STIMULI-RESPONSIVE HOST-GUEST SYSTEMS DECORATED WITH HEMITHIOINDIGO AND SPIROPYRAN UNITS

Giulia Moncelsi

UNIVERSITAT ROVIRA i VIRGILI

Stimuli-responsive host-guest systems decorated with hemithioindigo and spiropyran units

GIULIA MONCELSI

DOCTORAL THESIS
2019

STIMULI-RESPONSIVE HOST-GUEST SYSTEMS DECORATED WITH HEMITHIOINDIGO AND SPIROPYRAN UNITS

Giulia Moncelsi

UNIVERSITAT ROVIRA I VIRGILI
STIMULI-RESPONSIVE HOST-GUEST SYSTEMS DECORATED WITH HEMITHIOINDIGO AND SPIROPYRAN UNITS
Giulia Moncelsi

DOCTORAL THESIS

Giulia Moncelsi

STIMULI-RESPONSIVE HOST-GUEST SYSTEMS DECORATED WITH HEMITHIOINDIGO AND SPIROPYRAN UNITS

Supervised by Prof. Pablo Ballester Balaguer

**UNIVERSITAT
ROVIRA i VIRGILI**

Tarragona

2019

UNIVERSITAT ROVIRA I VIRGILI
STIMULI-RESPONSIVE HOST-GUEST SYSTEMS DECORATED WITH HEMITHIOINDIGO AND SPIROPYRAN UNITS
Giulia Moncelsi

ICIQ
Institut
Català
d'Investigació
Química

Av. Països Catalans,16
43007 Tarragona, Spain
Tel +34 977920200
Fax +34 977920221

UNIVERSITAT ROVIRA i VIRGILI
Dept. de Química Analítica
i Química Orgànica

Carrer de Marcel·lí Domingo, 1
43007, Tarragona, Spain
Tel +34 977559769
Fax +34 977558446

I STATE that the present study, entitled "Stimuli-responsive host-guest systems decorated with hemithioindigo and spiropyran units", presented by Giulia Moncelsi for the award of the degree of Doctor, has been carried out under my supervision at the Institute of Chemical Research of Catalonia (ICIQ).

Tarragona, 4th June 2019

Doctoral Thesis Supervisor

Dr. Pablo Ballester Balaguer

UNIVERSITAT ROVIRA I VIRGILI
STIMULI-RESPONSIVE HOST-GUEST SYSTEMS DECORATED WITH HEMITHIOINDIGO AND SPIROPYRAN UNITS
Giulia Moncelsi

UNIVERSITAT ROVIRA I VIRGILI
STIMULI-RESPONSIVE HOST-GUEST SYSTEMS DECORATED WITH HEMITHIOINDIGO AND SPIROPYRAN UNITS
Giulia Moncelsi

Acknowledgements

When reading the acknowledgements section in other theses, I often empathize with the writer as the words condensed in those few pages describe vividly some of the most important moments or ensembles of moments that occurred during the time of their studies. It happens to be my favorite part of the manuscript.

For now it's my turn, the time has come to squeeze these past three and a half years of life and doctorate into a couple of pages and describe with the best accuracy possible the separate or joint contribution that the following people have, consciously or not, given to my journey as a PhD candidate culminating with this thesis. To me, acknowledging someone for their help and advice is one of the most rewarding parts of personal and professional life.

If I got here to pursue my PhD studies is all thanks to one person, that is my supervisor and mentor **Pau**. Muchísimas gracias Pau por esa primera entrevista en Julio 2015; por aceptarme en tu grupo de investigación aún sabiendo que no tenía experiencia previa en el campo de la química supramolecular; por ser siempre tán paciente en enseñar, por empujarme fuera del estado fundamental cuando tenía que espabilarme y aprofundizar más en entender los resultados de mi investigación. Puedo no haber reconocido o apreciado todos tus esfuerzos constantes en haber intentado mejorarme como científica, pero ahora lo veo todo. Gracias por compartir parte de tu visión del mundo científico y de la sociedad conmigo, y por cuidar tanto a tus estudiantes.

When I first arrived in the PB4, the research was very new to me. At this time, a post-doc who later became one of my best pals here, **Frank**, guided me through the world of organic synthesis, photoswitches and molecular capsules. Later on, we shared many significant moments in and outside of the lab. Te agradezco muchísimo por tu amistad y apoyo, Frank. Thank you for all your original ideas, and your bright enthusiasm. Tambien quiero agradecer a **Dani**, que siempre tuvo tiempo para ayudarme con sus conocimientos de la química experimental, y por demonstrarme su amistad de tal manera que en realidad sospechaba caerle mal. During that time I shared the PB4 with other wonderful people that made the lab life and Tarragona much more enjoyable: thank you **Alejandro**, **Rajesh**, **Ramón**, **Nelson**, **Albano** and **Jordi** for the good times together. I would also like to thank the exchange students and research fellows with whom I had the pleasure to coincide at ICIQ, even for just a few months.

También quiero agradecer a toda la unidad de soporte a la investigación del ICIQ, en particular modo a las unidades de RMN y Chromtae, por la ayuda proporcionada durante estos años.

Outside of the lab, I had another large group of people, near and far, who were essential to get through the (many) bad times and make the good ones memorable. My experience here would have been completely different (and maybe miserable) if I had lacked your selfless support. Thank you Enisa, for being part of all this notwithstanding the distance, for the countless messages, pictures, memes and calls that formed part of my daily routine. Thank you for visiting me wherever I roam and bringing over your special luggage of perfume, flowers, wine, poetry, chocolate and *je-ne-sais-quoi*.

Un grazie molto speciale agli amici di sempre Gabriele, Federica, Valentina, per continuare ad accompagnarmi nei miei avventurosi spostamenti ed avere sempre un pensiero per me; per ricordarmi con affetto sincero le mie radici e chiedermi quando tornerò a vivere in Umbria, sapendo che la risposta probabilmente non vi piacerà. A Giulia, Nadina, Stefano ed Elena per il vostro sostegno continuo, i lunghi (e sottolineo lunghi) aggiornamenti e per rendere l'inesorabile transizione all'etá adulta meno temibile. A tutta la mia famiglia sparsa per l'Italia, composta da nonni, zii e cugini, per farmi sentire sempre coccolata e a casa.

For the invaluable and many new friends that I made here at ICIQ, in Tarragona and around the world, I want to mention in particular Franzi, probably my longest-lasting friend of these years: danke! danke! danke! for all the Fun (capital letter is required here) that we have together and also for comforting each other with earthy food, drinks, sports, unlikely cults and good conversation! Thank you Laura, Ilario, Sofia, Jesús, Cristina, Barbara, Giacomo, Giacomo, Luca, Luca, Elisa, Marcos, Conchi, Justine, Ivo, Joe, Rosie, Manu, Paulina, Bradley, Carla, Serena, Marta, Primavera and the Grande Italia crew. All you guys went beyond my expectations as colleagues and friends during our time together, and I can say without a doubt that my PhD experience here in Catalunya would not have been the same without you.

Infine, arriva il momento di ringraziare chi c'è sempre stato dall'inizio, chi è rimasto vicino durante questo percorso e chi ci sarà dopo, a vivere con me e attraverso me quello che sarà il mio futuro: grazie a mamma **Maddalena** e a **Lorenzo**, cardini indispensabili, colonne portanti, porto sicuro. Tutto quello che faccio, ogni risultato e successo che ottengo, lo dedico a voi e ad Alcide.

A mamma, Lorenzo e Alcide,

UNIVERSITAT ROVIRA I VIRGILI
STIMULI-RESPONSIVE HOST-GUEST SYSTEMS DECORATED WITH HEMITHIOINDIGO AND SPIROPYRAN UNITS
Giulia Moncelsi

Table of Contents

UNIVERSITAT ROVIRA I VIRGILI
STIMULI-RESPONSIVE HOST-GUEST SYSTEMS DECORATED WITH HEMITHIOINDIGO AND SPIROPYRAN UNITS
Giulia Moncelsi

Chapter 1

General introduction

Part of this chapter has been published in:

STIMULI-RESPONSIVE HOST-GUEST SYSTEMS DECORATED WITH HEMITHIOINDIGO AND SPIROPYRAN UNITS

Giulia Moncelsi

UNIVERSITAT ROVIRA I VIRGILI
STIMULI-RESPONSIVE HOST-GUEST SYSTEMS DECORATED WITH HEMITHIOINDIGO AND SPIROPYRAN UNITS
Giulia Moncelsi

General introduction

1.1 General introduction

Photochromism (*phos* = light; *chroma* = color), a term coined by Hirshberg in 1950,[1] defines the light-induced reversible transformation between two forms of a compound with different color/absorption spectrum. Nowadays, the phenomenon of photochromism is found coupled to a wide variety of chemical systems, ranging from photo-[2,3] and chiroptical switches[4] to light-driven molecular motors,[5,6] biological receptors[7,8,9] and materials[10] of daily use.[11] Within them, organic photoswitches can be regarded as the structurally simplest and most studied examples of photochromic molecules.[12] The switching motion is generated by a reversible structural change between the two isomeric states of a compound upon light-irradiation. In most cases the isomeric states of a photoswitch can be discriminated using standard spectroscopic techniques owing to the difference in their absorption and emission spectra. The human eye may also serve as a detector at the macroscopic scale, when the change in the absorption profile associated to the isomerization takes place in the visible region of the electromagnetic spectrum (380-740 nm). The photochromic feature, i.e. the light-induced change in color, is common to the several families of molecular photoswitches that have been studied and developed over the years. However, the instrinsic switching ability and the type of isomerization process experienced upon light-irradiation induce properties that are unique to each family of photoswitches.[13] Therefore, a common method of classification is based on the type of isomerization process of the different synthetic photoswitches.[14] For example, azobenzenes,[15] stilbenes,[16] hemiindigos/hemithioindigos[17] and acyl hydrazones[18,19] undergo *trans*/*cis* or *E*/*Z* isomerization. On the other hand, spiropyrans/spirooxazines,[20,21,22] diarylethenes,[23,24] chromenes,[25,26] fulgides/fulgimides[27,28,29] and donor-acceptor Stenhouse adducts (DASAs)[30,31,32] feature open/closed-ring isomerization. Photoswitches can also be classified as P-type or T-type depending on the thermal stability of the bistable system.[33] The metastable state of T-type photoswitches is thermally unstable and reverts spontaneously and at different rates to the thermally stable state. On the other hand, P-type photoswitches are thermally stable in both states and require light-irradiation to recover the thermodynamically more stable state. Despite the excellent photochromic properties displayed by many photoswitches (very different absorption spectra for the two isomeric states), their optimal performance remains limited by different factors. The problems most frequently encountered in the applications of molecular photoswitches include: non-quantitative switching efficiency, low quantum yields, photofatigue, synthetic accessibility and limited function at the bio-

Chapter 1

optical window (650-1350 nm). Hence, the real application of photoswitchable compounds in chemical and biocompatible systems still represents a challenging endeavor.[34] A further understanding of the functioning of the different molecular photoswitches is essential to overcome their limitations and warrant their application in the design of complex molecular photoresponsive architectures.[35] Having used azobenzenes in our research endeavors for several years, we became especially interested in studying the photochemical behavior and investigate the applicability to supramolecular systems of two other switches: hemithioindigos (HTIs)[36] and spiropyrans (SPs) (Scheme 1.1).[37]
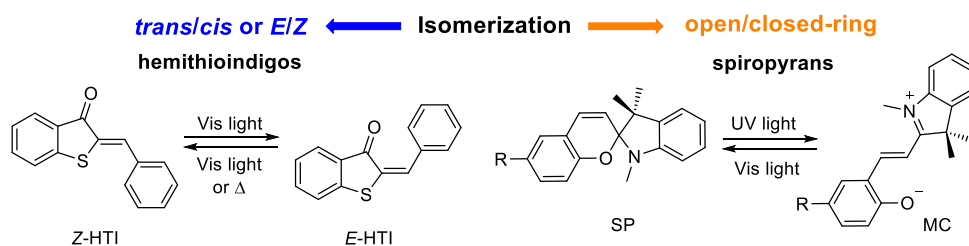
Scheme 1.1 Switching behavior of hemithioindigos and 6'-substituted spiropyrans.

Specifically, in this chapter we will go through selected examples of relevant host-guest systems incorporating these photoactive units in the receptor's or the guest's scaffold.[38] These examples serve to easily grasp the desired coupling between the photoswitching process and the modification of the composition of the host-guest systems (thermodynamic and dynamic equilibria).

1.2 Photoswitchable host-guest systems

Synthetic host-guest systems lead to the formation of supramolecular complexes between two or more chemical entities, which are held together by non-covalent, weak intermolecular forces. These forces are usually referred as molecular recognition interactions.[39,40] Simple host-guest systems may be decorated with moieties that display a selective and controllable response to an external stimulus: light, pH, temperature, solvation, metal ions, redox potential and mechanical force.[41] Photochromic compounds are nearly ideal candidates for this purpose. Light is a privileged external input given its typically non-damaging and non-invasive nature, and its high spatial and temporal resolution. In particular, organic photoswitches offer a higher ease of preparation with respect to other photochromic systems.

UNIVERSITAT ROVIRA I VIRGILI
STIMULI-RESPONSIVE HOST-GUEST SYSTEMS DECORATED WITH HEMITHIOINDIGO AND SPIROPYRAN UNITS
Giulia Moncelsi

General introduction

Hence, they have been employed in the functionalization of several smart materials, nanostructures, biopolymers and photopharmacophores.[42] As anticipated before, in this chapter we concern ourselves with host-guest systems incorporating hemithioindigos and spiropyrans. Although both photoswitches have been known for many years, more than 100 in the case of HTIs and more than 50 for SPs, their covalent attachment to organic receptors and guests, as well as the function of the resulting photoswitchable host-guest systems, has received limited attention in literature. Instead, photoswitchable supramolecular systems (host-guest and self-assembled) mainly based on azobenzene and diarylethene units are typically reviewed.[43,44,45] Hemithioindigos and spiropyrans feature reversible photoswitching in the ultraviolet and visible regions of the electromagnetic spectrum. However, they differ significantly in the light-induced isomerization process and in the modification of the physical properties of the metastable photoproducts. That is, irradiation of the thermally stable state of the photoswitch with UV light produces a photostationary state (PSS) rich in the metastable isomer. Subsequent irradiation with visible light produces a new PSS enriched in the thermodynamically stable state. Moreover, HTI and SP photoswitches are T-type, that is, their photoinduced metastable isomers undergo thermal relaxation to the original thermally stable state.[46] In the following sections, we describe a selection of fundamental studies involving HTI- and SP-based host-guest systems published in the last 30 years. Firstly, we discuss examples of synthetic receptors (hosts) covalently functionalized with HTI or SP units, and their use in molecular recognition studies of organic and biological molecules in solution. Secondly, we describe photoswitchable guests equipped with hemithioindigo or spiropyran units. We comment on the effects exerted by the switching process on the binding properties of the resulting complexes. We show that the intermolecular interactions involved in the stabilization of the host-guest complexes are modulated by the structural changes experienced by the photoswitches upon light-irradiation.[47] In some cases, the light-induced structural change experienced by the photoswitch does not translate into significant changes in the stability constants of the complexes. Nevertheless, other examples do reveal that it is possible to couple the photoprocess to dramatic changes in the composition of the host-guest systems.

Chapter 1

1.2.1 Applications of hemithioindigos in host-guest chemistry

1.2.1.1 *Z/E* photoisomerism of hemithioindigos

Hemithioindigos are a family of indigoid photoswitches that consist of a thioindigo fragment covalently connected to a stilbene fragment through a central double bond. Although the discovery of this hybrid chromophore dates back to 1906,[48] it was only recently that it became of high interest owing to the efficient photoswitching properties using visible light-irradiation.[49,50] In a similar manner to azobenzenes and stilbenes, the double bond of the hemithioindigos can be reversibly photoisomerized between the thermodynamically stable *Z*-configuration and the metastable *E*-configuration (Figure 1.1a). In the *Z*-configuration, the stilbene fragment is placed in a *cis* orientation with respect to the sulfur atom of the thioindigo. Irradiation with visible light ($\lambda > 400$ nm) produces the *Z*-to-*E* isomerization, with the stilbene fragment facing the thioindigo's carbonyl group. The *E*-to-*Z* photoisomerization is achieved at longer wavelengths of irradiation ($\lambda > 500$ nm). In general, the *Z*-isomer of hemithioindigos is lower in energy than the *E*-isomer. For the unsubstituted HTI, the thermal equilibrium is exclusively populated by *Z*-isomers (99.9%). The theoretical energy difference between the *Z/E* isomers in their electronic ground state is of 4.2 kcal·mol^{-1}.[51]
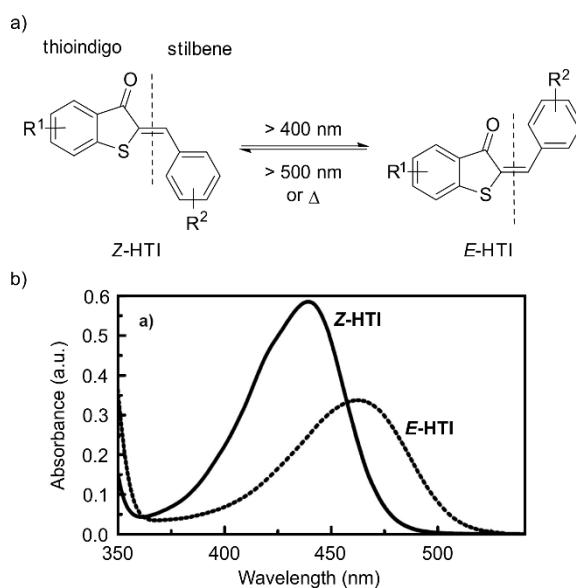
Figure 1.1 a) *Z/E* photoisomerization of hemithioindigos:[36] *Z*-HTI (left) and *E*-HTI (right). Thioindigo and stilbene fragments are indicated. b) UV/Vis absorption spectra of the *Z* and the *E*-isomers of unsubstituted HTI in dichloromethane solution.[52] [Adapted with permission from Ref. [46] (Copyright 2007 ACS Publications)]
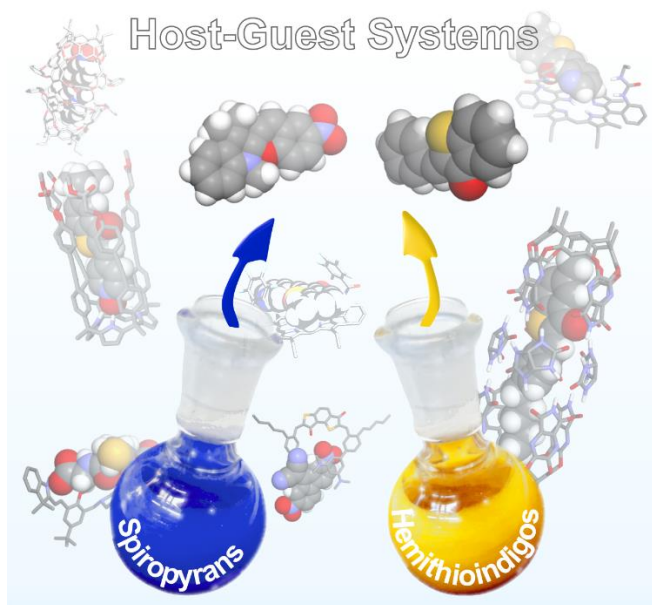
UNIVERSITAT ROVIRA I VIRGILI
STIMULI-RESPONSIVE HOST-GUEST SYSTEMS DECORATED WITH HEMITHIOINDIGO AND SPIROPYRAN UNITS
Giulia Moncelsi

General introduction

Additionally, the metastable *E*-isomer reverts thermally to the thermodynamic product, the *Z*-isomer. The barrier for the thermal *E/Z* isomerization (typically > 27 kcal·mol^{-1}) of the hemithioindigo is higher than that of the azobenzene photoswitch (> 25 kcal·mol^{-1}). Interestingly, the hemithioindigo switch can be photoisomerized in both directions using visible light. Despite the low quantum yields of the photoisomerization processes, the red-shifted absorption of the *E*-isomer (20-30 nm) allows the accumulation of both isomers in high yields at the respective PSSs (Figure 1.1b). In dichloromethane solution, the photoirradiation (λ = 420 nm, 60 min) of the *Z*-HTI affords the *E*-HTI to a 94% extent at the PSS. The *E*-to-*Z* back-conversion at 505 nm for 25 min restores quantitatively the starting *Z*-isomer. The *E*-isomer of unsubstituted hemithioindigo is stable for a remarkable 349 years at ambient conditions in toluene solution.[49] The introduction of substituents at either fragment of the hemithioindigo allows the modulation of its photoisomerization properties.[52,53] For example, the introduction of an electron-donating dimethyl-amino group in the *para*-position to the sulfur atom in the thioindigo fragment (R^1) significantly improves the thermal bistability of the photoswitch while rendering the compound susceptible to protonation.[54] In fact, protonation results in dramatic changes in the photophysical properties of the compound and can be used as a second independent input signal (light, pH) leading to 2-bit digital information processing behavior.

1.2.1.2 Hosts containing HTI units

Since the early work of Tanaka and co-workers in 2008 (*vide infra*),[55] there has been an increasing interest in the use of HTI photoswitches in host-guest supramolecular systems. Recently, Dube et al. developed photoresponsive molecular tweezers based on a HTI spacer unit equipped with two electron-rich biphenyl arms. In two representative works, they showed how the careful design of the HTI-based receptors (**1**-**3** in Scheme 1.2Scheme 1.3) is essential to achieve the desired binding geometry and subsequent light-induced cargo (guest) release. Electron-poor aromatic guests, such as 9-(dicyanomethylene)-2,7-dinitrofluorene (**4**) and 9-(dicyanomethylene)-2,4,7-trinitrofluorene (**5**), were suitable for binding with the HTI-tweezers. In the first report, the bis-HTI receptor **1** was synthesized by a condensation reaction of a tricyclic bis-thiophenone with two equivalents of biphenyl aldehyde.[56] The presence of two isomerizable double bonds implies the existence of **1** as four possible configurational isomers (*Z,Z*; *Z,E*; *E,Z* and *E,E*). The *Z,Z*-**1** isomer was isolated as the thermodynamically

Chapter 1

stable product, displaying a planar S-shaped geometry (Scheme 1.2). Remarkably, irradiation of the *Z,Z*-**1** isomer with visible light (λ = 420 nm) in toluene solution resulted in a highly selective conversion (94%) to the *E,Z*-**1** isomer, as confirmed by 2D NMR spectroscopic techniques. The steric congestion between the terminal anilines of the biphenyl arms of **1** forces the *E,Z*-**1** isomer to adopt a helically folded structure. The *E,Z*-**1** isomer binds one molecule of **4** producing a 1:1 complex with sandwich-like binding geometry (Scheme 1.2).
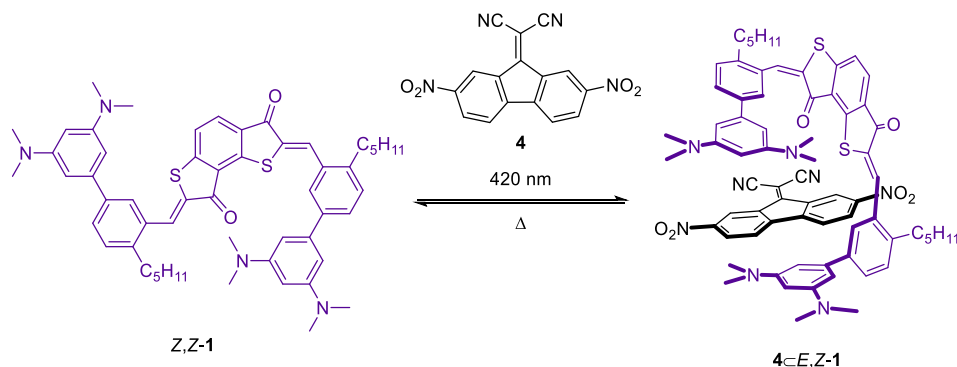
Scheme 1.2 First generation of HTI-based molecular tweezers reported by Dube and co-workers involving the cargo/release of guest **4** upon irradiation with visible light.[56]

The polar aromatic interactions (π-π) established between the two binding partners accounted for an association constant value K_a (**4**⊂*E,Z*-**1**) = 240 M^{-1} in toluene solution. In contrast, the binding constant value determined for the **4**⊂*Z,Z*-**1** complex was negligible. Therefore, the thermal treatment of a solution of the **4**⊂*E,Z*-**1** complex afforded the *Z,Z*-**1** isomer and **4**, as free components. This result demonstrated the efficient cargo-release of the bis-HTI receptor **1** owing to the large difference in binding affinity of the *E,Z*-**1** and *Z,Z*-**1** isomers for **4**. In the second generation of HTI-based molecular tweezers, the binding/release of the guest is achieved simultaneously by using two tweezers receptors, **2** and **3**, and a single light signaling event. The *Z*-isomers of receptors **2** and **3** are structurally complementary. That is, their electron-rich biphenyl arms are either oppositely directed to each other, *Z*-**2**, or face-to-face oriented one to another, *Z*-**3** (Scheme 1.3).[57] The different substitution of **2** and **3** does not perturb their absorption properties, thus, upon irradiation with visible light (λ = 435 nm), both receptors isomerized to their *E*-counterparts, to a 86% extent for *E*-**2** and 63% for *E*-**3** at the PSS. The *E*-isomers show opposite orientations of the biphenyl arms with respect to the *Z*-counterparts. In turn, irradiation at 530 nm triggered the back-conversion to a mixture of the *Z*-isomers of both receptors in high yields (80-84 %). The closed-tweezers forms, *E*-**2** and *Z*-

UNIVERSITAT ROVIRA I VIRGILI
STIMULI-RESPONSIVE HOST-GUEST SYSTEMS DECORATED WITH HEMITHIOINDIGO AND SPIROPYRAN UNITS
Giulia Moncelsi

General introduction

3, are expected to bind the electron-deficient guest **5** via polar aromatic interactions, analogously to receptor **1**.
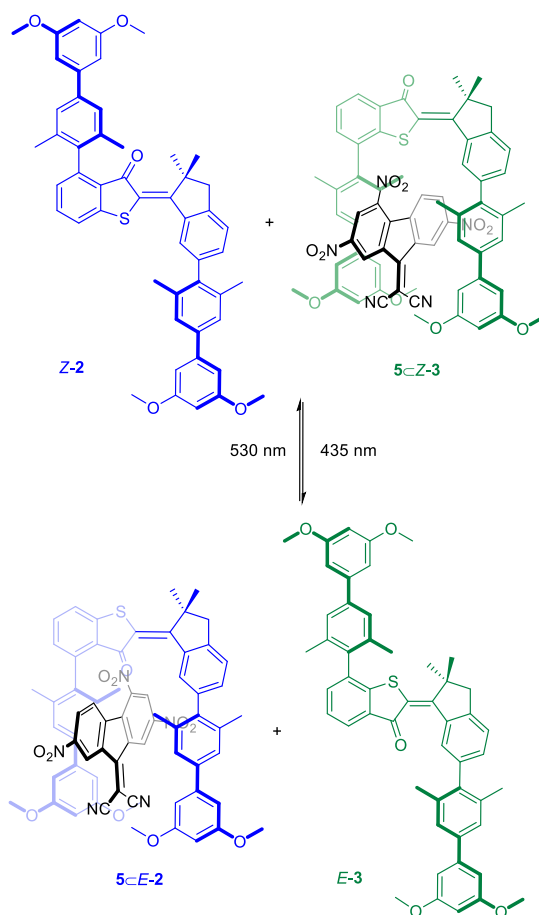
Scheme 1.3 Second generation of HTI-based molecular tweezers reported by Dube and co-workers involving the relocalization of guest **5** upon irradiation with visible light.[57]

A series of ^{1}H NMR titration experiments were performed using tweezers **2** and **3**, in both *Z* and *E* configurations, in order to assess their binding affinities with **5** in CDCl$_3$ solution at -20 °C. As expected, the open-tweezers forms, *Z*-**2** and *E*-**3**, showed a complete absence of binding towards **5**. On the other hand, when the closed-tweezers forms, *E*-**2** or *Z*-**3**, were titrated with **5** at -20 °C, they showed the formation of 1:1 complexes with sandwich-like binding geometry and high association constant values (K_a (**5**⊂*E*-**2**) = 1.2 × 10^4 M^{-1} and K_a (**5**⊂*Z*-**3**) = 2.3 × 10^3 M^{-1}). Using a sequential irradiation cycle, the authors demonstrated the dynamic relocation of guest **5** from its binding equilibrium with tweezers *Z*-**3** to a new binding

Chapter 1

equilibrium with tweezers *E*-**2**. An equimolar mixture of *Z*-**2** and *Z*-**3** containing 0.6 equiv. of **5** was irradiated at 435 nm in chloroform solution until reaching the PSS. At this point, two species with high affinity for **5**, *Z*-**3** and *E*-**2**, are present in solution to a different extent. *E*-**2** is predominant and it possesses the largest affinity for **5**. Consequently, **5** is primarily bound by *E*-**2**. Subsequent irradiation of the mixture at 530 nm reverses the relative ratio of high affinity species for **5**. *Z*-**3** is the predominant species under these circumstances. However, because *E*-**2** features a larger affinity for **5** than *Z*-**3**, the former reduces the relocation of the guest in tweezers *Z*-**3** to a 70%. A second irradiation cycle proved the complete reversibility of the translocation process, which was also evidenced using ^{1}H NMR spectroscopy.

1.2.1.3 HTI derivatives as guests

The use of photoswitchable guests constitutes an alternative methodology for the photochemical control of supramolecular host-guest systems. The introduction of molecular photoswitches in the guests' scaffolds is synthetically less demanding. Photoisomerizable guests can be addressed not only free in solution but also in the bound state.[58] In this vein, Rebek *et al.* showed that photoirradiation of azobenzene and hemithioindigo isomerizable guests can be used to expel them from the interior cavities of self-assembled hydrogen-bonded dimeric capsules based on the resorcin[4]arene cavitand **6** having 2-benzimidazolone bridges[59] (Figure 1.2a).[60] Initially, they used 4,4'-dimethylazobenzene, *trans*-**8**, to induce the quantitative thermal assembly of the encapsulation complex *trans*-**8**⊂**6**$_2$[61,62] in mesitylene solution. Likewise, working under strict stoichiometric control, a mixture of cavitand **6**, glycoluril **7** and HTI *Z*-**9** led to the quantitave formation of the extended capsular system *Z*-**9**⊂**6**$_2$·**7**$_4$ (Figure 1.2b).

UNIVERSITAT ROVIRA I VIRGILI
STIMULI-RESPONSIVE HOST-GUEST SYSTEMS DECORATED WITH HEMITHIOINDIGO AND SPIROPYRAN UNITS
Giulia Moncelsi

General introduction
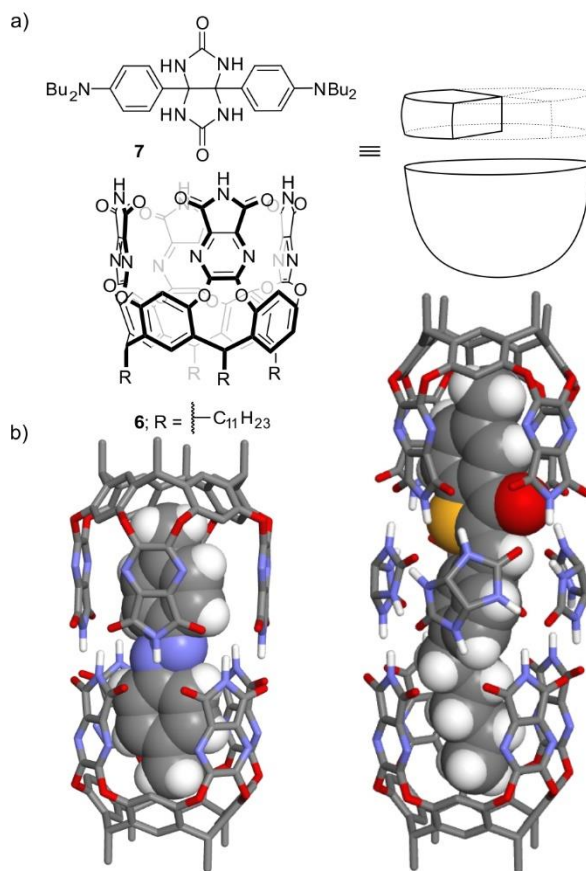
Figure 1.2 a) Line-drawing structures of resorcin[4]arene **6** and glycoluril **7**; b) energy-minimized (MM3) structures of the capsules *trans*-**8**⊂**6**$_2$ and *Z*-**9**⊂**6**$_2$·**7**$_4$. The hosts are depicted in stick representation and the included guests as CPK models. The undecyl chains in **6** were pruned to methyl groups and non-polar hydrogen atoms were removed for clarity. The Bu$_2$N-Ph substituents and non-polar hydrogen atoms of **7** were removed for clarity.

All capsular assemblies were characterized using ^{1}H NMR spectroscopy. With the systems *trans*-**8**⊂**6**$_2$ and *Z*-**9**⊂**6**$_2$·**7**$_4$ in hand, the authors were able to control the encapsulated guest and the type of assembly present in solution by combining an expectant mediocre guest with light and heat stimuli. Rebek and co-workers engineered a two modes light-triggered guest exchange by mixing cavitand **6**, the two photoswitchable guests, azobenzene *trans*-**8** and HTI *Z*-**9**, glycoluril **7** and the mediocre guests, 4,4'-dibromobenzil **10** and *p*-cymene **11** (Figure 1.3).

Chapter 1
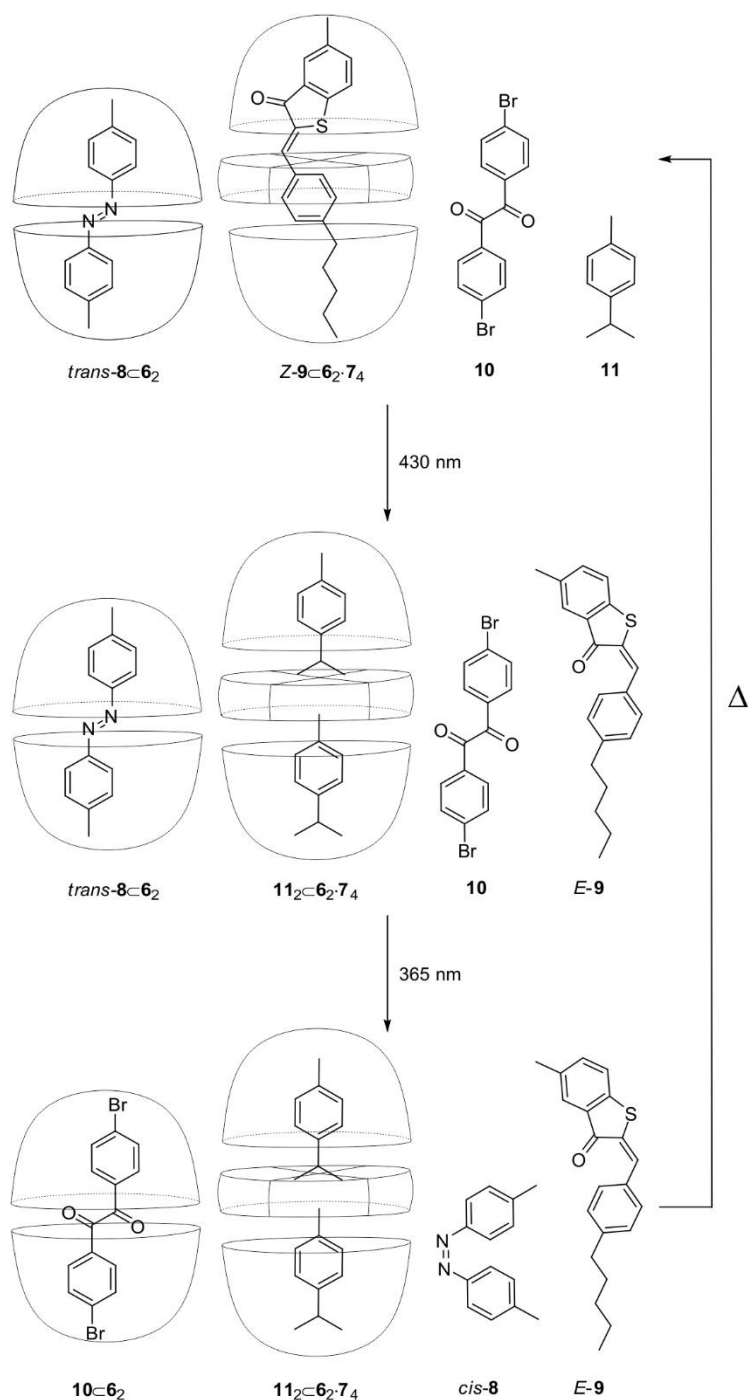
Figure 1.3 Sequential guest exchange triggered by distinct light inputs and thermal equilibration of the molecules described in the work of Dube and Rebek.[60]

UNIVERSITAT ROVIRA I VIRGILI
STIMULI-RESPONSIVE HOST-GUEST SYSTEMS DECORATED WITH HEMITHIOINDIGO AND SPIROPYRAN UNITS
Giulia Moncelsi

General introduction

When a mixture of all components, in proper stoichiometries, was heated to 160 °C for six minutes and then cooled down, only the two capsular assemblies *trans*-**8**⊂**6**$_2$ and *Z*-**9**⊂**6**$_2$·**7**$_4$ were detected in the ^{1}H NMR spectrum. Extensive light-irradiation of the mixture at 430 nm started the sequential guest exchange. No guest exchange occurred in the capsular dimer *trans*-**8**⊂**6**$_2$, but the guest exchange in the extended capsule was complete yielding **11**$_2$⊂**6**$_2$·**7**$_4$ owing to the *Z*-to-*E* isomerization of the bound HTI-**9** in the original assembly. Because HTI-*E*-**9** displays a pronounced bent shape compared to HTI-*Z*-**9**, it was not complementary to the cavity of **6**$_2$·**7**$_4$ and was readily replaced by two molecules of *p*-cymene (**11**). Subsequent irradiation at 365 nm generated the azobenzene *cis*-**8** isomer, which was released from the capsular dimer **6**$_2$ to the bulk solution, and replaced by one molecule of the dibromo derivative **10**. The two consecutive inputs of light at different wavelengths produced a whole different mixture of capsular assemblies in which both photoswitches are released to the solution and two new encapsulation complexes are formed. The original conditions of the experiment could be restored by thermal stabilization of the solution, proving the reversibility of the irradiation process. It is worth mentioning here that the driving force for the exchange processes depends both on the external stimulus (light irradiation) and the presence of the mediocre competing guests (**10** and **11**) that are complementary to the cavity volumes of the dimeric capsule and extended capsule, respectively.

In the work of Tanaka and co-workers mentioned at the beginning of this section,[55] a repeatable movement between two kinds of free-base porphyrins involving the HTI-pyridyl derivative **14** was controlled by photoirradiation. The free-base porphyrin hosts, **12** and **13**, formed 1:1 complexes with both *E*-**14** and *Z*-**14** isomers of the HTI-pyridyl guest (Figure 1.4). Remarkably, the bis-urea porphyrin **12** complexed the *E*-**14** isomer with substantially larger affinity than the *Z*-**14** counterpart (K_a (*E*-**14**⊂**12**) = 2.7 ± 0.7 × 10^3 M^{-1}, Figure 1.5a; K_a (*Z*-**14**⊂**13**) = 4.8 ± 0.1 × 10^2 M^{-1}). Conversely, the bis-amide porphyrin **13** preferred to bind the HTI-*Z*-**14** isomer (9.3 ± 0.1 × 10^2 M^{-1}) over the HTI-*E*-1**4** analogue (4.5 ± 1.8 × 10^2 M^{-1}, Figure 1.5b). All binding constant values were determined using ^{1}H NMR titrations in toluene-*d*$_8$ solutions.

Chapter 1
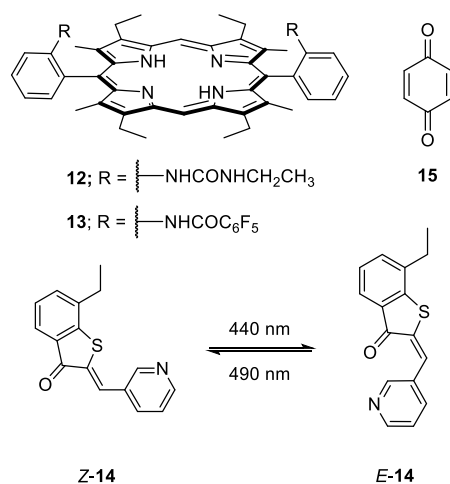
Figure 1.4 Line-drawing structures of the molecules described in Tanaka's work.[55]

The HTI-*E*-**14** isomer was prepared by irradiation of the thermodynamically stable HTI-*Z*-**14** analogue with 440 nm light and contained a 3% of the *Z*-isomer. In turn, the metastable *E*-isomer was reverted to the thermally stable conformer by irradiating at 490 nm. The superior binding ability of the ureido-porphyrin **12** for the HTI-*E*-**14** isomer was ascribed to tight *cis*-hydrogen bonding interactions between the two NH protons of one ureido group and the pyridine nitrogen and carbonyl oxygen atoms of the guest, together with two additional π-π stacking interactions (Figure 1.5a). For the HTI-*Z*-**14** isomer this ditopic hydrogen bonding interaction cannot be attained geometrically.
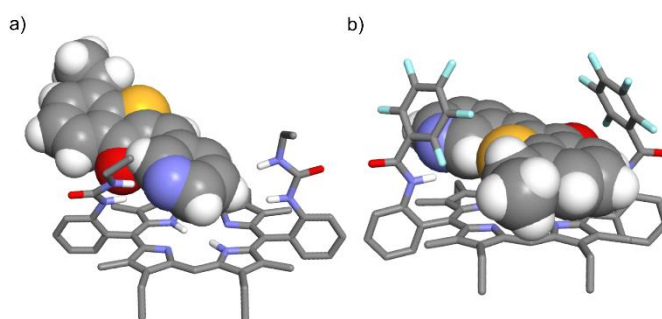
Figure 1.5 Energy-minimized (MM3) structures of the HTI⊂porphyrin complexes a) *E*-**14**⊂**12** and b) *Z*-**14**⊂**13**. The hosts are depicted in stick representation and the included guests as CPK models. Non-polar hydrogen atoms of the receptors were removed for clarity.

UNIVERSITAT ROVIRA I VIRGILI
STIMULI-RESPONSIVE HOST-GUEST SYSTEMS DECORATED WITH HEMITHIOINDIGO AND SPIROPYRAN UNITS
Giulia Moncelsi

General introduction

On the other hand, the preference of porphyrin **13** for the complexation of the HTI-*Z*-**14** isomer was assigned to a strong *trans*-hydrogen bonding of the pyridine nitrogen and carbonyl oxygen atoms of the guest and the two acidic pentafluorobenzamido protons (Figure 1.5b). The shuttling process of the HTI-**14** between the two porphyrins, **12** and **13**, was confirmed by ^{1}H NMR spectroscopy upon irradiation (440 nm) of a toluene-d_8 solution containing a 1 mM equimolar mixture of the porphyrins and 0.5 equiv. of HTI-*Z*-**14**. The preferential formation of the HTI-*E*-**14**⊂**12** complex was evidenced by the downfield shift experienced by the PhNH urea protons of **12**, while the amido protons of **13** moved upfield. Subsequent irradiation with 490 nm light produced the reversed chemical shift changes in the NH protons of **12** and **13**, supporting the preferential capture of the HTI-*Z*-**14** isomer by the pentafluorobenzamido porphyrin **13**. The observed chemical shift changes were reproduced three times by consecutive photo-irradiation processes. The authors noted that, at mM concentration and taking into consideration the calculated binding constants, 35% of the HTI-*Z*-**14** isomer is captured by **13** while 20% is bound to **12** and the remaining 45% is free in solution. Reversely, 13% of HTI-*E*-**14** binds to **13** and 58% to **12**, with 29% remaining free in solution. The binding preferences of receptors **12** and **13** towards a specific photoisomer of **14** were also used to control the photo-induced catch and release of *p*-benzoquinone **15** with the two porphyrins. The K_a values for the complexes of *p*-benzoquinone **15** with porphyrins **12** and **13** were slightly lower than those of HTI-**14** in its two isomeric forms. Nevertheless, irradiation with 440 nm light of a toluene-d_8 solution of bis-ureido porphyrin **12** (2 mM), *p*-benzoquinone **15** (0.2 mM) and HTI-*Z*-**14** (5 mM) showed a downfield shift of the olefinic protons of *p*-benzoquinone **15**. This result indicated that the *p*-benzoquinone **15** captured by porphyrin **12** was released to the solution due to the increased binding affinity of the porphyrin for the HTI-*E*-**14** isomer. Subsequent irradiation with 490 nm light returned the system to the original position. Similar light-irradiation experiments were performed using porphyrin **13** and also a mixture of the two porphyrins. In this latter case, the quantification of the quinone distribution (free and bound) was not possible because one porphyrin captures the quinone released by the other. Remarkably, chemical shift changes in the olefinic protons of **15** were still detectable, suggesting that the reversible distribution of the quinone between the two porphyrins is also triggered by the photoswitching and shuttling processes of HTI-**14**.

Recently, we studied the effect exerted by the isomerization process of two HTI-*N*-oxide derivatives, **17** and **18**, used as photoresponsive guests for a super aryl-extended calix[4]pyrrole receptor (**16**, Figure 1.6a).[63] The *Z*-isomers of 2-(4'-pyridyl-*N*-oxide)-

Chapter 1

substituted hemithioindigos, **17** and **18**, (Figure 1.6a) displayed the characteristic *Z/E* isomerization processes upon irradiation with blue light (λ = 450 nm). At the PSS the metastable *E*-isomer was present to an 80% extent. The *Z*-isomers of both HTIs were bound in the deep aromatic cavity provided by the elongated super aryl-extended calix[4]pyrrole **16**. The shape, size and function complementarity that exists between the receptor's cavity and the guests produced the formation of kinetically and thermodynamically stable 1:1 inclusion complexes in chloroform solution (Figure 1.6b).
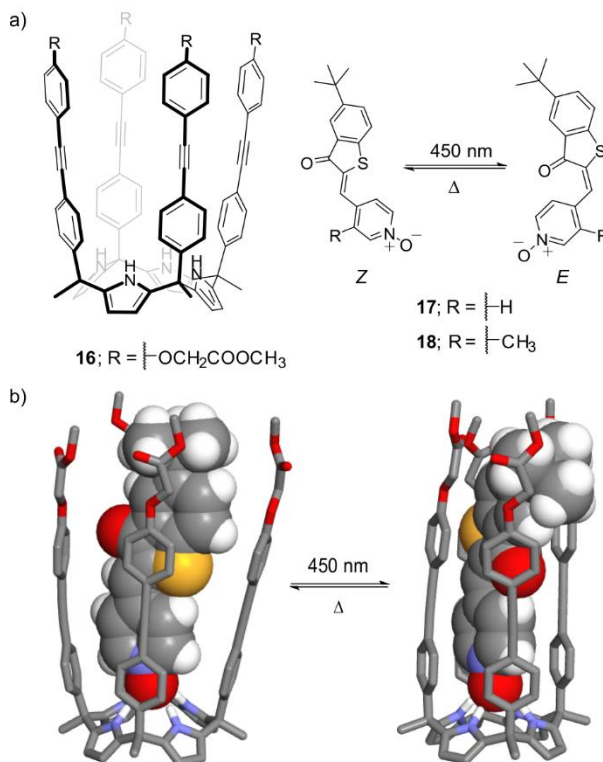
Figure 1.6 a) Line-drawing structures of calix[4]pyrrole **16** and *Z/E*-HTIs **17** and **18**; b) energy-minimized (MM3) structures of the inclusion complexes *Z*-**17**⊂**16** and *E*-**17**⊂**16**.[63] The host is depicted in stick representation and the included guest as CPK model. Non-polar hydrogen atoms of **16** were removed for clarity.

We used isothermal titration calorimetry (ITC) experiments to assess the binding constant values of the deep inclusion complexes. The calculated K_a values were of the order of 10^6 M^{-1}. Upon irradiation with 450 nm light, the bound *Z*-HTI *N*-oxides photoisomerized affording the corresponding *E*-HTI⊂**16** complexes. We evaluated the changes experienced by the photophysical properties of the free and bound chromophores. We discovered that the rates

UNIVERSITAT ROVIRA I VIRGILI
STIMULI-RESPONSIVE HOST-GUEST SYSTEMS DECORATED WITH HEMITHIOINDIGO AND SPIROPYRAN UNITS
Giulia Moncelsi

General introduction

of the *Z*-to-*E* photoisomerization processes and thermal relaxations of the HTIs were significantly reduced by the inclusion of the photoswitch in the receptor's cavity. Moreover, the conformational flexibility of the receptor was responsible for the reduced changes in the binding affinities measured for the two isomeric forms of the guests. The binding constant values of the HTI *E*-isomers were only 2.2-2.8 fold lower than those of the HTI *Z*-counterparts. This result suggested that the number and nature of the different interactions (CH-π, π-π, π-sulfur) between the photoswitchable guests and the macrocyclic host are not significantly modified by the photoisomerization process. Likewise, the small decrease in binding affinity experienced by the 1:1 complexes of the HTI *E*-forms of photoswitches explained the lack of release of the cargo to the solution.

1.2.2 Host-guest chemistry of spiropyran photoswitches

1.2.2.1 Ring-opening photoisomerization of spiropyrans

Spiropyrans (SPs) are a widely studied class of organic photoswitches used as prominent building blocks in the design of dynamic materials.[37] Their photo-, acido- and solvatochromism have been extensively investigated for many decades since their discovery by Fisher and Hirshberg in 1952.[64] The reversible switching of simple SPs was applied in the development of colorimetric molecular thermometers,[65] selective sensors for metal cations,[66] molecular logic gates,[67,68] polymer nanoparticles,[69,70] photoregulated oligonucleotides[71,72] and chiroptical materials, such as self-assembled supramolecular gels.[73,74]

The photo-induced isomerization of SPs relies on the reversible interconversion between the colorless closed SP-form and the open and colored zwitterionic merocyanine-form (MC) (Scheme 1.4). The closed SP-form consists of two perpendicular indoline and chromene moieties fused at the central sp^3 hybridized spiro-carbon. The UV light-irradiation of the SP-form gives rise to the open conjugated MC-form with a central *trans*-double bond between the methine carbon atoms. This is a first order process that has been extensively investigated both experimentally and theoretically. In-between the starting SP and the final *all-trans*-MC photoproduct, other *transoid* and *cisoid* merocyanine conformers are formed, although they are rarely detected (a priori 16 possible structures can exist for the open MC products).[20] The reverse MC-to-SP isomerization usually occurs spontaneously, and can be accelerated by visible light-irradiation. The *trans*-MC species, in its zwitterionic resonance form, is

Chapter 1

characterized by the concomitant presence of two charged moieties: the *N*-indolenium cation and the *O*-phenolate anion. The photogenerated charge separation gives rise to a large difference between the electric dipole moments of the SP isomer (4-6 D) and the MC isomer (14-18 D). Moreover, the stacking of the MC isomer is known to have a strong stabilizing effect and leads to the formation of aggregates in solution.[75] The dipoles of the MCs can arrange in a parallel (head-to-head) or antiparallel (head-to-tail) fashion to afford J- or H-aggregates, respectively. These assemblies experience a red (J-type) or blue (H-type) shift in their UV/Vis absorption spectra, as compared with the isolated merocyanine molecules. In general, the photoisomerization behavior of SP in solution is strongly dependent on the nature of the solvent. Interestingly, some SP derivatives show negative photochromism in polar environments i.e. water, silica, or reverse micelles. In such cases, the MC-form is the thermodynamically stable isomer and the SP-to-MC conversion occurs spontaneously with time, even in the dark.[76] The SP-form only exists if the system is exposed to visible light, that is why this property is referred to as inverse or reverse photochromism.[77] The absorption spectrum of the MC-isomer is also strongly solvent-dependent. Non-polar solvents favor the quinoidal form and decrease the energy gap between ground and excited state of MC, resulting in a red shift of the MC band.
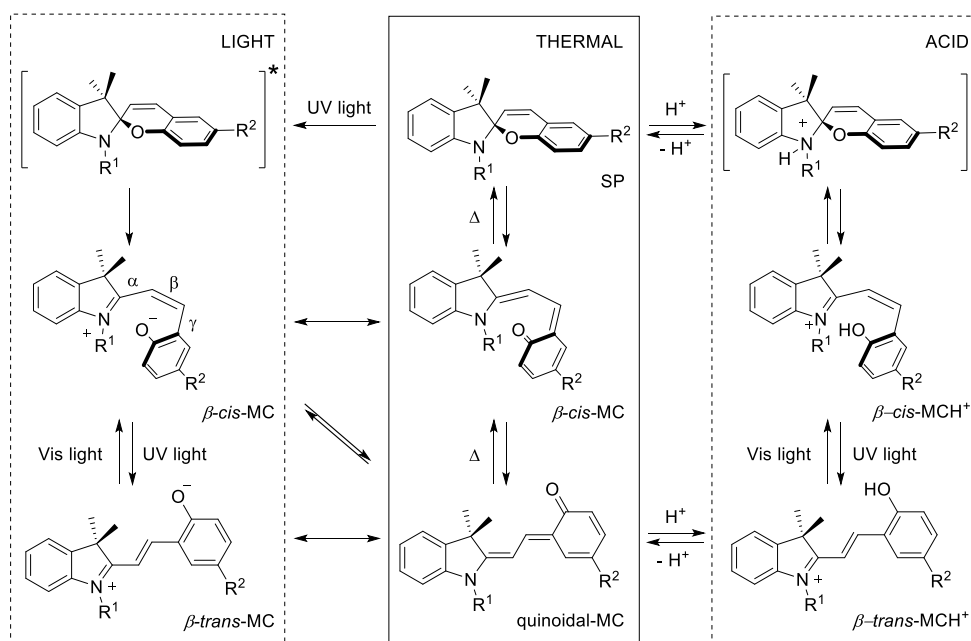
Scheme 1.4 Formation of the photo- and acido-products of the SP-to-MC conversion of 6'-substituted spiropyrans.

UNIVERSITAT ROVIRA I VIRGILI
STIMULI-RESPONSIVE HOST-GUEST SYSTEMS DECORATED WITH HEMITHIOINDIGO AND SPIROPYRAN UNITS
Giulia Moncelsi

General introduction

Further applicability of SP-based systems in aqueous media is limited by the instability of the MC towards hydrolysis at basic pH. The mechanism consists in the conjugate addition of water to the ene-iminium cation of the MC isomer, followed by a retro-aldol reaction to afford the corresponding Fischer's base and 4-substituted salicylaldehyde.[78]

Acidochromism is another distinct feature of SPs, that occurs in addition to photochromism. Typically, the open protonated merocyanine-form (MCH$^+$) and its conjugate base (MC) have distinctly different absorption spectra. This phenomenon is common to phenols and aromatic amines.[12] Several works on the pH-regulated conversion of SP derivatives into the MCH$^+$-form, even in the absence of any UV irradiation, have been reported.[79] The initial neutral SP can be restored by addition of a suitable base, usually a tertiary amine.[68,80] Browne *et al*. showed through a combined experimental and theoretical study that in aprotic solvents the acidochromism of SPs is highly dependent on the acid strength.[81] They also achieved a pH-gated photochromism switching cycle of simple SPs between four-states. The protonated *β-cis*-MCH$^+$ displayed an absorption spectrum very similar to the one of the neutral SP isomer and the authors warned about the possible wrong assignment of the closed-form in previous studies. The commercially available 6'-nitrospiropyran (1′,3′-dihydro-1′,3′,3′-trimethyl-6-nitrospiro[2H-1-benzopyran-2,2′-(2H)-indole]; NSP-**27**, *vide infra*) is the most extensively SP studied and, together with its derivatives, has been used as model compound to increase the understanding about the photo-, acido-, thermo- and solvatochromic properties of activated spiropyrans.[80,82,83]

1.2.2.2 Hosts containing SP units

Receptors based on mono- and bis-SP photoswitches have been employed as "smart" sensors for the detection of several ionic species, especially cyanide and metal cations.[84] The molecular recognition function is generally performed by the open MC isomer of the photoswitch owing to its reactive functions, phenolate and *N*-indolenium units of the zwitterionic resonance form, and its colored properties that are absent in the closed SP-form. In aqueous media, the cyanide anion is known to react selectively and reversibly with the N-indolenium unit of the MC, produced by UV light-irradiation, affording a covalent adduct. The reaction is associated with a change in color of the solution from pink (MC) to yellow (MC-CN-adduct). On the other hand, the phenolate unit either alone or in combination with a nearby heteroatom (N,O) has been extensively exploited for the interaction with metal cations.

Chapter 1

Using this strategy, Yang, Chan and co-workers described a SP functionalized with a dimethylamino methyl substituent in the 8' position that selectively chelated Cu^{2+} with the phenolate oxygen forming a 2:1 (MC:M) complex.[85] The same authors demonstrated the use of an ensemble of the SP with Cu^{2+} or Hg^{2+} for the efficient recognition and quantification of cysteine (Cys) and homocysteine (Hcy) in neutral aqueous solution. They proposed that the deprotonation of the Cys at the sulfhydryl group formed a bridged dimer (cystine) through the redox activity of the metal. Next, a complex involving two metal centers and one cystine self-assembled with two molecules of the chelating MC-form into a ternary aggregate (2:1:2 M:cystine:MC) producing a significant change (red-violet to yellow) in the color of the solution.[86] In an effort to extend the recognition and sensing properties of the SPs to organic guests and biomolecules, the research group of Inouye synthesized the spiropyridopyran **19** (Figure 1.7a), which could bind guanosine derivative **21a** in both the SP- and MC-forms.[87]
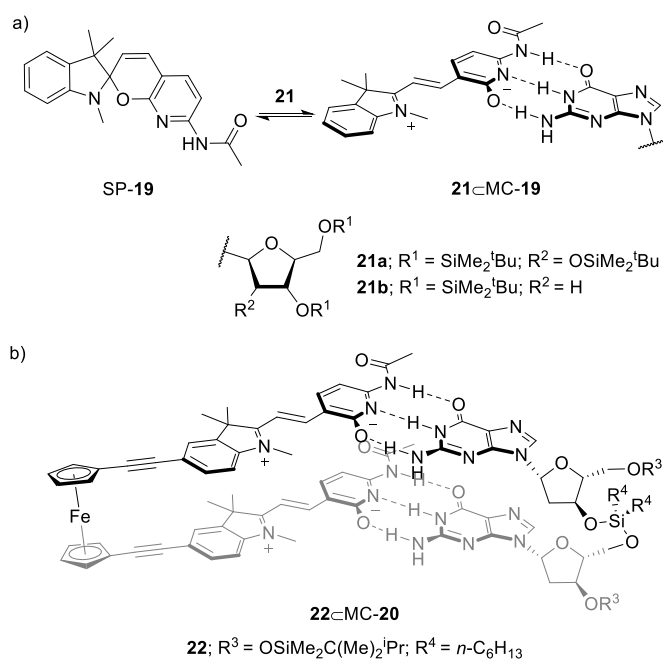
Figure 1.7 Line-drawing structures of the a) **21⊂MC-19** and b) **22⊂MC-20** complexes and the molecules described in Inouye's work.[87,88]

The binding process was monitored using UV/Vis and ^{1}H NMR spectroscopy. The profiles of the UV/Vis and ^{1}H NMR spectra registered during the incremental addition of guanosine **21a** to a chloroform solution of **19** suggested the concomitant formation of the **21a⊂SP-19** and

UNIVERSITAT ROVIRA I VIRGILI
STIMULI-RESPONSIVE HOST-GUEST SYSTEMS DECORATED WITH HEMITHIOINDIGO AND SPIROPYRAN UNITS
Giulia Moncelsi

General introduction

21a⊂MC-**19** complexes, which were in equilibrium. The equilibrium shifted towards the formation of the **21a**⊂MC-**19** complex as the concentration of the guanosine was increased (Figure 1.7a). Later, Inouye *et al*. also used the spiropyridopyran **19** to bind the guanosine derivative **21b**, and prepared a ferrocene-based bis(spiropyridopyran) receptor **20** for the recognition of guanine-guanine dinucleoside **22** (Figure 1.7b).[88] Notably, receptor **20** constitutes the first example of a molecular architecture containing two SP motifs for the recognition and binding of small organic molecules. Upon guest binding, receptors **19** and **20** adopt mainly the open-ring MC configuration using the generated phenolate anion to better satisfy the triple hydrogen-bonding complementarity interaction that is established with the purine base of the nucleosides. The authors performed UV/Vis titration experiments of the receptors with the mono- and bis-nucleosides in dichloromethane solutions. The titration data were mathematically analyzed assuming that all the 1:1 complexes of the SPs existed as the MC-forms **21b**⊂MC-**19** and **22**⊂MC-**20** (Figure 1.7). Indeed, the absorption profiles of the UV/Vis spectra showed the appearance of the characteristic band for the merocyanine species at *ca*. 575 nm. The fit of the titration data returned association constant values of 2.4×10^4 M^{-1} for the **21b**⊂MC-**19** complex, and 4.2×10^5 M^{-1} for the **22**⊂MC-**20** analogue. The authors noticed that the increase in binding energy was lower than expected for the double interaction featured by the **22**⊂MC-**20** complex. They suggested an electrostatic repulsion between the two MC units as responsible for this result.

Several years later, Yang, Chan and co-workers also synthesized a bis-SP receptor with a piperazine linker covalently connecting the 8' methylene substituents of the photoswitches, SP-**23** (Figure 1.8a). This tweezers-like receptor recognized dipolar organic molecules.[89] Significantly, host **23** was employed for the highly selective binding of glutathione (GSH) **24** (Figure 1.8a), a biologically relevant tripeptide. The interaction of receptor **23** with the tripeptide **24** in 20:80 ethanol:water solution was probed using UV/Vis and fluorescence spectroscopy. In solution, receptor **23** exists in the thermodynamically stable closed-form SP-**23**. Remarkably, irradiation of the solution with UV light did not produce changes in its absorption spectrum. This result was indicative of the almost complete absence of the open-ring MC-form of the free receptor under these conditions. It was also a positive premise for the use of the receptor as a molecular sensor because the photochromic behavior of the free host in solution should not interfere with its optical response in the presence of the analytes capable of complexation-inducing the conversion of the SP-form into the MC-form. Incremental addition of GSH **24** to an aqueous solution of SP-**23** produced significant spectral

Chapter 1

changes in the absorption spectrum. These changes reflected the conversion of the closed SP-form of **23** into the open MC counterpart induced by the complexation to the GSH **24**. The bound MC-**23** receptor features two zwitterionic motifs along with the pre-existing binding cleft of the molecule (Figure 1.8b).
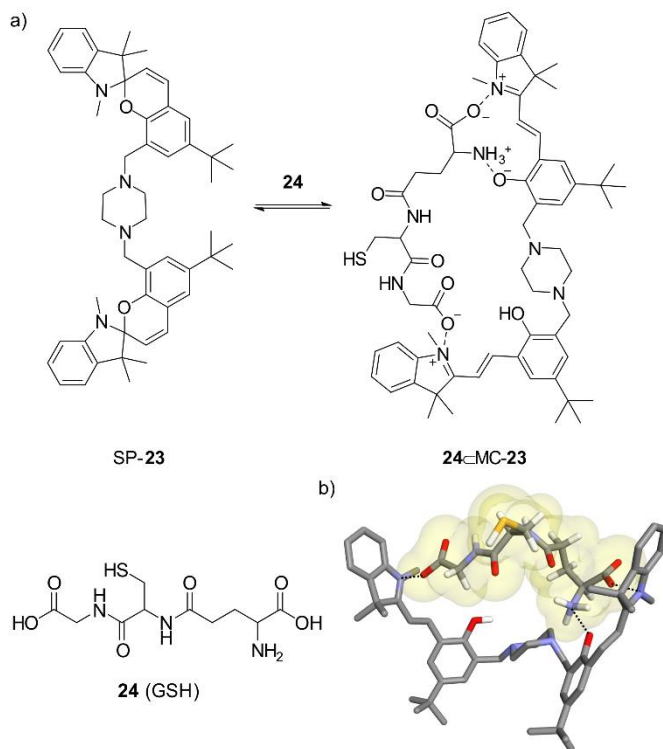
Figure 1.8 a) Line-drawing structures of bis-spiropyran SP-**23**, guest **24** and complex **24**⊂MC-**23**; b) Energy-minimized (MM3) structure of the inclusion complex **24**⊂MC-**23**.[89] The host and guest are depicted in stick representation and the bound guest is shown with a yellow transparent Van der Waals surface. Non-polar hydrogen atoms of **23** were removed for clarity. The electrostatic interactions are marked with dashed lines.

The MC units of MC-**23** have four possible binding sites: the two indolenium nitrogens and the two phenolate oxygens. Most likely, one of the phenolates is protonated upon complexation with GSH and does not participate in direct coulombic host-guest interactions but its participation in hydrogen-bonding interactions cannot be ruled out. The ^{1}H NMR spectrum of an equimolar mixture of SP-**23** and GSH **24** in ethanol-d_8 solution displayed characteristic proton signals for the MC-form. In particular, the signals for the vinyl protons of the MC units were observed and the two singlets of the magnetically non-equivalent methyl

UNIVERSITAT ROVIRA I VIRGILI
STIMULI-RESPONSIVE HOST-GUEST SYSTEMS DECORATED WITH HEMITHIOINDIGO AND SPIROPYRAN UNITS
Giulia Moncelsi

General introduction

protons of the SP-form coalesce into one singlet. The methylene protons of the spacer and the methylene protons of the piperazine unit moved downfield. Furthermore, the fit of the fluorescence titration data was consistent with a 1:1 binding model and returned an association constant value of the order of 10^4 M^{-1} for the **24**⊂MC-**23** complex. Although the recognition properties of MC-**23** are limited to non-directional coulombic/electrostatic interactions, the selectivity demonstrated by the receptor for the recognition of GSH over other dipolar substrates can be ascribed to the cooperativity in the multivalent binding displayed by the host-guest complex.[90] The **24**⊂MC-**23** complex was stable up to 6 h in the dark at RT, whereas visible light-irradiation for 15 min resulted in a 80% dissociation and conversion to the SP-form of the **23** receptor, as shown by the analysis of the emission spectra of the corresponding solutions. The complexation and irradiation de-complexation cycles could be repeated up to five times, showing complete reversibility and little fatigue of the host-guest system.

1.2.2.3 SP derivatives as guests

There are many examples in literature involving SP-based guests. In two representative works, Tiburcio and co-workers explored the binding properties of a dibenzo-24-crown-8 ether host towards hybrid spiropyran-viologen guests. In the first example, the acid- or photo-induced isomerization of the spiropyran-viologen induced the threading of the corresponding merocyanine-viologen through the macrocyle. The process was assisted by $N^+\cdots$O ion-dipole, C-H$\cdots$O hydrogen-bonding and π-stacking interactions. The resulting host-guest complex displayed a [2]pseudorotaxane topology.[91] In the second example, a spiropyran-methyl-viologen (SP-MV) guest is partially threaded through the crown ether by hydrogen-bonding interactions between the N^+-CH$_3$ moiety on the MV and the oxygen atoms of the host. The subsequent treatment with acid yielded two [2]pseudorotaxane architectures in equilibria between the partially and the fully threaded MC-MV guest, performing a shuttling motion in fast exchange.[92]

Recently, the groups of Mukherjee[93] and Klajn[94] independently demonstrated the stabilization of the MC-form of 6'-substituted SP by inclusion in the cavity of conformationally flexible coordination cages. With respect to purely organic receptors, it is known that in the solid state n-membered cyclodextrins (CD[n]; n = 6,7,8) bind spiropyrans yielding inclusion complexes with a 1:1 stoichiometry.[95,96] Sueishi and Nishimura investigated the complexation of 6-SO$_3^-$-SP with *β*- and *γ*-cyclodextrins in aqueous solution. Using UV/Vis absorption spectroscopy,

UNIVERSITAT ROVIRA I VIRGILI
STIMULI-RESPONSIVE HOST-GUEST SYSTEMS DECORATED WITH HEMITHIOINDIGO AND SPIROPYRAN UNITS
Giulia Moncelsi

Chapter 1

they demonstrated preferential inclusion of the SP-form in the 1:1 complexes formed with the cyclodextrins in solution.[97]

Conversely, cucurbit[n]urils and sulfonatocalix[n]arenes are suitable receptors for the MC-form of the SPs. We will focus our discussion on the studies performed with these receptors in aqueous solution. CB[n]s have two electron-rich open portals at the opposing ends of their cavities where several polar carbonyl groups converge. In addition, CB[n]s possess a highly hydrophobic cavity suitable for the inclusion of hydrophobic molecules or residues. These structural characteristics made CB[n]s suitable receptors for protonated akyl and arylamines, as well as neutral organic molecules and ions.[98] Miskolczy and Biczók investigated the influence of complex formation of 1-(2-hydroxyethyl)-3,3-dimethylindolino-6'-nitrobenzopyrylospiran **25** (Figure 1.9) with CB[8] on the MC-SP equilibrium in aqueous solution at different pHs. They showed that the MC and the protonated MCH$^+$ were the most stable forms both free in water solution and included in the cavity of CB[8].[99] Using absorption and fluorescence titrations, a binding constant value of $K_a = 1.7 \times 10^5$ M^{-1} was determined for the MC-**25**⊂CB[8] complex. Similar absorption titrations performed at pH 3.1 provided a binding constant value of $K_a = 2.0 \times 10^6$ M^{-1} for the analogous MCH$^+$-**25**⊂CB[8] complex.
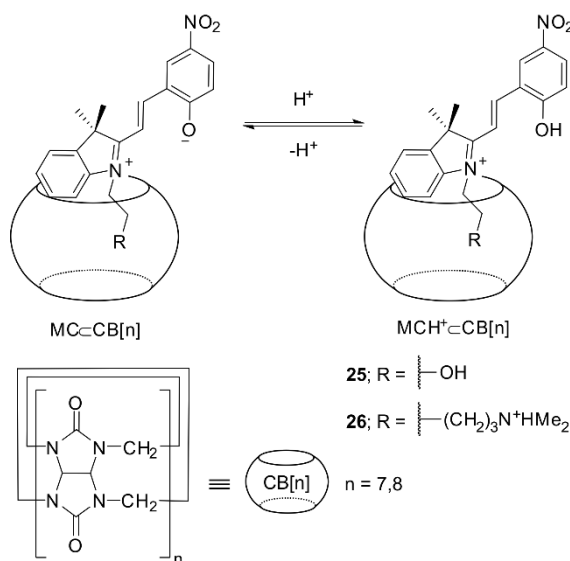
Figure 1.9 Line-drawing structures of merocyanine guests **25**-**26** and CB[n] receptors.

UNIVERSITAT ROVIRA I VIRGILI
STIMULI-RESPONSIVE HOST-GUEST SYSTEMS DECORATED WITH HEMITHIOINDIGO AND SPIROPYRAN UNITS
Giulia Moncelsi

General introduction

The complexes are stabilized by the hydrophobic effect derived from the deep inclusion of the *N*-alkyl substituent of **25** into the host's cavity, and the establishment of ion-dipole interactions between the carbonyl groups of the CB[8] and the cationic part of the guest at the portal of the cavity. Unfortunately, the structures of the two complexes could not be determined using ^{1}H NMR spectroscopy owing to the reduced solubility of the binding partners. Remarkably, the emission spectrum of MC-**25** turned out to be identical to the one of its protonated form MCH[+]-**25**. This result indicated that MCH[+]-**25** rapidly loses one proton in its excited state owing to acidity enhancement upon excitation. Nevertheless, the inclusion of MCH[+]-**25** in CB[8] diminishes the acidity of the dye. The presence of CB[8] significantly decelerated the light-induced (505 nm) formation of the SP-form. Most likely, the strong host-guest interactions stabilizing the MC-**25**⊂CB[8] complex and steric clashes hindered the *trans-cis* isomerization preceding the formation of the SP-form. The subsequent isomerization of the SP-form to the MC isomer carried out in the dark was faster for the SP-**25** included in CB[8] than free in water.

In a follow-up work, the authors reported a complete different thermodynamic and photochromic behavior for the inclusion of MC-**25** and its protonated counterpart in CB[7].[100] Firstly, only MCH[+]-**25** is bound by CB[7] and the stability constant of the complex is reduced almost two orders of magnitude ($K_a = 7.4 \times 10^4$ M^{-1}) compared to the inclusion complex with CB[8]. Probably, the larger cavity of CB[8] produces a deeper inclusion complex stabilized by stronger intermolecular interactions. Remarkably, the authors concluded that the cavity size does not influence the acidity change observed for the bound MCH[+]-**25**. Secondly and in striking contrast with the findings obtained for CB[8], the inclusion of MCH[+]-**25** in CB[7] accelerates the photoinduced transition of the merocyanine-form to the SP.

Andréasson, Pischel and co-workers[101] explored the binding of 6'-nitrospiropyran **26** featuring a cadaverine-substituted anchor to CB[7] in water solution using neutral or acidic conditions (Figure 1.9). At pH 7, the SP-form of **26** converted thermally to a 90% extent into the MC-form, as indicated by ^{1}H NMR spectroscopy. The kinetic data of the process were obtained from a bi-exponential fit of the time-dependent changes in the absorbance of MC-**26**. The observed "rise and decay" behavior was assigned to the reversible initial formation of MC-**26** ($\tau_1 = 6.5$ h) followed by its hydrolytic decomposition ($\tau_2 = 47.4$ h). We already mentioned that the hydrolytic instability of the MC-form is one of the limitations of the use of SP molecular switches in water. At pH < 3, the MC-**26** form is protonated and produces

Chapter 1

MCH$^+$-**26**. At this pH the hydrolysis is suppressed and no signs of absorbance decay were observed. The rapid conversion of SP-**26** into MC-**26** hampered the determination of a binding constant for the SP-**26**⊂CB[7] complex. However, binding experiments performed under continuous visible light-irradiation provided evidence for the complex formation. The fit of the titration data to a 1:2 theoretical binding model afforded $K_1 = 7.9 \times 10^5$ M^{-1} and $K_2 = 1.3 \times 10^3$ M^{-1} for the MCH$^+$-**26**⊂CB[7] complex. Tentatively, K_1 was assigned to the inclusion of the cadaverine-substituent in the cavity of CB[7]. The second binding event was considered to be related to an *exo* complex formation of CB[7] with the indolenium unit. The MC-**26** form was stable enough to be titrated with CB[7]. The data were also fitted to a 1:2 binding model ($K_1 = 1.2 \times 10^5$ M^{-1} and $K_2 = 8.6 \times 10^3$ M^{-1}). The diminution in magnitude of K_1 for MC was interpreted based on the existence of negative repulsions between the phenolate anion and the electron-rich portal of CB[7]. The analysis of the mixtures using ^{1}H NMR spectroscopy supported the idea that the preferential site for binding of MC-**26** with CB[7] is the cadaverine substituent. The formation of the inclusion complexes was also evidenced in the gas-phase using ESI-MS experiments. The formation of the MC-**26**⊂CB[7] complex accelerated 70-fold the thermally induced opening of the ring of SP-**26** ($\tau_1 = 5.2$ min) and increased the hydrolytic stability of the MC-form. This result highlights the importance of the cadaverine-substituent in **26**, because in the case of SP-**25** no kinetic effect of CB[7] for the thermal ring-opening reactions was observed at acidic pH. The rate acceleration observed for the ring-opening of SP-**26** was explained by considering the indolenium nitrogen as part of the binding unit. In contrast to the accelerations measured for the SP-**26** to MC/H$^+$-**26** reactions induced by the presence of CB[7], the photoinduced back-conversions of MC-**26** and MCH$^+$-**26** were not affected by inclusion in CB[7].

Biczók and co-workers also employed merocyanine dyes as guests for water-soluble sulfonatocalix[n]arenes (SCXn; n = 4-8).[102] In their work, the receptors did not inhibit the hydrolysis of the open-ring *trans*-MC species in aqueous solution at neutral or basic pH. This is in contrast with the previously discussed results with CB[n] hosts. The cavity of the calixarene receptors lacks to some extent the negative charge density of the carbonyl groups in cucurbiturils, which protects the iminium unit of MC from the nucleophilic attack of OH$^-$ at basic pH. Similarly to the previous findings with CB[8],[99] visible light-irradiation of the *trans*-MCH$^+$⊂SCXn complexes at acidic pH produced their *cis*-MCH$^+$⊂SCXn counterparts, confirming the lack of deprotonation of the switch when bound to the receptor.

UNIVERSITAT ROVIRA I VIRGILI
STIMULI-RESPONSIVE HOST-GUEST SYSTEMS DECORATED WITH HEMITHIOINDIGO AND SPIROPYRAN UNITS
Giulia Moncelsi

General introduction

Recently, Ramamurthy and co-workers showed that 6'-nitro substituted NSP-**27** formed a 1:2 capsular assembly with Gibb's water-soluble octa-acid calix[4]arene cavitand **28**[103] (Figure 1.10).[104] The photoinduced isomerization of NSP-**27** into the NMC-**27** form is coupled with the disassembly of the dimeric capsular aggregate and the formation of simple 1:1 NMC-**27**⊂**28** complexes to a reduced extent ($< 10\%$). The assembly-disassembly process of the capsular dimer was shown to be reversible. The inclusion of NMC-**27** in **28** protects the dye from the hydrolytic reaction and increases its excited-state singlet lifetime.
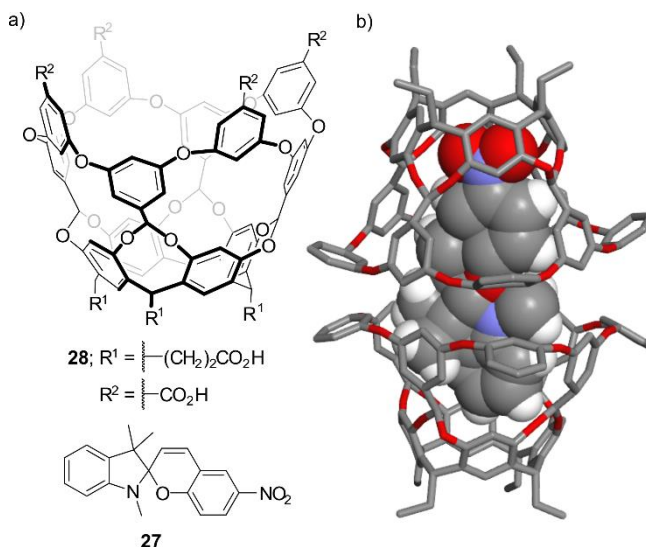
Figure 1.10 a) Line-drawing structures of NSP-**27** and calix[4]arene **28**; b) energy-minimized (MM3) structure of the capsule NSP-**27**⊂**28**$_2$. The host is depicted in stick representation and the included guest as CPK model. Non-polar hydrogen atoms and the terminal carboxylates of **28** were removed for clarity.

1.2.3 Conclusions

Hemithioindigos are visible light-responsive photoswitches that can be structurally tuned to isomerize at the bio-optical window with appropriate functionalization. Spiropyrans respond to a variety of external stimuli (light, heat, pH, etc.) which favors their use as multi-responsive molecular logic systems. The main photochemical and photophysical properties of unsubstituted HTI and 6'-nitrospiropyran NSP-**27** in different solvents are summarized in Table 1.1.

Chapter 1
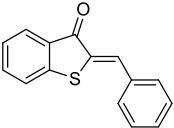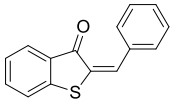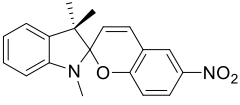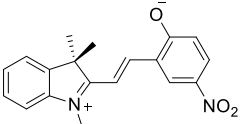
Compound	Extinction λ_{max} [nm] (ε [10^3 M^{-1}cm^{-1}])	Isomer yield at PSS (at irradiation λ in solvent)	Quantum yield ϕ (solvent)	Activation barrier of thermal isomerization [kcal·mol^{-1}]
Z-HTI 49	433 (12.6), 328 (17), 315 (19.8) in CH$_2$Cl$_2$	94% E (420 nm, CH$_2$Cl$_2$)	$\phi_{Z/E} = 0.23$ (CH$_2$Cl$_2$)	
E-HTI 49	457 (5.6), 321 (13.5) in CH$_2$Cl$_2$	100% Z (505 nm, CH$_2$Cl$_2$)	$\phi_{E/Z} = 0.05$ (CH$_2$Cl$_2$)	$\Delta G^* = 31$ (toluene)
NSP-**27**	298 (8.57) in EtOH[105]	100% NMC (334 nm, THF)[106]	$\phi_{SP} = 0.15$ (EtOH)[105]	
NMC-**27**	537 (36.8) in EtOH[105]		$\phi_{MC} = 0.04$ (EtOH)[105]	$\Delta G^* = 22$ (DMSO)[107]

Table 1.1 Comparison of the photochemical and photophysical properties of HTI with NSP-27.[36] [Adapted with permission from ref. [31] (Copyright 2015 Elsevier)]

Despite the clear differences in the structure and mechanism of isomerization of the two photochromic fragments, the tabulated data show similar trends. For instance, the quantum yield values for the *Z/E* and the NSP/NMC processes of the two switches are comparable in both directions, in a solvent suitable for their determination. Moreover, the switching efficiencies for the *Z/E*- HTI and the NSP-to-NMC isomerizations are quantitative, when the most appropriate irradiation wavelength and solvent system are employed. The molar extinction coefficient ε is similar for the *Z* and the *E*-isomer of hemithioindigo, whereas the ε of NMC-**27** is considerably higher with respect to that of NSP-**27** (in agreement with the known literature). In general, the photochemical and photophysical properties of these representative compounds of hemithioindigos and spiropyrans are of the same order of

UNIVERSITAT ROVIRA I VIRGILI
STIMULI-RESPONSIVE HOST-GUEST SYSTEMS DECORATED WITH HEMITHIOINDIGO AND SPIROPYRAN UNITS
Giulia Moncelsi

General introduction

magnitude, depending on the experimental conditions in which the measurements are carried out.

One of the goals of incorporating molecular switches to the scaffolds of receptors and their guests has to do with coupling their photoisomerization process with the thermodynamic stability of the resulting complexes. Based on the reviewed literature, we extract the following trends. The internal cavity of synthetic receptors is a privileged space for the confinement of photoswitchable molecules. Spiropyrans have been used as guests for a wide array of molecular receptors, whereas analogous studies with hemithioindigos are more limited. The photochromic properties of HTI and SP switches when included in molecular receptors might be significantly altered compared to their behavior in the bulk solution. At the molecular level, one might expect a significant response, for example, if the thermodynamically stable isomer of the photoswitch has high affinity for the receptor, whereas the photo- or acidogenerated counterpart cannot be accommodated in its binding cavity. Likewise, the binding properties of the receptors can be modified by the incorporation of one or more HTI or SP photoresponsive units into their scaffolds, however this approach is less commonly found in literature because it represents a more challenging synthetic effort. In the HTI-based tweezers, visible light-irradiation triggered an isomerization process that was coupled with a modification in the binding affinity of the receptor for the guest. In the examples of the SP-based receptors, the SP-to-MC isomerization was induced by the complexation of the receptor with a suitable guest. Such interaction could then be modulated by application of a light input. Typically, the light-induced photoisomerization processes experienced by the molecular switches are reversible, allowing the return to their initial state and the repetition of the cycle several times. The incorporation of molecular switches in host-guest systems aims at the modulation of their physicochemical properties with light. The photocontrolled release and uptake of cargo constitutes a general endeavor in this field. We are convinced that notwithstanding the successful applications of the HTI and SP molecular switches described in the reviewed examples, their use is still in the infancy state. The current research interest in the field of organic photoswitches is oriented towards the fabrication of smart materials and devices, as well as engineered biomolecules. For what concerns host-guest systems incorporating HTI and SP photoswitches, the main efforts translate into the design and preparation of molecular machines, nanoparticles, metal-organic assemblies, supramolecular polymers and self-assembled systems.[108] To warrant real-life applications and manufacturing of photocontrollable systems, i.e. as chemical sensors and biomimetic drug carriers, many

Chapter 1

practical challenges need yet to be overcome. Among them, we can highlight the synthetic cost and the retention of the photochemical and photophysical properties of the photoresponsive fragments guaranteeing the function of the resulting material or compound. Such challenges rise (and must be addressed) at the early stage of design of a simple molecular switch with its intrinsic limitations and amplify bottom-up to the host-guest systems and to the more elaborated molecular architectures discussed above. We expect that many photocontrolled host-guest systems and their applications will be developed in the years to come.

1.3 Aims of the thesis

The aim of the research work included in this thesis is the design and synthesis of stimuli-responsive inclusion complexes and molecular containers. In the host-guest systems presented herein, the photoactive unit is covalently incorporated into either the receptor's or the guest's scaffold. We use two photoswitches with distinct properties, hemithioindigos and spiropyrans, and two types of macrocyclic scaffolds based on calix[4]arene and calix[4]pyrrole. We aim at studying how light-irradiation and acid-base treatments induce the isomerization of the molecular switch. Moreover, we are interested in coupling the isomerization of the molecular switch with the binding affinity and the encapsulation properties of the synthesized molecular receptors and supramolecular capsules, respectively.

Specifically, we pursued the following objectives:

O.1) **Modulation of the reversible photoisomerization of two light-responsive hemithioindigo guests by inclusion in a super aryl-extended receptor.**

We sought the preparation of unprecedented *N*-oxide guests incorporating a photoisomerizable hemithioindigo unit. We aim at assessing their binding affinities towards a super aryl-extended calix[4]pyrrole receptor. Hemithioindigo switches photoisomerize between the thermodynamically stable *Z*-configuration and the metastable *E*-configuration under visible light-irradiation. The polar interior core and the deep aromatic cavity provided by the upper-rim extended aromatic walls of the calix[4]pyrrole receptor is, a priori, well suited for the binding of large polar guests with high affinity. We wanted to quantify the modulation in binding affinity with the calix[4]pyrrole receptor that is exerted by the *Z/E*

UNIVERSITAT ROVIRA I VIRGILI
STIMULI-RESPONSIVE HOST-GUEST SYSTEMS DECORATED WITH HEMITHIOINDIGO AND SPIROPYRAN UNITS
Giulia Moncelsi

General introduction

isomerization of the guest. The interaction between the receptor and the light-responsive guests was probed by different techniques (UV/Vis, ^{1}H NMR, ITC experiments).

O.2) **Upper-rim incorporation of four hemithioindigo switches on a tetraurea calix[4]arene scaffold.**

Recently, our group described the synthesis of light-responsive capsular dimers based on tetra-azobenzene tetraurea calix[4]arenes and calix[4]pyrroles. These macrocyclic scaffolds when decorated with four urea groups at their upper rims are known to form dimeric capsules in non-polar solvents. The dimerization process requires the presence of a suitable guest acting as template for the capsular self-assembly. Inspired by the previous systems, we designed two tetraurea calix[4]arenes containing four hemithioindigo units at their upper rim. We studied the coupling of the photoswitching properties of the responsive fragments to the self-assembly behavior (dimerization). We also investigated the encapsulation abilities of the assembled capsular dimers towards solvent molecules and small polar guests, as well as the light-controlled release of the capsular cargo.

O.3) **Homo- and hetero-dimeric capsules based on a tetraspiropyran tetraurea calix[4]arene. Studies on coupling of the light-mediated and acid-base modulated spiropyran-to-merocyanine isomerization of the switches with the assembly/disassembly processes of the capsular dimers.**

Following a similar molecular design to the one described in O.2), we sought to efficiently couple the switching properties of stimuli-responsive spiropyran units to the assembly/disassembly processes of capsular dimers based on tetraurea calix[4]arene and calix[4]pyrrole scaffolds. We prepared a tetraurea calix[4]arene featuring four appended spiropyran groups at its upper rim. We further explored the self-assembly of the tetraurea into homo- and hetero-dimeric capsules in organic solvents. Next, we investigated the photo- and acidochromic responsiveness of the capsules using UV/Vis and ^{1}H NMR spectroscopy techniques. We wanted to show that the capsular assembly/disintegration process is reversible owing to the acid/base properties of the spiropyran/merocyanine substituents.

Chapter 1

1.4 Outline of the thesis

This doctoral thesis is divided in 4 chapters: the present introduction (chapter 1), three chapters describing the results and their discussion (chapters 2-4) and a final chapter dedicated to the general conclusions of the work.

Following the general introduction, in chapter 2 we describe the synthesis and photochemical characterization of two hemithioindigos featuring a terminal *N*-oxide moiety. We probe their *Z/E* reversible photoisomerization with visible light ($\lambda = 450$ nm). We provide a detailed study of the binding processes of the two guests with a super aryl-extended calix[4]pyrrole receptor. We evaluated the binding properties of the *Z*- and *E*-HTI isomers. Finally, we studied the influence exerted by the inclusion of the molecular switch into the polar aromatic cavity of a super aryl-extended calix[4]pyrrole receptor to its photoswitching properties.

Chapter 3 deals with the design and synthesis of a series of tetraurea calix[4]arenes decorated with four hemithioindigo units at their upper rims. We describe the synthetic efforts to obtain these receptors and we investigate their dimerization in a variety of non-polar organic solvents and in the presence of tetramethyl phosphonium salts. We also report our attempts at the photoisomerization of the tetraureas in the monomeric state (in dimethylsulfoxide) and dimerized in capsular aggregates (in non-polar solvents).

Finally, chapter 4 reports the synthesis of a light- and pH-responsive tetraurea calix[4]arene featuring four appended spiropyran groups at its upper rim. The prepared tetraurea self-assembles into a homocapsule. Remarkably, in the presence of a calix[4]pyrrole counterpart and a suitable *N*-oxide template, both tetraureas experience a self-sorting process yielding exclusively the hetero-dimeric capsule. The self-assembly, self-sorting, photo- and acidochromic studies of the capsular systems in chlorinated solvents are discussed in this chapter. A summary of the preliminary encapsulation studies performed with tetramethyl phosphonium and tetramethyl ammonium cations is also described.

UNIVERSITAT ROVIRA I VIRGILI
STIMULI-RESPONSIVE HOST-GUEST SYSTEMS DECORATED WITH HEMITHIOINDIGO AND SPIROPYRAN UNITS
Giulia Moncelsi

General introduction

At the end of the thesis, we provide a concise summary of the most relevant conclusions drawn from the work carried out.

1.5 References and notes

[1] Y. Hirshberg, *Compt. Rend. Acad. Sci., Paris,* **1950**, *231*, 903.

[2] M.-M. Russew, S. Hecht, *Adv. Mater.* **2010**, *22*, 3348-3360.

[3] in *Molecular Switches*, 2 ed. (Eds.: B. L. Feringa, W. R. Browne), Wiley-VCH, Weinheim, **2011**.

[4] B. L. Feringa, R. A. van Delden, N. Koumura, E. M. Geertsema, *Chem. Rev.* **2000**, *100*, 1789-1816.

[5] A. Credi, *Aust. J. Chem.* **2006**, *59*, 157-169.

[6] T. van Leeuwen, A. S. Lubbe, P. Štacko, S. J. Wezenberg, B. L. Feringa, *Nat. Rev. Chem.* **2017**, *1*, 0096.

[7] T. Fehrentz, M. Schönberger, D. Trauner, *Angew. Chem., Int. Ed.* **2011**, *50*, 12156-12182.

[8] M. Volgraf, M. Banghart, D. Trauner, in *Molecular Switches*, 2 ed. (Eds.: B. L. Feringa, W. R. Browne), Wiley-VCH, Weinheim, **2011**.

[9] D. Wilson, N. R. Branda, in *Photochromic Materials* (Eds.: H. Tian, J. Zhang), Wiley-VCH, Weinheim, **2016**, pp. 361-391.

[10] J. Zhang, Q. Zou, H. Tian, *Adv. Mater.* **2013**, *25*, 378-399.

[11] S. Nigel Corns, S. M. Partington, A. D. Towns, *Color. Technol.* **2009**, *125*, 249-261.

[12] H. Bouas-Laurent, H. Dürr, *Pure Appl. Chem.* **2001**, *73*, 639-665.

[13] H. Dürr, H. Bouas-Laurent, *Photochromism: Molecules and Systems*, Elsevier Science, Amsterdam, **2003**.

[14] F. A. Jerca, V. V. Jerca, I.-C. Stancu, in *Polymer and Photonic Materials Towards Biomedical Breakthroughs, Vol. 4* (Eds.: J. Van Hoorick, H. Ottevaere, H. Thienpont, P. Dubruel, S. Van Vlierberghe), Springer, Cham, **2018**, pp. 3-47.

[15] H. M. D. Bandara, S. C. Burdette, *Chem. Soc. Rev.* **2012**, *41*, 1809-1825.

[16] D. H. Waldeck, *Chem. Rev.* **1991**, *91*, 415-436.

[17] C. Petermayer, H. Dube, *Acc. Chem. Res.* **2018**, *51*, 1153-1163.

[18] D. J. van Dijken, P. Kovaříček, S. P. Ihrig, S. Hecht, *J. Am. Chem. Soc.* **2015**, *137*, 14982-14991.

[19] I. Aprahamian, *Chem. Commun.* **2017**, *53*, 6674-6684.

[20] V. I. Minkin, *Chem. Rev.* **2004**, *104*, 2751-2776.

[21] V. I. Minkin, in *Molecular Switches*, 2 ed. (Eds.: B. L. Feringa, W. R. Browne), Wiley-VCH, Weinheim, **2011**.

[22] L. Kortekaas, W. R. Browne, *Chem. Soc. Rev.* **2019**. doi.org/10.1039/C9CS00203K

[23] M. Irie, *Chem. Rev.* **2000**, *100*, 1685-1716.

[24] M. Irie, T. Fukaminato, K. Matsuda, S. Kobatake, *Chem. Rev.* **2014**, *114*, 12174-12277.

[25] R. S. Becker, J. Michl, *J. Am. Chem. Soc.* **1966**, *88*, 5931-5933.

[26] B. Van Gemert, in *Organic Photochromic and Thermochromic Compounds: Volume 1: Main Photochromic Families, Vol. 1* (Eds.: J. C. Crano, R. J. Guglielmetti), Springer US, Boston, MA, **2002**, pp. 111-140.

[27] A. Santiago, R. S. Becker, *J. Am. Chem. Soc.* **1968**, *90*, 3654-3658.

[28] Y. Yokoyama, *Chem. Rev.* **2000**, *100*, 1717-1740.

[29] H. G. Heller, K. Koh, C. Elliot, J. Whittall, *Molecular Crystals and Liquid Crystals Science and Technology. Section A. Molecular Crystals and Liquid Crystals* **1994**, *246*, 79-86.

[30] S. Helmy, F. A. Leibfarth, S. Oh, J. E. Poelma, C. J. Hawker, J. Read de Alaniz, *J. Am. Chem. Soc.* **2014**, *136*, 8169-8172.

[31] S. Helmy, S. Oh, F. A. Leibfarth, C. J. Hawker, J. Read de Alaniz, *J. Org. Chem.* **2014**, *79*, 11316-11329.

[32] M. M. Lerch, S. J. Wezenberg, W. Szymanski, B. L. Feringa, *J. Am. Chem. Soc.* **2016**, *138*, 6344-6347.

[33] K. Nakatani, J. Piard, P. Yu, R. Métivier, in *Photochromic Materials* (Eds.: H. Tian, J. Zhang), Wiley-VCH, Weinheim, **2016**, pp. 1-45.

Chapter 1

[34] C. Brieke, F. Rohrbach, A. Gottschalk, G. Mayer, A. Heckel, *Angew. Chem., Int. Ed.* **2012**, *51*, 8446-8476.

[35] J. D. Harris, M. J. Moran, I. Aprahamian, *Proc. Natl. Acad. Sci.* **2018**.

[36] S. Wiedbrauk, H. Dube, *Tetrahedron Lett.* **2015**, *56*, 4266-4274.

[37] R. Klajn, *Chem. Soc. Rev.* **2014**, *43*, 148-184.

[38] D.-H. Qu, Q.-C. Wang, Q.-W. Zhang, X. Ma, H. Tian, *Chem. Rev.* **2015**, *115*, 7543-7588.

[39] J. J. Rebek, *Proc. Natl. Acad. Sci.* **2009**, *106*, 10423.

[40] K. Ariga, T. Kunitake, in *Supramolecular Chemistry - Fundamentals and Applications: Advanced Textbook*, Springer Berlin Heidelberg, Berlin, Heidelberg, **2006**, pp. 7-44.

[41] V. A. Azov, F. Diederich, in *Molecular Switches*, 2 ed. (Eds.: B. L. Feringa, W. R. Browne), Wiley-VCH, Weinheim, **2011**.

[42] Z. L. Pianowski, *Chem. Eur. J.* **2019**, *25*, 5128-5144.

[43] S. Yagai, A. Kitamura, *Chem. Soc. Rev.* **2008**, *37*, 1520-1529.

[44] X. Yao, T. Li, J. Wang, X. Ma, H. Tian, *Adv. Opt. Mater.* **2016**, *4*, 1322-1349.

[45] A. Díaz-Moscoso, P. Ballester, *Chem. Commun.* **2017**, *53*, 4635-4652.

[46] J. García-Amorós, D. Velasco, *Beilstein J. Org. Chem.* **2012**, *8*, 1003-1017.

[47] C. H. Huang, D. M. Bassani, *Eur. J. Org. Chem.* **2005**, *2005*, 4041-4050.

[48] P. Friedländer, *Ber. Dtsch. Chem. Ges.* **1906**, *39*, 1060-1066.

[49] B. Maerz, S. Wiedbrauk, S. Oesterling, E. Samoylova, A. Nenov, P. Mayer, R. de Vivie-Riedle, W. Zinth, H. Dube, *Chem. Eur. J.* **2014**, *20*, 13984-13992.

[50] A. Gerwien, T. Reinhardt, P. Mayer, H. Dube, *Org. Lett.* **2018**, *20*, 232-235.

[51] J. Plötner, A. Dreuw, *J. Phys. Chem. A* **2009**, *113*, 11882-11887.

[52] T. Cordes, T. Schadendorf, K. Rück-Braun, W. Zinth, *Chem. Phys. Lett.* **2008**, *455*, 197-201.

[53] T. Cordes, T. Schadendorf, M. Lipp, K. Rück-Braun, W. Zinth*, Vol. 92* (Eds.: P. Corkum, S. Silvestri, K. Nelson, E. Riedle, R. Schoenlein), Springer, Berlin, Heidelberg, **2009**, pp. 319-321.

[54] F. Kink, M. P. Collado, S. Wiedbrauk, P. Mayer, H. Dube, *Chem. Eur. J.* **2017**, *23*, 6237-6243.

[55] K. Tanaka, K. Kohayakawa, S. Iwata, T. Irie, *J. Org. Chem.* **2008**, *73*, 3768-3774.

[56] M. Guentner, E. Uhl, P. Mayer, H. Dube, *Chem. Eur. J.* **2016**, *22*, 16433-16436.

[57] S. Wiedbrauk, T. Bartelmann, S. Thumser, P. Mayer, H. Dube, *Nat. Commun.* **2018**, *9*, 1456.

[58] O. B. Berryman, H. Dube, J. Rebek, *Isr. J. Chem.* **2011**, *51*, 700-709.

[59] T. Heinz, D. M. Rudkevich, J. Rebek, *Nature* **1998**, *394*, 764.

[60] H. Dube, J. Rebek, *Angew. Chem., Int. Ed.* **2012**, *51*, 3207-3210.

[61] H. Dube, D. Ajami, J. Rebek, *Angew. Chem., Int. Ed.* **2010**, *49*, 3192-3195.

[62] H. Dube, M. R. Ams, J. Rebek, *J. Am. Chem. Soc.* **2010**, *132*, 9984-9985.

[63] G. Moncelsi, L. Escobar, H. Dube, P. Ballester, *Chem. Asian J.* **2018**, *13*, 1632-1639.

[64] E. Fisher, Y. Hirshberg, *J. Chem. Soc.* **1952**, *11*, 4522–4530.

[65] Y. Shiraishi, M. Itoh, T. Hirai, *Phys. Chem. Chem. Phys.* **2010**, *12*, 13737-13745.

[66] G. E. Collins, L.-S. Choi, K. J. Ewing, V. Michelet, C. M. Bowen, J. D. Winkler, *Chem. Commun.* **1999**, 321-322.

[67] F. M. Raymo, S. Giordani, *Org. Lett.* **2001**, *3*, 3475-3478.

[68] F. M. Raymo, S. Giordani, *J. Am. Chem. Soc.* **2001**, *123*, 4651-4652.

[69] M.-Q. Zhu, L. Zhu, J. J. Han, W. Wu, J. K. Hurst, A. D. Q. Li, *J. Am. Chem. Soc.* **2006**, *128*, 4303-4309.

[70] D. S. Achilleos, T. A. Hatton, M. Vamvakaki, *J. Am. Chem. Soc.* **2012**, *134*, 5726-5729.

[71] C. Brieke, A. Heckel, *Chem. Eur. J.* **2013**, *19*, 15726-15734.

[72] A. S. Lubbe, W. Szymanski, B. L. Feringa, *Chem. Soc. Rev.* **2017**, *46*, 1052-1079.

[73] C. Liu, D. Yang, Q. Jin, L. Zhang, M. Liu, *Adv. Mater.* **2016**, *28*, 1644-1649.

[74] W. Miao, S. Wang, M. Liu, *Adv. Funct. Mater.* **2017**, *27*, 1701368.

[75] G. Berkovic, V. Krongauz, V. Weiss, *Chem. Rev.* **2000**, *100*, 1741-1754.

[76] J. Sunamoto, K. Iwamoto, M. Akutagawa, M. Nagase, H. Kondo, *J. Am. Chem. Soc.* **1982**, *104*, 4904-4907.

[77] V. A. Barachevsky, *Review Journal of Chemistry* **2017**, *7*, 334-371.

[78] T. Stafforst, D. Hilvert, *Chem. Commun.* **2009**, 287-288.

[79] C. J. Roxburgh, P. G. Sammes, *Dyes Pigm.* **1995**, *27*, 63-69.

UNIVERSITAT ROVIRA I VIRGILI
STIMULI-RESPONSIVE HOST-GUEST SYSTEMS DECORATED WITH HEMITHIOINDIGO AND SPIROPYRAN UNITS
Giulia Moncelsi

General introduction

[80] J. T. C. Wojtyk, A. Wasey, N.-N. Xiao, P. M. Kazmaier, S. Hoz, C. Yu, R. P. Lemieux, E. Buncel, *J. Phys. Chem. A* **2007**, *111*, 2511-2516.

[81] L. Kortekaas, J. Chen, D. Jacquemin, W. R. Browne, *J. Phys. Chem. B* **2018**, *122*, 6423-6430.

[82] H. Görner, *Phys. Chem. Chem. Phys.* **2001**, *3*, 416-423.

[83] W. Tian, J. Tian, *Dyes Pigm.* **2014**, *105*, 66-74.

[84] M. Natali, S. Giordani, *Chem. Soc. Rev.* **2012**, *41*, 4010-4029.

[85] N. Shao, Y. Zhang, S. Cheung, R. Yang, W. Chan, T. Mo, K. Li, F. Liu, *Anal. Chem.* **2005**, *77*, 7294-7303.

[86] N. Shao, J. Y. Jin, S. M. Cheung, R. H. Yang, W. H. Chan, T. Mo, *Angew. Chem., Int. Ed.* **2006**, *45*, 4944-4948.

[87] M. Inouye, K. Kim, T. Kitao, *J. Am. Chem. Soc.* **1992**, *114*, 778-780.

[88] M. Takase, M. Inouye, *Chem. Commun.* **2001**, 2432-2433.

[89] N. Shao, J. Jin, H. Wang, J. Zheng, R. Yang, W. Chan, Z. Abliz, *J. Am. Chem. Soc.* **2010**, *132*, 725-736.

[90] G. Ercolani, *J. Am. Chem. Soc.* **2003**, *125*, 16097-16103.

[91] D. Hernández-Melo, J. Tiburcio, *Chem. Commun.* **2015**, *51*, 17564-17567.

[92] D. Hernández-Melo, R. Cervantes, J. Tiburcio, *J. Org. Chem.* **2017**, *82*, 4484-4488.

[93] P. Howlader, B. Mondal, P. C. Purba, E. Zangrando, P. S. Mukherjee, *J. Am. Chem. Soc.* **2018**, *140*, 7952-7960.

[94] D. Samanta, D. Galaktionova, J. Gemen, L. J. W. Shimon, Y. Diskin-Posner, L. Avram, P. Král, R. Klajn, *Nat. Commun.* **2018**, *9*, 641.

[95] T. Tamaki, M. Sakuragi, K. Ichimura, K. Aoki, I. Arima, *Polym. Bull.* **1990**, *24*, 559-564.

[96] S. Wan, Z. Ma, C. Chen, F. Li, F. Wang, X. Jia, W. Yang, M. Yin, *Adv. Funct. Mater.* **2016**, *26*, 353-364.

[97] Y. Sueishi, T. Nishimura, *J. Phys. Org. Chem.* **1995**, *8*, 335-340.

[98] J. W. Lee, S. Samal, N. Selvapalam, H.-J. Kim, K. Kim, *Acc. Chem. Res.* **2003**, *36*, 621-630.

[99] Z. Miskolczy, L. Biczók, *J. Phys. Chem. B* **2011**, *115*, 12577-12583.

[100] Z. Miskolczy, L. Biczók, *Photochem. Photobiol.* **2012**, *88*, 1461-1466.

[101] J. R. Nilsson, C. Parente Carvalho, S. Li, J. P. Da Silva, J. Andréasson, U. Pischel, *ChemPhysChem* **2012**, *13*, 3691-3699.

[102] Z. Miskolczy, L. Biczók, *J. Phys. Chem. B* **2013**, *117*, 648-653.

[103] C. L. D. Gibb, B. C. Gibb, *J. Am. Chem. Soc.* **2004**, *126*, 11408-11409.

[104] A. Mohan Raj, F. M. Raymo, V. Ramamurthy, *Org. Lett.* **2016**, *18*, 1566-1569.

[105] C. S. Santos, A. C. Miller, T. C. S. Pace, K. Morimitsu, C. Bohne, *Langmuir* **2014**, *30*, 11319-11328.

[106] R. T. F. Jukes, B. Bozic, F. Hartl, P. Belser, L. De Cola, *Inorg. Chem.* **2006**, *45*, 8326-8341.

[107] R. Kießwetter, N. Pustet, F. Brandl, A. Mannschreck, *Tetrahedron: Asymmetry* **1999**, *10*, 4677-4687.

[108] L. Wang, Q. Li, *Chem. Soc. Rev.* **2018**, *47*, 1044-1097.
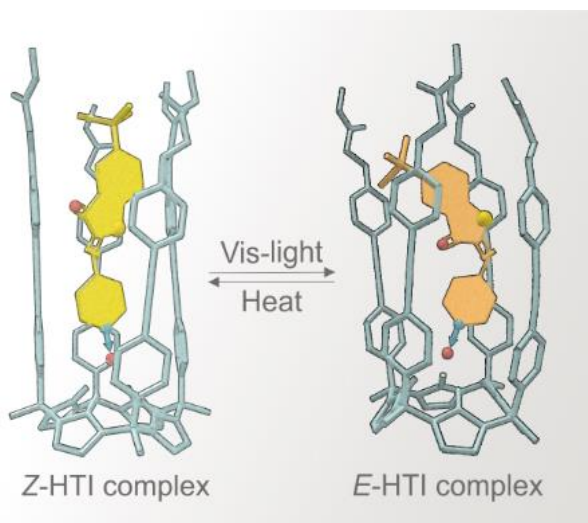
UNIVERSITAT ROVIRA I VIRGILI
STIMULI-RESPONSIVE HOST-GUEST SYSTEMS DECORATED WITH HEMITHIOINDIGO AND SPIROPYRAN UNITS
Giulia Moncelsi

Chapter 2

2-(4'-Pyridyl-*N*-oxide)-substituted hemithioindigos as photoresponsive guests for a super aryl-extended calix[4]pyrrole receptor
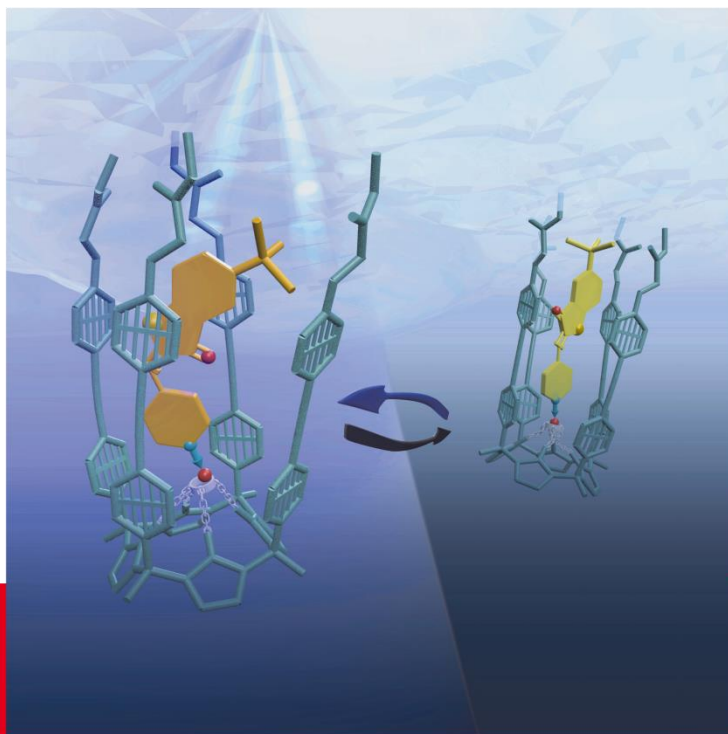

Part of this chapter has been published in:

CHEMISTRY
AN ASIANJOURNAL

www.chemasianj.org
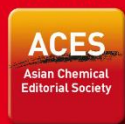
2-(4'-Pyridyl-N-oxide)-substituted hemithioindigos as photoresponsive guests for a super aryl-extended calix[4]pyrrole receptor

2.1 Introduction

The photocontrolled uptake and release of guest molecules from synthetic hosts relies on two strategies that share the use of appended photoswitchable units and differ in the selection of the binding partner (the host or the guest) to which they are covalently attached.[1] The isomerization of the photoswitch, induced by light or heat, modifies its shape, spectrum, size, polarity, hydrophobicity, and so on. In turn, these changes can be coupled to modulate the selectivity and affinity of the host–guest complex. Examples of unimolecular natural[2] and synthetic hosts[3,4] that bind photoresponsive guests have made extensive use of azobenzene groups as photochromic switches.[5,6,7] Likewise, photoresponsive guests containing azobenzene units have been employed for photocontrolled modulation of the binding affinity by using multicomponent host assemblies, that is, capsules[8] and cages.[9] Dube and Rebek introduced the *Z*/*E* photoinduced isomerization of hemithioindigo (HTI) derivatives to realize photocontrolled guest exchange in the encapsulation complexes of dimeric capsules derived from resorcinarene cavitands.[10] Irie and co-workers exploited the differences in binding ability exhibited by the *Z*/*E* isomers of 2-pyridyl-substituted HTIs with two Zn porphyrin receptors to control the shuttling of the former between the latter by using light irradiation.[11] The *Z*-to-*E* light-induced isomerization of HTI derivatives requires longer wavelengths ($\lambda =$ 410-430 nm) than the trans-to-cis photoisomerization of azobenzenes ($\lambda =$ 365 nm).[12] Remarkably, the *E*-HTI isomer can be reverted to the *Z* counterpart by subsequent irradiation at wavelengths > 500 nm or completely by thermal equilibration in the dark. The switching between the two states shows high efficiency and proceeds with little photofatigue. In recent years, HTI derivatives have been exploited as peptide modulators[13] and as prototypes of molecular logic gates,[14] machines,[15,16] and supramolecular receptors,[17,18] and their switching properties have been studied[19] and modulated[20] for possible applications at the bio-optical window ($\lambda =$ 650-900 nm). The tetra-α isomers of aryl- and super aryl-extended calix[4]pyrroles are known to form thermodynamically and kinetically stable 1:1 inclusion complexes with pyridyl-*N*-oxide derivatives. The association constant values determined for these inclusion complexes are in the range of 10^4 to $10^7 \, M^{-1}$.[21] The pyridyl-*N*-oxide is deeply included in the aromatic cavity and forms four convergent hydrogen bonds between the oxygen atom of the *N*-oxide and the pyrrole NHs of the receptor. Additional π-π and CH-π interactions are established between the two binding partners.

Chapter 2

In this chapter, we aimed at evaluating the affinity modulations experienced by super aryl-extended calix[4]pyrrole receptor **1** upon binding of photoresponsive pyridyl-*N*-oxides **2** and **3** containing an HTI molecular switch (Figure 2.1).
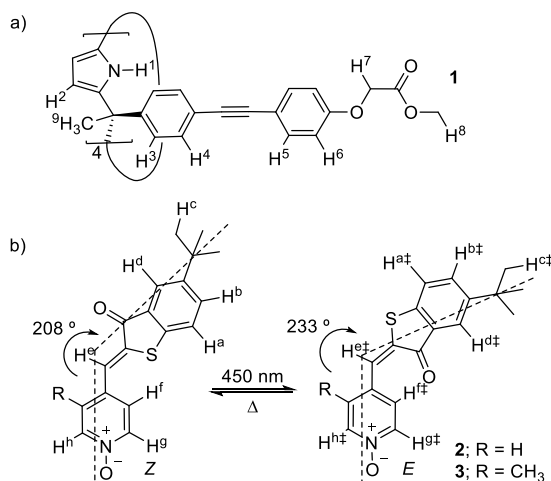
Figure 2.1 Molecular structures of a) super aryl-extended calix[4]pyrrole receptor **1** and b) 2-(4'-pyridyl-*N*-oxide)-substituted hemithioindigos **2** and **3**, *Z* (left) and *E* (right) isomers. In the case of **3**, the lower energy rotamers of the two isomers are shown. The values of the angles defined by the O, CH^e, and C(CH$_3$)$_3$ atoms are indicated in the *Z* and *E* isomers. The *E* isomer displays a pronounced bending of the pyridyl-*N*-oxide and the HTI unit, which suggests a less favorable fit in the cylindrical-shaped cavity of **1** in *cone* conformation (see text). Protons assigned to the *E* isomer are marked with a ‡ symbol.

We describe the synthesis of two 2-(4'-pyridyl-*N*-oxide)-substituted hemithioindigo derivatives. We study their photoresponsive behavior and probe the interaction of the *Z* isomers with super aryl-extended calix[4]pyrrole receptor **1** by using ^{1}H NMR spectroscopy. We investigate the photoisomerization processes induced by light irradiation of the formed inclusion complexes. Finally, we use isothermal titration calorimetry (ITC) experiments to assess the binding constants of the inclusion complexes formed by the *Z* and *E* isomers of the photoswitches with super aryl-extended calix[4]pyrrole **1** and quantify the binding affinity modulation exerted by the photoisomerization.

2-(4'-Pyridyl-N-oxide)-substituted hemithioindigos as photoresponsive guests for a super aryl-extended calix[4]pyrrole receptor

2.2 Results and discussion

2.2.1 Design and synthesis

The nucleophilic substitution reaction of 4-tert-butylbenzenethiol with 2-bromoacetic acid afforded aryl thioglycolic acid **4** in 69% yield.[22] The aryl acyl chloride formed "in situ" by reaction of **4** with thionyl chloride was cyclized under Friedel-Crafts acylation conditions to provide labile thioindoxyl **5**, which was used without further purification in condensation reactions with carboxaldehyde *N*-oxides **6** and **7**. Aldehyde **6** is commercially available. However, to the best of our knowledge, *N*-oxide **7** has not been previously described in the literature. Aldehyde derivative **7** was prepared in two synthetic steps starting from 3,4-lutidine. First, lutidine *N*-oxide **8** was isolated as white needles in 63% yield by using sodium perborate (PBS) in acetic acid as the oxidant.[23] Next, the *para*-methyl substituent of **8** was selectively oxidized by using SeO_2 to afford *N*-oxide **7** in 17% yield after purification of the reaction crude by column chromatography.[24] The reactions of thioindoxyl **5** with *N*-oxides **6** and **7** by using piperidine (PIP) as a base produced desired 2-(4'-pyridyl-*N*-oxide)-substituted HTI derivatives **2** and **3** as yellow powders in yields of 21 and 59%, respectively, after purification by column chromatography and trituration with ethyl acetate (see Scheme 2.1).
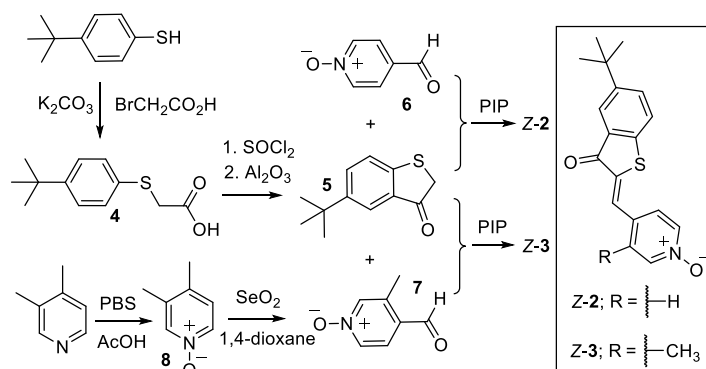
Scheme 2.1 Synthetic schemes for the preparation of hemithioindigo *N*-oxides *Z*-**2** and *Z*-**3**. The synthesis of the aldehyde *N*-oxide **8** is also shown. PIP = piperidine, PBS = sodium perborate tetrahydrate.

On the basis of ^{1}H NMR spectroscopy analyses of $CDCl_3$ solutions, the isolated solids of the HTI derivatives contained the thermodynamically stable *Z* isomers to an extent greater than 95%. The diagnostic vinylic proton (H^e) of the *Z*-HTI isomers is considerably downfield shifted with respect to the corresponding signal in the *E* isomers owing to the $+\delta$ anisotropy

Chapter 2

of the carbonyl group. On the contrary, the proton signal H^f resonates at lower chemical shift in the *Z* isomer with respect to the *E* counterpart; in this case, the anisotropic effect of the C=O oxygen atom towards H^f is more pronounced in the *E* isomer. These observations are in agreement with the assignment of the *Z/E* configuration of the isomers of hemithioindigos and related compounds prepared from the acid- or base-catalysed condensation with aromatic aldehydes (e.g. acetophenones, cyclohexanones, tetralones, flavanones, indanones and aurones) by simple ^{1}H NMR characterization.[25] Compounds **7**, *Z*-**2**, and *Z*-**3** were fully characterized by a complete set of high-resolution spectra (NMR and MS). In the case of HTI *Z*-**3**, the energy-minimized structures (MM3) returned a difference in energy of *ca*. 8 kcal·mol^{-1} for the two possible rotamers. Accordingly, it was possible to assign all the proton signals unambiguously and exclude one of the two rotamers of *Z*-**3** by using standard 2D NMR techniques. By means of NOE spectroscopy, we detected cross-peaks between the methyl proton H^i and protons H^h and H^e (Figure 2.2).
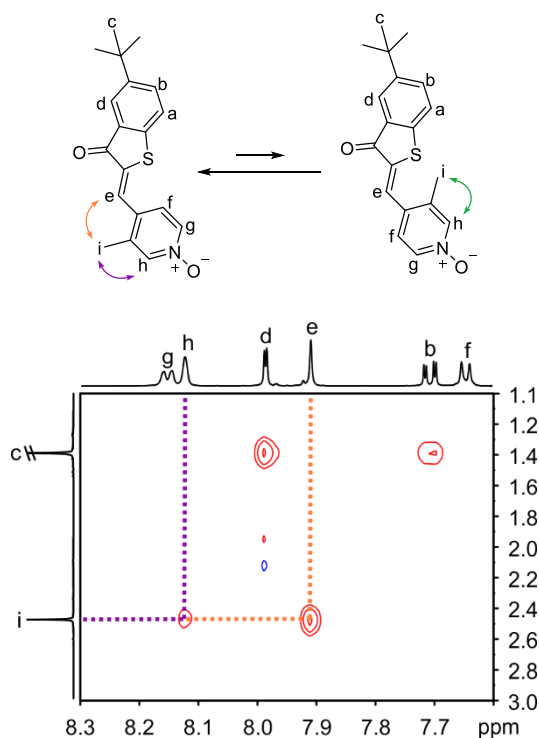
Figure 2.2 Selected region of the NOESY spectrum of HTI *Z*-**3** showing the diagnostic cross-peaks for the indicated protons.

60

2-(4'-Pyridyl-N-oxide)-substituted hemithioindigos as photoresponsive guests for a super aryl-extended calix[4]pyrrole receptor

Additionally, we obtained single crystals of *Z*-**3** suitable for X-ray diffraction analysis (Figure 2.3).
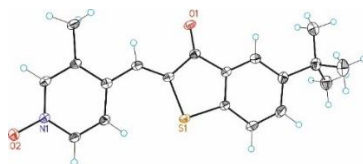
Figure 2.3 X-ray structure (ORTEP) of a single crystal of the *Z*-**3** isomer grown from a ACN:CHCl$_3$ 1:1 solution. Thermal ellipsoids are set at 50% probability.

In the solid state, the angle defined by the O, CH^e, and C(CH$_3$)$_3$ atoms of *Z*-**3** was 211°. This value is in good agreement with the one (208°) measured for its energy-minimized structure (MM3). Super aryl-extended calix[4]pyrrole **1** was synthesized using a procedure previously described by our group.[21]

2.2.2 Photoisomerization studies of hemithioindigos *Z*-**2** and *Z*-**3**

We monitored the photoisomerization process of HTI *N*-oxides *Z*-**2** and *Z*-**3** at micromolar concentration in chloroform solution by using UV/Vis absorption spectroscopy. We prepared a solution of **2** (30 µm) that mainly contained *Z*-**2**, and we acquired its UV/Vis absorption spectrum.
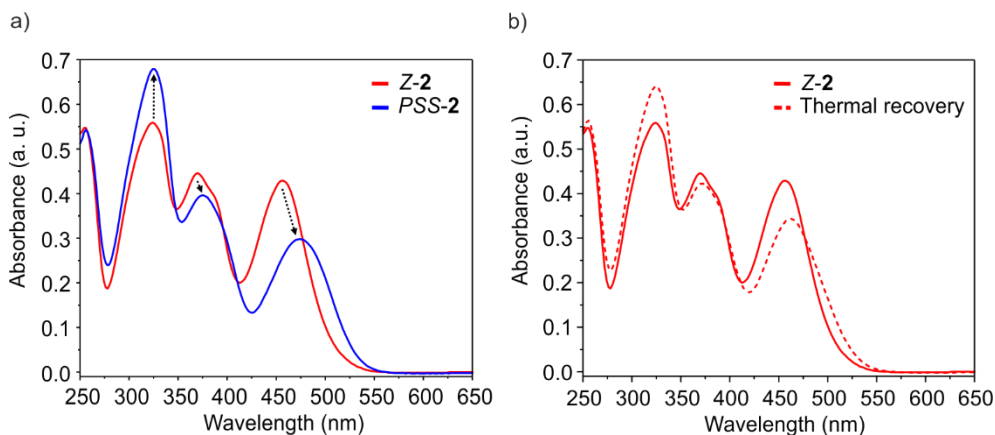
Figure 2.4 UV/Vis absorption spectra of chloroform solutions of **2** (30 µM): a) as the *Z* isomer (red), at the PSS after photoirradiation at λ = 450 nm for 30 s (blue) and b) as the *Z* isomer (red solid) and after thermal re-equilibration (red dashed).

Chapter 2

The absorption spectrum of *Z*-**2** showed three bands of similar intensity with maxima centered at λ = 324, 369 and 457 nm, respectively. Then, the same solution was photoirradiated at λ = 450 nm, and we recorded the UV/Vis spectra at different irradiation times. The photoirradiation process caused noticeable changes in the absorption bands of **2**. After 30 s of irradiation, the absorption spectrum remained unaltered, which indicated that the photostationary state (PSS) was reached. At the PSS, the high-energy band centered at λ = 324 nm increased in intensity. In contrast, the band appearing at λ = 369 nm displayed a decreased intensity, and a bathochromic shift (Δλ = +5 nm) was observed. The lower energy band with a maximum at λ = 457 nm was redshifted (Δλ = +17 nm) and was also diminished in intensity (Figure 2.4a). It is known that the absorption spectra of the *E* isomers of most HTIs are moderately bathochromically shifted relative to those of the *Z* isomers.[12] Consequently, the observed spectral changes are in agreement with an increase in the concentration of the *E*-**2** isomer in solution and support the *Z*-to-*E* photoisomerization process. An analogous photoirradiation experiment was performed with a freshly prepared solution (30 μM) of HTI *N*-oxide *Z*-**3**. The initial absorption spectrum of *Z*-**3** was almost identical to the one registered for *Z*-**2** (three bands centered at λ = 308, 370, and 460 nm). The chloroform solution was irradiated with λ = 450 nm light, and the PSS was reached within 30 s. The resulting UV/Vis spectrum of the solution showed the same earmarks for the *Z*-to-*E* photoisomerization of the HTI switch. Afterwards, the chloroform solutions of **2** and **3** at the PSSs were thermally equilibrated in the dark at 40 ºC for 12 h. The UV/Vis spectra of the equilibrated HTI *N*-oxide solutions were similar to the ones acquired for the *Z* isomers. All together, these results established that 1) *N*-oxides **2** and **3** are clearly responsive to light stimuli; 2) light irradiation at a wavelength of 450 nm induces the PSSs, in which the *E* isomer is the major component; 3) the *Z*-to-*E* photoisomerization process can be thermally reversed to a limited extent. The short times required to achieve the PSSs in the performed photoisomerization experiments are a direct consequence of the employed highly diluted conditions (30 μM) (see below). We also studied the photoisomerization process of both HTI *N*-oxides in millimolar chloroform solution by using ^{1}H NMR spectroscopy. Separate thermally equilibrated solutions of *Z*-**2** and *Z*-**3** (6-7 mM) were photoirradiated at λ = 450 nm. The solutions reached the PSSs after 7-10 min, as evidenced by the fact that the ^{1}H NMR spectra remained unchanged after this period of time. The mixture of HTI isomers at the PSSs showed *E*/*Z* compositions of 80:20 and 85:15 for **2** (Figure 2.5) and **3**, respectively. Most likely, the larger concentrations used in the ^{1}H NMR experiments are responsible for the

2-(4'-Pyridyl-N-oxide)-substituted hemithioindigos as photoresponsive guests for a super aryl-extended calix[4]pyrrole receptor

longer irradiation times required to achieve the PSSs in comparison to the analogous UV/Vis experiments.
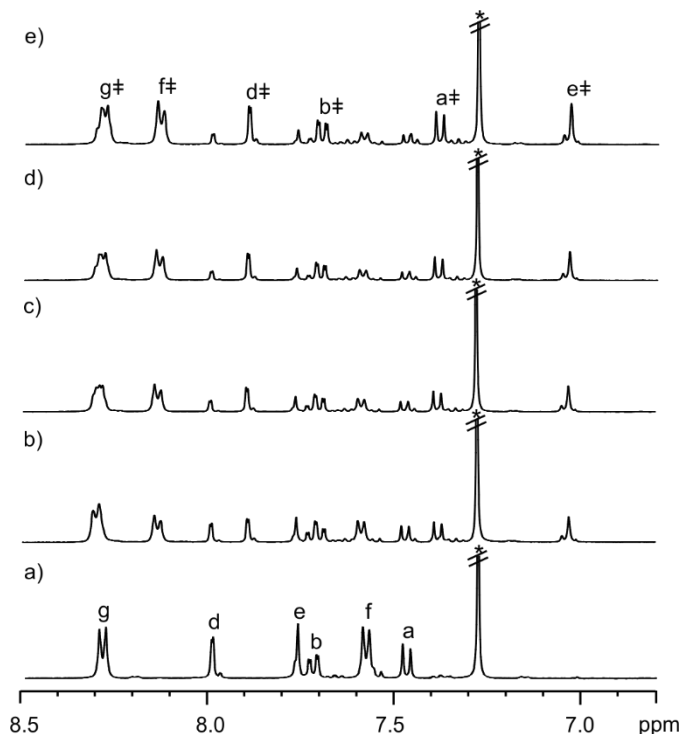
Figure 2.5 Selected region of the ^{1}H NMR spectra (400 MHz, CDCl$_3$, 298 K) recorded during photoirradiation at $\lambda = 450$ nm of a 6.5 mM solution of *Z*-**2** for a) 0, b) 3 min, c) 5 min, d) 7 min, and e) 10 min, reaching the PSS after 7 min with a final *Z/E* ratio of 20:80. Protons assigned to the *E*-**2** isomer are marked with a ‡ symbol. * Residual solvent signals.

2.2.3 Binding studies of hemithioindigos *Z*-**2** and *Z*-**3** with super aryl-extended calix[4]pyrrole **1**

We probed the interaction of HTI *N*-oxide *Z*-**2** with super aryl-extended calix[4]pyrrole **1** by using ^{1}H NMR titration experiments. The ^{1}H NMR spectrum of super aryl-extended **1** in CDCl$_3$ solution (3.5 mM) is in agreement with a C$_{4v}$ symmetry (Figure 2.6a). However, the NH and *β*-pyrrole proton signals are somewhat broadened, which suggests that **1** is involved in a dynamic equilibrium between conformers. The addition of 0.4 equiv. of HTI *Z*-**2** to the millimolar solution of **1** produced the appearance of a new set of signals that were assigned to the protons of bound **1** (Figure 2.6b). Significantly, the pyrrole NH protons (H$^{1'}$) of bound **1** appeared highly downfield shifted ($\delta = 9.8$ ppm, $\Delta\delta = +2.1$ ppm), which suggested their

Chapter 2

involvement in hydrogen-bonding interactions with the oxygen atom of the *N*-oxide. The *β*-pyrrole protons (H$^{2'}$) in bound **1** also moved downfield (Δδ = +0.3 ppm), and the four signals of its aromatic protons shifted upfield. The binding of *N* oxide *Z*-**2** locked receptor **1** in the *cone* conformation. As the amount of HTI *Z*-**2** increased, the new set of signals of bound **1** grew at the expense of those of free **1**. In the presence of 1 equiv. of *Z*-**2**, only the set of signals assigned to the protons of bound **1** was observed (Figure 2.6c).
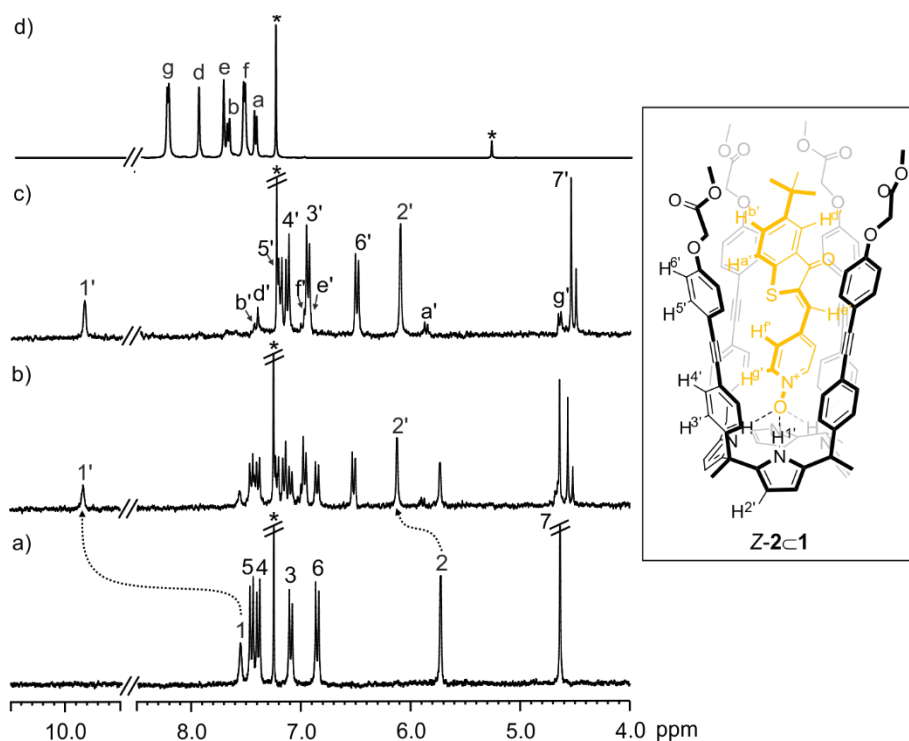
Figure 2.6 Selected region of the ^{1}H NMR spectra (300 MHz, CDCl$_3$, 298 K) acquired during titration of tetraester calix[4]pyrrole **1** with *Z*-**2**: a) **1**, b) **1** + 0.4 molar equiv. of *Z*-**2**, c) **1** + 1 molar equiv. of *Z*-**2**, and d) *Z*-**2**. Primed letters and numbers correspond to the proton signals of bound components. * Residual solvents signals.

Taken together, these results indicated that *Z*-**2** and **1** formed a 1:1 inclusion complex, *Z*-**2**⊂**1**, that was kinetically stable on the chemical shift timescale and for which a binding constant larger than 10^4 M^{-1} could be estimated. All proton signals of *Z*-**2** in the *Z*-**2**⊂**1** complex were upfield shifted relative to those of *Z*-**2** free in solution. The largest upfield shift was experienced by the *N*-oxide pyridyl protons α to the nitrogen atom, H$^{g''}$ (Δδ = -3.67 ppm). These observations support the deep inclusion of *Z*-**2** in the aromatic cavity defined by

2-(4'-Pyridyl-N-oxide)-substituted hemithioindigos as photoresponsive guests for a super aryl-extended calix[4]pyrrole receptor

the *meso*-aryl substituents of receptor **1** in the *cone* conformation. The inclusion is mainly driven by the formation of four simultaneous hydrogen bonds between the pyrrole NHs of **1** and the *N*-oxide oxygen atom of *Z*-**2**. We also probed the interaction of HTI *N*-oxide *Z*-**3** with calix[4]pyrrole **1** by using ^{1}H NMR titration experiments in CDCl$_3$ solution. The obtained results were completely analogous to the ones described above for the *Z*-**2** counterpart. Notably, the two chemically nonequivalent protons α to the nitrogen atom of included pyridyl-*N*-oxide *Z*-**3** (H$^{g''}$ and H$^{h'}$) experienced similar upfield shifts, $\Delta\delta$ = -3.6 and -3.1 ppm, respectively. Moreover, the magnitude of the upfield shifts is in agreement with the one experienced for the analogous protons of *Z*-**2**. This result supports similar binding geometries for the *Z*-**2**⊂**1** and *Z*-**3**⊂**1** inclusion complexes.

2.2.4 Light-irradiation experiments of the inclusion complexes

As discussed above, an equimolar mixture of *Z*-**2** and super aryl-extended **1**, at millimolar concentration, afforded the quantitative formation of the *Z*-**2**⊂**1** complex. The resulting CDCl$_3$ solution was photoirradiated with λ = 450 nm light and was analyzed at different time intervals by using ^{1}H NMR spectroscopy (Figure 2.7). After 10 min of irradiation, the ^{1}H NMR spectrum of the solution showed the diagnostic signals of the initial *Z*-**2**⊂**1** complex together with a new set of signals that were assigned to the protons of the *E*-**2**⊂**1** complex (Figure 2.7b). The complexes of the *E* and *Z* isomer of **2** could be easily identified, in the region of the NHs, as two separate singlets resonating at δ = 9.9 and 9.8 ppm, respectively. Further irradiation (20 and 40 min) induced an increase in the NH signal corresponding to the *E*-**2**⊂**1** complex (δ = 9.9 ppm) at the expense of the signals assigned to the *Z*-**2**⊂**1** counterpart (Figure 2.7c-d). After 60 min of irradiation, the ^{1}H NMR spectra of the solution remained unchanged, which indicated that the PSS was reached (Figure 2.7e).[26] Remarkably, the PSS of the mixture of inclusion complexes **2**⊂**1** was reached after 1 h of photoirradiation. The times required for free HTI **2** and the **2**⊂**1** complex to reach the PSS were significantly different, 7 min and 1 h, respectively. The intensity of the absorbance at λ = 450 nm in the UV/Vis absorption spectrum of the **2**⊂**1** complex is drastically reduced relative to that of free **2** (*vide infra*). This observation supports the finding that photoirradiation at this wavelength is less efficient in the case of the inclusion complex, and thus, longer irradiation times are required to achieve the PSS. At the PSS, the composition of the mixture of isomeric complexes *E*-**2**⊂**1**:*Z*-**2**⊂**1** was determined as approximately 75:25. This value is in good

Chapter 2

agreement with the 80:20 mixture of HTI isomers obtained at the PSS ($\lambda = 450$ nm) for free **2**. We did not observe any of the expected proton signals for either free receptor **1** or free HTI *N*-oxide *E*-**2**.
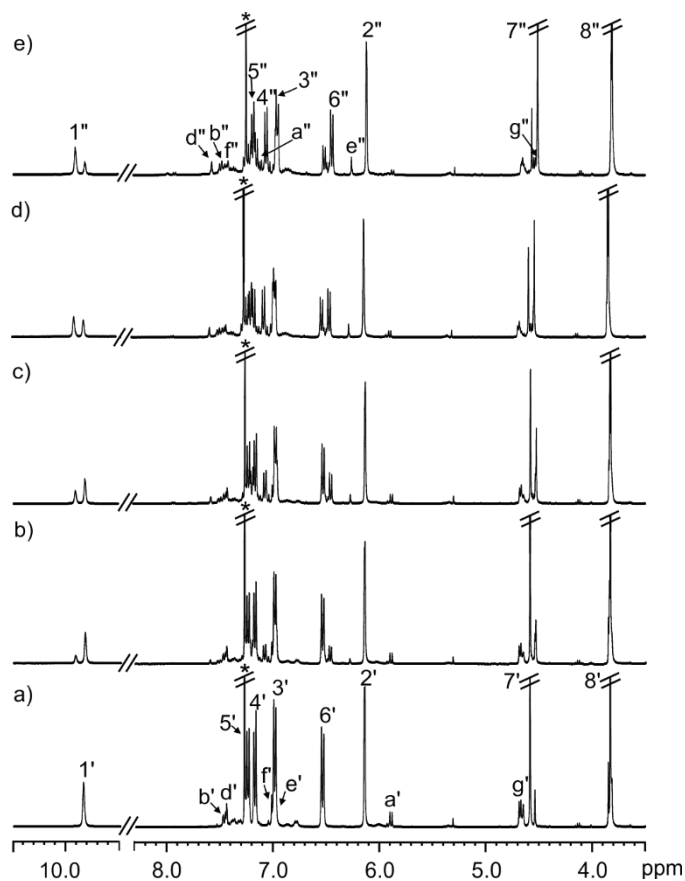
Figure 2.7 Selected region of the ^{1}H NMR spectra (400 MHz, CDCl$_3$, 298 K) acquired during photoirradiation at $\lambda = 450$ nm of the 1:1 *Z*-**2**⊂**1** complex for a) 0, b) 10, c) 20, d) 40, and e) 60 min. Primed letters and numbers correspond to the proton signals of the bound components of *Z*-**2**⊂**1**. Double primed letters and numbers correspond to the proton signals of irradiated bound components of *E*-**2**⊂**1**. * Residual solvent signals.

All together, these results show that the inclusion of the HTI *N*-oxide has little effect on the isomerization level of the molecular photoswitch and that its *E*-form is also bound by **1** with a stability constant larger than 10^4 M^{-1}. In short, at millimolar concentration, the *Z*-to-*E* photoisomerization of the bound guest did not modulate the binding constant of the resulting *E*-**2**⊂**1** inclusion complex at a level suitable to induce its dissociation. Thermal equilibration in the dark at 55 °C for 12 h of the mixture of isomeric complexes afforded a final composition

2-(4'-Pyridyl-N-oxide)-substituted hemithioindigos as photoresponsive guests for a super aryl-extended calix[4]pyrrole receptor

of approximately 5:95 E-$\mathbf{2}\subset\mathbf{1}$/$Z$-$\mathbf{2}\subset\mathbf{1}$, which is in agreement with the composition of free HTI $\mathbf{2}$ after thermal equilibration. Analogous results were obtained in the irradiation experiments performed with the Z-$\mathbf{3}\subset\mathbf{1}$ complex. Photoisomerization at $\lambda = 450$ nm produced an approximately 75:25 ratio of the E-$\mathbf{3}\subset\mathbf{1}$/$Z$-$\mathbf{3}\subset\mathbf{1}$ complexes, a value that is also in line with the photoisomerization level obtained for free Z-$\mathbf{3}$. As observed above for Z-$\mathbf{2}$, the inclusion of Z-$\mathbf{3}$ in calix[4]pyrrole receptor $\mathbf{1}$ does not affect the PSS composition significantly. To characterize the kinetic stability of the Z-$\mathbf{3}\subset\mathbf{1}$ complex, we determined its rate dissociation constant value as $k_{-1} = 1.8$ s^{-1} by using EXSY NMR experiments (entry 2 in Table 2.1).

Complex	k (s^{-1})	$\Delta G^{\ddagger}$ (kcal·mol^{-1})	k_{-1} (s^{-1})	$\Delta G^{\ddagger}_{-1}$ (kcal·mol^{-1})	k_1 (M^{-1}s^{-1})
Z-$\mathbf{2}\subset\mathbf{1}$	1.36	17.25	0.68	17.67	3.69×10^6
Z-$\mathbf{3}\subset\mathbf{1}$	1.84	17.07	0.92	17.48	4.83×10^6

Table 2.1 Magnetization rate constants (k), energy barriers of the magnetization exchange ($\Delta G^{\ddagger}$), magnetization rate constants and chemical exchange rate constants of the dissociation process ($k_{-1}' = k_{-1}$) and the energy barriers of dissociation ($\Delta G^{\ddagger}_{-1}$) for the complexes Z-$\mathbf{2}\subset\mathbf{1}$ and Z-$\mathbf{3}\subset\mathbf{1}$. Data obtained from 2D ^{1}H-EXSY experiments ($t_{mix} = 0.3$ s). Rate constants for the formation of both complexes (k_1) determined from K_a (ITC titrations) and k_{-1} (2D ^{1}H EXSY experiments).

This dissociation rate constant translates into an energy dissociation barrier of approximately 18 kcal·mol^{-1} at 298 K,[27] which is in complete agreement with the observed slow chemical exchange between the free and bound components. Using ^{1}H NMR spectroscopy, we also monitored the thermal E-to-Z isomerization processes at 25 ºC. First, separate CDCl$_3$ solutions of the free guests, $\mathbf{2}$ and $\mathbf{3}$, and their inclusion complexes, $\mathbf{2}\subset\mathbf{1}$ and $\mathbf{3}\subset\mathbf{1}$, at millimolar concentrations, were irradiated at $\lambda = 450$ nm in NMR tubes until the PSSs were reached (10 or 45 min for the free and the bound species, respectively). Immediately, the NMR tubes were introduced into the spectrometer probe previously thermostated at 25 ºC. Multiple ^{1}H NMR spectra of the evolving mixtures of stereoisomers were acquired every 5 min for the free guest and every 30 min for their inclusion complexes.

Compound	k (h^{-1})	$t_{1/2}$ (h)	$\Delta G^{\ddagger}$ (kcal·mol^{-1})
$\mathbf{2}$	0.50	1.38	22.69
$\mathbf{2}\subset\mathbf{1}$	0.16	4.33	23.36
$\mathbf{3}$	0.33	2.10	22.94
$\mathbf{3}\subset\mathbf{1}$	0.14	4.95	23.44

Table 2.2 Kinetic parameters (k, $t_{1/2}$ and $\Delta G^{\ddagger}$) of the E-to-Z isomerizations at RT of free and bound $\mathbf{2}$ and $\mathbf{3}$ obtained from the fit of the data to a first-order kinetic equation.

Chapter 2

The *E*-to-*Z* compositions of the mixtures were determined from the integral values of selected proton signals assigned to the respective isomers. The data obtained by monitoring the increase in concentration for the *Z* isomer, as well as the decrease in the *E* counterpart, were plotted versus time and fit to a first-order kinetic equation in all cases (Table 2.2). Remarkably, the half-lives for the thermally induced isomerization reactions of the free HTI guests were approximately three times shorter than those of the bound counterparts (1.5 vs. 4.5 h). These results indicate that the thermal *E*-to-*Z* isomerization of the HTIs is also affected by the inclusion in **1**. We calculated that the free-energy barriers for the isomerization processes are of the order of approximately 23 kcal·mol^{-1}. This magnitude corresponds to the lower range of values measured for related processes. It is known that the electron-donor or electron-acceptor nature of the *para* substituent at the stilbene fragment of HTIs has an effect on the *Z*-to-*E* photoisomerization and *E*-to-*Z* thermal isomerization rates.[12] The effect is more noticeable for the latter process, in which an increase in the electron-donor nature of the substituent promotes a faster thermal *E*-to-*Z* isomerization reaction.
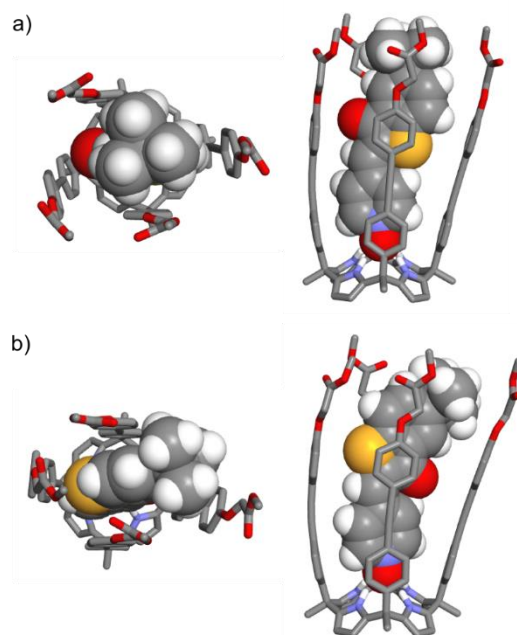

Figure 2.8 Energy-minimized structures (MM3) of the inclusion complexes (top and side view) of a) *Z*-**2**⊂**1** and b) *E*-**2**⊂**1**. Included guest molecules are shown as CPK models and receptor **1** is depicted in stick representation. Non-polar hydrogen atoms of **1** are omitted for clarity.

2-(4'-Pyridyl-N-oxide)-substituted hemithioindigos as photoresponsive guests for a super aryl-extended calix[4]pyrrole receptor

Surprisingly, the pyridyl *N*-oxide HTIs reported in this work show thermal isomerization rates that are similar to those of stilbene derivatives bearing a strong electron-donor dimethylamino *para* substituent ($\sigma+ = -1.7$).[28] The two inclusion complexes are stabilized by four simultaneous hydrogen bonds established between the *N*-oxide oxygen atom of the HTI and the pyrrole NHs of the calix[4]pyrrole unit. We surmise that the involvement of the *N*-oxide unit in hydrogen-bonding interactions might be responsible for the observed increase in the half-life for the thermal photoisomerization reactions of the inclusion complexes compared to those of the free guests. Simple molecular modeling studies (MM3) of the inclusion complexes, *Z*-**2**⊂**1** and *E*-**2**⊂**1**, show that bound HTI **2** isomers are somewhat shape, size, and function complementary to the aromatic polar cavity of **1** (Figure 2.8). This binding motif induces receptor **1** to adopt the *cone* conformation. In addition, multiple CH-π and π-π interactions take place between the aromatic rings of included HTI **2** and the four *meso*-aromatic substituents of **1**.[29,30] The linear shape of *Z*-**2** provides a better complementary to the deep and cylindrical aromatic cavity defined by the *meso*-aryl substituent of **1** in *cone* conformation. Upon complex formation, the bent shape of the *E*-**2** isomer provokes significant flexing in the aryl-extended aromatic walls of receptor **1**. This is mainly due to maximization of CH-π and π-π interactions. Likewise, the shape complementarity between the host and the guest in the *E*-**3**⊂**2** complex is reduced relative to that in the *Z*-**3**⊂**2** analogue. In contrast, π-sulfur interactions seem to be favored for the *E*-**3**⊂**2** complex. These types of interactions are observed in the crystal structures of folded proteins. They are established between methionine or cysteine residues and aromatic side chains of neighboring amino acids.[31,32,33] All in all, the calculated energy difference for the two isomeric complex is approximately 3 kcal·mol^{-1}, in favor of the *Z*-**3**⊂**2** complex, which is the one including the thermodynamically stable *Z*-**3** isomer of the HTI derivative.

2.2.5 Determination of accurate association constant values for the inclusion complexes

We performed a series of isothermal titration calorimetry (ITC) experiments to assess the modulation of thermodynamic stability experienced by the inclusion complexes of **1** as a function of the included photoisomer of **2** and **3**. The ^{1}H NMR binding studies discussed above indicated that the four possible 1:1 isomeric inclusion complexes featured association constant values larger than 10^4 M^{-1}. First, we determined the thermodynamic parameters for the formation of the 1:1 complexes of **1** with the thermodynamically stable *Z*-form of the two

Chapter 2

photoswitches. We also performed UV/Vis titrations of the *Z*-**2**/**3** isomers with incremental amounts of calix[4]pyrrole **1** in order to determine the association constants for the 1:1 inclusion complexes based on the changes in the absorption profiles. Small aliquots of a solution of receptor **1** (1.4-1.7 mM) were added to a 30 µM solution of compound *Z*-**2** (Figure 2.9) or *Z*-**3** in the same solvent. The UV/Vis spectra were acquired after the addition of each aliquot. The titration data were fit to a simple 1:1 binding model at the wavelength corresponding to the maximum of absorbance of the lower-energy band of the inclusion complexes (*ca*. 470 nm) using the *HypSpec* module.
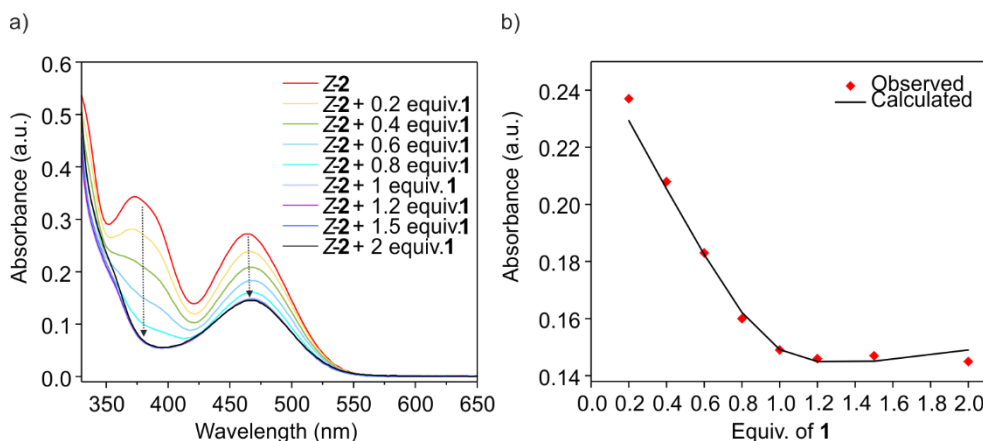

Figure 2.9 a) UV/Vis absorption spectra acquired during the titration of a 30 µM CHCl$_3$ solution of HTI *N*-oxide *Z*-**2** with super aryl-extended calix[4]pyrrole **1** and b) observed (red) and calculated (black line) absorbances at 470 nm plotted against the equivalents of **1**.

Because saturation was achieved after the addition of 1 equiv. of the host to the solution of the guest, the data were only useful to determine the 1:1 stoichiometry of the complexes and to estimate that their binding constants are larger than 10^6 M^{-1}. An accurate assessment of the binding constants of the two complexes *Z*-**2**/**3**⊂**1** would require working at concentrations that are too diluted for UV/Vis spectroscopy titrations. Accordingly, we determined the corresponding values using ITC titration experiments. The timed injection of incremental aliquots (15-20 µl) of chloroform solutions of *Z*-**2** (Figure 2.10a) or *Z*-**3** by using a computer-controlled microsyringe to a solution of super aryl-extended **1** in the same solvent produced the release of heat pulses. Next, we performed analogous ITC experiments by charging the syringe with diluted chloroform solutions of mixtures of HTIs isomers obtained by irradiating photoswitches **2** (Figure 2.10b) and **3** with λ = 450 nm light until their PSSs were achieved.

2-(4'-Pyridyl-N-oxide)-substituted hemithioindigos as photoresponsive guests for a super aryl-extended calix[4]pyrrole receptor

In all cases, the concentration of guest solutions (0.72-0.76 mM) was *ca*. 9 times the concentration of the calix[4]pyrrole (0.07-0.08 mM).
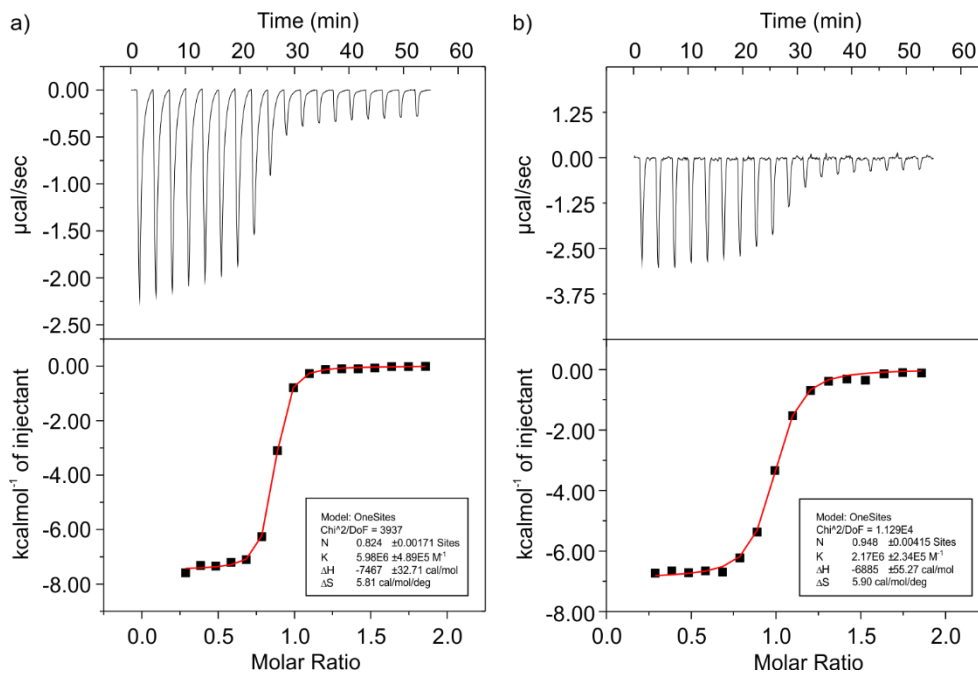

Figure 2.10 Top - Trace shows raw data for one set of experiments for the titration of the guest into the host: a) Z-**2**⊂**1** and b) E-**2**⊂**1**. Titration was performed at 25 °C in chloroform by timed injection of 15 µl of guest solution into the host solution. Bottom - Binding isotherm of the calorimetric titration shown on top. The enthalpy of binding for each injection is plotted against the molar ratio of host:guest in the cell. The continuous line represents the least-squares-fit of the data to a single-site binding model.

The photoisomerization levels were analyzed by using ^{1}H NMR spectroscopy before and after performing the ITC experiments. For the ITC titration of isomers E-**2** and E-**3** with **1**, control NMR experiments were conducted on the same sample, before and after irradiation to the PSS: a 3 mM solution of Z-**2** or Z-**3** in CDCl₃ was placed in a NMR tube and irradiated with a LED source at 450 nm for 10 min. NMR spectra showed a 15:85 E-**2**:Z-**2** or a 80:20 E-**3**:Z-**3** ratio, in accordance with expected values for the PSS. Then, aliquots were taken from the irradiated solutions and diluted for use in the ITC experiments. To assess the ratio of E/Z isomers after completion of an ITC experiment, we titrated a PSS-photoirradiated CDCl₃ solution of HTI **2** (80:20) with receptor **1** (reverse ITC experiment). An aliquot of the solution in the calorimeter cell was analyzed by using NMR spectroscopy immediately after finishing the experiment (~ 1 h). The ^{1}H NMR spectrum of the mixture showed that the

Chapter 2

composition of the E-$2 \subset 1$ and Z-$2 \subset 1$ complexes was close to the initial 80:20 ratio. As discussed above, the E isomers were present in the photoisomerized mixtures at approximately 80%. This result indicated that by the end of the ITC experiment the isomeric thermal equilibration did not evolve to a significant extent. The integrated and normalized data of all titrations provided sigmoidal binding isotherms with inflection points centered at a guest:host molar ratio equal to 1. The experimental binding isotherm showed very good fits to the "one set of sites" binding model implemented in the *Microcal* analysis software. The thermodynamic parameters determined from the fits (K_a, ΔH) are summarized in Table 2.3 together with those calculated from them (ΔG and $T\Delta S$). Because the thermodynamic values of the binding constants derived from the ITC experiments performed with the mixtures of photoisomers (entries 2 and 5 in Table 2.3) are weighted averages of the two inclusion complexes that are formed, we consider them as maximum estimates for the inclusion complexes of the E isomers.

Complex[a]	$K_a/10^{6[a]}$	ΔH[b]	$T\Delta S$[c]	ΔG[c]
Z-$2 \subset 1$	5.4 ± 0.5	-8.1 ± 0.6	1.1 ± 0.6	-9.2 ± 0.1
Z-$2 \subset 1$/E-$2 \subset 1$	2.6 ± 0.4	-6.8 ± 0.1	1.9 ± 0.1	-8.7 ± 0.1
E-$2 \subset 1$[d]	1.9 ± 0.5			
Z-$3 \subset 1$	5.2 ± 0.7	-11.6 ± 0.3	-2.4 ± 0.3	-9.2 ± 0.1
Z-$3 \subset 1$/E-$3 \subset 1$	2.9 ± 1.0	-10.1 ± 1.4	-1.3 ± 1.4	-8.8 ± 0.2
E-$3 \subset 1$[d]	2.3 ± 1.2			

[a] M^{-1}. [b] kcal·mol^{-1}. [c] kcal·mol^{-1} at 298 K. [d] Values calculated using equation (1).

Table 2.3 Thermodynamic constant values (K_a, ΔH, $T\Delta S$ and ΔG) determined for the complexation of HTIs Z-**2** and Z-**3** and the photoisomerized mixtures at the PSS (450 nm) with receptor **1** in chloroform solutions. All values represent the average of at least two ITC titration experiments. Errors in K_a and ΔH are reported as standard deviations.

Using Equation (1), we determined more accurate stability constant values for the E inclusion complexes (entries 3 and 6 in Table 2.3):

$$K_{a(E \subset 1)} = [K_{a(Z \subset 1/E \subset 1)} - \chi_{Z \subset 1} \cdot K_{a(Z \subset 1)}]/ \chi_{E \subset 1} \qquad (1)$$

in which $\chi_{Z \subset 1}$ and $\chi_{E \subset 1}$ are the molar fractions of the two complexes and $K_{a(Z \subset 1/E \subset 1)}$ is the stability constant as derived from the fits of the titrations with the mixtures of photoisomers. Thus, the calculated stability constant values are $K_{a[E-2 \subset 1]} = (1.9 \pm 0.5) \times 10^6$ M^{-1} and $K_{a[E-3 \subset 1]} = (2.3 \pm 1.2) \times 10^6$ M^{-1}. Several conclusions can be drawn from the tabulated and calculated data. First, the formation of all inclusion complexes is mainly enthalpically driven. Second, entropy favors the formation of the complexes with HTI **2** but opposes the formation of the

2-(4'-Pyridyl-N-oxide)-substituted hemithioindigos as photoresponsive guests for a super aryl-extended calix[4]pyrrole receptor

complexes with HTI **3**. We assign this dissimilar behavior mainly to different solvation/desolvation processes of the HTI. Third, enthalpy-entropy compensation effects[34] are also evident in the studied binding processes. The fact that the binding constant values for the pair of complexes *Z*-**2**/*Z*-**3** and *E*-**2**/*E*-**3** with receptor **1** are very similar indicates that the presence of the methyl group in the *meta* position of the pyridyl-*N*-oxide residue of **3** does not impact the thermodynamic stability of the inclusion complexes. Remarkably, the *Z*-to-*E* photoisomerization of the HTI guests produces a very small reduction in the binding constant value (2.2-2.8-fold), which corresponds to a free-energy difference of approximately 0.5-0.6 kcal·mol⁻¹. This value is significantly smaller than the 3 kcal·mol⁻¹ estimated from the molecular modeling studies (MM3). We attribute the experimentally measured decrease in binding affinity to the fewer CH-π and π-π interactions in the *E*-HTI⊂**1** complexes with respect to the *Z*-HTI⊂**1** counterparts and to the worst fit of shapes between the host and guest.

2.2.6 Binding and photoisomerization studies of **1** with tetramethylammonium 4-(phenylazo)benzoate **9**

We probed the interaction of receptor **1** with tetramethylammonium 4-(phenylazo)benzoate (**9**) (Figure 2.11), an azobenzene derivative in order to assess the modulation of its binding affinity.
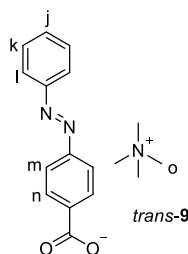

Figure 2.11 Molecular structure of tetramethylammonium 4-(phenylazo)benzoate **9** in the *trans* conformation.

In principle, the *trans*-to-*cis* photoisomerization produces a more dramatic conformational change between the two isomers with respect to the hemithioindigo fragment. Initially, a millimolar solution of **9** in CDCl₃ was thermally equilibrated at 60 ºC in the dark overnight (Figure 2.12a). The irradiation (λ = 365 nm) of the *trans*-**9** isomer produced a mixture enriched in the *cis*-**9** counterpart after 30 min, with a final *trans*:*cis* ratio of 15:85 at the PSS (Figure 2.12c). A small amount of unknown compound could be observed in the freshly

Chapter 2

dissolved sample and throughout the experiment: it was attributed to a decomposition product of **9** in this solvent.

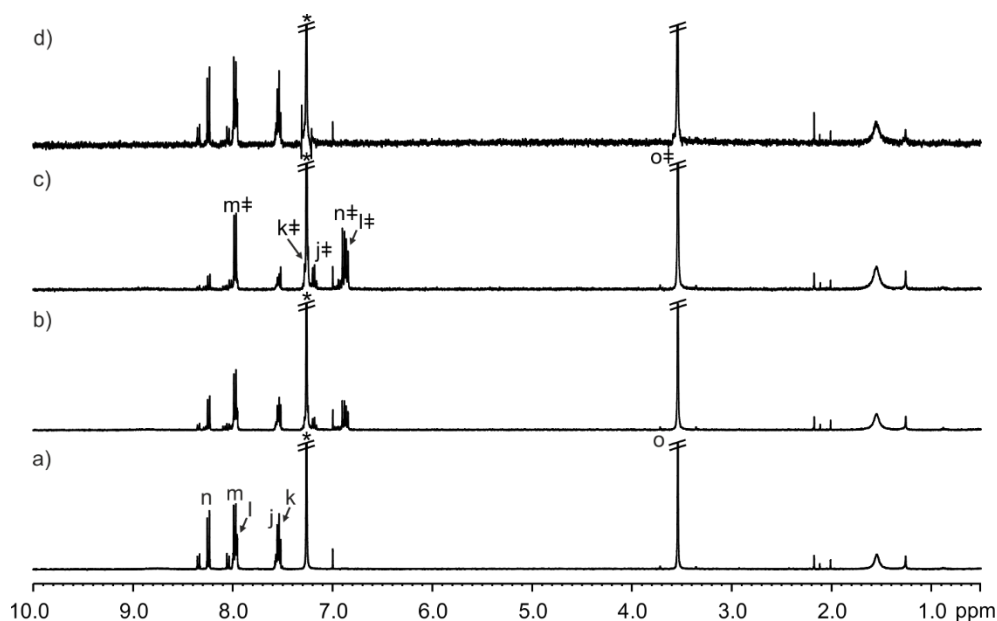**Figure 2.12** ^{1}H NMR spectra (400 MHz, CDCl₃, 298 K) recorded during photoirradiation at λ = 365 nm of a 1.6 mM solution of *trans*-**9** for a) 0, b) 10 min, and c) 30 min, reaching the PSS after 30 min with a final *trans*:*cis* ratio of 15:85. d) Thermally equilibrated sample at 60 ºC in the dark overnight. Protons assigned to the *cis*-**9** isomer are marked with a ‡ symbol. * Residual solvent signals.

A ^{1}H NMR titration experiment was performed by the addition of incremental amounts of *trans*-**9** to a CD₂Cl₂ solution of receptor **1** (Figure 2.13). Upon addition of 1 molar equiv. of the guest to the solution of the host, we observed the diagnostic proton peaks of the bound host and guest indicating the formation of the *trans*-**9**⊂**1** complex, for which a binding constant larger than 10^4 M⁻¹ could be estimated. In this solvent, the decomposition product of **9** was not detected. Afterwards, the *trans*-**9**⊂**1** complex was photoirradiated at 365 nm until the PSS was reached (15 min). The irradiation provoked the formation of the inclusion complex containing the *cis* isomer, *cis*-**9**⊂**1**. At the PSS, the composition in the inclusion complexes was 65:35 *trans*-**9**⊂**1**:*cis*-**9**⊂**1** by integration of the pyrrole NH protons (H[1'] and H[1'']) of **1**. Similarly to our results obtained for the HTI-**2**/**3**⊂**1** complexes, the absence of the diagnostic signals of free *cis*-**9** indicated the lack of photoinduced release of the guest to the bulk solution at millimolar concentration.

2-(4'-Pyridyl-N-oxide)-substituted hemithioindigos as photoresponsive guests for a super aryl-extended calix[4]pyrrole receptor
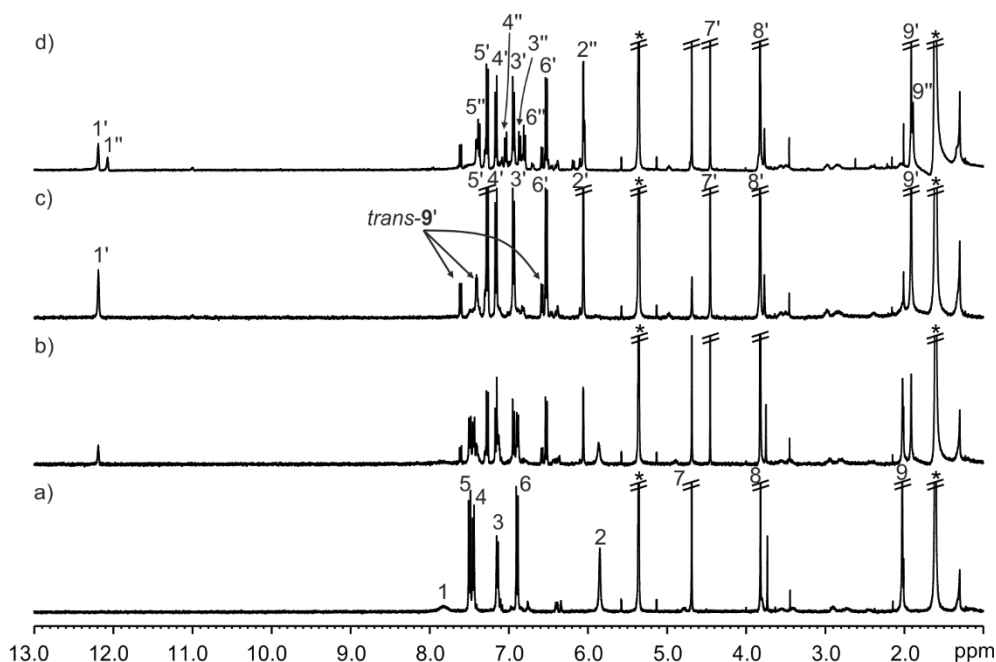

Figure 2.13 ^{1}H NMR spectra (400 MHz, CD$_2$Cl$_2$, 298 K) acquired during titration of a 0.9 mM solution of: a) **1**, b) **1** + 0.5 molar equiv. of *trans*-**9**, c) **1** + 1 molar equiv. of *trans*-**9** before and d) after photoirradiation at λ = 365 nm for 15 min (PSS). Primed and double primed numbers correspond to the proton signals of bound components. * Residual solvents signals.

2.2.7 Binding and photoisomerization studies of HTI **2** with tetranitro calix[4]pyrrole **10**

We also probed the interaction of HTI *Z*-**2** with tetranitro tetraester calix[4]pyrrole (**10**) by ^{1}H NMR titration in CDCl$_3$ solution. Aryl-extended calix[4]pyrroles adopt mainly the 1,3-alternate conformation in non-polar organic solvents, and the binding of a polar molecule (**2** or **3**) induces the receptor to adopt the *cone* conformation. The ^{1}H NMR spectrum of **10** in chloroform solution (4.6 mM) showed sharp and well-defined proton signals. The addition of incremental amounts of HTI *Z*-**2** to a millimolar solution of **10** provoked chemical shifts changes on the proton signals of the receptor. The *β*-pyrrole protons of **10** suffered a downfield shift, while its aromatic protons experienced an upfield shift. The NH pyrrole protons of **10** became too broad for their observation. Overall, the proton signals of *Z*-**2** experienced an upfield shift with respect to those of *Z*-**2** free in solution. These observations indicated that *Z*-**2** was included in the aromatic cavity of **10** and the presence of only one set of proton signals for the host and the guest after each addition of *Z*-**2** was indicative of a fast chemical exchange on the ^{1}H NMR chemical shift timescale between the free and bound components (Figure 2.14).
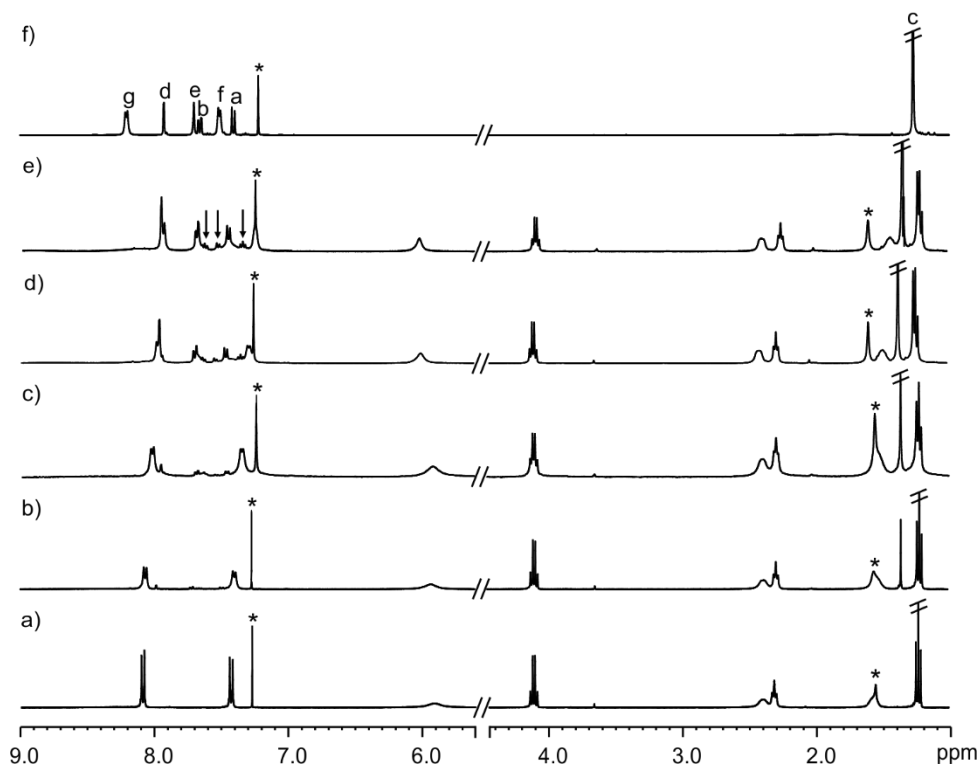
75

Chapter 2

Figure 2.14 ^{1}H NMR spectra (400 MHz, CDCl$_3$) acquired during the titration of a 4.6 mM solution of tetranitrocalix[4]pyrrole **10** with a) 0; b) 0.5; c) 1; d) 3 and e) 5 equiv. of *Z*-**2**; f) *Z*-**2**. * Residual solvents peaks.

The fit of the titration data returned an association constant for the complexation event that was indicative of weak interaction between the two binding partners. Specifically, the changes in the chemical shift of the diagnostic *β*-pyrrolic protons from the ^{1}H NMR titration and the corresponding concentration of guest *Z*-**2** in chloroform solution were fit to a 1:1 binding model using the software *HypNMR2008*. From the fitting of the experimental data (Figure 2.15) we estimated a value for the association constant of $1.0 \cdot 10^2$ M^{-1}.

2-(4'-Pyridyl-N-oxide)-substituted hemithioindigos as photoresponsive guests for a super aryl-extended calix[4]pyrrole receptor

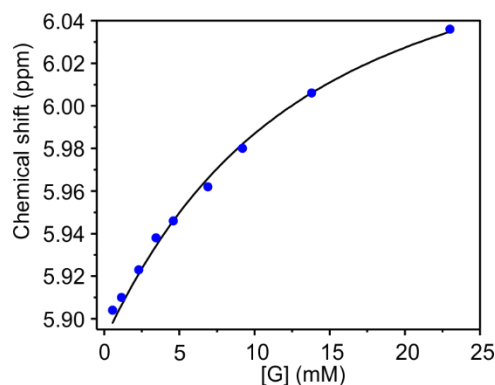**Figure 2.15** Observed (blue dots) and calculated (black line) chemical shifts of the diagnostic β-pyrrolic protons of receptor **10** vs. the concentration of guest Z-**2** added to the solution.

The ^{1}H NMR spectrum of an equimolar solution of Z-**2** and **10** in CD_2Cl_2 also showed the proton signals of Z-**2** upfield shifted with respect to those of the free guest in solution due to its inclusion in the aromatic cavity of tetranitro **10**. Based on the speciation profile, 26 % of HTI Z-**2** was bound to host **10**. The solution was photoirradiated at 450 nm for 15 min producing 85 % of the E-**2** isomer at the *PSS*. The proton signals of E-**2** appeared also upfield shifted with respect to those of free E-**2** in solution.
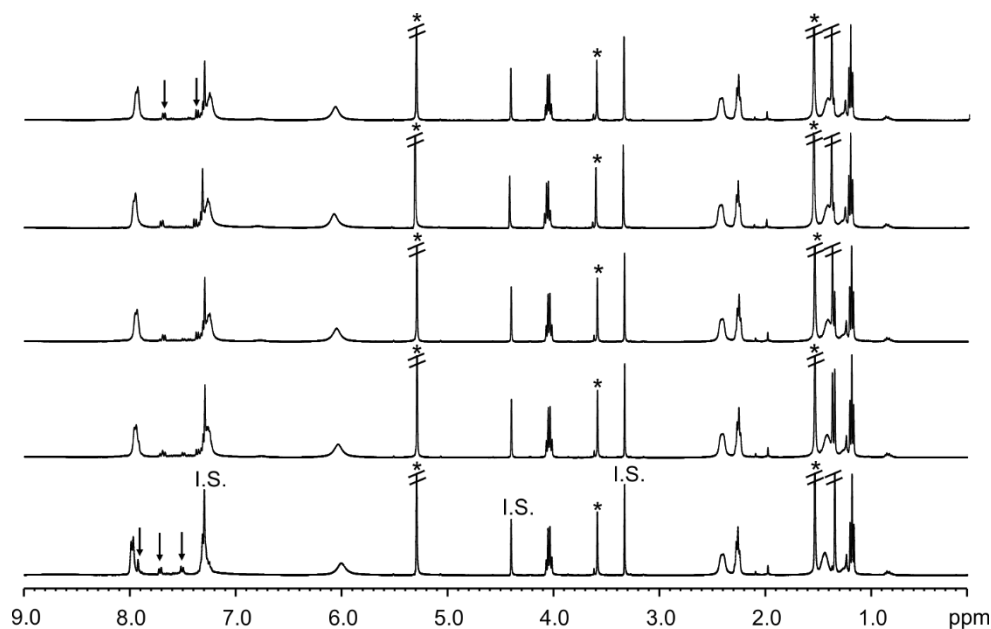

Figure 2.16 ^{1}H NMR spectra (400 MHz, CD_2Cl_2) acquired during the photoirradiation at 450 nm of a 1:1 millimolar solution of tetranitro calix[4]pyrrole **10** with HTI Z-**2** for: a) 0; b) 2; c) 4; d) 10; e) 15 min. Benzyl methyl ether was used as internal standard (I.S.). * Residual solvents peaks.

Chapter 2

This observation suggested that photoirradiation of the *Z*-**2**⊂**10** complex induced the appearance of the *E*-**2**⊂**10** counterpart without promoting the release of *E*-**2** to the bulk solution. As in the case of receptor **1**, the *Z*-to-*E* photoisomerization of **2** did not provoke a reduction in thermodynamic stability of the inclusion complex dramatic enough to induce the release of the guest to the bulk at millimolar concentrations. Afterwards, the mixture of inclusion complexes was back-irradiated (*E*-to-*Z*) at 530 nm for 40 min and returned to its original state, as monitored by ^{1}H NMR spectroscopy.

2.3 Conclusions

In conclusion, we reported the synthesis and characterization of two photoswitchable hemithioindigo *N*-oxides, *Z*-**2** and *Z*-**3**, that were found to be suitable for deep inclusion in the polar aromatic cavity defined by the *cone* conformation of super aryl-extended calix[4]pyrrole **1**. Photoirradiation of thermally stabilized milli- and micromolar chloroform solutions of the HTI derivatives, *Z*-**2** and *Z*-**3**, with λ = 450 nm light produced isomeric mixtures enriched with the *E*-form to an extent >80% at the PSS. The *Z*-to-*E* photoisomerization of the HTI derivatives could be reversed by a thermal equilibration process, which produced mainly the *Z*-form. ^{1}H NMR titration experiments evidenced the formation of kinetically and thermodynamically stable 1:1 inclusion complexes of the HTI derivative *Z*-forms of **2** and **3** and super aryl-extended receptor **1**. Photoirradiation of the *Z*-HTI⊂**1** complexes produced mixtures enriched with the *E*-HTI⊂**1** counterparts, which required extensive irradiation times to achieve the PSSs compared to the analogous experiments performed with the free *Z*-HTI. Photoirradiation of the inclusion complexes produced identical levels of isomerization of the HTI derivatives to those obtained for the free guest. At millimolar concentration, the *Z*-to-*E* photoisomerization of the HTI guests did not induce their release to detectable extents to the bulk solution. The results from the isothermal titration calorimetry experiments allowed us to determine that the binding constant values of all isomeric inclusion complexes were of the order of 10^6 M^{-1} (ΔG ~ 9.5 kcal·mol^{-1}). Likewise, we quantified that the modulation in binding affinity exerted by the isomerization of the guest was approximately 0.5 kcal·mol^{-1}. The design of related host–guest systems capable of efficient "cargo release" by light stimulus remains a challenging endeavor in our laboratory.

2-(4'-Pyridyl-N-oxide)-substituted hemithioindigos as photoresponsive guests for a super aryl-extended calix[4]pyrrole receptor

2.4 Experimental section

2.4.1 General information and instrumentation

All syntheses were carried out using chemicals as purchased from commercial sources unless otherwise noted. All commercial solvents and chemicals were of reagent grade quality and were used without further purification except as noted. Dry solvents were taken from a solvent system MB SPS 800 (*MBraun*) and freshly distilled unless otherwise stated. Thin-layer chromatography (TLC) and flash column chromatography were performed with DC-Alufolien Kieselgel 60 F_{254} (*Merck*) and silica gel 60 Å for chromatography (*Sigma-Aldrich*), respectively. Routine ^{1}H and ^{13}C NMR spectra were recorded on *Bruker* Avance 300 (300 MHz for ^{1}H NMR), Avance 400 (400 MHz for ^{1}H NMR) or Avance 500 (500 MHz for ^{1}H NMR) ultrashield spectrometers, or on a *Bruker* Avance III 500 with a QNP cryoprobe. Deuterated solvents (*Sigma-Aldrich*) used are indicated in the characterization and chemical shifts are given in ppm. Residual solvent peaks were used as reference. All NMR *J* values are given in Hz. High Resolution Mass Spectrometry (HRMS) experiments were performed on a MicroTOF, *Bruker Daltonics ESI*. The diagnostic peaks are reported in m/z units. UV/Vis spectra were recorded on a *Shimadzu* UV-2401PC spectrophotometer (equipped with a photomultiplier detector, double beam optics and D_2 and W light sources). The spectra were recorded in a quartz cuvette (10 mm path length). Chloroform for spectroscopy was obtained from *Merck*. IR spectra were recorded on a *Bruker Optics* FT-IR Alpha spectrometer equipped with a DTGS detector, KBr beam splitter at 4 cm^{-1} resolution using a one bounce ATR accessory with diamond windows. Melting points were measured on a MP70 Melting Point System instrument from *Mettler Toledo*. Irradiation experiments for the HTI derivatives and inclusion complexes were conducted using a high power LED-diode from *Roithner Lasertechnik GmbH* (450 nm, 26 mW·cm^{-2}) mounted on a heat sink from *Fischer Elektronik*. Isothermal titration calorimetry experiments were carried out on a *MicroCal VP-ITC* microcalorimeter. Chloroform of HPLC grade was passed through basic alumina (*Merck*) prior to use.

2.4.2 Synthetic procedures

The syntheses of super aryl-extended calix[4]pyrrole **1** and tetranitro tetraester calix[4]pyrrole **10** were carried out following procedures reported in literature.[21,35] 4-Pyridinecarboxaldehyde *N*-oxide **6** was purchased from *Sigma-Aldrich*.

2-(4'-Pyridyl-*N*-oxide)-HTI *Z*-**2**: 5-(tert-butyl)benzo[b]thiophen-3(2H)-one **5** (210 mg, 1.02 mmol, 1 equiv.) was added to a 25 mL Schlenk flask and dried under vacuum for 30 min, then dissolved in 10 mL anhydrous benzene turning to a red color. Afterwards, 5 drops of piperidine were added, and subsequently 4-Pyridinecarboxaldehyde *N*-oxide **6** (82 mg, 0.67 mmol, 0.65 equiv.) in one portion. All reagents were added under nitrogen flow. Reaction was carried out under nitrogen at 45°C and protected from light. After 5 h it was stopped according to TLC (DCM:MeOH 99:1), that indicated the absence of the starting materials. The crude was dissolved in 50 mL EtOAc and partitioned once between 50 mL 3:2 water:NH$_4$Cl saturated solution. The aqueous phase was then extracted with EtOAc (2x 50 mL). The organic phases were combined, dried over sodium sulfate and *in vacuo* to afford a deep red solid. The crude was redissolved in acetone. Column chromatography (SiO$_2$, acetone:MeOH 98:2) afforded the product as a bright yellow solid. The compound was triturated in ethyl acetate, sonicated thoroughly until a golden dispersion appeared, filtered out and dried under high vacuum to afford a yellow powder (67 mg, 0.215 mmol, 21% yield). R$_f$ = 0.37 (acetone:MeOH 99:1). M.p. = >200 °C (decompose). ^{1}H NMR (CDCl$_3$, 400 MHz) δ (ppm): 8.24 (d, *J* = 6.5 Hz, 2H); 7.96 (d, *J* = 2.0 Hz, 1 H); 7.74 (s, 1 H); 7.69 (dd, *J* = 8.3, 2.1 Hz, 1 H); 7.55 (d, *J* = 6.4 Hz, 2 H); 7.45 (d, *J* = 8.3 Hz, 1 H); 1.36 (s, 9 H). ^{13}C {^{1}H} NMR (CDCl$_3$, 101 MHz) δ (ppm): 188.24; 150.10; 141.72; 139.55; 136.01; 133.90; 131.73; 129.52; 127.03; 126.91; 124.04; 123.65; 34.83; 31.23. FT-IR ν (cm^{-1}) = 2951; 1674 (C=O stretching); 1581; 1476; 1441; 1362; 1326; 1263 (N-O stretching); 1213; 1174; 1070; 1020; 909; 824; 740; 575; 538; 513; 491. HRMS (EI): *m/z* calcd. for C$_{18}$H$_{17}$NO$_2$S: 311.0979; found: 311.0974.

2-(4'-Pyridyl-*N*-oxide)-HTI *Z*-**3**: 5-(tert-butyl)benzo[b]thiophen-3(2H)-one **5** (55 mg, 0.27 mmol, 1 equiv.) was added to a 25 mL Schlenk flask and dried under vacuum for 30 min, then dissolved in 10 mL anhydrous benzene turning to a red color. Afterwards, 2 drops of piperidine were added, and subsequently *N*-oxide **7** (29.25 mg, 0.21 mmol, 0.80 equiv.) in one portion. All reagents were added under nitrogen flow. Reaction was carried out under

UNIVERSITAT ROVIRA I VIRGILI
STIMULI-RESPONSIVE HOST-GUEST SYSTEMS DECORATED WITH HEMITHIOINDIGO AND SPIROPYRAN UNITS
Giulia Moncelsi

*2-(4'-Pyridyl-N-oxide)-substituted hemithioindigos as photoresponsive guests for a super
aryl-extended calix[4]pyrrole receptor*

nitrogen at 45 °C and protected from light. After 12 h it was stopped according to TLC (DCM:MeOH 98:2), that indicated the absence of the starting materials. The crude was dissolved in 40 mL EtOAc and partitioned once between 35 mL 3:2 water:NH_4Cl saturated solution. The aqueous phase was then extracted with EtOAc (2x 40 mL). The organic phases were combined, dried over sodium sulfate and *in vacuo*. Column chromatography (SiO_2, acetone:MeOH 98:2) afforded the product as a golden solid. The compound was triturated in ethyl acetate, sonicated thoroughly until a golden dispersion appeared, filtered out and dried under high vacuum to afford a yellow powder (51 mg, 0.16 mmol, 59% yield). R_f = 0.55 (DCM:MeOH 98:2). M.p. = > 240 °C (decompose). ^{1}H NMR ($CDCl_3$, 400 MHz) δ (ppm): 8.12 (d, *J* = 7.0 Hz, 1H); 8.09 (s, 1 H); 7.96 (d, *J* = 1.85 Hz, 1 H); 7.88 (s, 1 H); 7.68 (dd, *J* = 8.3 Hz, 1 H); 7.62 (d, *J* = 6.8 Hz, 1 H); 7.43 (d, J = 8.3 Hz, 1 H); 2.44 (s, 3 H); 1.36 (s, 9 H). ^{13}C {^{1}H} NMR ($CDCl_3$, 101 MHz) δ (ppm): 188.38; 150.18; 142.15; 139.36; 137.29; 137.10; 134.87; 133.95; 131.47; 129.92; 124.81; 124.74; 124.10; 123.72; 34.93; 31.33; 17.30. FT-IR ν (cm^{-1}) = 3026; 2952; 1669 (C=O stretching); 1598; 1575; 1553; 1462; 1266 (N-O stretching); 1212; 1065; 921; 819; 743; 575; 550; 487; 440. HRMS (EI): *m/z* calcd. for $C_{19}H_{19}O_2NS$: 325.11365; found: 325.1133.

2-((4-(*Tert*-butyl)phenyl)thio)acetic acid **4**: commercially available 4-tert-butylbenzenethiol (1 g, 6.01 mmol, 1 equiv.) was added with a syringe to a Schlenk flask, then dried under high vacuum until bubbling stopped, due to the hygroscopicity of the reagent. The thiol was then dissolved in 20 mL of HPLC grade THF. Afterwards, K_2CO_3 (1.66 g, 12.03 mmol, 2 equiv.) and 2-bromoacetic acid (877.4 mg, 6.31 mmol, 1.05 equiv.) were added at once to the flask. The whole procedure was carried out under nitrogen atmosphere at room temperature. The flask was equipped with a nitrogen balloon and stirred. After 3 h the reaction was stopped upon formation of a white precipitate. The excess of THF was removed and the reaction crude was dissolved in 100 mL water. The aqueous phase was acidified to pH = 2 with HCl 2 M, then extracted with EtOAc (2x 100 mL). The organic phase was dried over sodium sulfate and *in vacuo*, to afford a colorless sticky solid (930 mg, 4.15 mmol, 69% yield). R_f = 0.43 (DCM:MeOH 98:2). M.p. = 53-54 °C. ^{1}H NMR (MeOD, 400 MHz) δ (ppm): 7.34 (s, 4 H); 3.64 (s, 2 H); 1.30 (s, 9 H). ^{13}C {^{1}H} NMR ($CDCl_3$, 101 MHz) δ (ppm): 173.48; 151.10; 133.17; 130.68; 126.96; 37.44; 35.19; 31.51. FT-IR ν (cm^{-1}) = 2956; 2905; 1708 (C=O stretching); 1497; 1419; 1302; 1270; 1192; 1121; 1011; 876; 815; 740; 660; 542; 470; 440. HRMS (EI): *m/z* calcd. for $C_{12}H_{16}O_2S$: 224.0871; found: 224.0877.

Chapter 2

5-(*Tert*-butyl)benzo[b]thiophen-3(2H)-one **5**: 2-((4-(tert-butyl)phenyl)thio)acetic acid **4** (543 mg, 2.42 mmol, 1 equiv.) was added to a 50 mL Schlenk flask and dried under high vacuum for 1h, until bubbling stopped, due to its hygroscopicity. Afterwards, thionyl chloride (1.4 mL, 19.37 mmol, 8 equiv.) was added dropwise under nitrogen atmosphere. Upon addition of the chloride the mixture took on a golden color. After 15 min at 70 °C the solution was cooled at RT and excess $SOCl_2$ was removed *in vacuo*. The resulting golden oil was dissolved in 20 mL dry 1,2-dichloroethane. Upon addition of coarse $AlCl_3$ (1.29 g, 9.67 mmol, 4 equiv.) at 0 °C over 5 min, the mixture turned green and then, slowly, brown with a red shade. The mixture was left stirring under nitrogen flow and protected from light. After 3 h the mixture was quenched with ice and water under nitrogen flow until it became light orange, then the crude was extracted with CH_2Cl_2 (2x 50mL). The orange organic phase was washed twice with water (2x 50 mL), dried over sodium sulfate and *in vacuo*, protected from light. A red brown oil (392.2 mg, 1.71 mmol, apparent 71% yield) was isolated and used for the next step without further purification due to its instability. R_f = 0.68 (CH_2Cl_2). ^{1}H NMR (CD_2Cl_2, 400 MHz) δ (ppm): 7.75 (s, 1 H); 7.65 (dd, J = 8.3 Hz, 1 H), 7.38 (d, J = 8.5 Hz, 1 H); 3.79 (s, 2 H); 1.33 (s, 9 H).

4-Formyl-3-methylpyridine *N*-oxide **7**: 3,4-lutidine *N*-oxide was oxidized to the corresponding aldehyde via benzylic oxidation:[36] a mechanically stirred mixture of **8** (1.10 g, 8.93 mmol, 1 equiv.), dioxane (9.57 mL, 112.18 mmol, 12.56 equiv.), and powdered selenium dioxide (961 mg, 8.66 mmol, 0.97 equiv.) was refluxed at 109 °C. The SeO_2 slowly darkens to black. After 24 h the reaction was stopped according to TLC (DCM:MeOH 98:2). The hot yellow mixture was filtered through a short celite column and washed with 300 mL DCM. The crude was concentrated under vacuum to afford a yellowish solid. The solid was purified with column chromatography (DCM:MeOH 97:3), to afford the desired aldehyde as a white solid (213 mg, 1.55 mmol, 17 % yield). R_f = 0.26 (DCM:MeOH 98:2). M.p. = 151-153 °C. ^{1}H NMR (CDCl$_3$, 400 MHz) δ (ppm): 10.16 (s, 1 H), 8.15 (d, J = 6.9 Hz, 1 H), 8.10 (s, 1 H), 7.67 (d, J = 6.9 Hz, 1 H), 2.61 (s, 3 H). ^{13}C{^{1}H} NMR (CDCl$_3$, 101 MHz) δ (ppm): 187.85; 140.90; 137.87; 137.72; 129.93; 127.12; 16.27. FT-IR ν (cm^{-1}) = 3035; 1688 (C=O stretching); 1604; 1528; 1457; 1379; 1308; 1263 (N-O stretching); 1227; 1122; 844; 803; 737; 632; 545; 497; 448. HRMS (EI): *m/z* calcd. for $C_7H_7NO_2$: 137.04768; found: 137.0473.

3,4-Lutidine *N*-oxide **8**: commercially available 3,4-lutidine (200 mg, 1.87 mmol, 1 equiv.) was oxidized to the corresponding *N*-oxide following a known procedure for π-deficient

2-(4'-Pyridyl-N-oxide)-substituted hemithioindigos as photoresponsive guests for a super aryl-extended calix[4]pyrrole receptor

azines:[37] the reagent was added with a syringe to a round bottom flask. Acetic acid (1.87 mL, 32.66 mmol, 17.5 equiv.) was added dropwise and finally, sodium perborate tetrahydrate (PBS, 316 mg, 2.05 mmol, 1.1 equiv.) in two portions. The flask was left stirring overnight at 45 °C leading to a turbid milky mixture. The acetic acid was carefully evaporated under vacuum, then the crude was redissolved in 20 mL saturated $NaHCO_3$ solution and extracted with chloroform (3x 50 mL). The organic phase was dried over sodium sulfate and under reduced pressure to afford white crystalline needles (144 mg, 1.17 mmol, 63 % yield). R_f = 0.20 (DCM:MeOH 98:2). M.p. = 68-69 °C. ^{1}H NMR ($CDCl_3$, 400 MHz) δ (ppm): 8.0 (s, 1 H); 7.96 (d, J = 6.4 Hz, 1 H); 6.99 (d, J = 6.4 Hz, 1 H); 2.21 (s, 3 H); 2.16 (s, 3 H). ^{13}C {^{1}H} NMR ($CDCl_3$, 101 MHz) δ (ppm): 138.82; 137.32; 136.31; 135.51; 126.59; 18.38; 16.80. FT-IR ν (cm^{-1}) = 3374; 3075; 2958; 1682; 1485; 1458; 1288; 1247 (N-O stretching); 1213; 1122; 1016; 959; 890; 840; 743; 567; 517; 467; 436. HRMS (EI) *m/z* calcd. for C_7H_9NO: 123.0684; found: 123.0678.

Tetramethylammonium 4-(phenylazo)benzoate **9**: commercially available 4-(phenylazo)benzoic acid (151 mg, 0.67 mmol, 1 equiv.) and TMAOH (121 mg, 0.67 mmol, 1 equiv.) were added to a 50 mL round bottom flask. Then, MeOH (10 mL) was added and the mixture was stirred vigorously at RT for 2 h. The color of the solution was dark red. Afterwards, the reaction was stopped and MeOH was removed under reduced pressure. Finally, hexane (0.2 mL) was added and the dispersion sonicated. The resulting solid was dried under high vacuum and with P_2O_5 overnight to afford a dark green solid (200 mg, 0.67 mmol, 99% yield). ^{1}H NMR (ACN-d_3, 500 MHz) δ (ppm): 8.11 (d, J = 8.3 Hz, 2H); 7.93 ppm (d, J = 7.7 Hz, 2H); 7.83 (d, J = 8.3 Hz, 2H); 7.59 (m, 3H); 3.13 (s, 12H). ^{13}C {^{1}H} NMR (ACN-d_3, 126 MHz) δ (ppm): 169.60; 153.74; 153.46; 145.80; 132.02; 130.97; 130.31; 123.53; 122.60; 56.14.

Chapter 2

2.4.3 Figures and tables
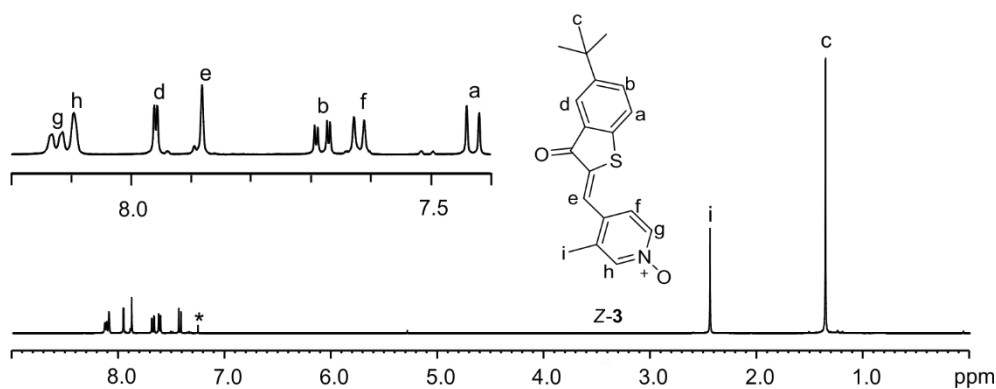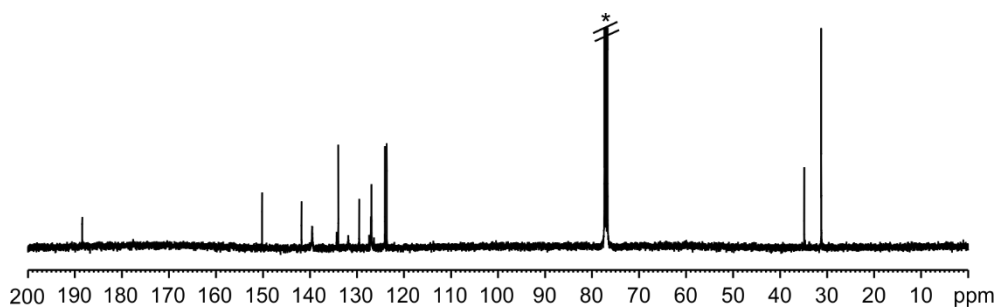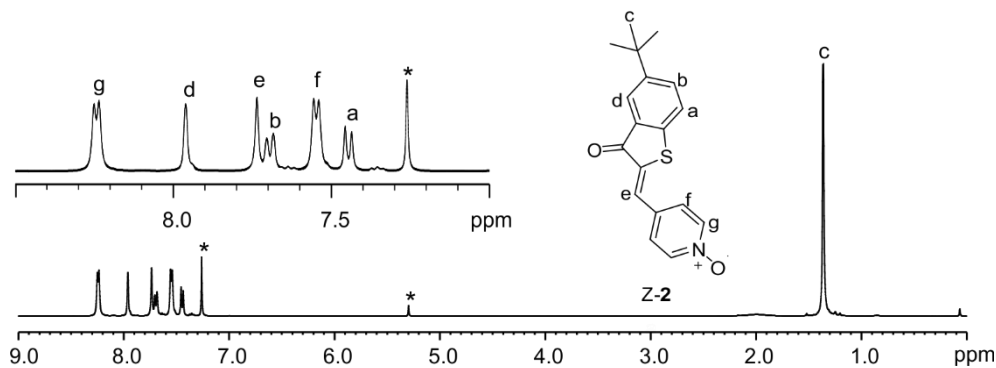
Figure 2.17 ^{1}H NMR (CDCl$_3$, 400 MHz) of 2-(4'-Pyridyl-*N*-oxide)-HTI *Z*-**2**. * Residual solvent peaks.

Figure 2.18 ^{13}C NMR (CDCl$_3$, 101 MHz) of 2-(4'-Pyridyl-*N*-oxide)-HTI *Z*-**2**. * Residual solvent peaks.

Figure 2.19 ^{1}H NMR (CDCl$_3$, 400 MHz) of 2-(4'-Pyridyl-*N*-oxide)-HTI *Z*-**3**. * Residual solvent peaks.

2-(4'-Pyridyl-N-oxide)-substituted hemithioindigos as photoresponsive guests for a super aryl-extended calix[4]pyrrole receptor
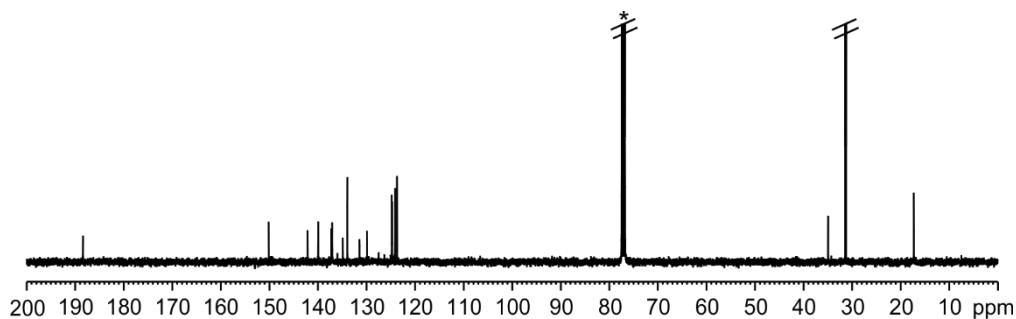
**Figure 2.20** ^{13}C NMR (CDCl$_3$, 101 MHz) of 2-(4'-Pyridyl-*N*-oxide)-HTI *Z*-**3**. * Residual solvent peaks.
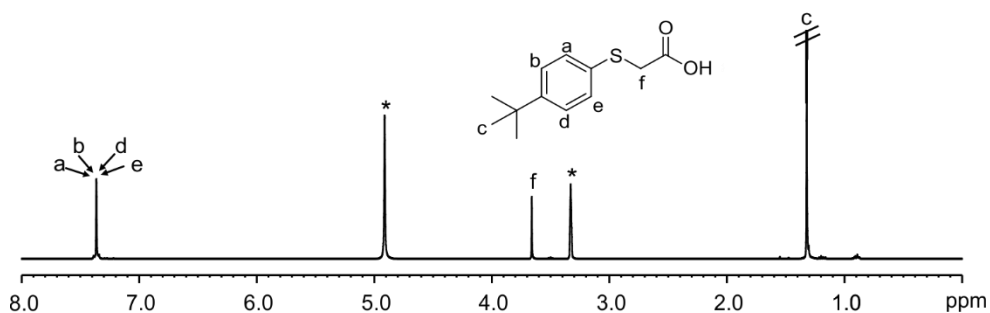
Figure 2.21 ^1H NMR (MeOD, 400 MHz) of 2-((4-(tert-butyl)phenyl)thio)acetic acid **4**. * Residual solvent peaks.
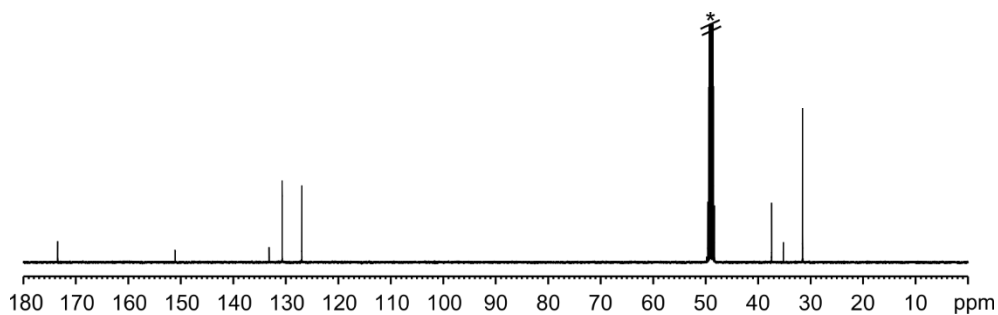
Figure 2.22 ^{13}C NMR (MeOD, 101 MHz) of 2-((4-(tert-butyl)phenyl)thio)acetic acid **4**. * Residual solvent peaks.

85

Chapter 2
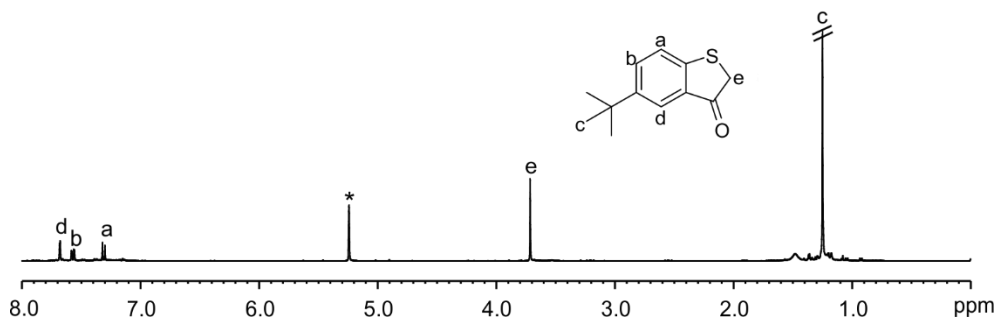
Figure 2.23 ^{1}H NMR (CD$_2$Cl$_2$, 400 MHz) of 5-(tert-butyl)benzo[b]thiophen-3(2H)-one **5**. * Residual solvent peaks.
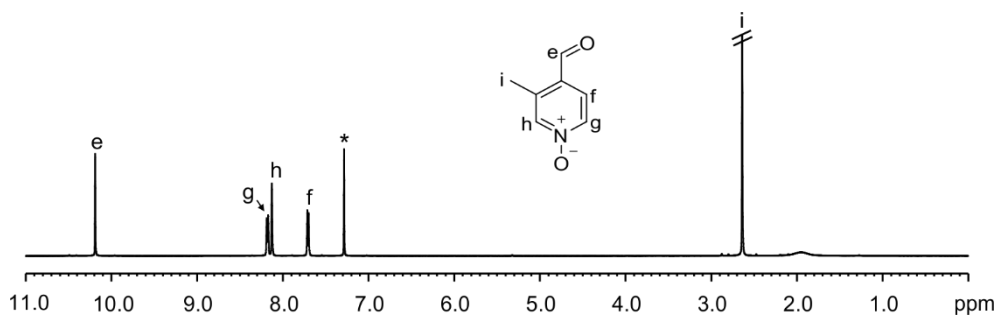
Figure 2.24 ^{1}H NMR (CDCl$_3$, 400 MHz) of 4-formyl-3-methylpyridine *N*-oxide **7**. * Residual solvent peaks.
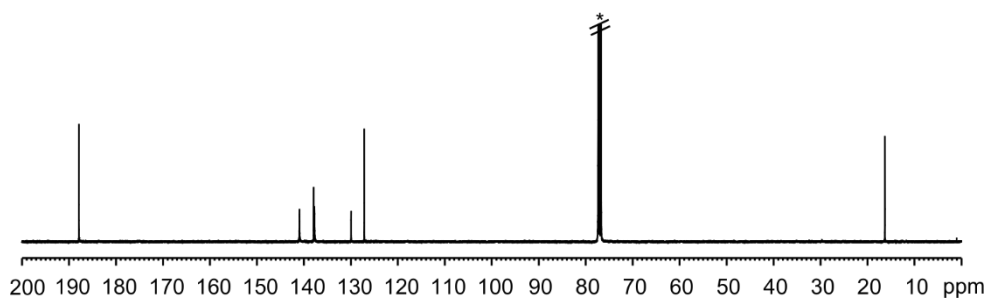
Figure 2.25 ^{13}C NMR (CDCl$_3$, 101 MHz) of 4-formyl-3-methylpyridine *N*-oxide **7**. * Residual solvent peaks.

Single crystals suitable for X-Ray diffraction were grown by slow diffusion of heptane in dichloromethane solution of **7** in order to distinguish between the position isomers 4-formyl-3-methylpyridine and 3-formyl-4-methylpyridine *N*-oxides. The latter was unequivocally excluded.

86

2-(4'-Pyridyl-N-oxide)-substituted hemithioindigos as photoresponsive guests for a super aryl-extended calix[4]pyrrole receptor
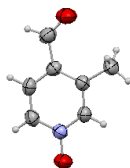
Figure 2.26 Preliminary solution of the X-ray structure (ORTEP) of compound **7**: thermal ellipsoids set at 50% probability and hydrogens shown as fixed spheres of 0.15 Å.
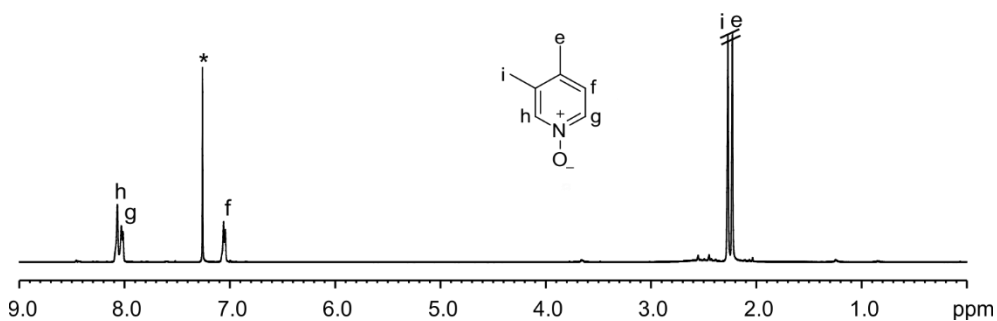

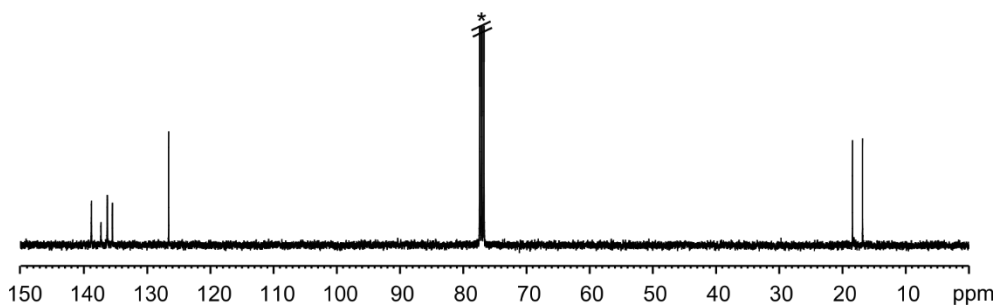**Figure 2.27** ^{1}H NMR (CDCl$_3$, 400 MHz) of 3,4-lutidine *N*-oxide **8**. * Residual solvent peaks.

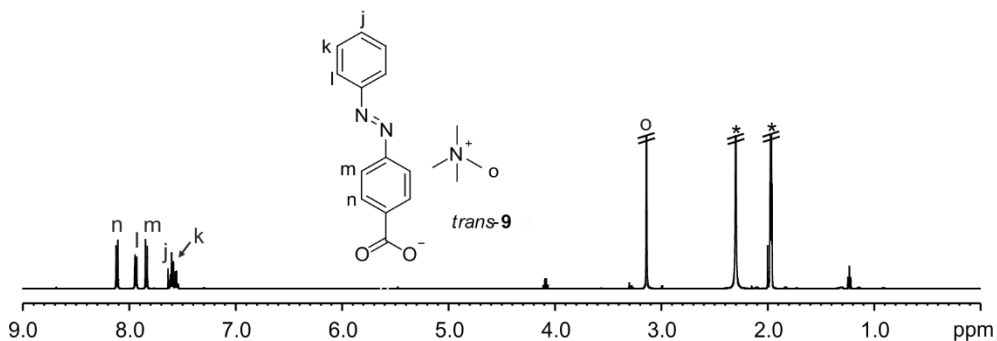**Figure 2.28** ^{13}C NMR (CDCl$_3$, 101 MHz) of 3,4-lutidine *N*-oxide **8**. * Residual solvent peaks.

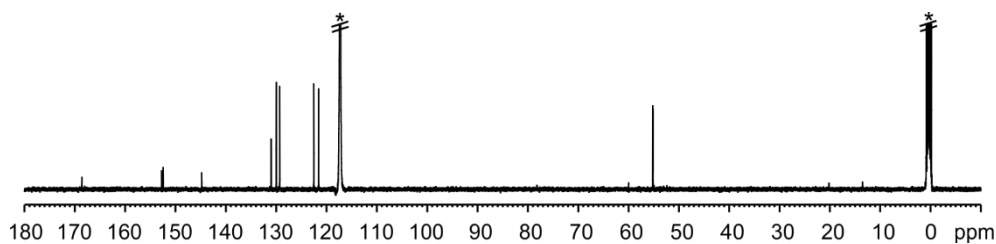**Figure 2.29** ^{1}H NMR (ACN-d$_3$, 500 MHz) of tetramethylammonium 4-(phenylazo)benzoate **9**. * Residual solvent peaks.

Chapter 2

Figure 2.30 ^{13}C NMR (ACN-d$_3$, 126 MHz) of tetramethylammonium 4-(phenylazo)benzoate **9**. * Residual solvent peaks.
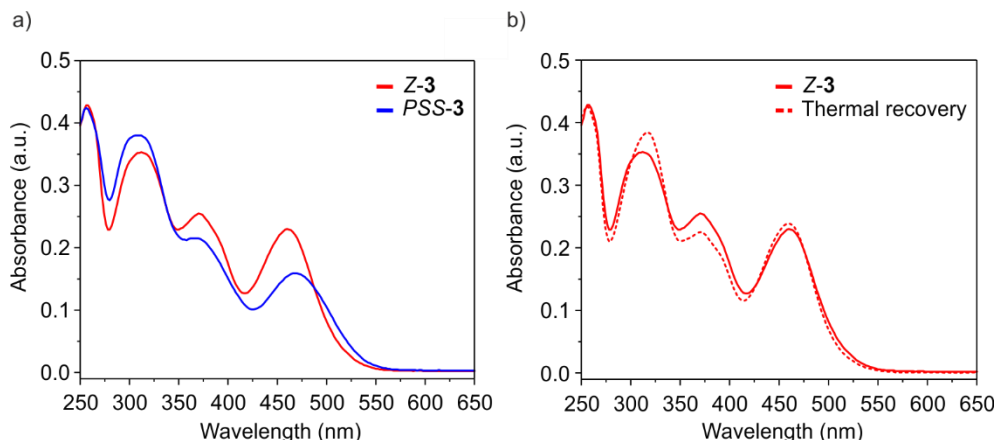

Figure 2.31 UV/Vis absorption spectra of chloroform solutions of **3** (30 µM): a) as the Z isomer (red), at the PSS after photoirradiation at λ = 450 nm for 30 s (blue) and b) as the Z isomer (red solid) and after thermal re-equilibration (red dashed).
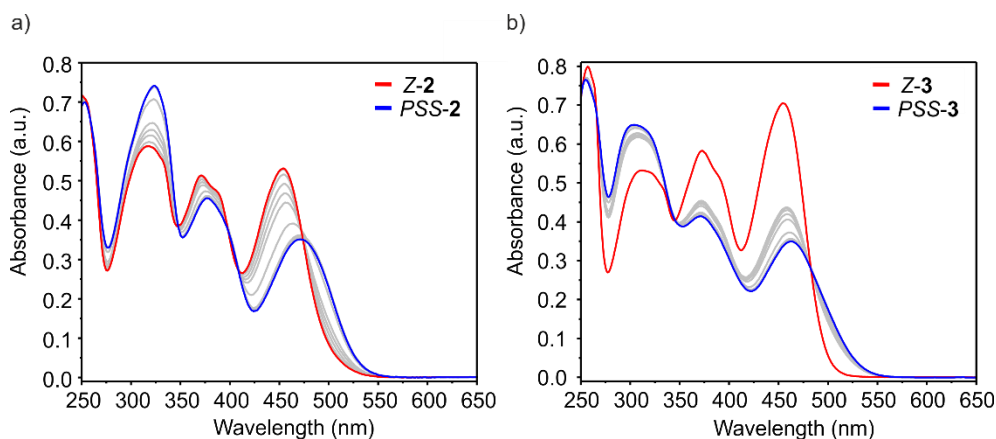

Figure 2.32 UV/Vis absorption spectra of a dichloromethane solution of a) Z-**2** (30 µM) light-irradiated at 435 nm at different times up to 3 min and b) Z-**3** (40 µM) light-irradiated at 365 nm at different times up to 40 s.

2-(4'-Pyridyl-N-oxide)-substituted hemithioindigos as photoresponsive guests for a super aryl-extended calix[4]pyrrole receptor
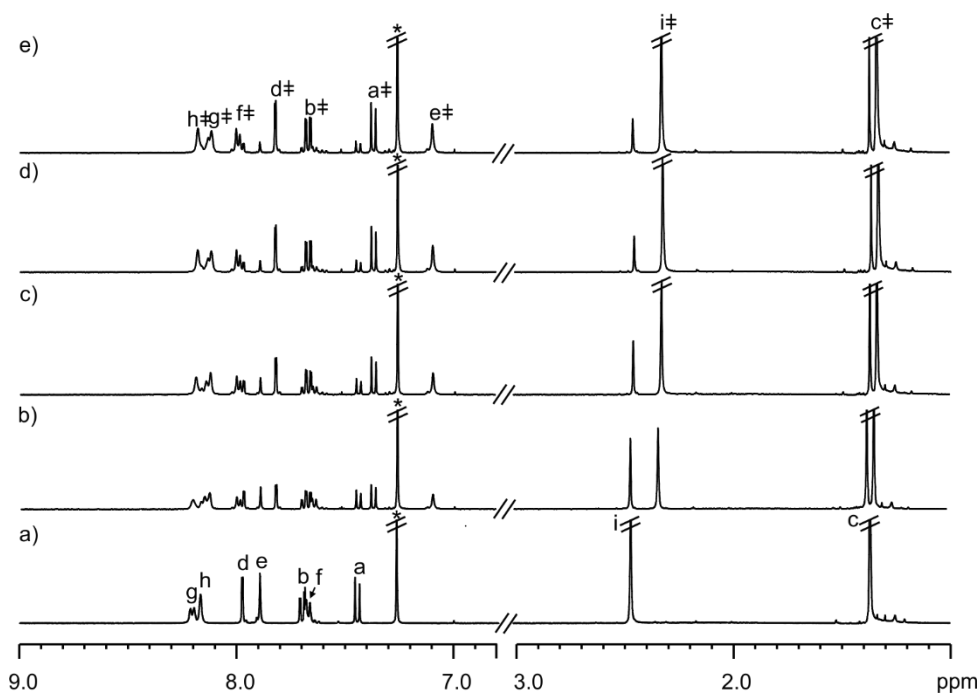

Figure 2.33 ^{1}H NMR spectra (400 MHz, CDCl$_3$) recorded during the photoirradiation at 450 nm of a 7 mM solution of compound *Z*-**3** for a) 0; b) 3 min; c) 5 min; d) 10 min and e) 15 min, reaching the PSS after 10 min with a final *Z*:*E* ratio of 15:85. Protons assigned to the *E*-**3** isomer are marked with a ‡. * Residual solvent peaks.
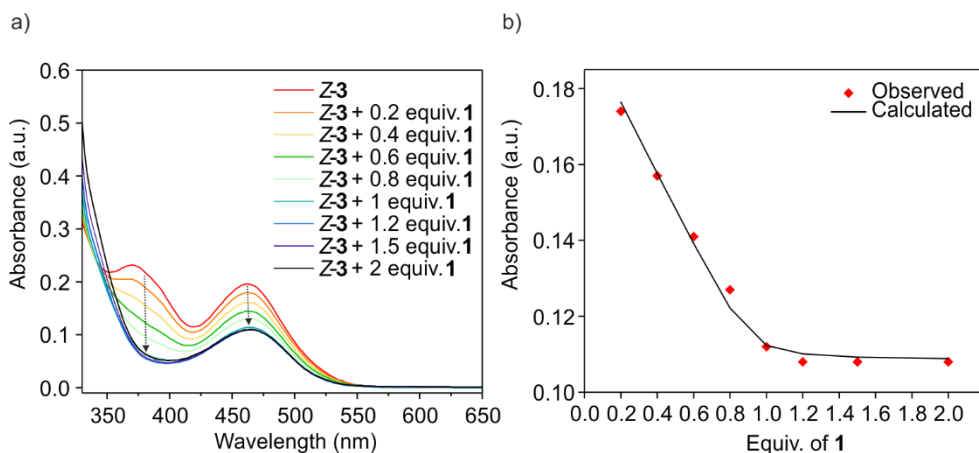

Figure 2.34 a) UV/Vis absorption spectra acquired during the titration of a 30 µM CHCl$_3$ solution of hemithioindigo *N*-oxide *Z*-**3** with super aryl-extended calix[4]pyrrole **1** and b) observed (red) and calculated (black) absorbances at 470 nm plotted against the equivalents of **1**.
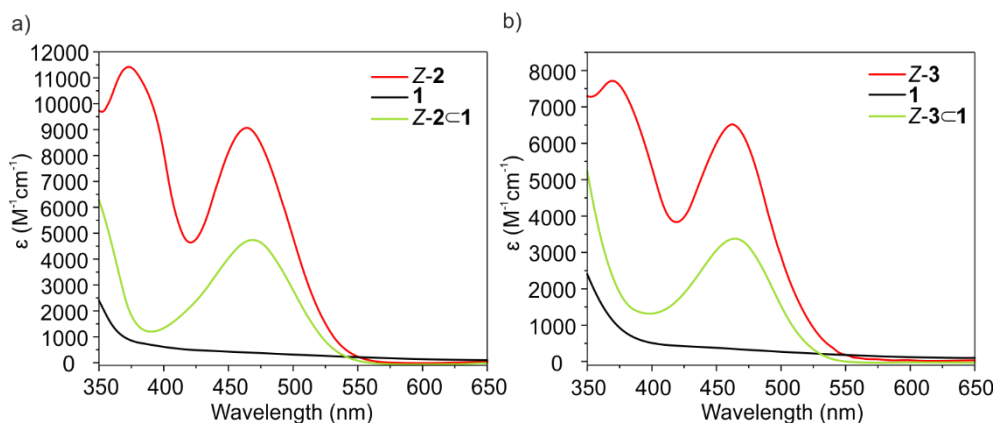
Chapter 2

Figure 2.35 Molar absorption coefficients ε of: a) the experimental spectra of 30 μM CHCl₃ separate solutions of *Z*-**2** and **1** and the calculated spectrum of *Z*-**2**⊂**1**; and b) the experimental spectra of 30 μM CHCl₃ separate solutions of *Z*-**3** and **1** and the calculated spectrum of *Z*-**3**⊂**1**. The spectra of the inclusion complexes *Z*-**2**⊂**1** and *Z*-**3**⊂**1** were calculated from the fitting of the titration data with *HypSpec*.

Z-**2**⊂**1**				*E*-**2**⊂**1**			
Signal	δ_{free}	δ_{bound}	$\Delta\delta$	Signal	δ_{free}	δ_{bound}	$\Delta\delta$
g	8.35	4.68	-3.67	g	8.25	4.55	-3.70
d	7.97	7.43	-0.54	d	7.87	7.58	-0.29
e	7.72	7.03	-0.69	e	7.01	6.27	-0.74
b	7.70	7.45	-0.25	b	7.67	7.47	-0.20
f	7.59	7.00	-0.59	f	8.10	7.36	-0.74
a	7.44	5.89	-1.55	a	7.36	7.08	-0.28
c	1.36	1.35	-0.01	c	1.35	1.34	-0.01

Table 2.4 Chemical shifts of the proton signals of *Z*-**2** (δ, ppm) and complexation induced chemical shifts (Δδ, ppm) between free and bound guest to receptor **1** in CDCl₃.

2-(4'-Pyridyl-N-oxide)-substituted hemithioindigos as photoresponsive guests for a super aryl-extended calix[4]pyrrole receptor
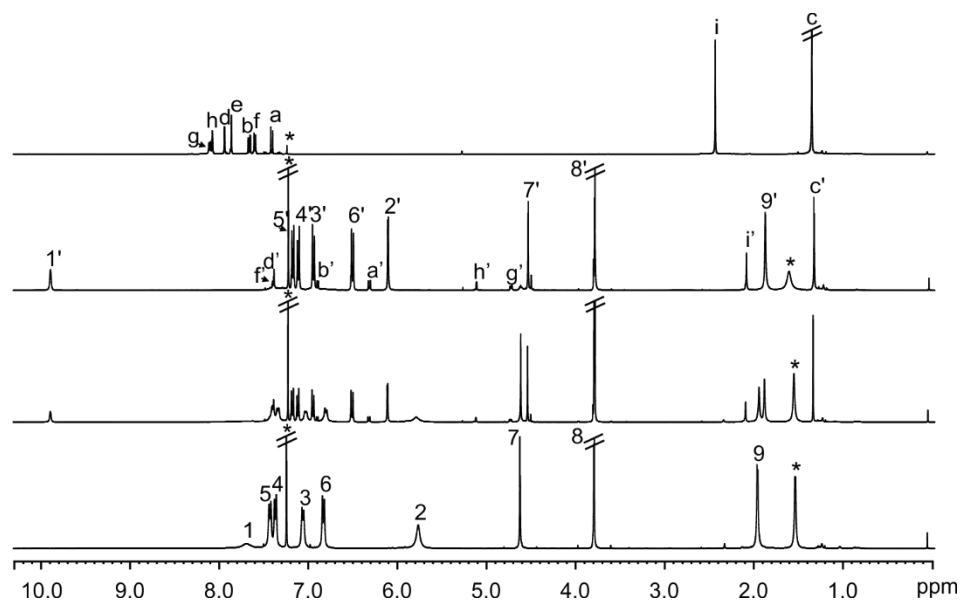

Figure 2.36 ^{1}H NMR spectra (400 MHz, CDCl$_3$) acquired during the titration of super aryl-extended calix[4]pyrrole **1** with hemithioindigo *N*-oxide *Z*-**3**: a) 3.9 mM solution of **1**; b) **1** + 0.5 eq. of *Z*-**3**; c) equimolar amount of **1** and *Z*-**3** and d) *Z*-**3**. Primed letters and numbers correspond to proton signals of bound components.* Residual solvents peaks.
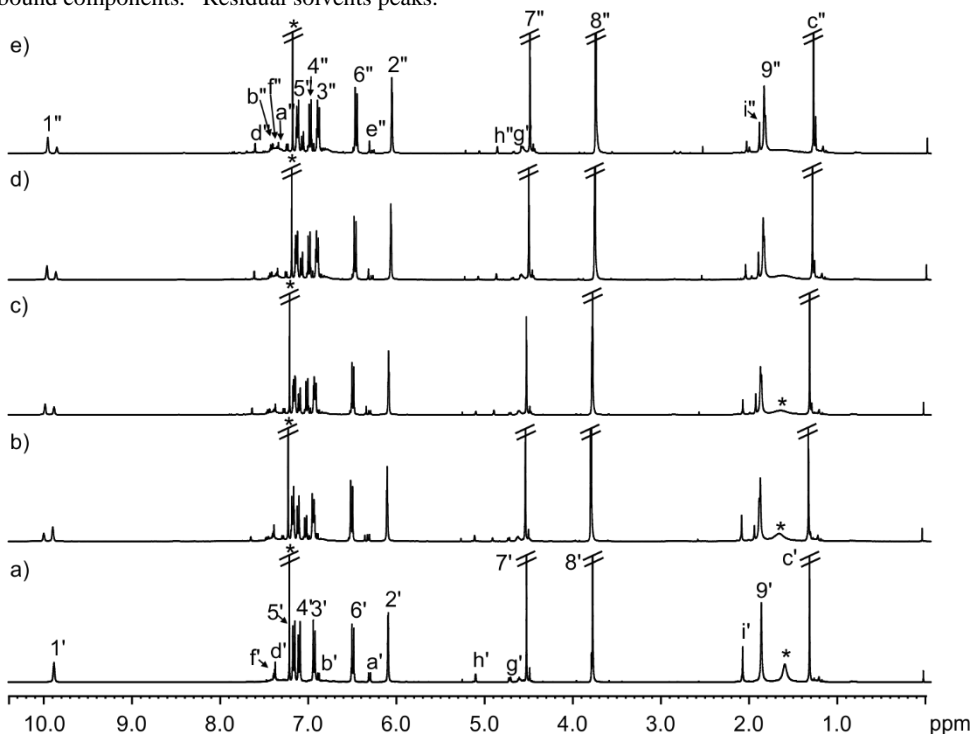

Figure 2.37 ^{1}H NMR spectra (400 MHz, CDCl$_3$) acquired during the photoirradiation (450 nm) of the 1:1 *Z*-**3**⊂**1** complex for: a) 0; b) 1; c) 5; d) 30 and e) 60 min. Primed letters and numbers correspond to

Chapter 2

proton signals of bound components. Double primed letters and numbers correspond to proton signals of irradiated bound components. * Residual solvents peaks.

Z-3⊂1				E-3⊂1			
Signal	δ_{free}	δ_{bound}	$\Delta\delta$	Signal	δ_{free}	δ_{bound}	$\Delta\delta$
g	8.37	4.77	-3.6	g	8.13	4.54	-3.59
h	8.28	5.15	-3.13	h	8.18	4.95	-3.23
d	7.96	7.42	-0.54	d	7.82	7.68	-0.14
e	7.85	7.21	-0.64	e	7.10	6.38	-0.72
b	7.74	6.93	-0.81	b	7.67	7.49	-0.18
f	7.70	7.42	-0.28	f	7.99	7.32	-0.67
a	7.42	6.37	-1.05	a	7.37	7.32	-0.05
i	2.48	2.11	-0.37	i	2.33	1.97	-0.36
c	1.37	1.35	-0.02	c	1.34	1.35	0.01

Table 2.5 Chemical shifts of the proton signals of *Z*-**3** (δ, ppm) and complexation induced chemical shifts ($\Delta\delta$, ppm) between free and bound guest to receptor **1** in CDCl$_3$.
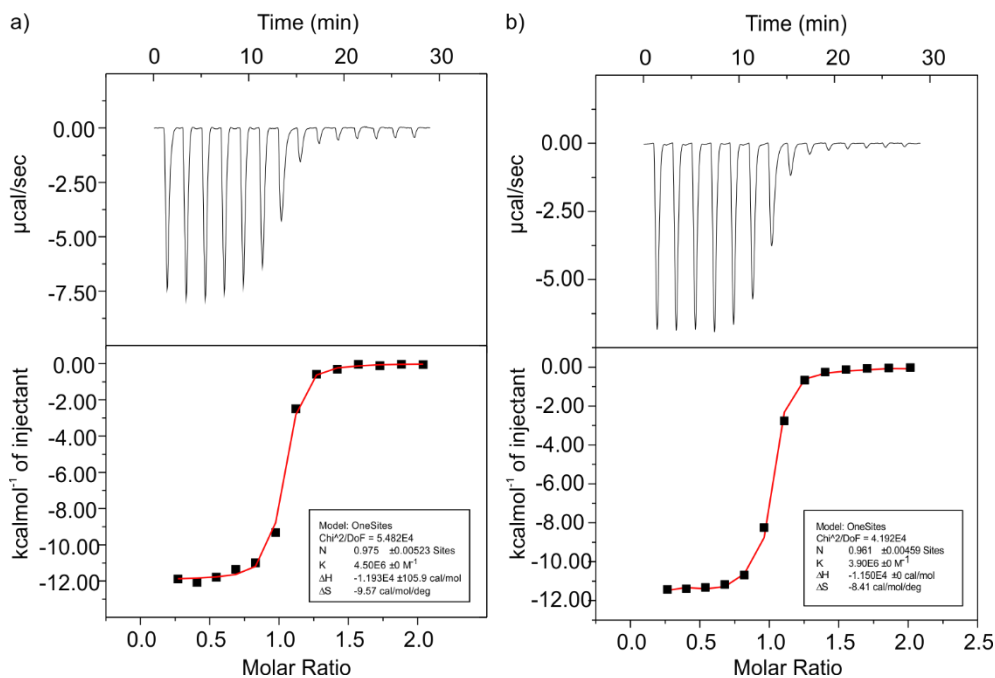

Figure 2.38 Top - Trace shows raw data for one set of experiments for the titration of the guest into the host: a) *Z*-**3**⊂**1** and b) *E*-**3**⊂**1**. Titration was performed at 25 °C in chloroform by timed injection of 20 µl of guest solution into the host solution. Bottom - Binding isotherm of the calorimetric titration shown on top. The enthalpy of binding for each injection is plotted against the molar ratio of host:guest in the cell. The continuous line represents the least-squares-fit of the data to a single-site binding model.

2-(4'-Pyridyl-N-oxide)-substituted hemithioindigos as photoresponsive guests for a super aryl-extended calix[4]pyrrole receptor
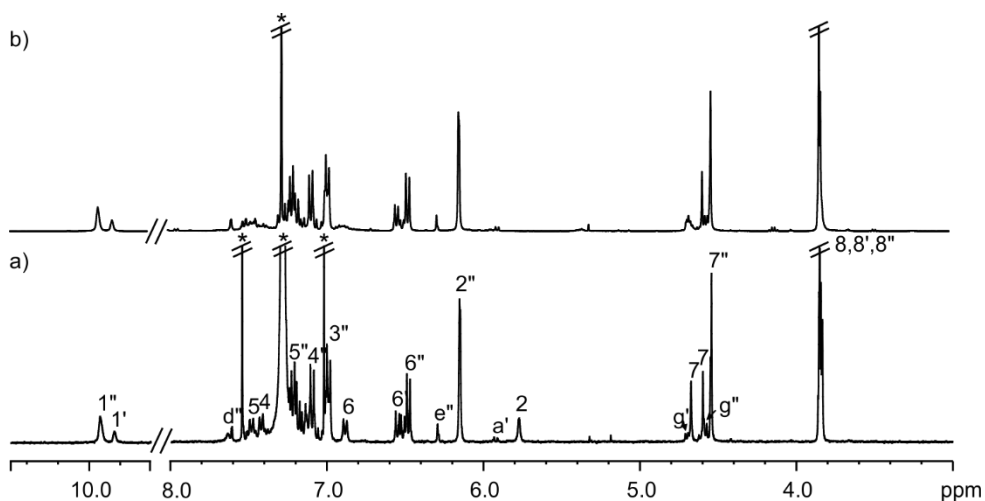

Figure 2.39 Selected regions of the ^{1}H NMR spectra (400 MHz, CDCl$_3$). a) Solution taken from the calorimeter cell after finishing a reverse ITC run for the complexation of *E*-**2** with **1**. A 5 mM solution of *Z*-**2** in CDCl$_3$ was placed in a NMR tube and irradiated with a LED source at 450 nm for 7 min until the PSS. Then, an aliquot was taken from the irradiated solution and diluted to 0.3 mM for use in the ITC experiment. The ITC run was carried out by timed injection of 15 μl of a 2.1 mM solution of the host into the 0.3 mM solution of the guest in the same solvent. b) Photoirradiated solution at 450 nm of the *Z*-**2**⊂**1** complex during 60 min. Primed letters and numbers correspond to proton signals of bound components. Double primed letters and numbers correspond to proton signals of irradiated bound components. * Residual solvents peaks.
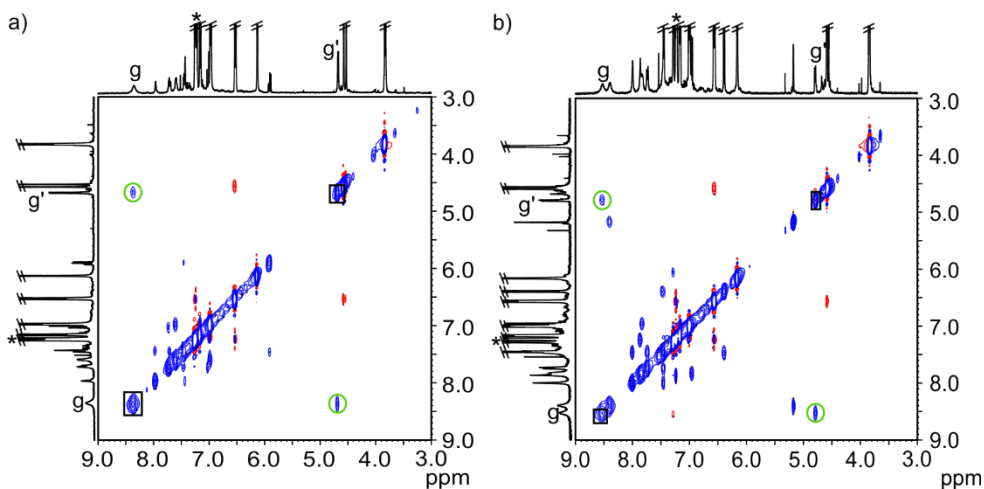

Figure 2.40 Selected regions of the 2D ^{1}H EXSY NMR (500 MHz, CDCl$_3$, 298 K) experiments (t_{mix} = 0.3 s) of a) *Z*-**2**+**1** and b) *Z*-**3**+**1** (2:1 molar ratio). Primed letters correspond to proton signals of the guest in the inclusion complex *Z*-**2**/**3**⊂**1**. Diagonal and EXSY cross-peaks are positive (blue) and NOESY cross-peaks are negative (red).

Chapter 2

Figure 2.41 a) ^{1}H NMR analysis of the kinetics of thermal *E*-to-*Z* isomerization of a 1.7 mM solution of **2** in CDCl₃ at RT. Starting point is a mixture of *Z*-**2** and *E*-**2** in a ratio of 14:86. The starting *E*:*Z* ratio is reversed after 4 h of thermal equilibration. The composition in the *E*-**2** isomer was determined from the integration of protons H^{d‡} of the *E* isomer and H^d of the *Z* counterpart. The concentration in the *E* conformers was then calculated from the mass balance [**2**] = [*Z*-**2**] + [*E*-**2**]. b) First order kinetic analysis of the ^{1}H NMR data recorded every 5 min at RT for 6 h of thermal equilibration.
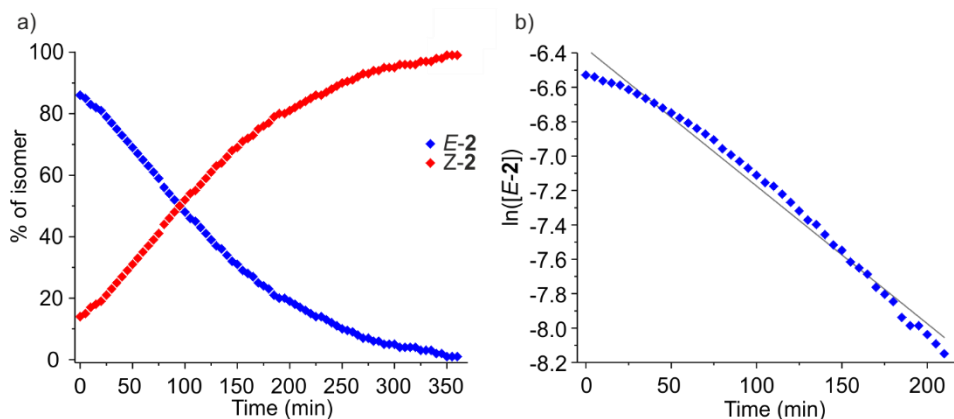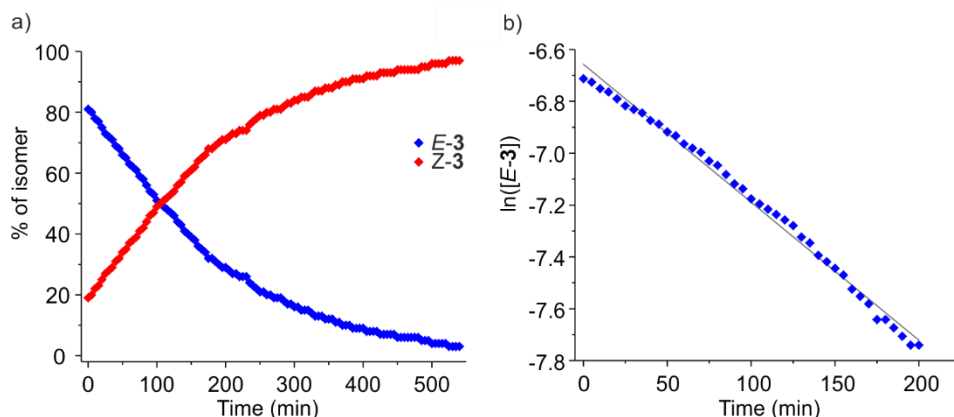

Figure 2.42 a) ^{1}H NMR analysis of the kinetics of thermal *E*-to-*Z* isomerization of a 1.5 mM solution of **3** in CDCl₃ at RT. Starting point is a mixture of *Z*-**3** and *E*-**3** in a ratio of 19:81. The starting *E*:*Z* ratio is reversed after 5 h of thermal equilibration. The composition in the *E*-**3** isomer was determined from the integration of protons H^{c‡} of the *E* isomer and H^c of the *Z* counterpart. The concentration in the *E* conformers was then calculated from the mass balance [**3**] = [*Z*-**3**] + [*E*-**3**]. b) First order kinetic analysis of the ^{1}H NMR data recorded every 5 min at RT for 9 h of thermal equilibration.

The concentration changes in the *E* isomers were fit to a first-order kinetic equation and the rate constant (*k*) (3), half-life (*t*$_{1/2}$) (4) and energy barrier ($\Delta G^\#$) (5) values were determined. The first-order rate constant $k_{(therm.\ E \rightarrow Z)}$ is the slope of the linear fit:[15]

(1) *Z*-**2** → *E*-**2** or *Z*-**3** → *E*-**3**
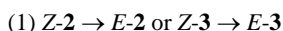
(2) d[*Z*-**2**]/dt = -d[*E*-**2**]/dt = $k_1 \cdot$[*E*-**2**] or d[*Z*-**3**]/dt = -d[*E*-**3**]/dt = $k_2 \cdot$[*E*-**3**]

94

2-(4'-Pyridyl-N-oxide)-substituted hemithioindigos as photoresponsive guests for a super aryl-extended calix[4]pyrrole receptor

(3) $\ln[E\text{-}2] = \ln[E\text{-}2]_0 - k_1 \cdot t$ or $\ln[E\text{-}3] = \ln[E\text{-}3]_0 - k_2 \cdot t$; $k = k_{(therm.\ E \to Z)}$ = rate constant

(4) $t_{1/2} = (\ln 2)/k$; $t_{1/2}$ = half-life

(5) $k = (k_B \cdot T/h) \cdot e^{(-\Delta G\#/RT)}$; k_B = Boltzmann's constant; h = Planck's constant; R = Gas constant; T = Temperature and $\Delta G^{\#}$ = Energy barrier.

Figure 2.43 a) ^{1}H NMR analysis of the kinetics of thermal *E*-to-*Z* isomerization of a 1.7 mM solution of **2⊂1** in CDCl$_3$ at RT. Starting point is a mixture of *Z*-**2⊂1** and *E*-**2⊂1** in a ratio of 27:73. The *Z*-**2⊂1** complex is quantitatively restored after 17 h. The concentration in the *E* complex was determined from the pyrrolic N-H$^{1'}$ bound protons assigned to the *E* and *Z* counterparts and the mass balance [**2⊂1**] = [*Z*-**2⊂1**] + [*E*-**2⊂1**]. b) First order kinetic analysis of the ^{1}H NMR data recorded every 30 min at RT for 10 h of thermal equilibration.
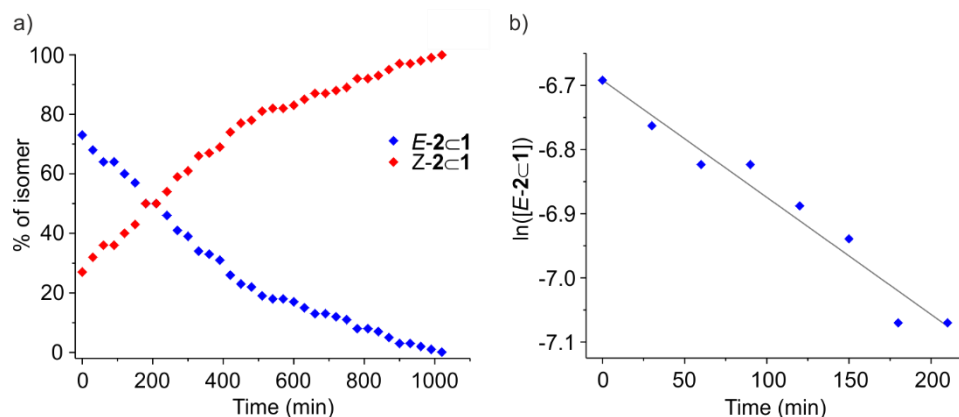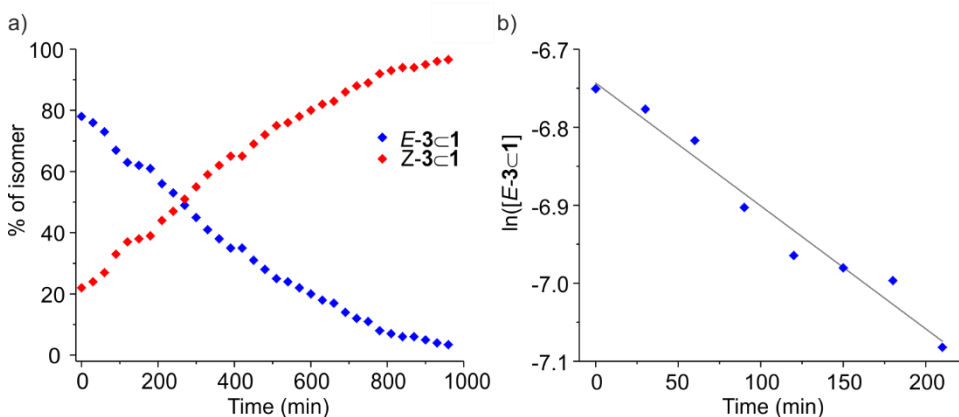

Figure 2.44 a) ^{1}H NMR analysis of the kinetics of thermal *E*-to-*Z* isomerization of a 1.5 mM solution of **3⊂1** in CDCl$_3$ at RT. Starting point is a mixture of *Z*-**3⊂1** and *E*-**3⊂1** in a ratio of 22:78. The *Z*-**3⊂1** complex is quantitatively restored after 16 h. The concentration in the *E* complex was determined from the pyrrolic N-H$^{1'}$ bound protons assigned to the *E* and *Z* counterparts and the mass balance [**3⊂1**] = [*Z*-**3⊂1**] + [*E*-**3⊂1**]. b) First order kinetic analysis of the ^{1}H NMR data recorded every 30 min at RT for 10 h of thermal equilibration.
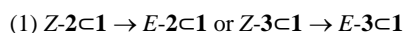
Chapter 2

The concentration changes in the *E* complexes were fit to a first-order kinetic equation and the rate constant (k) (3), half-life ($t_{1/2}$) (4) and energy barrier ($\Delta G^{\#}$) (5) values were determined.

(1) Z-**2**⊂**1** → E-**2**⊂**1** or Z-**3**⊂**1** → E-**3**⊂**1**

(2) d[Z-**2**⊂**1**]/dt = -d[E-**2**⊂**1**]/dt = k_1[E-**2**⊂**1**] or d[Z-**3**⊂**1**]/dt = -d[E-**3**⊂**1**]/dt = k_2[E-**3**⊂**1**]

(3) ln[E-**2**⊂**1**] = ln[E-**2**⊂**1**]$_0$ – k_1·t or ln[E-**3**⊂**1**] = ln[E-**3**⊂**1**]$_0$ – k_2·t; k = $k_{(therm. E \rightarrow Z)}$ = rate constant

(4) $t_{1/2}$ = (ln 2)/k; $t_{1/2}$ = half-life

(5) k = (k_B·T/h)·e $^{(-\Delta G\#/RT)}$; k_B = Boltzmann's constant; h = Planck's constant; R = Gas constant; T = Temperature and $\Delta G^{\#}$ = Energy barrier.

Eq. of Z-**2**	[Z-**2**] (mM)	δ_{obs}	δ_{calc}
0.12	0.5	5.904	5.898
0.25	1.1	5.910	5.906
0.5	2.3	5.923	5.921
0.75	3.4	5.938	5.934
1	4.6	5.946	5.946
1.5	6,9	5.962	5.966
2	9.2	5.98	5.982
3	13.8	6.006	6.006
5	23	6.036	6.035

Table 2.6 Chemical shifts of the proton signals of Z-**2** (δ, ppm) and complexation induced chemical shifts ($\Delta\delta$, ppm) between free and bound guest to receptor **10** in CDCl$_3$.

2-(4'-Pyridyl-N-oxide)-substituted hemithioindigos as photoresponsive guests for a super aryl-extended calix[4]pyrrole receptor

2.5 References and notes

[1] D. H. Qu, Q. C. Wang, Q. W. Zhang, X. Ma, H. Tian, *Chem. Rev.* **2015**, *115*, 7543-7588.

[2] A. Ueno, K. Takahashi, T. Osa, *J. Chem. Soc., Chem. Commun.* **1980**, 837-838.

[3] G. Yu, C. Han, Z. Zhang, J. Chen, X. Yan, B. Zheng, S. Liu, F. Huang, *J. Am. Chem. Soc.* **2012**, *134*, 8711-8717.

[4] T. Ogoshi, K. Kida, T.-a. Yamagishi, *J. Am. Chem. Soc.* **2012**, *134*, 20146-20150.

[5] H. Huang, A. Juan, N. Katsonis, J. Huskens, *Tetrahedron* **2017**, *73*, 4913-4917.

[6] J. del Barrio, S. T. J. Ryan, P. G. Jambrina, E. Rosta, O. A. Scherman, *J. Am. Chem. Soc.* **2016**, *138*, 5745-5748.

[7] M. M. Lerch, M. J. Hansen, W. A. Velema, W. Szymanski, B. L. Feringa, *Nat. Commun.* **2016**, *7*, 12054.

[8] H. Dube, D. Ajami, J. Rebek, Jr., *Angew. Chem., Int. Ed.* **2010**, *49*, 3192-3195.

[9] G. H. Clever, S. Tashiro, M. Shionoya, *J. Am. Chem. Soc.* **2010**, *132*, 9973-9975.

[10] H. Dube, J. Rebek, *Angew. Chem., Int. Ed.* **2012**, *51*, 3207-3210.

[11] K. Tanaka, K. Kohayakawa, S. Iwata, T. Irie, *J. Org. Chem.* **2008**, *73*, 3768-3774.

[12] S. Wiedbrauk, H. Dube, *Tetrahedron Lett.* **2015**, *56*, 4266-4274.

[13] S. Kitzig, M. Thilemann, T. Cordes, K. Rück-Braun, *ChemPhysChem* **2016**, *17*, 1252-1263.

[14] F. Kink, M. P. Collado, S. Wiedbrauk, P. Mayer, H. Dube, *Chem. Eur. J.* **2017**, *23*, 6237-6243.

[15] M. Guentner, M. Schildhauer, S. Thumser, P. Mayer, D. Stephenson, P. J. Mayer, H. Dube, *Nat. Commun.* **2015**, *6*, 8406.

[16] L. A. Huber, K. Hoffmann, S. Thumser, N. Böcher, P. Mayer, H. Dube, *Angew. Chem., Int. Ed.* **2017**, *56*, 14536-14539.

[17] M. Guentner, E. Uhl, P. Mayer, H. Dube, *Chem. Eur. J.* **2016**, *22*, 16433-16436.

[18] S. Wiedbrauk, T. Bartelmann, S. Thumser, P. Mayer, H. Dube, *Nat. Commun.* **2018**, *9*, 1456.

[19] S. Wiedbrauk, B. Maerz, E. Samoylova, A. Reiner, F. Trommer, P. Mayer, W. Zinth, H. Dube, *J. Am. Chem. Soc.* **2016**, *138*, 12219-12227.

[20] J. E. Zweig, T. R. Newhouse, *J. Am. Chem. Soc.* **2017**, *139*, 10956-10959.

[21] L. Escobar, G. Aragay, P. Ballester, *Chem. Eur. J.* **2016**, *22*, 13682-13689.

[22] H. Meier, W. Luettke, *Liebigs Ann. Chem.* **1981**, 1303-1333.

[23] A. McKillop, D. Kemp, *Tetrahedron* **1989**, *45*, 3299-3306.

[24] A. D. Dunn, *Org. Prep. Proced. Int.* **1999**, *31*, 120-123.

[25] L. S. S. Reamonn, W. I. O'Sullivan, *J. Chem. Soc. Perkin Trans. 1* **1977**, 1009-1012.

[26] The photoirradiation at λ = 450 nm of a millimolar solution of super aryl-extended calix[4]pyrrole **1** in chloroform resulted in its total decomposition after 1 h. This indicated that the highly efficient light-absorption properties of included HTI **2** inhibited photodegradation of the receptor to a significant extent.

[27] The Eyring-Polanyi equation was used to calculate the energy barrier ($\Delta G^{\ddagger}$): $k = ((k_B T)/h)e^{(-\Delta G^{\ddagger}/RT)}$, where k is the rate constant, k_B is the Boltzmann constant ($1.38 \cdot 10^{-23}$ J·K^{-1}), T is the temperature, h is the Planck constant ($6.63 \cdot 10^{-34}$ J·s), and R is the ideal gas constant (8.31 J·mol^{-1}·K^{-1}).

[28] J. E. Leffler, E. Grunwald, *Rates and Equilibria of Organic Reactions*, Wiley, New York, **1963**.

[29] G. Aragay, D. Hernandez, B. Verdejo, E. C. Escudero-Adan, M. Martinez, P. Ballester, *Molecules* **2015**, *20*, 16672-16686.

[30] P. Ballester, S. M. Biros, in *The Importance of Pi-Interactions in Crystal Engineering*, John Wiley & Sons, Ltd, **2012**, pp. 79-107.

[31] A. R. Viguera, L. Serrano, *Biochemistry* **1995**, *34*, 8771-8779.

[32] K. N. M. Daeffler, H. A. Lester, D. A. Dougherty, *J. Am. Chem. Soc.* **2012**, *134*, 14890-14896.

[33] J. C. Gómez-Tamayo, A. Cordomí, M. Olivella, E. Mayol, D. Fourmy, L. Pardo, *Protein Sci.* **2016**, *25*, 1517-1524.

[34] J. D. Dunitz, *Chem. Biol.* **1995**, *2*, 709-712.

[35] L. Escobar, F. A. Arroyave, P. Ballester, *Eur. J. Org. Chem.* **2017**, 1097-1106.

[36] A. D. Dunn, *Org. Prep. Proced. Int.* **1999**, *31*, 120-123.

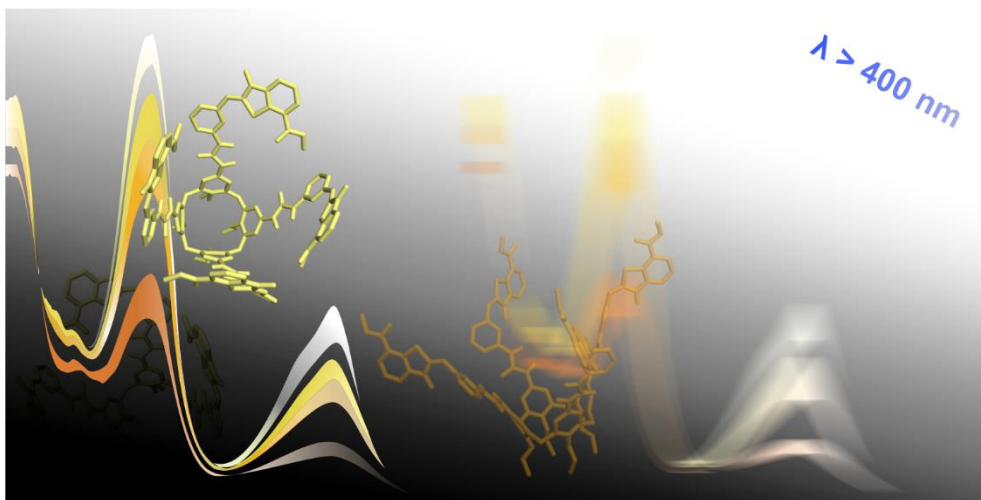[37] A. McKillop, D. Kemp, *Tetrahedron* **1989**, *45*, 3299-3306.

UNIVERSITAT ROVIRA I VIRGILI
STIMULI-RESPONSIVE HOST-GUEST SYSTEMS DECORATED WITH HEMITHIOINDIGO AND SPIROPYRAN UNITS
Giulia Moncelsi

Chapter 3

Synthesis of hemithioindigo-decorated tetraurea calix[4]arenes. Study of their dimerization into capsular assemblies

Unpublished results

Synthesis of hemithioindigo-decorated tetraurea calix[4]arenes. Study of their dimerization into capsular assemblies

3.1 Introduction

In the previous chapter, we have described two hemithioindigo-hemistilbene (HTI) 2-(4'-pyridyl)-*N*-oxides that were used as photoresponsive guests for inclusion in the deep aromatic cavity of a super aryl-extended calix[4]pyrrole. While working on the synthesis of these organic photoswitches, we envisaged the covalent functionalization of a tetraurea calix[4]arene scaffold with multiple photoresponsive HTI units in order to modulate its dimerization process in capsular assemblies. In recent years, there has been a considerable increase in the design of light-responsive molecular containers and their application in supramolecular[1,2] and materials chemistry.[3,4] We focused our attention on tetraurea derivatives of calix[4]arenes in *cone* conformation.[5] These compounds are known to dimerize quantitatively in non-polar organic solution affording discrete capsular assemblies,[6,7] which can be further functionalized to perform specific chemical tasks.[8] For instance, azobenzene photoswitches[9] were incorporated in calix[4]arene scaffolds,[10,11] at both their upper[12,13] and lower rims.[14,15,16] In 2015, our group reported a series of tetraurea calix[4]arenes (tuC[4]As **1a-c**, Figure 3.1) decorated with differently substituted azobenzene groups at their upper rims. The prepared tetra-azobenzene tetraurea derivatives underwent a reversible *trans/cis* photoisomerization upon UV light-irradiation (λ = 365 nm) and subsequent thermal equilibration in the dark.[17] In a sequel, we demonstrated the exclusive assembly of the tetra-azobenzene tetraurea calix[4]arene **1b** with a tetraurea calix[4]pyrrole counterpart in a heterodimeric capsule.[18] This result was in agreement with the previously reported self-sorting dimerization process exhibited by structurally related tetraureas not incorporating the photoswitchable units.[19,20,21,22] More interestingly, the reversible photoisomerization of the appended azo groups in (all-*trans*)-capsular dimers yielded *cis*-enriched counterparts *(tttc*; *ttcc*; *tctc*; *tccc*; *cccc)* in equilibrium with non-capsular aggregates. This methodology allowed the control of the assembly/disassembly process of capsular dimers and the concomitant uptake and release of polar guests using light irradiation.
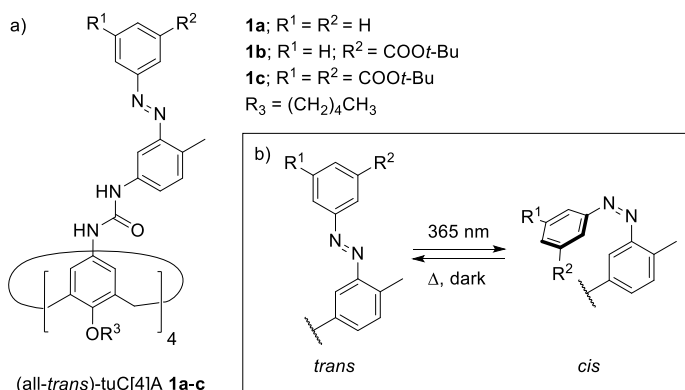
Chapter 3

Figure 3.1 Schematic representation of the a) (all-*trans*)-tetra-azo tetraurea calix[4]arenes **1a-c** and b) *trans*/*cis* switching of the attached azobenzene fragments.[17,18]

Inspired by these works, we designed two tetraurea calix[4]arenes containing four hemithioindigo (HTI) units at their upper rim (Scheme 3.1). Our aim was to couple the *Z*/*E* isomerization process of the HTIs with the assembly/disassembly process of the capsular aggregates resulting from the dimerization process of the tetraurea calix[4]arenes decorated with HTI units. In principle, the possibility of using a visible light-input ($\lambda > 400$ nm) for the isomerization of the HTIs constitutes an advantage with respect to our previous photoswitchable designs based on UV light-irradiation. In due course, such containers were expected to provide systems for transport and release of cargo compatible with biological applications owing to the less-damaging energy of the light employed in the isomerization process.

Herein, we describe the synthesis of two tetrahemithioindigo tetraurea calix[4]arenes. We report preliminary studies of the dimerization process of the synthesized tetraurea derivatives into capsular aggregates. We describe our attempts to encapsulate tetramethylphosphonium cation in the putative dimeric aggregates assembled in solution.

3.2 Results and discussion

3.2.1 Design and synthesis

The macrocyclic building blocks for the synthesis of our target compounds were the known tetra-amino[23] (**6**, Figure 3.25) and tetracarbamate[17] (**7**, Figure 3.26) calix[4]arene derivatives. For the synthesis of the HTI switching units, we developed a synthetic route that started with a Fischer's esterification reaction of thiosalicylic acid with EtOH.[24] Next, the nucleophilic

Synthesis of hemithioindigo-decorated tetraurea calix[4]arenes. Study of their dimerization into capsular assemblies

substitution reaction of the obtained (2-carboxyethyl)benzene thiol with 2-bromoacetic acid afforded the aryl thioglycolic acid **9** (see the experimental part for more details). The labile thioindoxyl **8** was prepared by intramolecular Friedel-Crafts acylation reaction of the "in situ" prepared acyl chloride of **9**. The HTI photoswitches bearing terminal amino and diethyl ester groups were prepared by reacting **8** with the commercially available *m*-amino-, *p*-amino- or *p*-aminomethyl- benzaldehyde. The conditions of the Knoevenagel condensation reaction were adapted to the synthesis of HTI derivatives.[25] Finally, cleavage of the *N*-Boc protecting group with trifluoroacetic acid afforded free amines **3**, **4** and **5**. The aminomethyl-HTI **5** was reacted with *p*-nitrochloroformate to afford the corresponding carbamate derivative **5b**. The X-ray structures of the prepared amino- and carbamate-HTI derivatives showed that in the solid state all compounds adopted the *Z*-conformation (Figure 3.2). In solution and at ambient conditions, the ^{1}H NMR spectra of the isolated solids evidenced the existence of **3**, **4** and **5a** as mixtures of *Z/E* photoisomers in different ratios. However, the use of an amber NMR tube prior to the dissolution of the compound for the spectroscopic analysis, or heating the solutions of *Z/E* isomers protected from light, produced ^{1}H NMR spectra displaying exclusively the proton signals corresponding to the *Z* isomers. We assigned the configuration of the HTI derivatives based on the methodology described in chapter 2.[26]
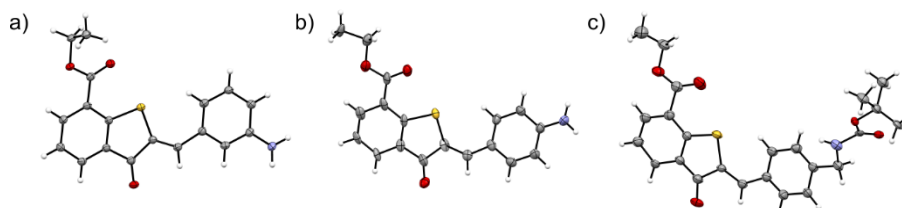

Figure 3.2 Preliminary single crystal X-Ray structures of compounds a) *Z*-**3**, b) *Z*-**4** and c) *Z*-**5a** (thermal ellipsoids set at 50% probability and hydrogen atoms shown as fixed spheres of 0.15 Å).

Amino-HTI *Z*-**3** was reacted with tetracarbamate (**7**) to produce the tetra-HTI tetraurea calix[4]arene, *Z*-**1**. On the other hand, the tetra-amino (**6**) calix[4]arene was coupled with four equiv. of the carbamate-HTI **5b** affording tetra-HTI tetraurea calix[4]arene, *Z*-**2**.[27,28] Both tetra-HTI tetraurea calix[4]arenes were obtained as the (all-*Z*)-**1** and (all-*Z*)-**2** in moderate yields after purification of the reaction crudes (Scheme 3.1).
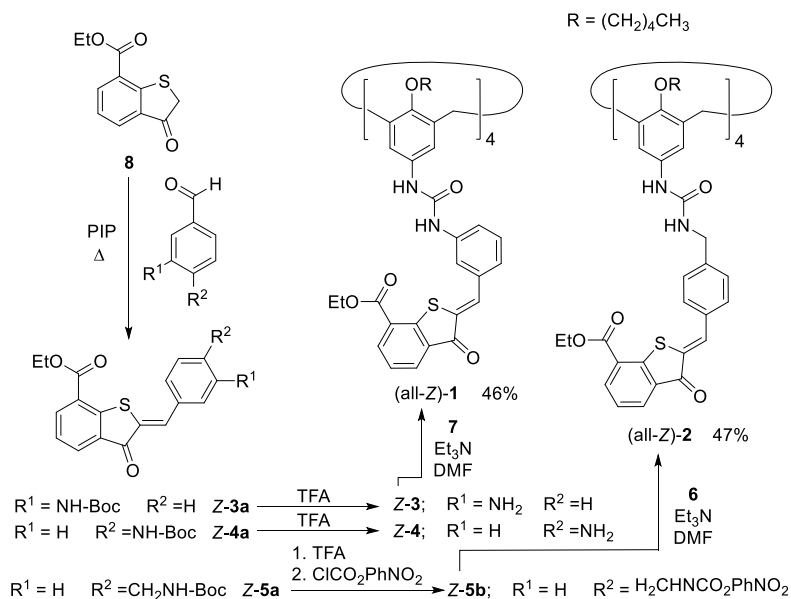
Chapter 3

Scheme 3.1 Synthetic routes for the preparation of the hemithioindigo derivatives and the corresponding tetra-HTI tetraurea calix[4]arenes described in this chapter. The tetra-amino (**6**) and tetracarbamate calix[4]arene (**7**) derivatives were prepared according to reported procedures.[17,29]

Surprisingly, while the synthesis of tetra-HTI tetraurea calix[4]arene (all-*Z*)-**1** from amino-derivative *Z*-**3** was straightforward, the preparation of (all-*Z*)-**2** from the carbamate-HTI derivative *Z*-**5b** and the tetra-amino calix[4]arene **6** proved to be tricky. In our hands, this reaction could not be scaled up. The coupling of the amino-HTI *Z*-**4** with calix[4]arene tetracarbamate **7** did not lead to the isolation of the expected tetra-HTI tetraurea calix[4]arene. Most likely, the HTI *Z*-**4** featuring the amino substituent in *para* position had an even reduced reactivity in the nucleophilic reaction with tetracarbamate **7** than the *meta*-amino-HTI *Z*-**3**, leading to the recovery of the starting HTI. The preparation of *Z*-**1** and *Z*-**2** was also undertaken using the complementary reaction conditions, that is coupling the carbamate of the HTI with the tetra-amino calix[4]arene **6** and the tetracarbamate calix[4]arene **7** with the amino-HTI, respectively. However, the reaction conditions described above provided better yields.

3.2.2 Photoisomerization studies of HTI-**3a** and the tetraurea monomers

Initially, we analyzed the photoisomerization process of the hemithioindigo **3a** by means of ^{1}H NMR and UV/Vis spectroscopies. The ^{1}H NMR spectrum of **3a** under ambient conditions

Synthesis of hemithioindigo-decorated tetraurea calix[4]arenes. Study of their dimerization into capsular assemblies

revealed the existence of the compound as a mixture of *Z/E* isomers in 83:17 ratio. We obtained a ^{1}H NMR spectrum displaying the exclusive signals of the protons of the *Z*-**3a** isomer by dissolving the isolated solid in an amber NMR tube. We probed the photoisomerization process of a 30 μM chloroform solution of *Z/E*-**3a** using UV/Vis spectroscopy. Based on literature precedents, the initial irradiation of the mixture with 425 nm light produced spectral changes that are consistent with a preferential *Z*-to-*E* isomerization of the photoswitch.[29,30,31,32,33] We reached a PSS enriched in the *E*-**3a** isomer after 5 min of irradiation. During the irradiation process, we observed the emergence of an isosbestic point at 452 nm. At the PSS, the strongest absorption band of the *E*-**3a** enriched mixture has a maximum at 449 nm. Subsequently, we irradiated the solution with 475 nm light for 5 min. The resulting absorption spectrum was consistent with the almost quantitative formation of the *Z*-**3a** isomer. For the *Z*-**3a** isomer the largest absorption band is red-shifted compared to the *E*-isomer ($\Delta\lambda$ = +10 nm) displaying a maximum at 439 nm. Analogous irradiation experiments monitored by ^{1}H NMR spectroscopy using a millimolar solution of *Z*-**3a** gave consistent results with those obtained by UV/Vis spectroscopy. A millimolar solution of *Z*-**3a** was photoirradiated (λ = 425 nm) until the PSS was reached (5 min). At the PSS, the composition of the *Z:E* mixture was 9:91 by integration of the diagnostic proton signals assigned to the respective isomers. The sample was irradiated again using 475 nm light for 5min. The new PSS showed a *Z:E* composition of 74:26. This ratio of isomers is similar to the one obtained by letting the solution exposed to ambient light for a whole day (Figure 3.3).
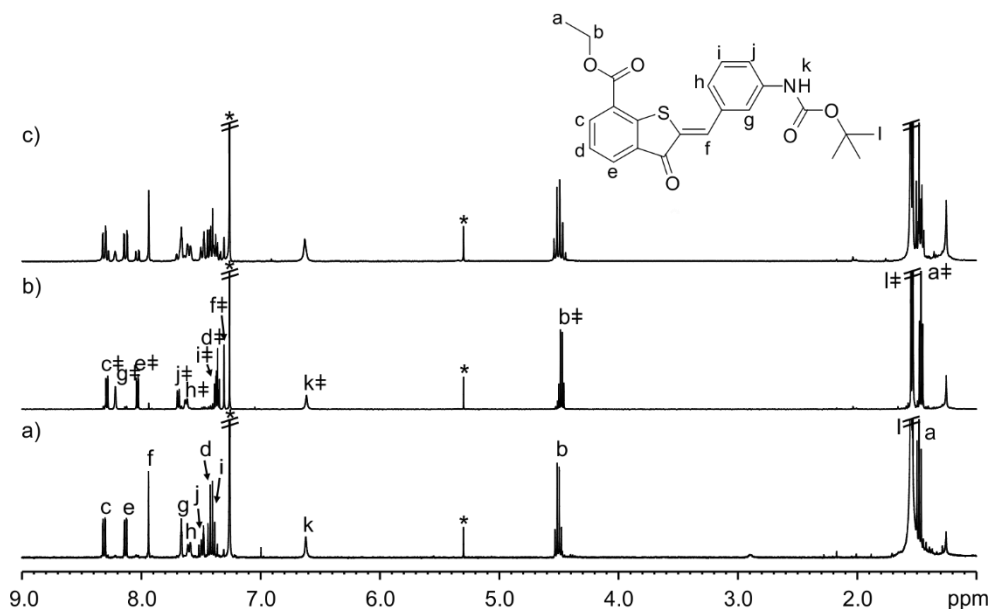
Chapter 3

Figure 3.3 ¹H NMR (CDCl₃, 400 MHz) spectra at 298 K of a 7 mM solution of a) *Z*-**3a**; b) *Z*-**3a** photoirradiated at 425 nm for 5 min (*Z:E* 9:91 ratio) and c) *Z*-**3a** photoirradiated at 475 nm for 5 min (*Z:E* 74:26 ratio). Protons assigned to the *E*-**3a** isomer are marked with a ‡ symbol. * Residual solvents peaks.

Upon irradiation with 425 nm light, the color of the solution changed from yellow to orange. The isomerization state of most hemithioindigos can be detected by the naked eye, because the change in their absorption spectrum takes places in the visible region.

Having studied the photoisomerization properties of a simple HTI derivative, we focused on evaluating the photochemical behavior of receptors **1** and **2** in solution. In polar solvents that compete for hydrogen-bonding interactions with the urea moieties (i.e. dimethyl sulfoxide, dimethylformamide, acetone), receptors **1** and **2** are in the monomeric state and the four covalently attached photoswitchable HTI units can be isomerized to the thermodynamically more stable conformer, (all-*Z*)-**1** and (all-*Z*)-**2**, by thermal equilibration in the dark. Starting from this single isomer, in principle, the four photoresponsive groups appended to the calix[4]arene scaffold can be isomerized by visible light-irradiation producing a mixture containing up to six different conformational isomers (all-*Z*; *Z,Z,Z,E*; *Z,Z,E,E*; *Z,E,Z,E*; *Z,E,E,E* and all-*E*). The mixture should be enriched in the isomers having the HTI units in the *E*-form. We investigated the behavior of (all-*Z*)-**1** to visible light-irradiation ($\lambda = 450$ nm) at micromolar concentration in different solvents using UV/Vis spectroscopy. Interestingly,

106

Synthesis of hemithioindigo-decorated tetraurea calix[4]arenes. Study of their dimerization into capsular assemblies

the absorption spectra of **1** in $(CH_3)_2SO$, $CHCl_3$ and CH_2Cl_2 solutions were very similar and all showed a decrease in the absorbances of the bands centered at *ca*. 325 and 438 nm upon light-irradiation (Figure 3.4). We did not observe shifts to the red for the maxima of these bands. On the contrary, the band having a maximum at 275 nm experienced a slight increase in intensity and a blue-shift. These findings are in striking contrast with our observations for the simple HTI derivative (*vide supra*).
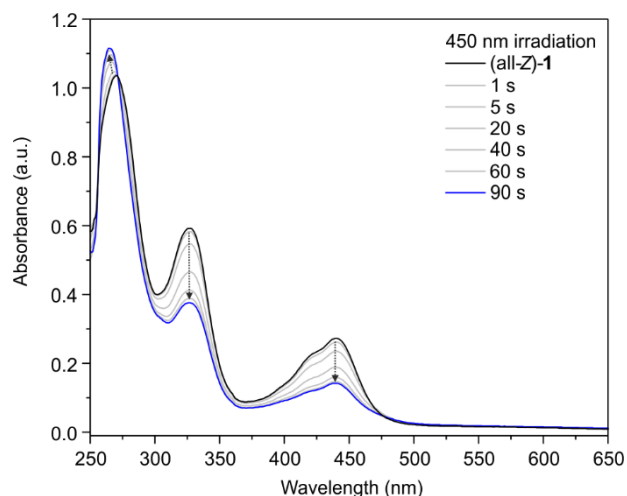

Figure 3.4 UV/Vis absorption spectra of a 10 µM $(CH_3)_2SO$ solution of (all-*Z*)-**1** light-irradiated at 450 nm at different times.

Next, we studied the changes experienced by a millimolar solution of (all-*Z*)-**1** in $(CH_3)_2SO$ to 425 nm visible light-irradiation using ^{1}H NMR spectroscopy (Figure 3.5). After a prolonged irradiation time (30 min), the diagnostic peaks of the tetraurea monomer were not detectable. We continued the irradiation for an additional 60 min: the ^{1}H NMR spectrum of the solution showed multiple broad and ill-defined proton signals and was very similar to the one acquired after the initial 30 min of irradiation. This result is consistent with the *Z*-to-*E* isomerization of the HTI units in **1** producing a complex mixture of isomers having reached the PSS after 30 min. Subsequently, we thermally equilibrated the solution at 80 ºC for 12 h in the dark and recovered, to some extent, the proton signals that are diagnostic to the (all-*Z*)-**1** isomer. We concluded that the photoisomerization process of the HTI units in **1** is reversible but under the employed irradiation conditions compound **1** is not fully photostable.
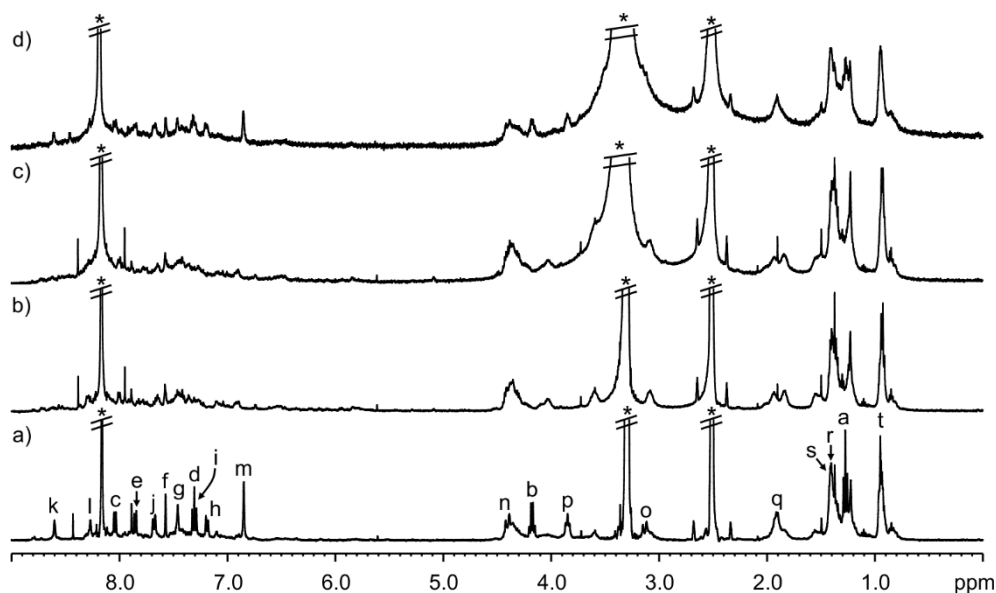
Chapter 3

Figure 3.5 ^{1}H NMR ((CD$_3$)$_2$SO:CDCl$_3$ 70:30, 400 MHz) spectra at 298 K of a millimolar solution of (all-*Z*)-**1** photoirradiated at 425 nm for a) 0, b) 30 and c) 90 min and d) thermally equilibrated at 80 ºC for 12 h. * Residual solvents peaks.

The analysis of an analogous irradiation experiment performed on a millimolar solution of (all-*Z*)-**2** in (CD$_3$)$_2$SO solution using ^{1}H NMR spectroscopy provided similar results to those described for (all-*Z*)-**1** in the same solvent.

3.2.3 Dimerization and photoisomerization studies of **1** and **2** in non-polar organic solvents

We were interested in studying the dimerization of all-*Z* tetra-HTI tetraurea calix[4]arenes **1** and **2** in organic solvents to produce well-defined capsular assemblies. Our aim was to evaluate the coupling of the *Z*-to-*E* photoisomerization process of the HTI units with the assembly/disassembly process of the putative dimeric cage. The energy minimized structure (MM3) of the homodimeric capsule (all-*Z*)-**1**$_2$ is depicted in (Figure 3.6a). The two calix[4]arene components dimerize by establishing an array of 16 hydrogen bonds through the unidirectional orientation of the urea groups. Additionally, the *Z*-HTI substituents of the hemispheres are closely packed without experiencing steric clashes. These observations augured well for the dimerization of the all-*Z* ureas in solution. In contrast, the energy minimized structure of the (all-*E*)-**1**$_2$ dimer shows a reduced close contact of the *E*-HTI substituents that might translate in a change of the thermodynamic stability of the assembly.

108

Synthesis of hemithioindigo-decorated tetraurea calix[4]arenes. Study of their dimerization into capsular assemblies
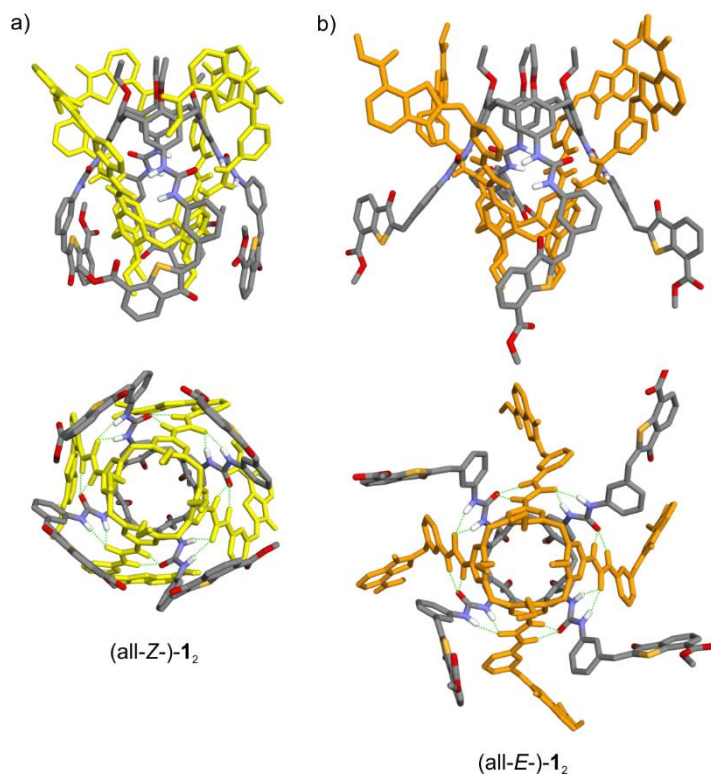

a)

b)

(all-*Z*-)-**1**$_2$

(all-*E*-)-**1**$_2$

Figure 3.6 Side and top views of the energy minimized structures (MM3) of the putative homodimers a) (all-*Z*)-**1**$_2$ and b) (all-*E*)-**1**$_2$. The two tetraurea monomers of **1** are shown as in stick representation, one using the atom color code and the other with all atoms in yellow ((all-*Z*)-**1**$_2$) or orange ((all-*E*)-**1**$_2$). The O-pentyl chains were pruned to ethyl groups and the HTI-ethyl esters were pruned to methyls. Non-polar hydrogen atoms were removed for clarity. Hydrogen bonds are evidenced by green dashed lines in the top view representations.

Unfortunately, the ^{1}H NMR spectra of (all-*Z*)-**1** at millimolar concentrations in chloroform-d, dichloromethane-d$_2$, benzene-d$_6$, nitrobenzene-d$_5$, toluene-d$_8$ and tetrachloroethane-d$_2$ solutions showed broad and not-resolved proton signals. These observations suggested that the (all-*Z*)-**1** tetraurea did not assemble into a structurally well-defined dimeric capsules in any of the solvents. Most likely, (all-*Z*)-**1** prefers to assemble in ill-defined polymeric aggregates. Another sensible explanation is the presence of at least one *E*-arm in the dominant isomer of tetraurea **1** in these solvents. The addition of 0.5 equiv. of tetramethylphosphonium hexafluorophosphate[17] (Me$_4$P$^+$PF$_6^-$, **10**), as a solid, to the solutions above followed by thermal equilibration in the dark did not produce noticeable changes in the corresponding ^{1}H NMR spectra. The Me$_4$P$^+$ cation was expected to act as a template and induce the dimerization of the ureas owing to the good fit with the volume of the aromatic cavity and the formation of additional cation-π interactions. Taken together, these observations indicated that (all-*Z*)-**1**

Chapter 3

did not assemble significantly into dimeric capsules even in the presence of unknown concentrations of the Me_4P^+ cation.

Because the $Me_4P^+PF_6^-$ salt, **10**, had a reduced solubility in the used solvents, we envisaged the possibility to use an alternative anion to increase the salt's solubility and thus the concentration of the Me_4P^+ cation in solution. Hence, we prepared tetramethylphosphonium tetrakis(3,5-bis(trifluoromethyl)phenyl)borate ($BArF^-$) Me_4P^+ salt, **12**. The ^1H NMR spectra of a millimolar solution of (all-*Z*)-**1** in $CDCl_3$ containing incremental amounts of **12** displayed the sharpening of the aromatic proton signals of (all-*Z*)-**1** and the emergence of two separate set of signals for the protons of the Me_4P^+. The doublet resonating at $\delta = 1.5$ ppm corresponds to the methyl protons of Me_4P^+ free in solution. The broad signal appearing at $\delta = -0.90$ ppm was assigned to bound Me_4P^+ (Figure 3.7). The chemical shift value of the bound Me_4P^+ is in nice agreement with the one observed for the same guest encapsulated in tetra-azo tetraurea calix[4]arene dimeric capsules.[17]
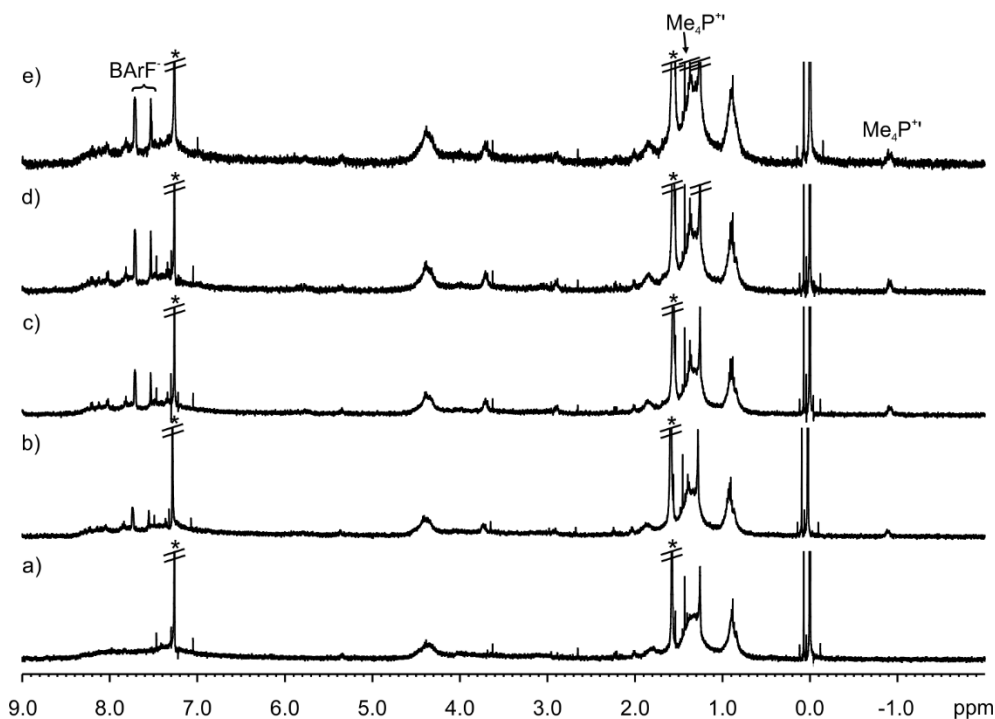

Figure 3.7 ^1H NMR ($CDCl_3$, 500 MHz) spectra at 298 K of a 1 millimolar solution of a) (all-*Z*)-**1** + b) 0.25; c) 0.5; d) 0.75 and e) 1 equiv. of **12**. Primed letters and numbers correspond to proton signals of bound components. * Residual solvents peaks.

Synthesis of hemithioindigo-decorated tetraurea calix[4]arenes. Study of their dimerization into capsular assemblies

We concluded that the Me_4P^+ cation was effective in templating the assembly of (all-*Z*)-**1** in dimeric capsules in $CDCl_3$ solution to a limited extent. Surprisingly, an analogous experiment, performed in CD_2Cl_2 solution (in which **12** is completely soluble) displayed a ^1H NMR spectrum lacking the diagnostic signals of the capsular assembly.

Based on the results obtained with tetraurea (all-*Z*)-**1**, we investigated the dimerization of (all-*Z*)-**2** (Figure 3.8).
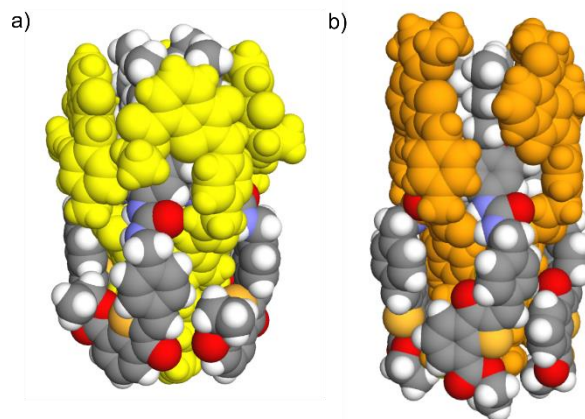

Figure 3.8 Side-view of the energy minimized molecular models (MM3) of the putative homodimeric capsules a) (all-*Z*)-**2**$_2$ and b) (all-*E*)-**2**$_2$. The two tetraurea monomers are shown as CPK models, one using the atom color code and the other with all atoms in yellow ((all-*Z*)-**2**) or orange ((all-*E*)-**2**).

The ^1H NMR spectra of millimolar solutions of (all-*Z*)-**2** in $CDCl_3$ and CD_2Cl_2 revealed that the tetraurea does not assemble into well-defined and discrete homodimers (all-*Z*)-**2**$_2$ (the spectra in these solvents showed broad, ill-defined non-capsular aggregates). The addition of incremental amounts of $Me_4P^+PF_6^-$ (**10**) to a $CDCl_3$ solution of (all-*Z*)-**2** induced the formation of encapsulation complexes, $Me_4P^+ \subset$**2**$_2$, as evidenced by the appearance of a broad doublet resonating at $\delta = -0.92$ ppm and the sharpening of the aromatic proton signals of (all-*Z*)-**2**. Most likely, the encapsulation dimeric complex is in equilibrium with ill-defined, non-capsular aggregates. These latter aggregates constitute the major species present in solution producing the observed base-line broadened proton signals. (Figure 3.9).
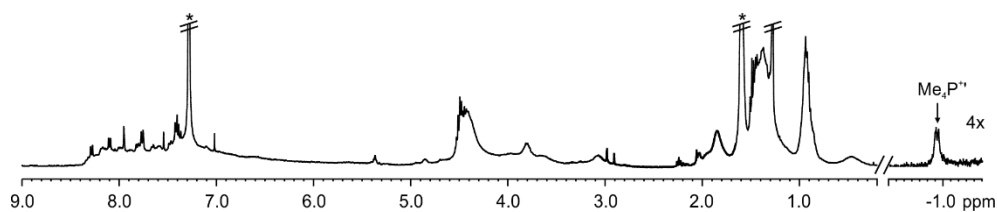
Chapter 3

Figure 3.9 ^{1}H NMR (CDCl$_3$, 400 MHz) spectrum at 298 K of a 0.8 millimolar solution of (all-*Z*)-**2** + 0.5 equiv. of **10** after thermal equilibration at 50 ºC in the dark for 6 h. Primed letters and numbers correspond to proton signals of bound components. * Residual solvents peaks.

We attribute the complexity of the ^{1}H NMR spectra assigned to the dimeric encapsulation complexes Me$_4$P$^+$⊂**1**$_2$ and Me$_4$P$^+$⊂**2**$_2$ to the existence in solution of tetraureas as multiple diastereoisomers owing to their HTI units adopting *E* and *Z* configurations. The observation of a broad doublet for the methyl proton signals of the encapsulated Me$_4$P$^+$ cation provided additional support to the hypothesis of multiple conformers of the tetraureas that can dimerize to form the encapsulation complexes. All our attempts to induce the assembly of heterodimeric capsules of the HTI tetraurea calix[4]arenes with a *p*-tolyl counterpart (**11**)[34,35] were unsuccessful.

It is worthy to note that the low solubility of Me$_4$P$^+$PF$_6^-$ salt **10** in the employed chlorinated solvents hampered the accurate calculation of the equivalents added.

The irradiation at 425 or 450 nm of millimolar solutions of (all-*Z*)-**1** in chloroform-d, dichloromethane-d$_2$, benzene-d$_6$, nitrobenzene-d$_5$, toluene-d$_8$ and tetrachloroethane-d$_2$ did not produce detectable changes in the ^{1}H NMR spectra. We performed light-irradiation experiments with tetra-HTI tetraurea (all-*Z*)-**2** at micromolar concentration. The UV/Vis absorption spectra of a 1 µM chloroform solution of receptor (all-*Z*)-**2** registered at different times during light-irradiation at 450 nm are showed in Figure 3.10.

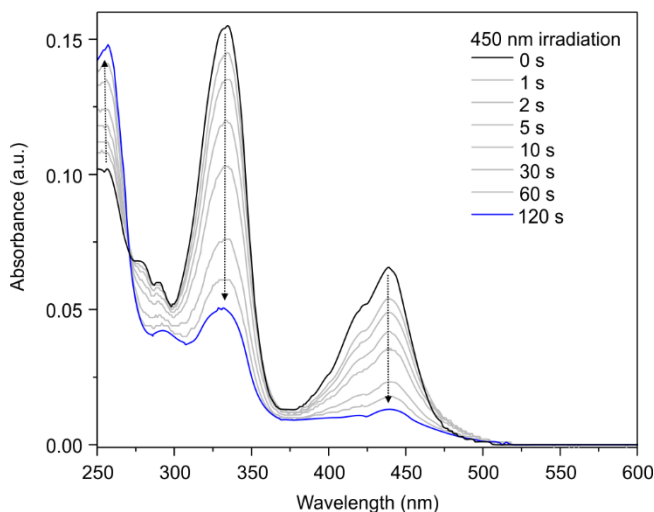*Synthesis of hemithioindigo-decorated tetraurea calix[4]arenes. Study of their dimerization into capsular assemblies*

Figure 3.10 UV/Vis absorption spectra of a 1 µM CHCl₃ solution of (all-*Z*)-**2** light-irradiated at 450 nm at different times.

The changes observed by UV/Vis spectroscopy are in line with those discussed above for (all-*Z*)-**1**.

3.3 Conclusions

In this chapter, we have presented the synthesis of different hemithioindigo derivatives and their incorporation onto a macrocyclic calix[4]arene scaffold. We initially probed the visible light-induced *Z/E* photoisomerization of HTI **3a**, which was consistent with the photochemical behavior of reported hemithioindigo analogs. Afterwards, we were able to isolate moderate amounts of the desired tetraurea compounds in their thermodynamically stable conformations (all-*Z*)-**1** and (all-*Z*)-**2**. They were used in photophysical and binding studies in different organic solvents and in the presence of tetramethylphosphonium cation as the target guest for the binding cavity of the hosts.

We showed the nice photochemical and photophysical behavior of the simple HTI **3a** by UV/Vis and ¹H NMR techniques. However, the absorption profiles of visible light-irradiated solutions of (all-*Z*)-**1** and (all-*Z*)-**2** indicated that their "aggregates" in apolar organic solvents do not experience the blue- or red-shifts typical of the *E*-HTI isomers. The lack of these characteristic photochromic feature might explain in part the absence of changes in the NMR spectra upon irradiation of the encapsulation complexes of **1** and **2**, indicative of a reduced/hampered switching of the responsive fragments.

Chapter 3

Finally, the exclusive self-assembly into discrete capsules was not achieved when the responsive units were incorporated onto the calix[4]arene scaffold. The use of Me_4P^+ salts as the designed guests (with either PF_6^- or $BArF^-$ as counteranions) did not favor the homodimerization of tetraureas (all-*Z*)-**1** and (all-*Z*)-**2**. The scarce amount of **2** synthesized did not allow us to perform complete titrations and additional ^1H NMR experiments using guest **12**. However, with the experimental data available we could conclude that these types of functionalized macrocycles are not the ideal candidates for the construction of photoresponsive capsular architectures. In fact, the only response to the external light stimulus was detected in the case of the tetra-HTI tetraurea monomers by NMR studies in dimethyl sulfoxide solution. Analogous systems with the HTI switches directly attached to the macrocyclic core (thus lacking the urea moieties responsible for the formation of capsular/non-capsular aggregates) could be devised as unimolecular receptors to explore their photochemical and molecular recognition properties in apolar organic solvents.

3.4 Experimental section

3.4.1 General information and instrumentation

All syntheses were carried out using chemicals as purchased from commercial sources unless otherwise noted. All commercial solvents and chemicals were of reagent grade quality and were used without further purification except as noted. Dry solvents were taken from a solvent system MB SPS 800 (*MBraun*) and freshly distilled unless otherwise stated. Thin-layer chromatography (TLC) and flash column chromatography were performed with DC-Alufolien Kieselgel 60 F_{254} (*Merck*) and silica gel 60 Å for chromatography (*Sigma-Aldrich*), respectively. Routine ^1H and ^{13}C NMR spectra were recorded on *Bruker* Avance 300 (300 MHz for ^1H NMR), Avance 400 (400 MHz for ^1H NMR) or Avance 500 (500 MHz for ^1H NMR) ultrashield spectrometers, or on a *Bruker* Avance III 500 with a QNP cryoprobe. Deuterated solvents (*Sigma-Aldrich*) used are indicated in the characterization and chemical shifts are given in ppm. Residual solvent peaks were used as reference. All NMR *J* values are given in Hz. High Resolution Mass Spectrometry (HRMS) experiments were performed on a MicroTOF, *Bruker Daltonics ESI*. The diagnostic peaks are reported in m/z units. UV/Vis spectra were recorded on a *Shimadzu* UV-2401PC spectrophotometer (equipped with a photomultiplier detector, double beam optics and D_2 and W light sources). The spectra were recorded in a quartz cuvette (10 mm path length). IR spectra were recorded on a *Bruker*

Optics FT-IR Alpha spectrometer equipped with a DTGS detector, KBr beam splitter at 4 cm^{-1} resolution using a one bounce ATR accessory with diamond windows. Melting points were measured on a MP70 Melting Point System instrument from *Mettler Toledo*. Elemental analyses were carried out with a microanalyzer *LECO* CHNS-932. Irradiation experiments for the HTI derivatives and tetra-HTI tetraurea calix[4]arenes were conducted either by choosing the appropriate wavelength (λ = 425 and 475 nm) on a custom-made portable photoreactor, or by using a single high power LED-diode from *Roithner Lasertechnik GmbH* (450 nm, 26 mW·cm^{-2}) mounted on a heat sink from *Fischer Elektronik*.

3.4.2 Synthetic procedures

Ethyl 2-mercaptobenzoate: commercially available thiosalicylic acid (5 g, 32.4 mmol, 1 equiv.) was dissolved in 300 mL anhydrous EtOH. Then, 3 mL of H_2SO_4 (37.5 mmol, 1.1 equiv.) were added dropwise and the solution was refluxed at 100°C for 3 days under argon atmosphere. Afterwards, the excess solvent was removed under reduced pressure leaving around 50 mL, then solid NaHCO$_3$ was added until pH = 4-5. 50 mL of DCM were added, and the solution washed with 100 mL water; then, the organic phase was dried over sodium sulfate and concentrated to dryness to afford a colorless oil (4.58 g, 77% yield). R$_f$ = 0.67 (Hex:Et$_2$O 3:1). HRMS (ESI-TOF): m/z calcd. for $C_9H_{10}NaO_2S$ [M+Na]$^+$: 205.0294; found: 205.0285. ^{1}H NMR (CDCl$_3$, 500 MHz) δ (ppm): 8.01 (d, *J* = 7.8 Hz, 1H); 7.29 (dd, *J* = 5.1, 2.9 Hz, 2H); 7.14 (m, *J* = 8.2 Hz, 1H); 4.69 (s, 1H); 4.38 (q, *J* = 7.1 Hz, 2H); 1.39 (t, *J* = 7.1 Hz, 3H). ^{13}C NMR (CDCl$_3$, 126 MHz) δ (ppm): 166.8; 138.2; 132.4; 131.7; 130.9; 126.3; 124.7; 61.3; 14.3. FT-IR ν (cm^{-1}) = 2981; 2549 (S–H stretching); 1698 (C=O stretching); 1589; 1564; 1467; 1436; 1390; 1367; 1286; 1250 (C–O stretching); 1168; 1144; 1112; 1060 (C–O stretching); 1015; 969; 871; 789; 740; 690; 652; 524; 490.

Tetra-HTI tetraurea calix[4]arene (all-*Z*)-**1**: tetracarbamate calix[4]arene **6** (42 mg, 0.03 mmol, 1 equiv.) was dissolved in 1 mL anhydrous DMF and added to a Schlenk tube under Ar atmosphere. To this solution, 25 μl of dry Et$_3$N (0.178 mmol, 6 equiv.) were added with a syringe. Finally, hemithioindigo Z-**3** (53 mg, 0.163 mmol, 5.49 equiv.) previously dissolved in 1 mL anhydrous DMF was added to the reaction vessel. The solution was stirred at 50 °C for 24 h under argon atmosphere, protected from light. Afterwards, the reaction mixture was added dropwise to 20 mL of water, and stirred for a couple of minutes upon formation of a yellow suspension. The precipitate was vacuum filtered, washed thoroughly with water to

UNIVERSITAT ROVIRA I VIRGILI
STIMULI-RESPONSIVE HOST-GUEST SYSTEMS DECORATED WITH HEMITHIOINDIGO AND SPIROPYRAN UNITS
Giulia Moncelsi

Chapter 3

remove *p*-nitrophenol and air dried. The resulting solid was purified by column chromatography on silica gel (DCM:MeOH 99:1): the isolated fraction was dissolved in 2 mL DCM and precipitated with an equal amount of diethyl ether. The solvents were evaporated to afford the product as a yellow-orange powder (30 mg, 46 % yield). $R_f = 0.57$ (DCM:MeOH 98:2). HRMS (ESI/-): m/z calcd. for $C_{124}H_{118}N_8O_{20}S_4$ $[M - 2H]^{2-}$: 1083.3678; found: 1083.3672. ^{1}H NMR $((CD_3)_2SO:CDCl_3$ 80:20, 500 MHz) δ (ppm): 8.62 (s, 4H); 8.29 (s, 4H); 8.03 (dd, *J* =7.7,0.8 Hz, 4H); 7.85 (dd, *J* =7.7,0.8 Hz, 4H); 7.67 (d, *J* = 8.1 Hz, 4H); 7.56 (s, 4H); 7.45 (s, 4H); 7.32 (m, 8H); 7.19 (d, *J* = 7.5 Hz, 4H); 6.85 (s, 8H); 4.39 (d, *J* = 12.8 Hz, 4H); 4.16 (q, *J* = 7.1 Hz, 8H); 3.84 (t, *J* = 6.9 Hz, 8H); 3.13 (d, *J* = 13.1 Hz, 4H); 1.91 (br s, 8H); 1.40 (m, 16H); 1.26 (t, *J* = 7.0 Hz, 12H); 0.94 (br s, 12H). ^{13}C{^{1}H} NMR $(((CD_3)_2SO:CDCl_3$ 80:20, 126 MHz) δ (ppm): 186.7; 163.8; 152.2; 151.2; 147.1; 140.5; 135.9; 134.5; 133.8; 133.6; 133.2; 131.0; 130.3; 130.0; 129.2; 129.0; 125.5; 124.3; 124.0; 119.8; 119.3; 118.0; 79.0; 74.6; 61.1; 29.3; 27.9; 22.2; 13.8.

Tetra-HTI tetraurea calix[4]arene (all-Z)-**2**: tetra-amino calix[4]arene **7** (5 mg, 6.63 μmol, 1 equiv.) was added to an oven-dried 5 mL Schlenk tube and the system was purged with 3x vacuum-Ar cycles. Then, the compound was dissolved in 0.5 mL anhydrous DMF, under Ar atmosphere. Dry Et$_3$N (4.6 μl, 33 μmol, 5 equiv.) was added dropwise with a hamilton syringe. Finally, compound *Z*-**5** (17 mg, 33 μmol, 5 equiv.) was dissolved in 0.2 mL anhydrous DMF and added dropwise to the reaction vessel. The resulting yellow solution was left stirring at RT protected from light. After 4 h the solution was heated up to 35°C and left stirring. After 2 days the reaction was stopped, a yellow dispersion formed. The reaction mixture was transferred to a flask and 1 mL of 1 M aq. K$_2$CO$_3$ solution was added, and the newly formed yellow dispersion sonicated. Then, the resulting yellow solid was filtered *in vacuo*, washed with water (2-3 mL) to remove *p*-nitrophenolate until water came out clear, air dried, then stored in desiccator under argon in the dark (7 mg. 47 % yield). $R_f = 0.39$ (DCM:MeOH 99:1). HRMS (ESI/+): m/z calcd. for $C_{128}H_{128}N_8Na_2O_{20}S_4$ $[M+2Na]^{2+}$: 1135.3970; found: 1135.3956. ^{1}H NMR $((CD_3)_2SO$, 500 MHz) δ (ppm): 8.17 (s, 4H); 8.04 (d, *J* = 7.7 Hz, 4H); 7.81 (d, *J* = 7.7 Hz, 4H); 7.57 (s, 4H); 7.54 (d, *J* = 7.7 Hz, 4H); 7.33 (m, 8H); 6.75 (s, 8H); 6.33 (s, 4H); 4.30 (d, *J* = 13.0 Hz, 4H); 4.23 (m. 16H); 3.79 (t, *J* = 6.9 Hz, 8H); 3.04 (d, *J* = 13.0 Hz, 4H); 1.88 (br s, 8H); 1.38 (m, 16H); 1.29 (t, *J* = 7.0 Hz, 12H); 0.92 (br s, 12H).

Synthesis of hemithioindigo-decorated tetraurea calix[4]arenes. Study of their dimerization into capsular assemblies

(*m-N*-Boc-amino)-HTI *Z*-**3a**: thioindoxyl **8** (0.168 g, 0.76 mmol, 1 equiv.) was added to a Schlenk flask and dissolved in 9 mL anhydrous benzene. Afterwards, dry piperidine (0.37 mL, 3.78 mmol, 5 equiv.) was added dropwise over a period of 2 min. Finally, *tert*-butyl (3-formylphenyl)carbamate (0.25 g, 1.13 mmol, 1.49 equiv.) was dissolved in 1 mL anhydrous benzene and added dropwise to the reaction mixture. The solution was left stirring at 82°C under Ar atmosphere. After 2 h the reaction was stopped according to TLC monitoring (DCM). The crude was dissolved in DCM and partitioned with water (3x 80 mL) to remove residual base. The organic phase was isolated, dried over sodium sulfate and in vacuo. Finally, the compound was precipitated in Hex, filtered under vacuum and collected as a yellow powder (0.294 g, 91% yield). $R_f = 0.27$ (DCM). ^{1}H NMR (CDCl$_3$, 400 MHz) δ (ppm): 8.31 (dd, $J = 7.7, 1.3$ Hz, 1H); 8.13 (dd, $J = 7.7, 1.3$ Hz, 1H); 7.93 (s, 1H); 7.66 (s, 1H); 7.59 (d, $J = 8.4$ Hz, 1H); 7.48 (d, $J = 7.7$ Hz, 1H); 7.42 (t, $J = 7.7$ Hz, 1H); 7.40 (t, $J = 7.7$ Hz, 1H); 6.62 (s, 1H); 4.50 (q, $J = 7.1$ Hz, 2H); 1.54 (s, 9H); 1.48 (t, $J = 7.1$ Hz, 3H).

(*m*-Amino)-HTI *Z*-**3**: *N*-Boc-amino compound *Z*-**3a** (115 mg, 0.27 mmol, 1 equiv.) was dissolved in 4 mL anhydrous dichloromethane inside a 25 mL round-bottom flask. Then, 2 mL of TFA were added dropwise over a period of 2 min and the solution turned red. The *N*-Boc deprotection was run under ambient conditions. After 1 h the reaction was stopped as judged by TLC monitoring (DCM:EtOAc 98:2, ninhydrin staining). The excess solvent and acid were removed under reduced pressure and the resulting solid was dissolved in 40 mL DCM, washed with 50 mL of satd. aq. NaHCO$_3$ solution, and finally with water (1x 30 mL). The organic phase was extracted, dried over sodium sulfate and excess solvent was removed in vacuo. Column chromatography (DCM:EtOAc 98:2): afforded the desired product as the second fraction, which was dried under reduced pressure and isolated as an orange powder (87 mg, 99% yield). $R_f = 0.46$ (DCM:EtOAc 98:2). M.p. = >185 ºC (decompose). HRMS (ESI/+): m/z calcd. for $C_{18}H_{16}NO_3S$ [M+H]$^+$: 326.0845; found: 326.0844. ^{1}H NMR (CDCl$_3$, 500 MHz) δ (ppm): 8.30 (dd, $J = 7.5, 1.3$ Hz, 1H); 8.12 (dd, $J = 7.5, 1.3$ Hz, 1H); 7.89 (s, 1H); 7.39 (t, $J = 7.3$ Hz, 1H); 7.27 (t, $J = 7.6$ Hz, 1H); 7.20 (d, $J = 7.3$ Hz, 1H); 7.10 (t, $J = 1.9$ Hz, 1H); 6.76 (ddd, $J = 7.9, 2.5, 0.7$ Hz, 1H); 4.49 (q, $J = 7.3$ Hz, 2H); 3.84 (s, 2H); 1.47 (t, $J = 7.3$ Hz, 3H). FT-IR ν (cm^{-1}) = 3421 (N–H stretching); 2922; 2853; 1704 (C=O stretching); 1667; 1631; 1586; 1556; 1464; 1445; 1392; 1367; 1293; 1260 (C–O stretching); 1184; 1142; 1074; 1024; 908; 856; 827; 749; 701; 668; 568; 497; 450.

Chapter 3

(*p-N*-Boc-amino)-HTI *Z*-**4a**: thioindoxyl **8** (138 mg, 0.62 mmol, 1 equiv.) was added to a 25 mL Schlenk flask and dissolved in 7 mL anhydrous benzene. The flask was heated and stirred at 75°C, protected from light. Afterwards, anhydrous piperidine (0.30 mL, 3.10 mmol, 5 equiv.) was added dropwise. Finally, *tert*-butyl (4-formylphenyl)carbamate (165 mg, 0.74 mmol, 1.2 equiv.) was added at once under Ar flow. The reaction mixture slowly turned to a deep brown color, then to deep dark green. After 2h the reaction was stopped according to TLC monitoring (DCM:Et$_2$O 99:1). The crude was dissolved in 10 mL DCM and washed with NH$_4$Cl satd. solution (2x20 mL). The organic red phase was isolated, dried over sodium sulfate and under reduced pressure. The resulting solid was precipitated in a 1:1 Hex:Et$_2$O mixture and a yellow dispersion appeared: it was filtered *in vacuo* and collected as a red powder (200 mg, 76% yield). R$_f$ = 0.57 (DCM:Et$_2$O 99:1). M.p. = 178-180 ºC. HRMS (ESI/+): m/z calcd. for C$_{23}$H$_{23}$NNaO$_5$S [M+Na]$^+$: 448.1189; found: 448.1200. ^{1}H NMR (CDCl$_3$, 500 MHz) δ (ppm): 8.30 (dd, *J* = 7.7, 1.3 Hz, 1H); 8.13 (dd, *J* = 7.7, 1.3 Hz, 1H); 7.94 (s, 1H); 7.76 (d, *J* = 8.7 Hz, 2H); 7.50 (d, *J* = 8.7 Hz, 2H); 7.39 (t, *J* = 7.7 Hz, 1H); 6.65 (br s, 1H); 4.50 (q, J = 7.1 Hz, 2H); 1.54 (s, 9H); 1.47 (t, *J* = 7.1 Hz, 3H). ^{13}C{^{1}H} NMR (CDCl$_3$, 126 MHz) δ (ppm): 188.3; 165.5; 152.3; 148.5; 140.7; 136.5; 134.7; 132.9; 132.6; 130.9; 129.6; 128.9; 125.3; 125.1; 118.5; 81.4; 61.9; 28.4; 14.5. FT-IR ν (cm^{-1}) = 3325 (N–H stretching); 2976; 2919; 1725 (C=O stretching); 1701; 1658 (C=O stretching); 1580; 1553; 1503; 1411; 1366; 1317; 1290; 1268; 1230; 1152 (C–O stretching); 1065; 1043; 1017; 901; 834; 769; 742; 666; 564; 533; 500.

(*p*-Amino)-HTI *Z*-**4**: a) *N*-Boc-amino compound *Z*-**4a** (141 mg, 0.32 mmol, 1 equiv.) was added to a 25 mL two-neck round-bottom flask and dissolved in 2 mL anhydrous DCM under argon flow. Then, 1 mL TFA was added dropwise under argon flow. The deprotection reaction was run at RT under inert atmosphere and protected from light. The solution turned dark red upon addition of the acid. After 1 h it was stopped as judged by TLC monitoring (EtOAc), and excess solvent/acid removed *in vacuo*. The resulting red solid was triturated by addition of 2 mL of DCM, and over time a golden solid precipitated. The solid was filtered under vacuum: the orange/red TFA salt of the hemithioindigo compound was collected and dried in the desiccator, protected from light. The liberation of the amine was performed *in situ*. b) The HTI-salt was dissolved in 10 mL of DCM. Then, the same amount of 4% aq. NaHCO$_3$ was added and the two phases partitioned (2x 20 mL). The organic phase was separated, dried over sodium sulfate and under vacuum for 30 min to afford the desired product as small red crystals (102 mg, 98% yield). R$_f$ = 0.84 (EtOAc). ^{1}H NMR (CDCl$_3$, 400

Synthesis of hemithioindigo-decorated tetraurea calix[4]arenes. Study of their dimerization into capsular assemblies

MHz) δ (ppm): 8.28 (dd, J = 7.6,1.3 Hz, 1H); 8.13 (dd, J = 7.6,1.3 Hz, 1H); 7.93 (s, 1H); 7.66 (d, J = 8.5 Hz, 2H); 7.37 (t, J = 7.4 Hz, 1H); 6.74 (d, J = 8.5 Hz, 2H); 4.49 (q, J = 7.2 Hz, 2H); 4.12 (br s, 2H); 1.47 (t, J = 7.2 Hz, 3H).

(*p-N*-Boc-aminomethyl)-HTI *Z*-**5a**: Thioindoxyl **8** (200 mg, 0.90 mmol, 1 equiv.) was added to a 25 mL Schlenk flask and dissolved in 10 mL anhydrous benzene. The flask was heated and stirred at 75°C, protected from light. Afterwards, anhydrous piperidine (0.45 mL, 4.50 mmol, 5 equiv.) was added dropwise. Finally, *tert*-butyl (4-formylbenzyl)carbamate (254 mg, 1.08 mmol, 1.2 equiv.) was added at once under Ar flow. The reaction mixture turned to a red-brown color, then to deep brown, and finally to deep dark green. After 2h the reaction was stopped according to TLC monitoring (DCM:Et$_2$O 99:1). The crude was dissolved in DCM and partitioned with NH$_4$Cl satd. solution (2x50 mL). The organic red phase was isolated, dried over sodium sulfate and under reduced pressure. The resulting solid was precipitated in Et$_2$O and a yellow dispersion appeared: it was filtered *in vacuo* and collected as a golden powder (345 mg, 87% yield). R$_f$ = 0.34 (DCM: Et$_2$O 99:1). M.p. = 176-177 ºC. HRMS (ESI/+): m/z calcd. for $C_{24}H_{25}NNaO_5S$ [M+Na]$^+$: 462.1351; found: 462.1347. ^{1}H NMR (CDCl$_3$, 400 MHz) δ (ppm): 8.29 (dd, J = 7.6,1.3 Hz, 1H); 8.12 (dd, J = 7.6,1.3 Hz, 1H); 7.94 (s, 1H); 7.76 (d, J = 8.2 Hz, 2H); 7.39 (d, J = 8.2 Hz, 2H); 7.37 (t, J = 6.8 Hz, 1H); 4.93 (br s, 1H); 4.49 (q, J = 7.1 Hz, 2H); 4.37 (d, J = 5.4 Hz, 2H); 1.47 (s, 9H); 1.46 (t, J = 7.1 Hz, 3H). ^{13}C{^{1}H} NMR (CDCl$_3$, 101 MHz) δ (ppm): 188.3; 165.2; 148.6; 141.7; 136.4; 134.3; 133.2; 132.7; 132.2; 131.6; 131.1; 131.0; 130.8; 127.9; 125.3; 125.0; 61.8; 44.3; 28.4; 14.3. FT-IR ν (cm^{-1}) = 3352 (N–H stretching); 2990; 2938; 1702; 1678 (C=O stretching), 1589, 1559; 1511; 1466; 1412; 1365; 1289; 1260 (C–O stretching); 1170, 1147 (C–O stretching); 1105; 1065; 1048; 1023; 965; 904; 870; 809; 742; 723; 671; 644; 550; 502; 470.

(*p-Tert*-butyl *N*-methylcarbamate)-HTI *Z*-**5b**: a) compound *Z*-**5a** (217 mg, 0.49 mmol, 1 equiv.) was added to a 10 mL Schlenk tube, and purged 3x with Ar-vacuum cycles. Afterwards, it was dissolved in 5 mL dry DCM. Then, 1 mL of TFA was added dropwise to the tube under Ar flow. The *N*-Boc deprotection was run at RT under Ar atmosphere, protected from light. After 2 h the reaction was stopped as judged by TLC (DCM:Et2O 95:5, ninhydrin staining). Excess solvent/acid were removed under reduced pressure, and the resulting TFA salt was dispersed in 2 mL of DCM and filtered under vacuum to afford an orange solid (186 mg, 83% yield). b) (*p*-aminomethyl)-HTI *Z*-**5** was reacted immediately for the formation of the corresponding carbamate: 15 mL of HPLC DCM were added to the salt.

Chapter 3

The yellow dispersion was sonicated for 3 min in order to have fine particles in suspension. Then, the dispersion was transferred to a 50 mL extraction funnel. The same amount of 4% $NaHCO_3$ aq. solution was added and the 2 phases partitioned (2x 15 mL). The orange organic phase was separated, dried over sodium sulfate and under reduced pressure to afford an orange-yellow oil (139 mg, 83% yield). The amine (139 mg, 0.41 mmol, 1 equiv.) was dissolved in 4 mL dry DCM and added to a 25 mL Schlenk flask kept under Ar flow. The solution was cooled to 0 °C in a water/ice bath. Then, 4-nitrophenyl chloroformate (116 mg, 0.57 mmol, 1.4 equiv.) was added to a vial equipped with a septum, purged 3x with Ar-vacuum cycles, dissolved in 2 mL dry DCM and added dropwise to the solution of the amine. After 5 min the reaction was brought to RT and equipped with an Ar-filled balloon. At RT there's appearance of a yellow precipitate. After 12 h the reaction was stopped according to TLC monitoring (DCM:Et$_2$O 98:2). The excess solvent was evaporated under vacuum, then the crude was triturated in Et$_2$O and filtered out under vacuum to afford a golden solid (130 mg, 62% yield). R_f = 0.60 (DCM:Et$_2$O 98:2). M.p. = >185 ºC (decompose). HRMS (ESI/+): m/z calcd. for $C_{26}H_{20}N_2NaO_7S$ [M+Na]$^+$: 527.0883; found: 527.0883. ^{1}H NMR (CDCl$_3$, 300 MHz) δ (ppm): 8.31 (dd, J = 7.7, 1.2 Hz, 1H); 8.27 (d, J = 9.2 Hz, 2H); 8.14 (dd, J = 7.7, 1.2 Hz, 1H); 7.97 (s, 1H); 7.82 (d, J = 8.3 Hz, 2H); 7.47 (d, J = 8.3 Hz, 2H); 7.41 (t, J = 7.6 Hz, 1H); 7.37 (d, J = 9.2 Hz, 2H); 5.51 (br s, 1H); 4.54 (d, J = 5.8 Hz, 2H); 4.50 (q, J = 7.1 Hz, 2H); 1.47 (t, J = 7.1 Hz, 3H). ^{13}C{^{1}H} NMR (CDCl$_3$, 126 MHz) δ (ppm): 188.3; 165.3; 155.7; 153.2; 148.5; 144.9; 139.7; 139.2; 136.5; 133.9; 133.8; 132.1; 131.8; 130.9; 128.2; 125.4; 125.1; 125.0; 122.0; 61.8; 45.0; 14.3. FT-IR ν (cm^{-1}) = 3359 (N–H stretching); 1747; 1720; 1671 (C=O stretching); 1589; 1561; 1523; 1488; 1438; 1409; 1365; 1346; 1277; 1221 (C–O stretching); 1144; 1105; 1077; 1049; 1015; 951; 925; 866; 854; 805; 742; 673; 599; 522; 488.

Tetra-amino calix[4]arene **6** was synthesized adapting a reported procedure:[23] two scoops of Ni Raney were carefully washed with water, ethanol, and then anhydrous toluene (3x each solvent) in an Ace pressure tube, leaving the Ni Raney in solution with 10 mL of toluene. Tetranitro calix[4]arene (1.5 g, 1.69 mmol, 1 equiv.) was added to the reaction vessel and the reagents were dissolved in a total of 60 mL of anhydrous toluene. The hydrogenation reaction was carried out in a *Parr* shaker hydrogenator at a pressure of 4 bar for 6 h. Afterwards, the reaction micture was filtered through celite in a small chromatography column under nitrogen flow with toluene as the eluent. The column was continuously checked by TLC to confirm that all the product came out. After that, the Ni Raney was quenched with acetone, then water and stored in its waste container. The collected solution was dried under reduced pressure

Synthesis of hemithioindigo-decorated tetraurea calix[4]arenes. Study of their dimerization into capsular assemblies

and under high vacuum to afford an off-white solid (1.14 g, 88% yield). ^{1}H NMR ($(CD_3)_2SO$, 400 MHz) δ (ppm): 5.93 (s, 8H); 4.20 (br s, 8H); 4.16 (d, J = 12.7 Hz, 4H); 3.66 (t, J = 7.4 Hz, 8H); 2.78 (d, J = 12.7 Hz, 4H); 1.83 (m, 8H); 1.34 (m, 16H); 0.90 (t, J = 8.7 Hz, 12H). The ^{1}H NMR spectrum is in total agreement with what is reported in the literature.

Tetracarbamate calix[4]arene **7** was synthesized following a reported procedure:[17] compound **6** (300 mg, 0.39 mmol, 1 equiv.) was added to an oven dried 2-necked 100 mL round-bottom flask equipped with a magnet.and dissolved in 56 mL of a CHCl₃:THF 3:2 mixture. The *p*-nitrophenyl chloroformate (391 mg, 1.94 mmol, 4.95 equiv.) was added in one portion. Finally, the flask was equipped with a condenser and refluxed at 84 ºC for 12 h under argon flow. Afterwards, the reaction mixture was dried under reduced pressure and the resulting solid was sonicated in diethyl ether, filtered out and dried under high vacuum to afford an off-white solid (410 mg, 73% yield). ^{1}H NMR (CDCl₃, 400 MHz) δ (ppm): 8.21 (d, J = 8.3 Hz, 8H); 7.30 (d, J = 8.3 Hz, 8H); 6.76 (br s, 8H); 4.46 (d, J = 13.7 Hz, 4H); 3.88 (s, 8H); 3.15 (d, J = 13.7 Hz, 4H); 1.89 (m, 8H); 1.39 (br s, 16H); 0.95 (t, J = 7.2 Hz, 12H). The ^{1}H NMR spectrum is in total agreement with what is reported in the literature.

7-(Propanoyl)benzo[b]thiophen-3(2H)-one **8**: compound **9** (0.253 g, 1.05 mmol, 1 equiv.) was added to a two-neck amber round-bottom flask and dissolved in SOCl₂ (1.05 mL, 14.5 mmol, 13 equiv.), under Ar atmosphere; the mixture was heated at 75 °C and equipped with a bubbler for HCl release. The reaction was completed after 15 min, cooled at 70°C for 10 min and at RT, then the crude was concentrated to dryness. The resulting aryl acyl chloride was dissolved in 9 mL of anhydrous 1,2-dichloroethane. The solution was protected from light and cooled down to 0°C. AlCl₃ (0.561 g, 4.21 mmol, 4 equiv.) was added slowly over a period of 2 min, the mixture was stirred at 0°C for 5 min and afterwards at RT. The flask was equipped with a bubbler for HCl release until no more bubbling was observed, then left stirring with an Ar balloon. After 4 h the reaction was completed as judged by TLC; the mixture was quenched with ice and water, then extracted twice between 30 mL water and 30 mL DCM. The organic phase was dried over sodium sulfate and under reduced pressure. The resulting pink solid was triturated with a 1:1 Hex:Et₂O mixture and filtered under vacuum (0.17 g, 73% yield). The beige solid was used for the next reactions without further purification due to its instability to light and moisture. R_f = 0.65 (DCM:Et₂O 99:1). M.p. = 101-102 ºC. HRMS (ESI-TOF): m/z calcd. for $C_{11}H_{10}NaO_3S$ [M+Na]⁺ : 245.0243; found: 245.0242. ^{1}H NMR (CDCl₃, 500 MHz) δ (ppm): 8.29 (dd, J = 7.4, 1.2 Hz, 1H), 7.95 (dd, J =

Chapter 3

7.3, 1.2 Hz, 1H), 7.31 (t, *J* = 7.6 Hz, 1H), 4.45 (q, *J* = 7.1 Hz, 2H), 3.76 (s, 2H), 1.44 (t, *J* = 7.1 Hz, 3H). $^{13}C\{^1H\}$ NMR (CDCl$_3$, 126 MHz) δ (ppm): 200.0; 165.3; 157.0; 137.3; 132.9; 130.7; 125.9; 124.6; 61.8; 39.7; 14.4. FT-IR ν (cm^{-1}) = 3055; 2992; 2934; 1695 (C=O stretching); 1589; 1563; 1472; 1409; 1384; 1291 (C–O stretching); 1266; 1203; 1182; 1145; 1102; 1052; 1016; 867; 817; 753; 730; 598; 561; 502; 477.

2-[(Carboxymethyl)thio]-1-benzoic acid ethyl ester **9**: ethyl 2-mercaptobenzoate (1.02 g, 5.60 mmol, 1 equiv.) and 2-bromoacetic acid (0.7 g, 5.04 mmol, 0.9 equiv.) were added to a two-neck round-bottom flask. Then, they were dissolved in 20 mL freshly distilled THF. Finally, oven-dried K$_2$CO$_3$ (1.55 g, 11.19 mmol, 2 equiv.) was added at once. Upon addition of the base, the reaction mixture took swiftly a milky color. The reaction was carried out under Ar flow at RT, vigorous stirred. Within 30 min a white precipitate formed. The reaction was stopped and excess solvent was removed *in vacuo*. The reaction crude was dispersed in 10 mL of water. The aqueous phase was acidified with HCl 2M until pH = 2, then extracted with EtOAc (2x 150 mL). The organic phase was dried over sodium sulfate and over reduced pressure, to afford a white solid. The solid was triturated in a 1:1 DCM:Hex mixture (10 mL) and filtered out to afford a white crystalline solid (1.1 g, 84% yield). R$_f$ = 0.56 (DCM:MeOH 90:10). M.p. = 137-139 ℃. HRMS (ESI/-): m/z calcd. for C$_{11}$H$_{11}$O$_4$S [M-H]$^-$: 239.0384; found: 239.0379. ^{1}H NMR (THF-d$_8$, 500 MHz) δ (ppm): 7.95 (dd, *J* = 7.8 Hz, 1H); 7.53 (d, *J* = 8.2 Hz, 1H); 7.47 (td, *J* = 7.7, 1.5 Hz, 1H); 7.19 (t, J = 7.6 Hz, 1H); 4.36 (q, *J* = 7.1 Hz, 2H); 3.73 (s, 2H); 1.39 (t, 3H); 7.91 (dd, *J* = 7.8, 1.5 Hz, 1H); 7.48 (d, *J* = 7.9 Hz, 1H); 7.42 (td, *J* = 7.7, 1.5 Hz, 1H); 7.14 (td, *J* = 8.1, 1.1 Hz, 1H); 4.31 (q, *J* = 7.1 Hz, 2H); 3.67 (s, 2H); 1.34 (t, *J* = 7.1 Hz, 3H). $^{13}C\{^1H\}$ NMR (THF-d$_8$, 126 MHz) δ (ppm): 169.9; 165.4; 141.3; 136.1; 131.9; 130.6; 128.1; 125.9; 123.7; 60.4; 34.1; 13.6. FT-IR ν (cm^{-1}) = 1697 (C=O stretching); 1586; 1558; 1427; 1388; 1368; 1309; 1294; 1275; 1247 (C–O stretching); 1193; 1176; 1146; 1108; 1061 (C–O stretching); 1043; 1022; 880; 865; 750; 708; 690; 670; 649; 527; 498; 468; 453.

Tetramethylphosphonium hexafluorophosphate (V) (Me$_4$P$^+$PF$_6$$^-$) **10**: Two separate water solutions (5 mL each) of Me$_4$P$^+$Cl$^-$ (150 mg, 1.185 mmol, 1 equiv.) and Na$^+$PF$_6$$^-$ (201 mg, 1.197 mmol, 1.01 equiv.) were prepared. Me$_4$P$^+$Cl$^-$ was completely soluble at RT, whereas Na$^+$PF$_6$$^-$ was warmed up at 40°C for 2-3 min until completely dissolved. The two stirred solutions were then mixed together. Within seconds, a white precipitate appeared. The mixture was left stirring for 30 min at RT. Afterwards, the precipitate was filtered out and

Synthesis of hemithioindigo-decorated tetraurea calix[4]arenes. Study of their dimerization into capsular assemblies

dried under high vacuum to afford an off-white solid (163 mg, 58 % yield). ^{1}H NMR ((CD$_3$)$_2$SO, 400 MHz) δ (ppm): 1.82 (d, J = 15.2 Hz, 12H). ^{31}P NMR ((CD$_3$)$_2$SO, 162 MHz) δ (ppm): 28.37 (s); -141.08 (sept, J = 710.8 Hz). Elemental analysis (C$_4$H$_{12}$P$^+$·F$_6$P$^-$): Meas. %C = 20.21; %H = 5.24; %N = 0. Calc. %C = 20.35; %H = 5.12; %N = 0.

p-Tolyl tetraurea calix[4]arene **11** was synthesized adapting a reported procedure:[34] A two-neck 100 mL round-bottom flask was oven dried and equipped with a magnet, then put under argon flow (vacuum-Ar 3x). The tetraamino calix[4]arene **6** (300 mg, 0.39 mmol, 1 equiv.) was added in one portion to the flask, then 30 mL of DCM were added with a syringe and the flask stirred. Finally, *p*-tolyl isocyanate (261 mg, 1.96 mmol, 5 equiv.) was added dropwise with a syringe into the reaction flask. The brownish homogeneous solution was left stirring at RT for 24 h. After that time a white precipitate formed. The crude mixture was dried under reduced pressure, redissolved in a DCM:MeOH mixture to induce the precipitation of an ivory solid. The solid was filtered in vacuo and collected (380 mg, 75% yield). The ^{1}H NMR spectrum is in total agreement with what is reported in the literature.

Tetramethylphosphonium tetrakis(3,5-bis(trifluoromethyl)phenyl)borate (Me$_4$P$^+$BArF$^-$) **12**: a solution of sodium tetrakis(3,5-bis(trifluoromethyl)phenyl)borate (Na$^+$BArF$^-$, 260 mg, 0.29 mmol, 1.2 equiv.) in 4 mL of anhydrous MeOH was added dropwise to a 3 mL solution of tetramethylphosphonium chloride (31 mg, 0.24 mmol, 1 equiv.) in the same solvent, under argon flow. The transparent reaction was stirred at room temperature and equipped with an Ar balloon. After 12 h the reaction was stopped. The solution was dried under reduced pressure and redissolved in 5 mL of Milli-Q water. The mixture was sonicated to generate a white suspension. The product was filtered out and washed several times with Milli-Q water, then dried under high vacuum to afford a white solid (156 mg, 67% yield). ^{1}H NMR (CD$_2$Cl$_2$, 400 MHz) δ (ppm): 7.72 (br s, 8H); 7.57 (s, 4H); 1.86 (d, J = 13.8 Hz, 12H). ^{13}C NMR (CD$_2$Cl$_2$, 101 MHz) δ (ppm): 162.14 (q, $^1J_{B-C}$ = 50 Hz); 135.21; 129.26 (q, $^2J_{C-F}$ = 32 Hz); 126.36; 123.65; 120.94; 117.91; 10.97 (d, J = Hz). ^{31}P NMR (CD$_2$Cl$_2$, 162 MHz) δ (ppm): 25.76. ^{19}F NMR (CD$_2$Cl$_2$, 376 MHz) δ (ppm): -62.89. ^{11}B NMR (CD$_2$Cl$_2$, 128 MHz) δ (ppm): -6.61.
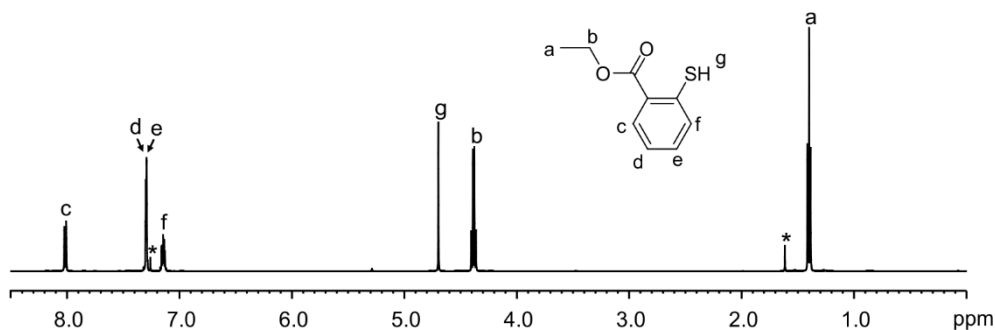
3.4.3 Figures

Figure 3.11 ^{1}H NMR (CDCl$_3$, 500 MHz) spectrum of ethyl 2-mercaptobenzoate. * Residual solvent peaks.
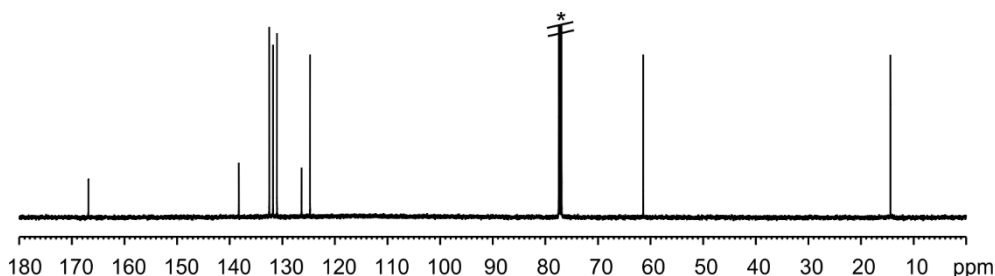

Figure 3.12 ^{13}C NMR (CDCl$_3$, 126 MHz) spectrum of ethyl 2-mercaptobenzoate. * Residual solvent peaks.
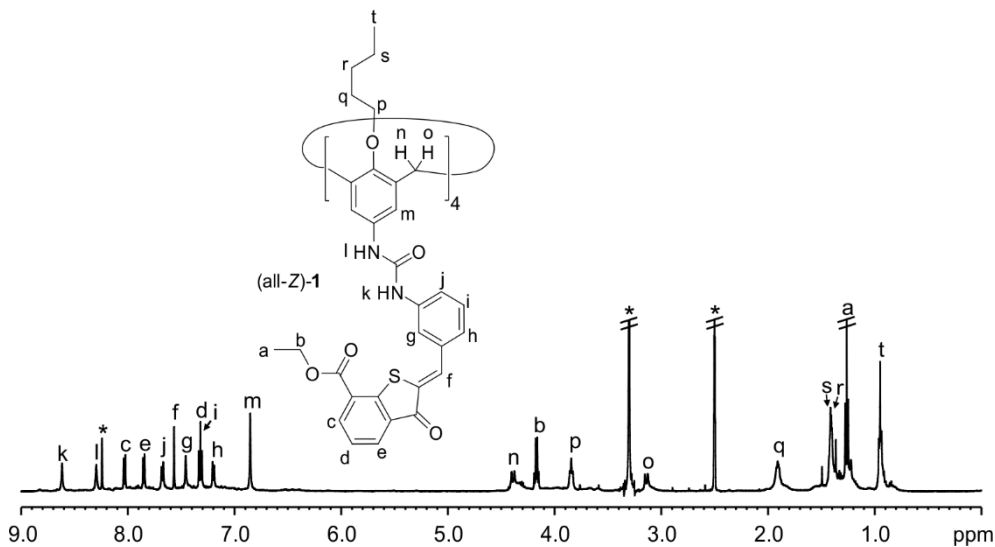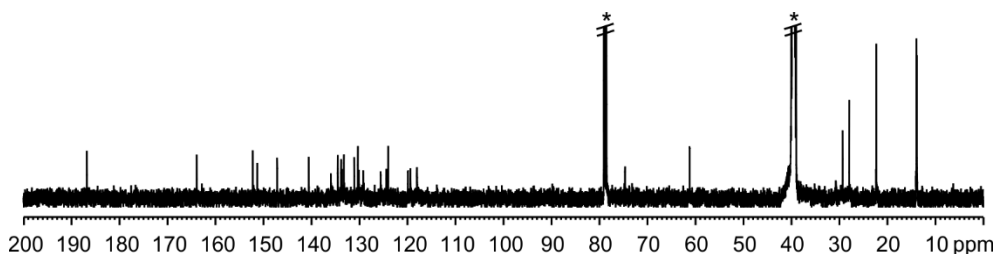

Figure 3.13 ^{1}H NMR ((CD$_3$)$_2$SO:CDCl$_3$ 80:20, 500 MHz) spectrum of (all-Z)-**1**. * Residual solvents peaks.

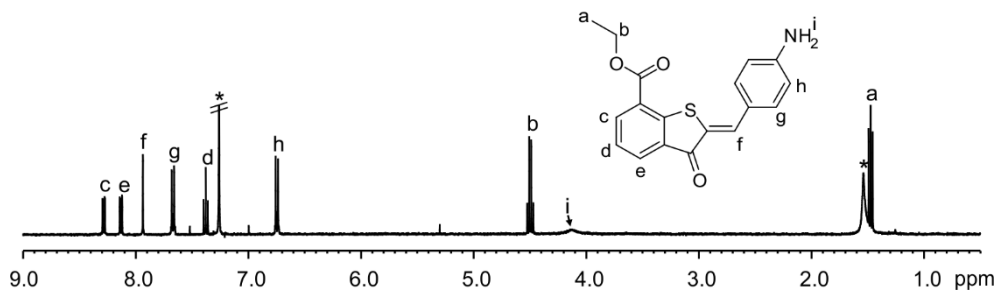*Synthesis of hemithioindigo-decorated tetraurea calix[4]arenes. Study of their dimerization into capsular assemblies*


Figure 3.14 ^{13}C NMR ((CD$_3$)$_2$SO:CDCl$_3$ 80:20, 126 MHz) spectrum of (all-*Z*)-**1**. * Residual solvent peaks.
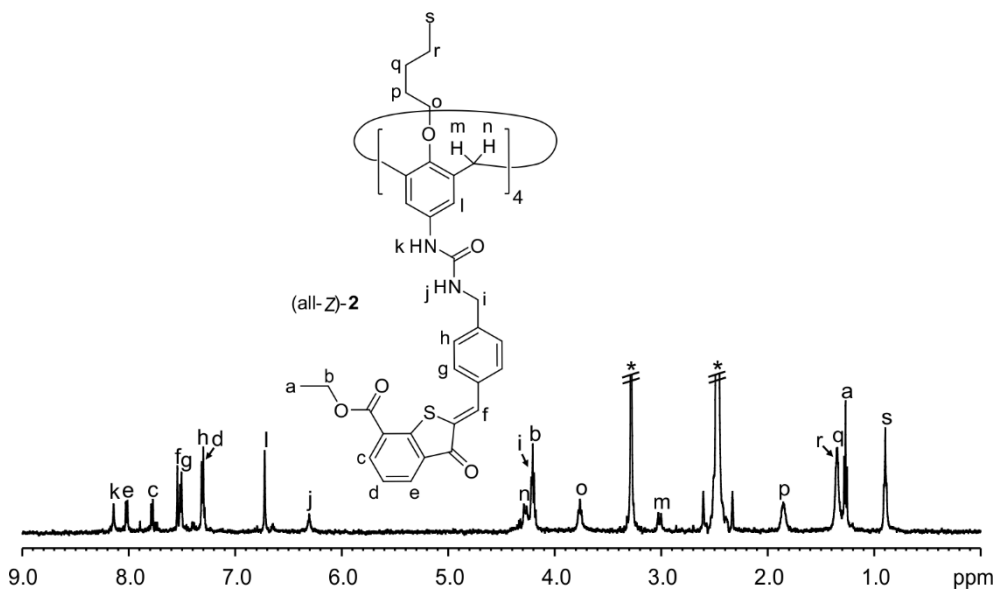
Figure 3.15 ^{1}H NMR ((CD$_3$)$_2$SO, 500 MHz) spectrum of (all-*Z*)-**2**. * Residual solvents peaks.
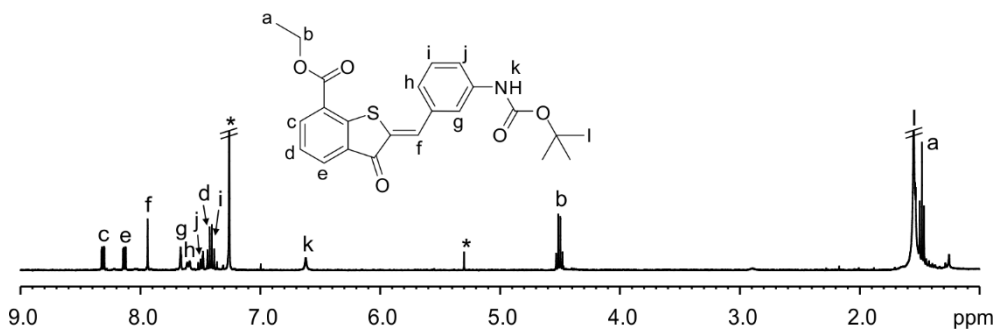
Figure 3.16 ^{1}H NMR spectrum of *Z*-**3a** (CDCl$_3$, 400 MHz). * Residual solvent peaks.

Chapter 3
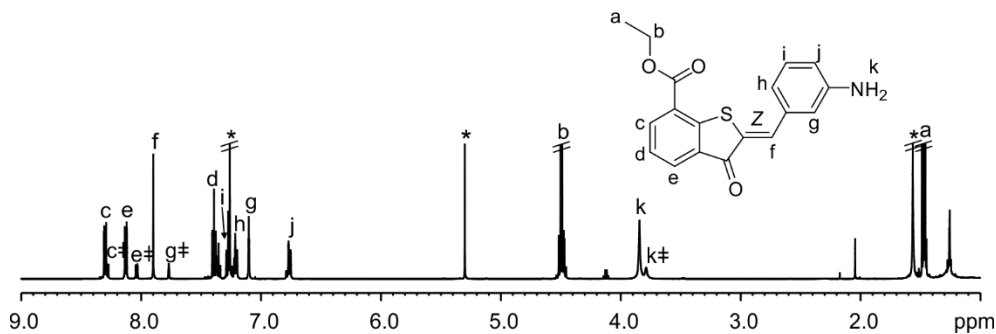
Figure 3.17 ^{1}H NMR (CDCl$_3$, 500 MHz) spectrum of **3** in a *Z:E* 80:20 ratio at ambient conditions. Protons assigned to the *E*-**3** isomer are marked with a ‡ symbol. * Residual solvent peaks.
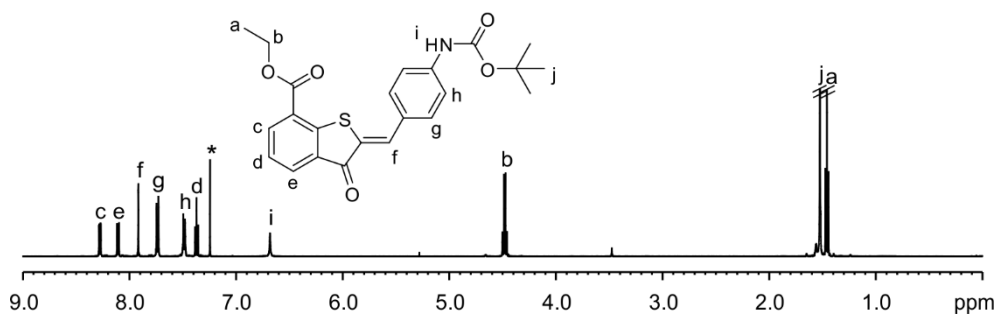
Figure 3.18 ^{1}H NMR (CDCl$_3$, 500 MHz) spectrum of Z-**4a**. * Residual solvent peaks.
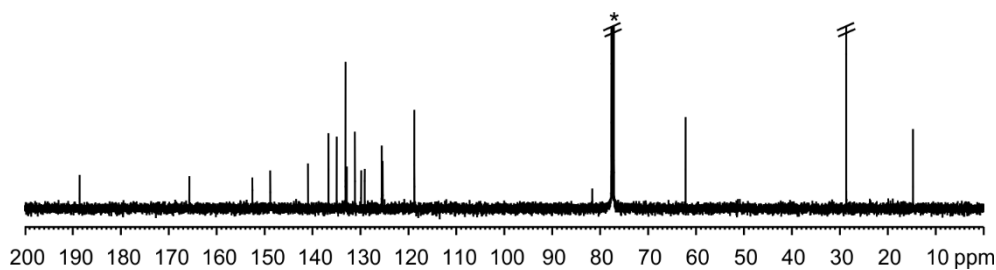
Figure 3.19 ^{13}C NMR (CDCl$_3$, 126 MHz) spectrum of Z-**4a**. * Residual solvent peaks.

Figure 3.20 ^{1}H NMR (CDCl$_3$, 400 MHz) spectrum of Z-**4**. * Residual solvent peaks.
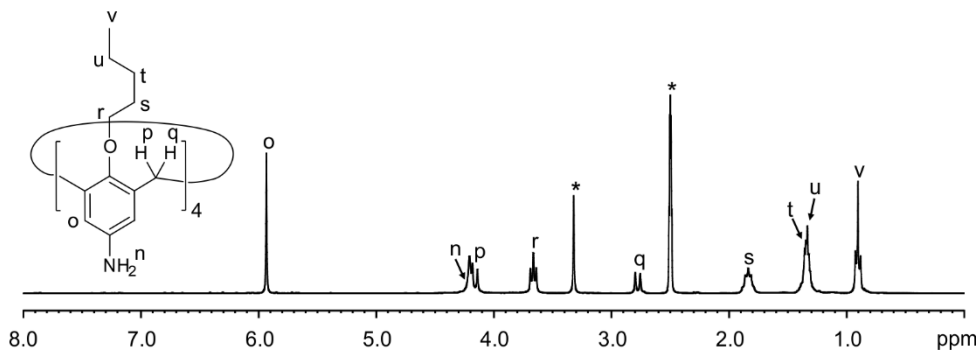
Synthesis of hemithioindigo-decorated tetraurea calix[4]arenes. Study of their dimerization into capsular assemblies
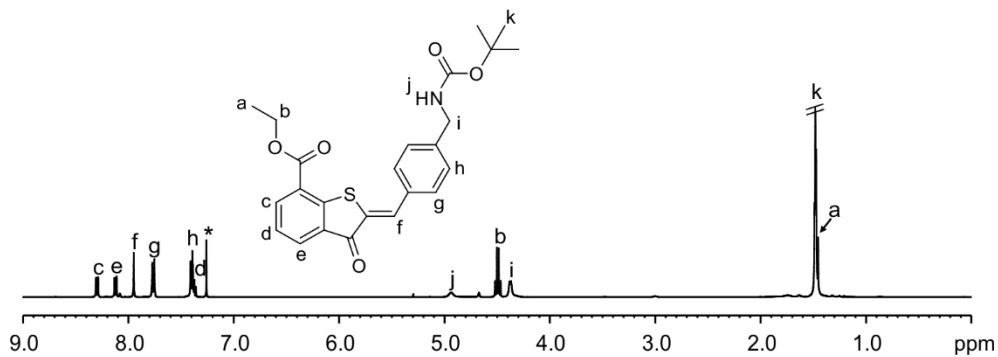
Figure 3.21 ^{1}H NMR (CDCl$_3$, 400 MHz) spectrum of Z-**5a**. * Residual solvent peaks.
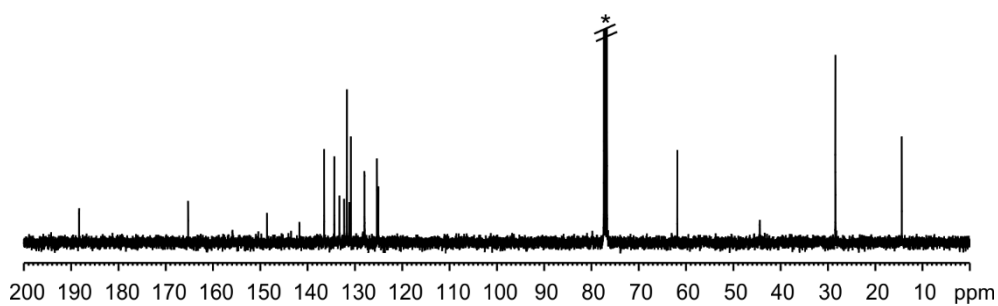
Figure 3.22 ^{13}C NMR (CDCl$_3$, 101 MHz) spectrum of Z-**5a**. * Residual solvent peaks.
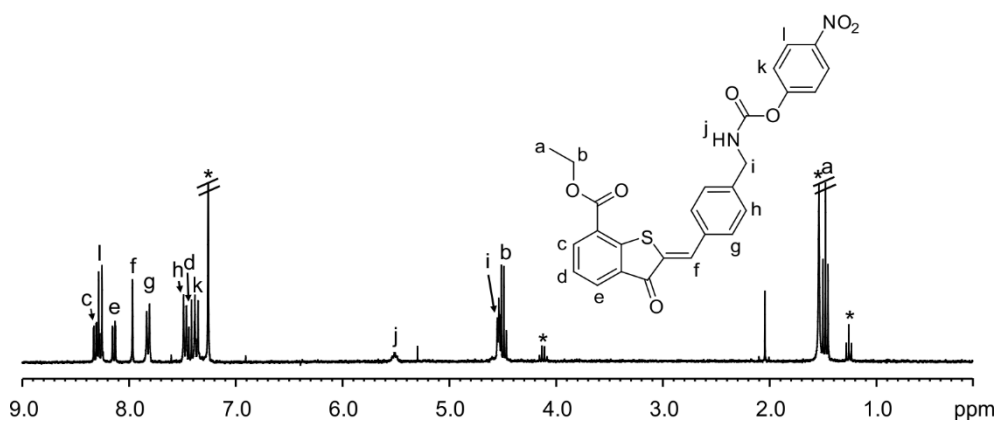
Figure 3.23 ^{1}H NMR (CDCl$_3$, 300 MHz) spectrum of Z-**5b**. * Residual solvent peaks.

127

Chapter 3
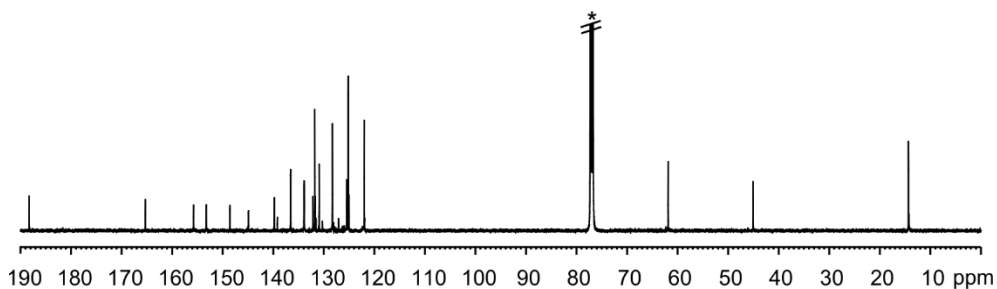
Figure 3.24 ^{13}C NMR (CDCl$_3$, 126 MHz) spectrum of *Z*-**5b**. * Residual solvent peaks.

Figure 3.25 ^{1}H NMR ((CD$_3$)$_2$SO, 400 MHz) of tetra-amino calix[4]arene **6**. * Residual solvent peaks.
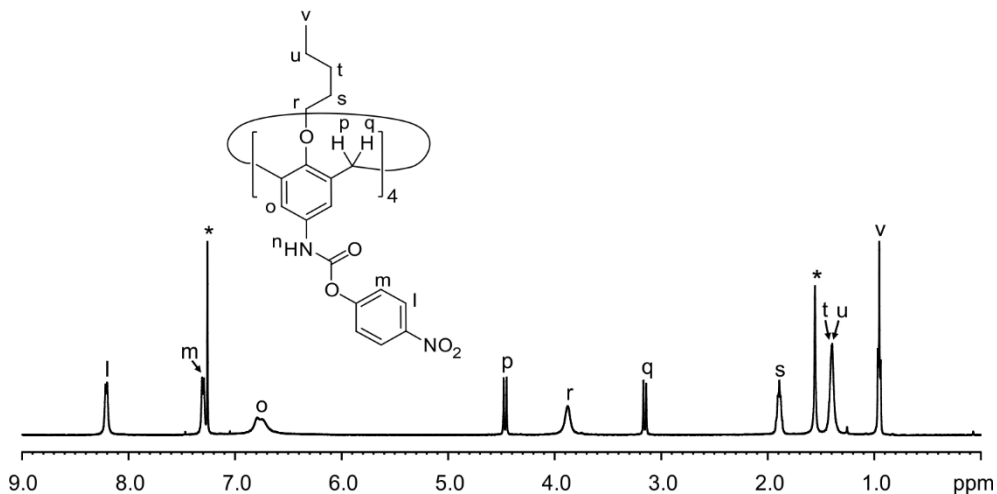

Figure 3.26 ^{1}H NMR (CDCl$_3$, 400 MHz) of tetracarbamate calix[4]arene **7**. * Residual solvent peaks.

128

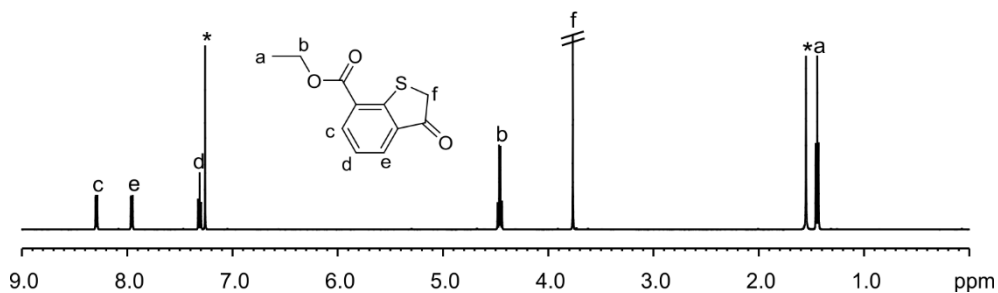*Synthesis of hemithioindigo-decorated tetraurea calix[4]arenes. Study of their dimerization into capsular assemblies*

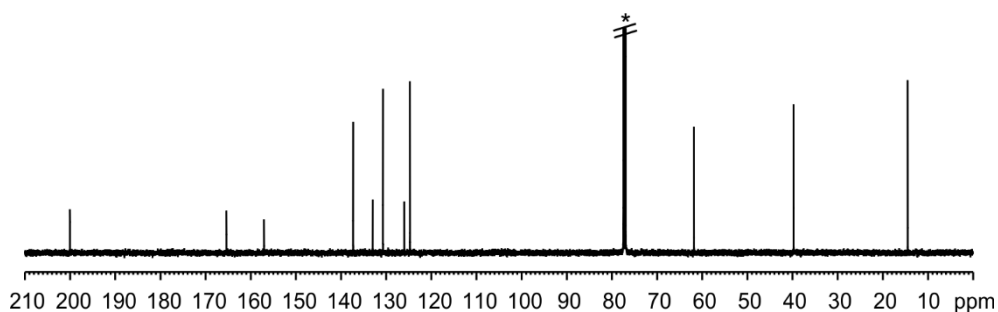**Figure 3.27** ^{1}H NMR (CDCl$_3$, 500 MHz) spectrum of **8**. * Residual solvent peaks.

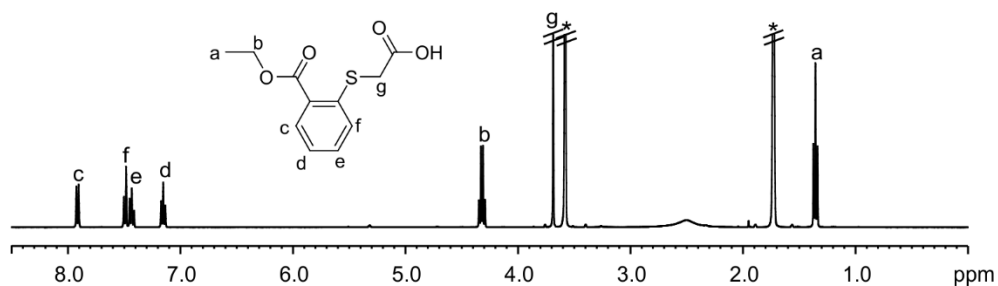**Figure 3.28** ^{13}C NMR (CDCl$_3$, 126 MHz) spectrum of **8**. * Residual solvent peaks.

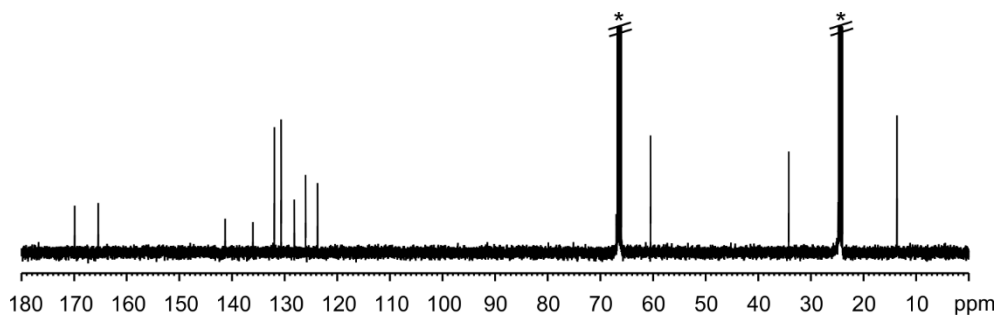**Figure 3.29** ^{1}H NMR (THF-d$_8$, 400 MHz) spectrum of **9**. * Residual solvent peaks.

Figure 3.30 ^{13}C NMR (THF-d$_8$, 126 MHz) spectrum of **9**. * Residual solvent peaks.
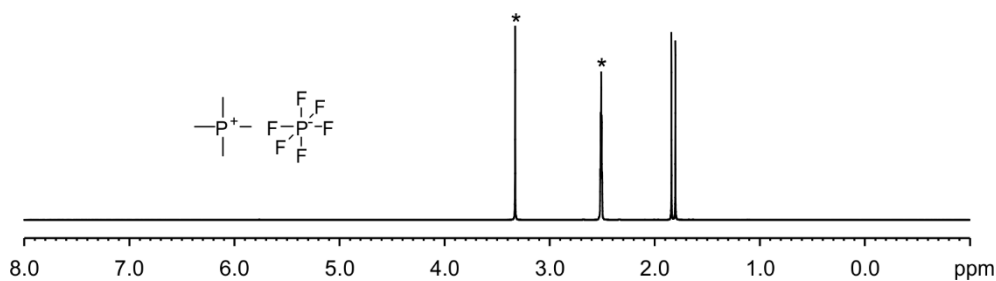
Chapter 3

Figure 3.31 ^{1}H NMR (CDCl$_3$, 400 MHz) spectrum of **10**. * Residual solvent peaks.

Figure 3.32 ^{31}P NMR (CDCl$_3$, 162 MHz) spectrum of **10**. * Residual solvent peaks.

Figure 3.33 ^{1}H NMR ((CD$_3$)$_2$CO, 300 MHz) spectrum of **11**. * Residual solvent peaks.

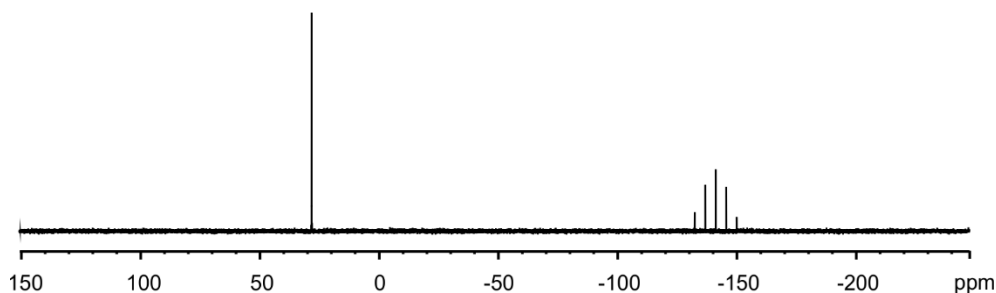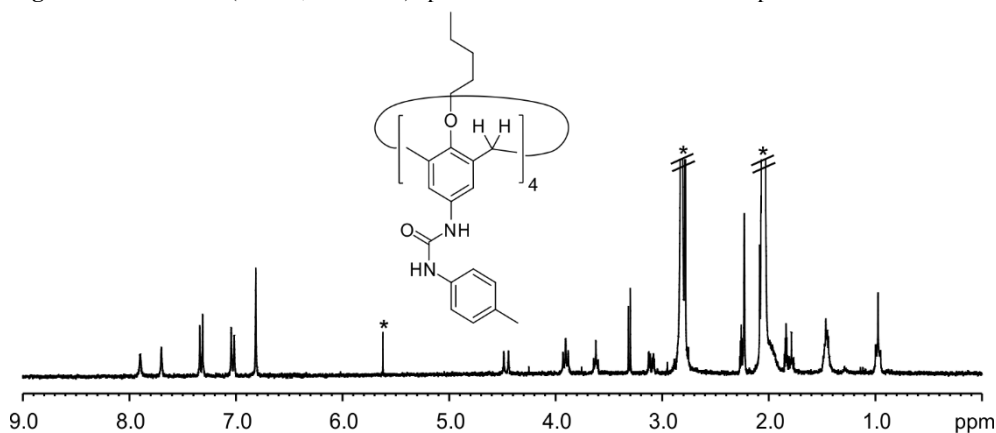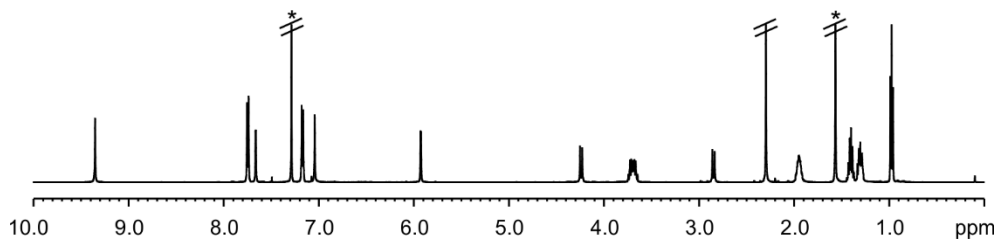**Figure 3.34** ^{1}H NMR (CDCl$_3$, 500 MHz) spectrum of **11$_2$**. * Residual solvent peaks.

Synthesis of hemithioindigo-decorated tetraurea calix[4]arenes. Study of their dimerization into capsular assemblies
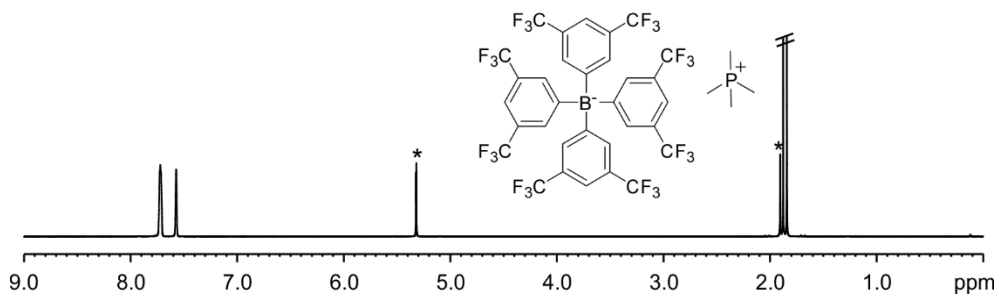
Figure 3.35 ^{1}H NMR (CD$_2$Cl$_2$, 400 MHz) of Me$_4$P$^+$BArF$^-$ **12**. * Residual solvent peaks.
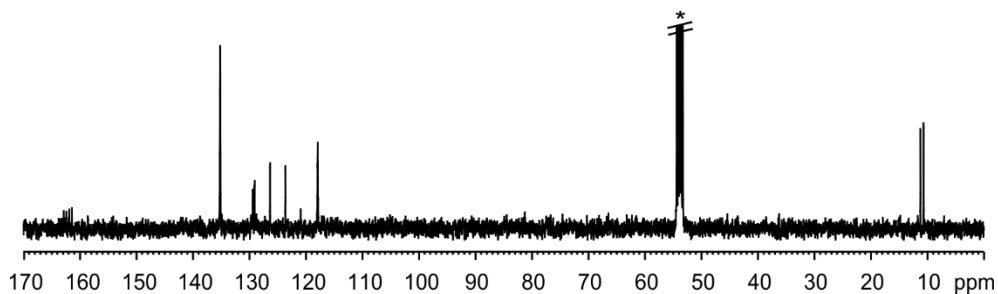
Figure 3.36 ^{13}C NMR (CD$_2$Cl$_2$, 101 MHz) of Me$_4$P$^+$BArF$^-$ **12**. * Residual solvent peaks.
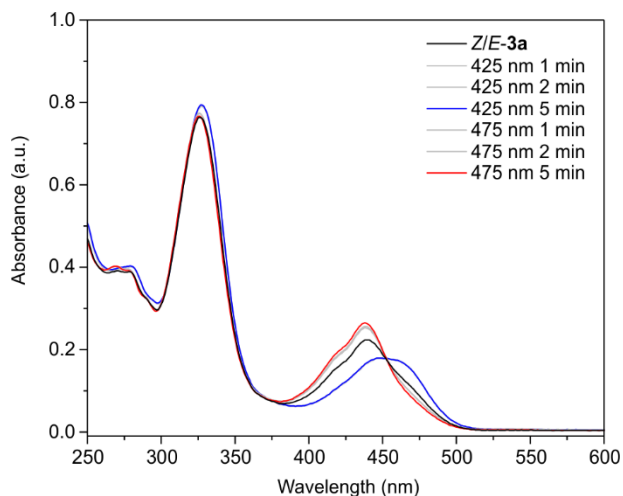
Figure 3.37 UV/Vis absorption spectra of a 30 µM CHCl$_3$ solution of *Z/E*-**3a** (ambient mixture) light-irradiated at 425 and 475 nm at different times.

UNIVERSITAT ROVIRA I VIRGILI
STIMULI-RESPONSIVE HOST-GUEST SYSTEMS DECORATED WITH HEMITHIOINDIGO AND SPIROPYRAN UNITS
Giulia Moncelsi

Chapter 3
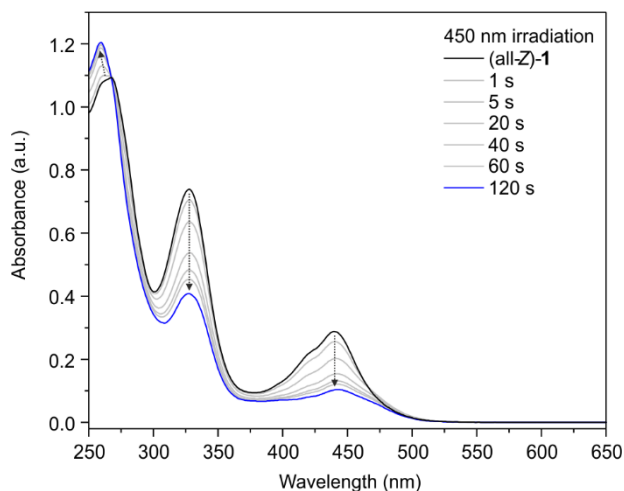
Figure 3.38 UV/Vis absorption spectra of a 10 µM CHCl$_3$ solution of (all-*Z*)-**1** light-irradiated at 450 nm at different times.
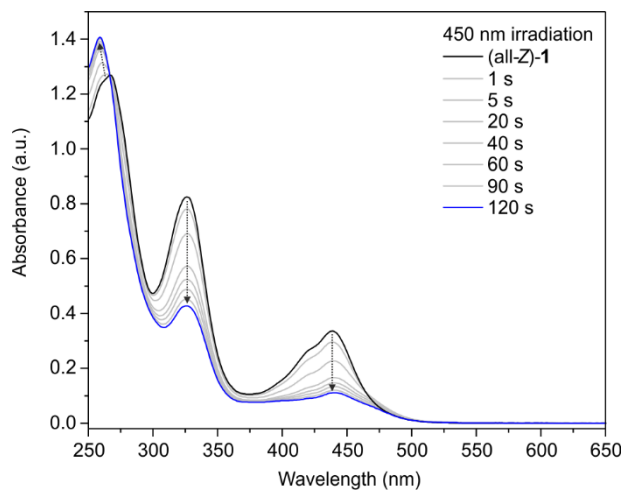
Figure 3.39 UV/Vis absorption spectra of a 10 µM CH$_2$Cl$_2$ solution of (all-*Z*)-**1** light-irradiated at 450 nm at different times.

Synthesis of hemithioindigo-decorated tetraurea calix[4]arenes. Study of their dimerization into capsular assemblies

**Figure 3.40** ^{1}H NMR ((CD$_3$)$_2$SO, 400 MHz) spectra at 298 K of a millimolar solution of (all-*Z*)-**2** photoirradiated at 450 nm for a) 0, b) 1 and c) 10 min. * Residual solvents peaks.
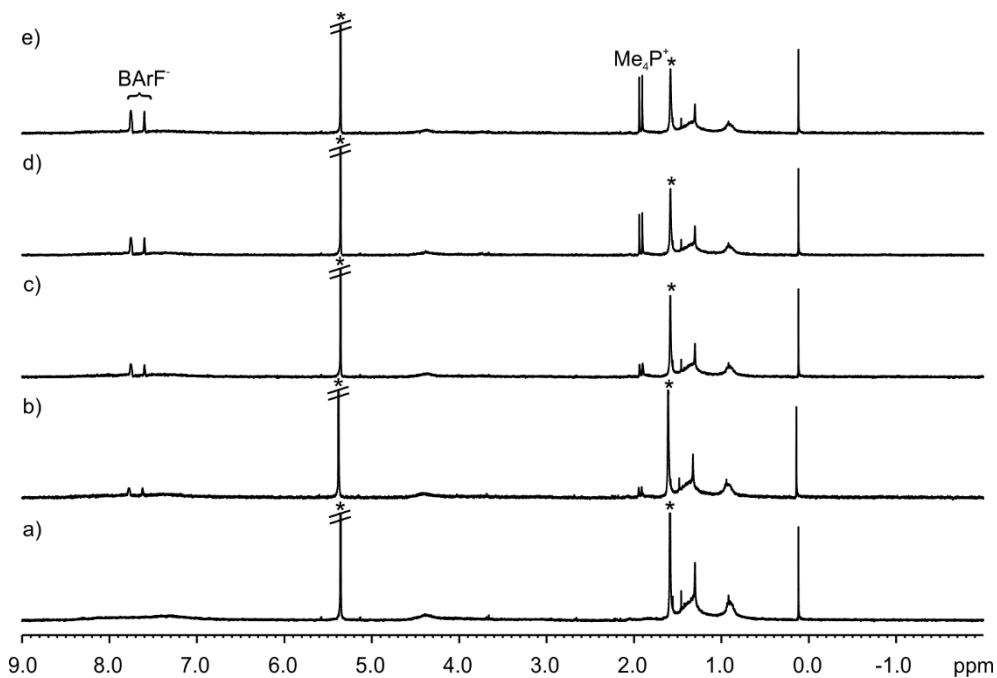
Figure 3.41 ^{1}H NMR (CD$_2$Cl$_2$, 400 MHz) spectra at 298 K of a 1 millimolar solution of a) (all-*Z*)-**1** + b) 0.25; c) 0.5; d) 0.75 and e) 1 equiv. of **12**. Primed letters and numbers correspond to proton signals of bound components. * Residual solvents peaks.

Chapter 3
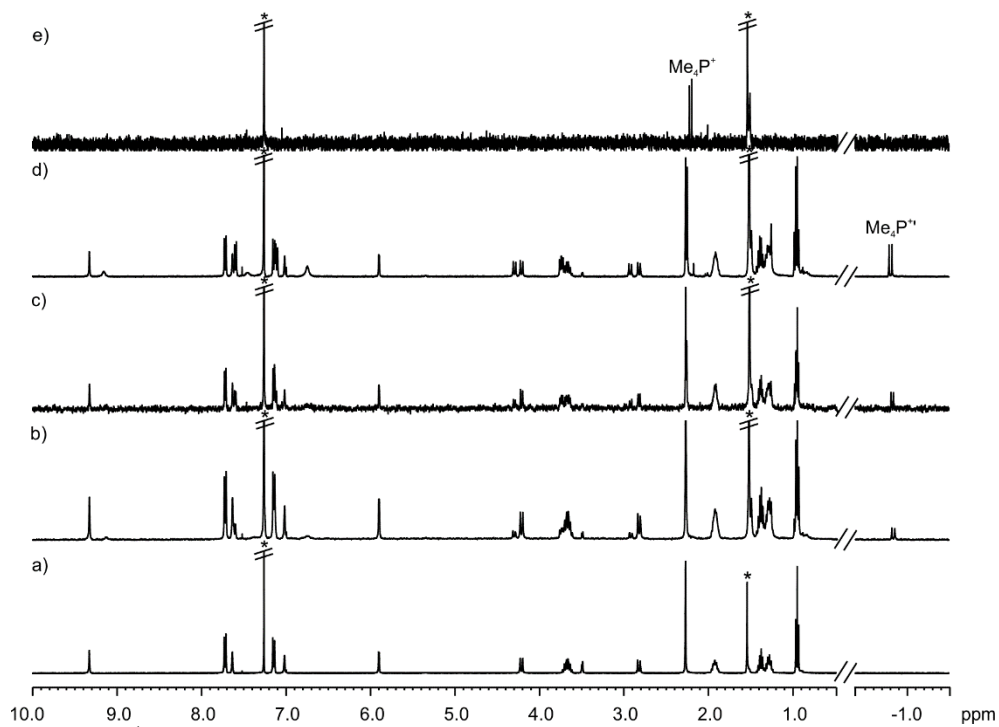
Figure 3.42 ^{1}H NMR (CDCl$_3$, 400 MHz) spectra at 298 K of a millimolar solution of **11** + a) 0 equiv.; b) 0.5 equiv.; c) 1 equiv.; d) 2 equiv. of **10** and e) pure **10**. Primed letters and numbers correspond to proton signals of bound components. * Residual solvents peaks.

Synthesis of hemithioindigo-decorated tetraurea calix[4]arenes. Study of their dimerization into capsular assemblies

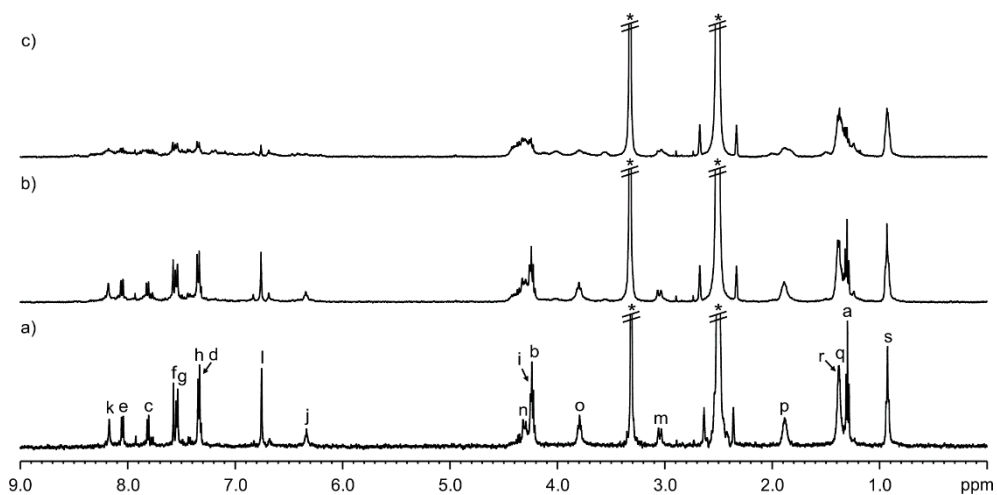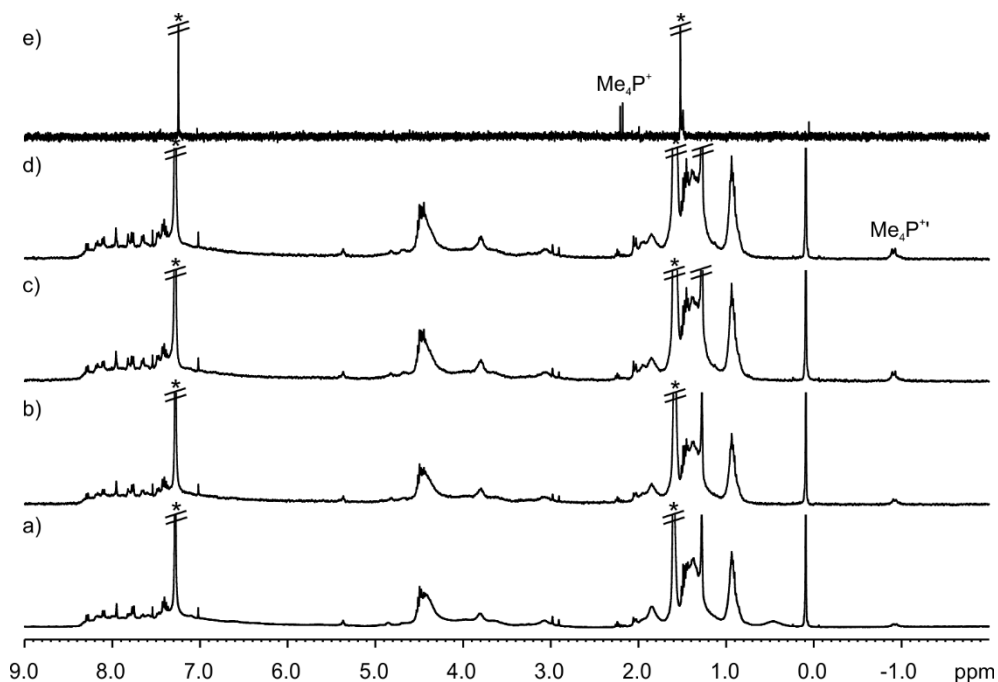**Figure 3.43** ^{1}H NMR (CDCl3, 400 MHz) spectra at 298 K of a millimolar solution of (all-*Z*)-**2** + a) 0.5 equiv; b) 1 equiv.; c) 2 equiv.; d) 2.5 equiv. of **10** and e) pure **10**. Primed letters and numbers correspond to proton signals of bound components. * Residual solvents peaks.
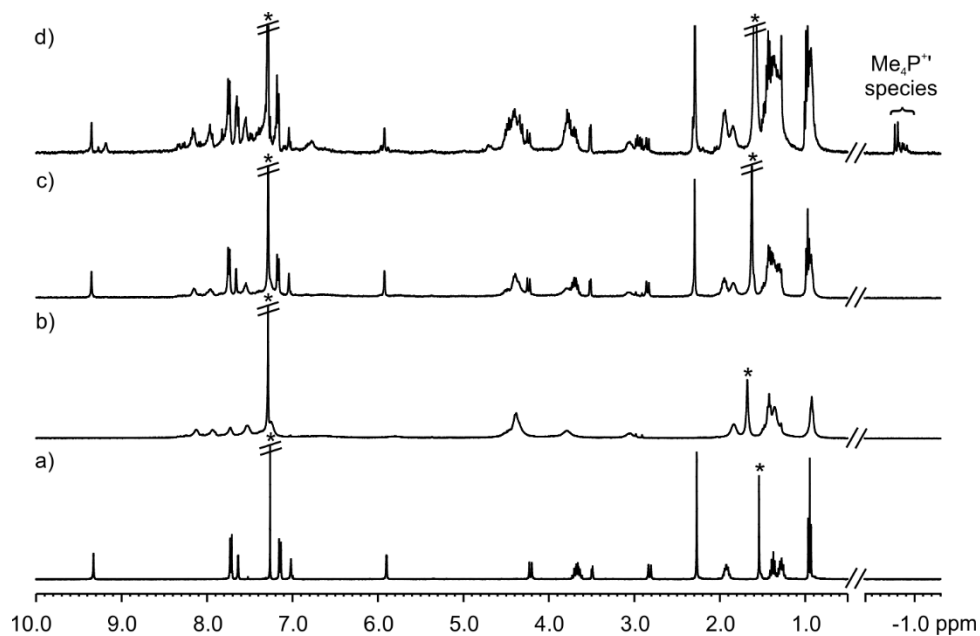
Figure 3.44 ^{1}H NMR (CDCl3, 400 MHz) spectra at 298 K of 1 millimolar solutions of a) **11**$_2$; b) (all-*Z*)-**2**$^-$; c) **11**$_2$ + (all-*Z*)-**2** (0.5:1 molar ratio); d) **11**$_2$ + (all-*Z*)-**2** + **10** (0.5:1:1 molar ratio). Primed letters and numbers correspond to proton signals of bound components. * Residual solvents peaks.

135

Chapter 3

3.5 References and notes

[1] O. B. Berryman, H. Dube, J. J. Rebek, *Isr. J. Chem.* **2011**, *51*, 700-709.

[2] A. Díaz-Moscoso, P. Ballester, *Chem. Commun.* **2017**, *53*, 4635-4652.

[3] D.-H. Qu, Q.-C. Wang, Q.-W. Zhang, X. Ma, H. Tian, *Chem. Rev.* **2015**, *115*, 7543-7588.

[4] L. Wang, Q. Li, *Chem. Soc. Rev.* **2018**, *47*, 1044-1097.

[5] K. Iwamoto, K. Araki, S. Shinkai, *J. Org. Chem.* **1991**, *56*, 4955-4962.

[6] K. D. Shimizu, J. Rebek, *Proc. Natl. Acad. Sci. U. S. A.* **1995**, *92*, 12403-12407.

[7] J. J. Rebek, *Chem. Commun.* **2000**, 637-643.

[8] R. K. Castellano, S. L. Craig, C. Nuckolls, J. Rebek, *J. Am. Chem. Soc.* **2000**, *122*, 7876-7882.

[9] H. M. D. Bandara, S. C. Burdette, *Chem. Soc. Rev.* **2012**, *41*, 1809-1825.

[10] W.-C. Geng, H. Sun, D.-S. Guo, *J. Inclusion Phenom. Macrocyclic Chem.* **2018**, *92*, 1-79.

[11] E. Wagner-Wysiecka, N. Łukasik, J. F. Biernat, E. Luboch, *J. Inclusion Phenom. Macrocyclic Chem.* **2018**, *90*, 189-257.

[12] N. Y. Kim, S.-K. Chang, *J. Org. Chem.* **1998**, *63*, 2362-2364.

[13] I. T. Ho, G.-H. Lee, W.-S. Chung, *J. Org. Chem.* **2007**, *72*, 2434-2442.

[14] F. Hamada, T. Masuda, Y. Kondo, *Supramol. Chem.* **1995**, *5*, 129-131.

[15] F. Hamada, Y. Kondo, I. Okubo, *Int. J. of The Soc. of Mat. Eng. for Resources* **1995**, *3*, 88-94.

[16] F. Vögtle, D. Udelhofen, S. Abramson, B. Fuchs, *J. Photochem. Photobiol., A* **2000**, *131*, 41-48.

[17] F. A. Arroyave, P. Ballester, *J. Org. Chem.* **2015**, *80*, 10866-10873.

[18] A. Diaz-Moscoso, F. A. Arroyave, P. Ballester, *Chem. Commun.* **2016**, *52*, 3046-3049.

[19] M. O. Vysotsky, I. Thondorf, V. Böhmer, *Angew. Chem., Int. Ed.* **2000**, *39*, 1264-1267.

[20] Y. Rudzevich, M. O. Vysotsky, V. Böhmer, M. S. Brody, J. J. Rebek, F. Broda, I. Thondorf, *Org. Biomol. Chem.* **2004**, *2*, 3080-3084.

[21] D. Braekers, C. Peters, A. Bogdan, Y. Rudzevich, V. Böhmer, J. F. Desreux, *J. Org. Chem.* **2008**, *73*, 701-706.

[22] Y. Rudzevich, V. Rudzevich, V. Böhmer, *Chem. Eur. J.* **2010**, *16*, 4541-4549.

[23] R. A. Jakobi, V. Böhmer, C. Gruettner, D. Kraft, W. Vogt, *New J. Chem.* **1996**, *20*, 493−501.

[24] R. Chaubey, N. D. Jasuja, G. Garg, *Int. J. Pharm. Sci. Res.* **2017**, *8*, 2249-2257.

[25] M. T. Konieczny, W. Konieczny, *Heterocycles* **2005**, *65*, 451-464.

[26] L. S. S. Réamonn, W. I. O'Sullivan, *J. Chem. Soc. Perkin Trans. 1* **1977**, 1009-1012.

[27] A. Bogdan, M. O. Vysotsky, T. Ikai, Y. Okamoto, V. Böhmer, *Chem. Eur. J.* **2004**, *10*, 3324-3330.

[28] O. Molokanova, A. Bogdan, M. O. Vysotsky, M. Bolte, T. Ikai, Y. Okamoto, V. Böhmer, *Chem. Eur. J.* **2007**, *13*, 6157-6170.

[29] W. Steinle, K. Rück-Braun, *Org. Lett.* **2003**, *5*, 141-144.

[30] T. Schadendorf, C. Hoppmann, K. Rück-Braun, *Tetrahedron Lett.* **2007**, *48*, 9044-9047.

[31] T. Cordes, T. Schadendorf, B. Priewisch, K. Rück-Braun, W. Zinth, *J. Phys. Chem. A* **2008**, *112*, 581-588.

[32] B. Maerz, S. Wiedbrauk, S. Oesterling, E. Samoylova, A. Nenov, P. Mayer, R. de Vivie-Riedle, W. Zinth, H. Dube, *Chem. Eur. J.* **2014**, *20*, 13984-13992.

[33] J. Wang, K. Rueck-Braun, *ChemPhotoChem* **2017**, *1*, 493-498.

[34] O. Mogck, V. Böhmer, W. Vogt, *Tetrahedron* **1996**, *52*, 8489-8496.

[35] O. Mogck, M. Pons, V. Böhmer, W. Vogt, *J. Am. Chem. Soc.* **1997**, *119*, 5706-5712.

Chapter 4

## Self-assembly of homo- and heterodimeric capsules based on a tetraspiropyran tetraurea calix[4]arene

Manuscript in preparation

UNIVERSITAT ROVIRA I VIRGILI
STIMULI-RESPONSIVE HOST-GUEST SYSTEMS DECORATED WITH HEMITHIOINDIGO AND SPIROPYRAN UNITS
Giulia Moncelsi

Self-assembly of homo- and heterodimeric capsules based on a tetraspiropyran tetraurea
calix[4]arene
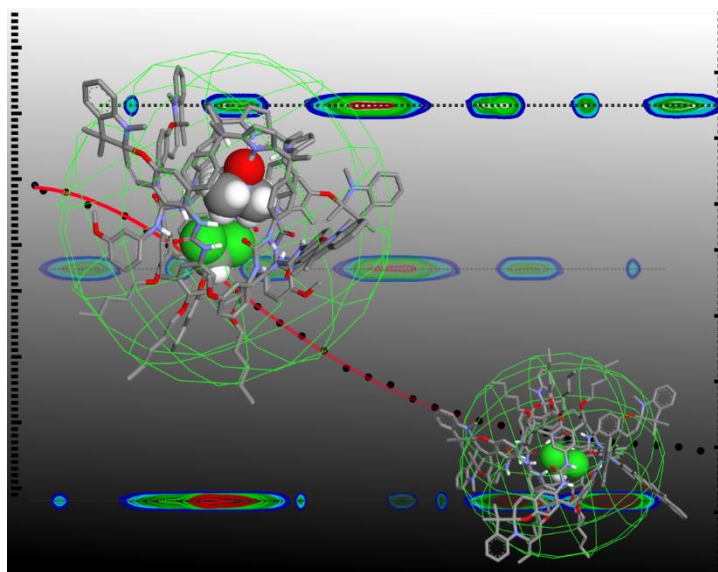
4.1 Introduction

In previous chapters, we already commented that a large number of fatigue-resistant small molecules able to undergo important structural changes when irradiated with UV or visible light have been designed.[1] Well-established and promising families of photoswitches include: azobenzenes,[2] hemithioindigos,[3] acyl hydrazones,[4,5] spiropyrans,[6,7] diarylethenes,[8,9] and donor-acceptor Stenhouse adducts.[10,11,12] Spiropyrans are organic photoswitches that undergo a reversible isomerization process between the colorless, closed-ring (SP) form and the colored open-ring neutral (MC) or protonated (MCH$^+$) merocyanine counterpart. The reversible SP-to-MC isomerization can be promoted by UV light and/or protonation (Scheme 4.1).[6]
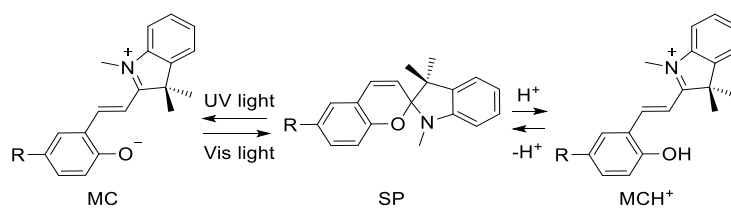
Scheme 4.1 Photo- and acidochromic reversible isomerization processes between a 6'-substituted spiropyran (SP) and its merocyanine (MC) and protonated merocyanine (MCH$^+$) isomers.

The intrinsic photochromic properties of spiropyran switches make them ideal candidates for their use in the design of photo-responsive molecular containers. The SP-to-MC conversion is accompanied by a dramatic change in the geometry of the switch and by a significant difference in the dipole moment between the closed SP-form and the open MC-form. In addition, the SP is susceptible to protonation, which induces its conversion to the MCH$^+$ isomer.

The controlled uptake/release of cargo using molecular containers is usually targeted by the covalent attachment of appropriate responsive fragments onto the receptor's scaffold. The goal consists on coupling the isomerization of the responsive fragment with the binding properties of the container. Thus, the application of an external stimulus (light, pH, etc.) induces a modification of the host-guest properties of the container/receptor.[13,14] To this end, azobenzene photoswitches have been coupled to a wide variety of synthetic macrocycles[15,16,17] and biomolecules.[18,19,20,21]

Chapter 4

The adequate choice of the receptor's scaffold and the location of the isomerizable substituents is essential to impart the construct with the desired property: modulation of its binding affinity through external stimuli. Calix[4]arenes are well-known macrocyclic receptors and their molecular recognition properties have been extensively reported in literature.[22] The upper-rim functionalization of calix[4]arene scaffolds, fixed in the *cone* conformation, with four urea groups produced tetraurea derivatives that self-assemble into dimeric homo- and hetero-capsular assemblies. In non-polar solvents, the resulting capsular containers are stabilized by a cyclic array of sixteen hydrogen bonds. The formed array involves eight head-to-tail hydrogen-bonded urea groups that are unidirectional oriented.[23,24,25] These elegant dimeric assemblies have been exploited for the encapsulation of a wide variety of guests.[26,27,28,29] Many other examples of self-assembled containers, cages and capsules based on hydrogen-bonding and metal-ligand interactions have already been described.[30,31,32,33,34]

Recently, we reported photoresponsive homo- and heterodimeric capsules based on tetraurea calix[4]arenes decorated with differently substituted azobenzene groups at their upper rims.[35,36] On the other hand, Kobayashi *et al.* described the self-assembly of a hexameric capsule based on resorcin[4]arene units bearing azobenzene dendrons at the lower rim.[37] In these examples, the *cis/trans* photoisomerization of the appended azo groups allowed to control the partial assembly/disassembly processes of the hydrogen-bonded capsules and the concomitant uptake and release of the encapsulated guests. We envisioned that the incorporation of SP units to a tetraurea calix[4]arene scaffold would endow the resulting hydrogen-bonded dimeric capsules with photoresponsive behavior. Our aim was to investigate the coupling of the isomerization process of the SP units with the assembly/disassembly process of the capsular dimers.

Herein, we describe the synthesis of the tetra-SP tetraurea calix[4]arene **1**. We study the self-assembly process of the thermodynamically more stable isomer, all-SP-**1**, into a homodimeric capsule in chloroform solution. We also disclose the exclusive self-sorting process that takes places between the tetraurea all-SP-**1** and the photochemical non-responsive tetraurea calix[4]pyrrole **2**. The two tetraureas dimerize quantitatively encapsulating one molecule of trimethylamine *N*-oxide (**3**). Finally, we investigate the photochemical and acid-base modulation of the SP-to-MC equilibria occurring in both the homo- and the heterocapsular

assemblies. To this end, we use UV light-irradiation (λ = 365 nm) and the sequential treatment of the capsular dimers with trifluoromethanesulfonic acid and triethylamine.

4.2 Results and discussion

4.2.1 Design and synthesis

Tetraspiropyran tetraurea calix[4]arene SP-**1** was synthesized in three steps (Scheme 4.2). First, commercially available 6'-nitrospiropyran (**BIPS**) was reduced to the corresponding amine SP-**4** with stannous chloride dihydrate by refluxing the mixture in EtOH solution.[38] After work-up, the isolated SP-**4** was used for the next synthetic step without further purification owing to the degradation of the compound under ambient conditions. In turn, tetracarbamate calix[4]arene **5** was prepared from the tetraamino counterpart[39] following a reported procedure.[35] SP-**4** was reacted with tetracarbamate **5** in DMF solution using triethylamine as base. The work-up of the quadruple acyl substitution reaction afforded tetraspiro tetraurea calix[4]arene SP-**1** in a remarkable 67% yield. Tetraspiro tetraurea calix[4]arene SP-**1** was characterized by a set of high-resolution spectra (NMR, HRMS). Spiropyrans are chiral switches possessing a stereogenic spiro-carbon atom. Thus, they can easily racemize through a *cis*-merocyanine intermediate that is prochiral.[40,41] The energy barrier for the epimerization reaction of spiropyrans is *ca*. 21-22 kcal/mol in non-polar organic solvents.[42] In the case of SP-**1**, this translates into the possibility of obtaining SP-**1** as a mixture of several diastereomers. Moreover, the SP units appended to the tetraurea calix[4]arene scaffold in SP-**1** are prone to be isomerized to the open-ring merocyanine isomer (MC) by UV light-irradiation, acid-treatment or solvent-induced conversion.[43,44] Therefore, the tetraurea SP-**1** can exist also as a mixture of possible isomeric conformers: all-SP; SP,SP,SP,MC; SP,SP,MC,MC; SP,MC,SP,MC; SP,MC,MC,MC and all-MC. In order to induce the conversion of all isomers into the all-SP counterpart, a mM $(CD_3)_2SO$ solution of the isolated solid of SP-**1** was thermally equilibrated at 60 °C for 12 h in the dark. The resulting solution was cooled down at RT and analyzed using ^{1}H NMR spectroscopy. In $(CD_3)_2SO$ solution, SP-**1** is a monomer owing to the competitive nature of the solvent for hydrogen-bonding interactions with the urea moieties. The ^{1}H NMR spectrum of thermally equilibrated SP-**1** displayed a single set of sharp and well-resolved proton signals in agreement with a C_{4v} symmetry. We assigned this set of signals to the thermodynamically stable all-SP-**1** isomer.[45] We obtained similar results in the thermal equilibration processes

Chapter 4

performed with tetra-azobenzene tetraurea calix[4]arene[35] and calix[4]pyrrole derivatives.[46] Because SP-**1** shows a single set of proton signals, we assume that the barrier for the (*R*)/(*S*)-SP racemization process is low and its dynamics are fast on the chemical shift timescale.
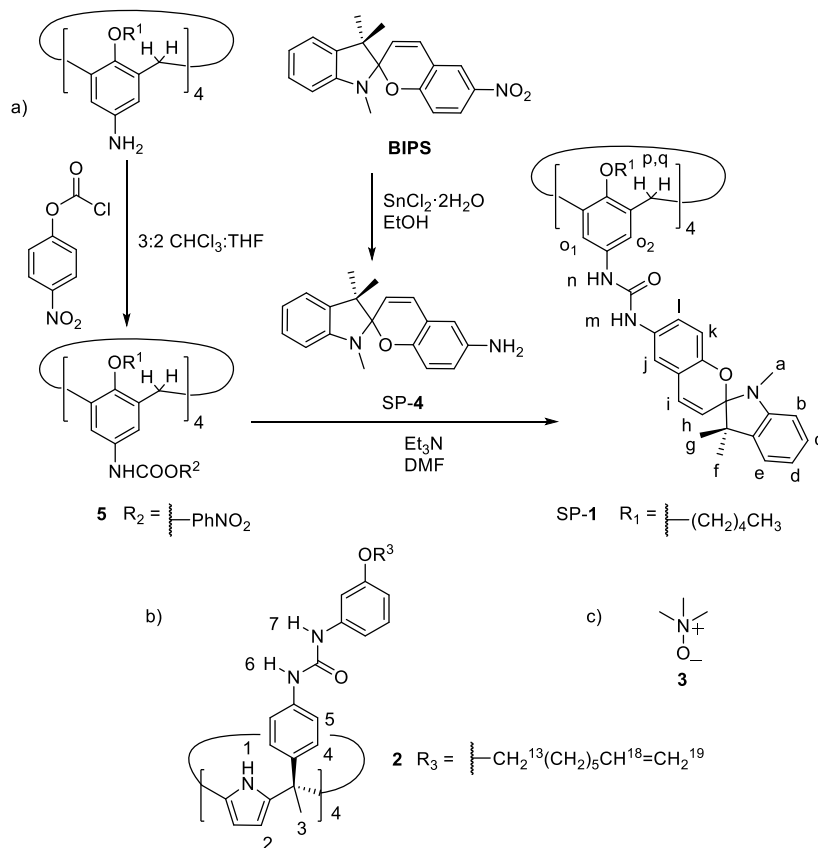
Scheme 4.2 a) Synthetic scheme for the preparation of tetraspiropyran tetraurea calix[4]arene SP-**1**; the line-drawing structures of the b) tetraurea calix[4]pyrrole **2** and c) trimethylamine *N*-oxide **3** are also shown.

4.2.2 Photoisomerization studies of all-SP-**1**

As mentioned above, the upper rim SP groups in all-SP-**1** can undergo light-induced isomerization to the open-ring MC-form. Firstly, we probed the photoisomerization process of all-SP-**1** as a discrete molecule in $(CH_3)_2SO$ solution using UV/Vis spectroscopy. The absorption spectrum of all-SP-**1** shows an intense band centered at 345 nm with a shoulder having a maximum at 390 nm (Figure 4.1). Irradiation of the $(CH_3)_2SO$ solution of all-SP-**1** with 365 nm light produced dramatic changes in the absorption spectrum. The shoulder band

UNIVERSITAT ROVIRA I VIRGILI
STIMULI-RESPONSIVE HOST-GUEST SYSTEMS DECORATED WITH HEMITHIOINDIGO AND SPIROPYRAN UNITS
Giulia Moncelsi

Self-assembly of homo- and heterodimeric capsules based on a tetraspiropyran tetraurea calix[4]arene

at 390 nm increased significantly. A new band with strong absorption appeared at 460 nm. Taken together, these spectral changes are diagnostic of the conversion of some SP units in all-SP-**1** into the open-ring MC-form.[47] After 30 min of light-irradiation, the photostationary state of the mixture was reached.
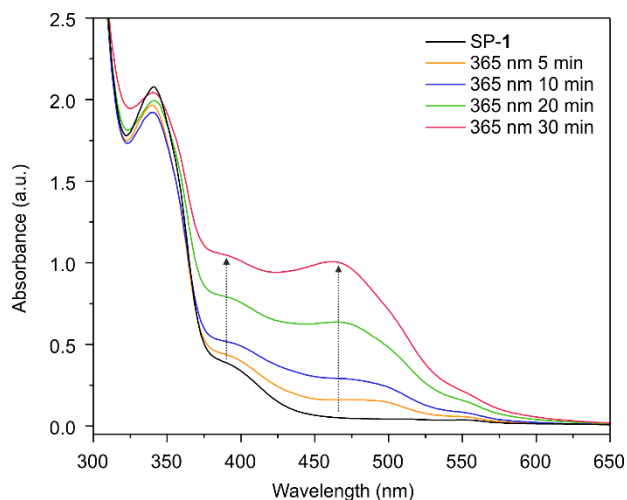

Figure 4.1 UV/Vis absorption spectra acquired for all-SP-**1** (50 µM) dissolved in (CH$_3$)$_2$SO solution upon the time-course (5 to 30 min) of a light-irradiation experiment with 365 nm light.

Remarkably, the intense absorption band centered at 345 nm, which is assigned to the SP-form, was not significantly modified. The results of the analysis of the light-irradiation experiment using UV/Vis spectroscopy did not allow us to quantify the extent of the SP-to-MC isomerization process. For this reason, we repeated the light-irradiation experiment using a 1 mM (CD$_3$)$_2$SO solution of all-SP-**1**. In this case, we monitored the evolution of the mixture every 5 min during 1 h using ^{1}H NMR spectroscopy. Surprisingly to us, the irradiation experiment did not produce noticeable changes in the acquired ^{1}H NMR spectra. Most likely, the concentration of the mixture of MC-enriched isomers of **1** produced by the photo-induced isomerization process is too low to be detected by ^{1}H NMR spectroscopy (i.e. <5 %).[48]

4.2.3 Self-assembly of a homodimeric capsule derived from all-SP-**1** in chloroform

The ^{1}H NMR spectrum of all-SP-**1** in CD$_2$Cl$_2$ solution showed broad and unresolved proton signals indicative of the formation of ill-defined polymeric aggregates. It is known that

Chapter 4

simple tetraurea calix[4]arenes show a reduced tendency to dimerize into well-defined capsular assemblies when dissolved in CH_2Cl_2 solution. The size of the CH_2Cl_2 does not provide a good fit for the cavity of the dimeric capsule.[26] In striking contrast with the above results, the ^{1}H NMR spectrum of a 1 mM solution of all-SP-**1** in $CDCl_3$ displayed an intense set of sharp proton signals together with other proton signals experiencing baseline broadening (Figure 4.2). The set of intense and sharp proton signals was diagnostic of the dimerization of all-SP-**1** into a structurally well-defined hydrogen-bonding capsular dimer, (all-SP-**1**)$_2$. The urea NH protons of (all-SP-**1**)$_2$, $H^{m'}$ and $H^{n'}$, resonated at 9.2 and 7.0 ppm, respectively. The dimer features a S_8 symmetry owing to the desymmetrization of the aryl protons ($H^{o1'}$ and $H^{o2'}$) produced by the unidirectional orientation of the urea bond belt, whose rotation is slow on the NMR time scale. [49] It is known that the observation of two separated *meta*-coupled aryl doublets is diagnostic of the dimerization of tetraurea calix[4]arenes in solution.[23]
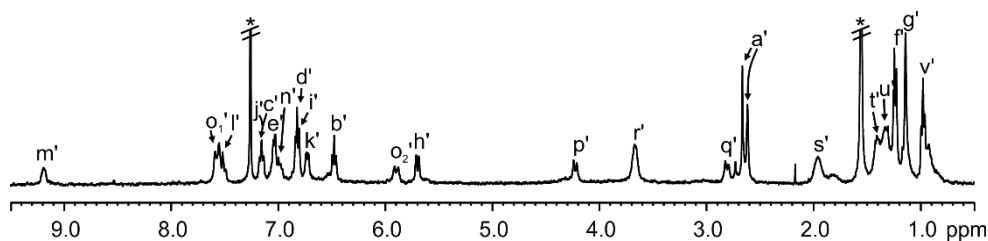

Figure 4.2 ^{1}H NMR ($CDCl_3$, 400 MHz) spectrum of a 1 mM solution of (all-SP-**1**)$_2$. Primed letters and numbers correspond to proton signals of bound components. See Scheme 4.2 for proton assignment. * Residual solvent peaks.

The observation of broadened proton signals suggested the existence of a dynamic equilibrium in solution. Most likely, the all-SP-**1** units of the dimeric capsule (all-SP-**1**)$_2$ are in equilibrium with other aggregates of higher stoichiometry. Interestingly, the diagnostic *N*-methyl proton signal of the SP units ($H^{a'}$) split into two singlets of different intensities at δ = 2.66 and 2.61 ppm. This observation is consistent with a higher energy barrier for the $(R)/(S)$ epimerization of the SP units when **1** is involved in the dimeric assembly. Therefore, the *N*-CH_3 will produce a different signal depending if it is inwardly or outwardly directed with respect to the capsular environment. Simple molecular modelling studies (MM3) on the homodimeric capsule (all-SP-**1**)$_2$ together with previous investigations with structurally related tetraurea calix[4]arene capsules supported the encapsulation of one chloroform molecule in its cavity. In order to provide evidence to the encapsulation of $CHCl_3$ in (all-SP-

1)$_2$, we performed a 1D GOESY NMR experiment. We used a 2 mM solution of (all-SP-**1**)$_2$ in a 9:1 CHCl$_3$:CDCl$_3$ mixture. The selective excitation of the proton signal corresponding to the bulk CHCl$_3$ produced the observation in the GOESY spectrum of a small singlet with the same phase and resonating at $\delta = 4.43$ ppm (Figure 4.3).
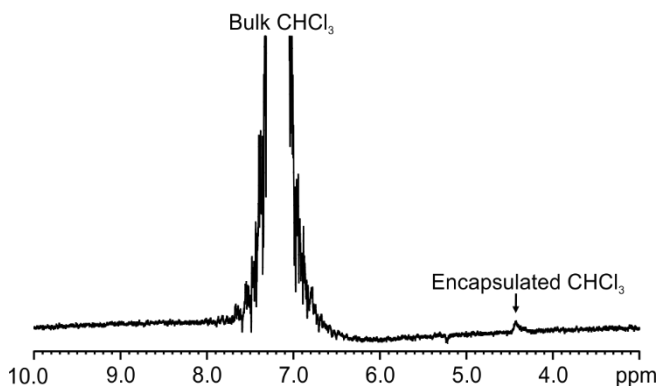

Figure 4.3 Selected region of the ^{1}H GOESY NMR spectrum (298 K, 500 MHz) of (all-SP-**1**)$_2$ in a 9:1 CHCl$_3$:CDCl$_3$ mixture with selective excitation of the solvent signal.

We assigned this signal to the proton of the encapsulated CHCl$_3$ experiencing a chemical exchange process with the bulk solvent molecules that is slow on the chemical shift timescale.[50] The packing coefficient, or volume of filled space, for capsular assemblies is defined as the ratio between the van der Waals volumes of the guest molecules and that of the internal cavity of the capsule ($PC = (V_{guest/s}/V_{host})$ x 100) obtained from energy-minimized models. The calculated PC for the CHCl$_3$⊂(all-SP-**1**)$_2$ complex is *ca*. 42%. This value is relatively small compared to the optimal 55% reported by Rebek and co-workers[51] and might explain the reduced thermodynamic stability of the dimeric capsule, (all-SP-**1**)$_2$ and its existence in equilibria with ill-defined aggregates of all-SP-**1**. Steric clashes between adjacent spiropyran substituents can cause the suboptimal arrangement of the two halves in the CHCl$_3$⊂(all-SP-**1**)$_2$ capsular assembly compared to other derivatives with less-bulky substituents, i.e. the phenyl in **2**. The assembly of the homodimeric capsule, (all-SP-**1**)$_2$ in CDCl$_3$ solution was further evidenced by performing a diffusion ordered spectroscopy (DOSY) experiment. DOSY NMR is a fundamental analytical technique for the characterization of capsular systems in solution.[52] The decays of the proton signals assigned to (all-SP-**1**)$_2$ *vs*. the gradient strength showed a good fit to a monoexponential function and returned a diffusion coefficient of 3.35 ± 0.12 x 10^{-10} m^2/s ($-\log D = 9.47$). This value is

translated into a diffusing spherical particle having a radius of 12.2 Å. The volume of the diffusing particle is consistent with the size of the energy-minimized structure (MM3) of the (all-SP-**1**)$_2$ dimeric capsule. To the best of our knowledge, all-SP-**1** constitutes the first example of a calix[4]arene scaffold decorated with four spiropyrans at its upper rim. Other examples of scaffolds with attached spiropyran groups include a tetra(spiropyran)-substituted porphyrin[53] and calix[4]arenes functionalized at the lower rim with one[54,55] or two spiropyran fragments.[56,57]

4.2.4 Exclusive self-sorting of tetraureas all-SP-**1** and **2** into a heterodimeric capsule in dichloromethane

Tetraurea calix[4]arenes are capable to self-sort with tetraurea calix[4]pyrroles to produce quantitatively heterodimeric capsules. In this vein, we investigated the self-sorting process of all-SP-**1** with tetraurea calix[4]pyrrole **2**[58] in dichloromethane solution using trimethylamine *N*-oxide **3** as template (Scheme 4.2). The ^{1}H NMR spectrum of an equimolar mixture of **2** and *N*-oxide **3** in dichloromethane solution produced the proton signals that are diagnostic of the quantitative formation of the homodimeric capsular assembly, **3**$_2$⊂**2**$_2$ (Figure 4.4a).[58] Notably, the pyrrole NHs appeared at δ = 10.6 ppm owing to the formation of hydrogen bonds with the oxygen atom of **3**. The urea NHs, H[6] and H[7], resonated at δ = 6.3 and 8.7 ppm, respectively. These chemical shift values indicated their involvement in hydrogen bonding interactions. In line with previous findings, we observed that the *meso*-phenyl protons *ortho* to the urea groups (H[5]’ and H[8]’ in the proton assignment) of the calix[4]pyrrole **2** resonated as separate broad signals. This observation suggested that the change in the unidirectional orientation of the urea groups was intermediate on the chemical shift timescale. The signal of the methyl protons of the encapsulated *N*-oxide **3** (**3**-CH$_3$’) resonated at δ = 0.8 ppm. The upfield shift experienced by the methyl protons (Δδ = -2.4 ppm) is caused by the shielding effect of the *meso*-phenyl groups that define the polar aromatic cavity in which the *N*-oxide is deeply included. The addition of a CD$_2$Cl$_2$ solution of SP-**1** (1 equiv., Figure 4.4c) to the one containing the homodimeric capsular assembly, **3**$_2$⊂**2**$_2$, produced a new set of sharp proton signals. The urea NHs of calix[4]pyrrole **2** resonated at δ = 9.1 and 5.4 ppm. These chemical shift values are different to those observed for **3**$_2$⊂**2**$_2$. Additionally, the urea NH protons of all-SP-**1** assembled into a dimeric capsule were observed at 8.8 and 8.0 ppm. Based on previous findings, we assigned the new set of

Self-assembly of homo- and heterodimeric capsules based on a tetraspiropyran tetraurea calix[4]arene

signals to the heterodimeric capsular complex, $3 \subset$(all-SP-$1 \cdot 2$) that was quantitatively assembled in the equimolar mixture (Figure 4.4b). In the case at hand, the signal of the methyl protons of encapsulated **3** (**3**-CH$_3$'') appeared at $\delta = 0.6$ ppm ($\Delta\delta = -2.6$). The small difference in complexation induced shift (CIS), 0.2 ppm, experienced by the methyl protons of **3** in its homo- and hetero-encapsulation complexes, $3_2 \subset 2_2$ and $3 \subset$(all-SP-$1 \cdot 2$), reflects the different magnetic environments of the two capsules' interiors.
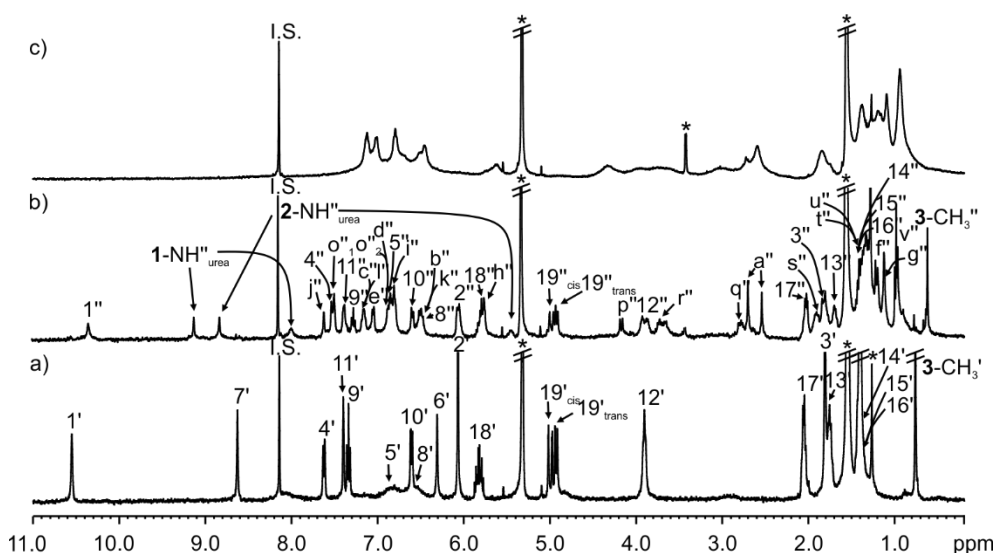

Figure 4.4 ^{1}H NMR (CD$_2$Cl$_2$, 400 MHz) spectra at 298 K of 1.3 mM solutions of a) all-SP-**1**; b) all-SP-**1**, **2** and **3** (1:1:1 molar ratio) (0.65 mM) and c) $3_2 \subset 2_2$. Primed letters and numbers correspond to proton signals of bound components. Double primed letters and numbers correspond to proton signals of bound components involved in the heterocapsular assembly $3 \subset$(all-SP-$1 \cdot 2$). 1,3,5-tris(trifluoromethyl)benzene was used as internal standard (I.S.). See Scheme 4.2 for proton assignment. * Residual solvent peaks.

The energy-minimized structure (MM3) of the heterocapsular complex $3 \subset$(all-SP-$1 \cdot 2$) begs for the co-encapsulation of a dichloromethane molecule with the *N*-oxide **3**. We determined a *PC* value of 63% for the co-encapsulation complex (CH$_2$Cl$_2 \cdot$**3**)$\subset$(all-SP-$1 \cdot 2$) complex. Although the calculated value is slightly larger than the optimal 55%, it is in agreement with those we determined for the encapsulation complexes of polar molecules in dimeric capsules with polar interiors.[59] The energy minimized structure of the (CH$_2$Cl$_2 \cdot$**3**)$\subset$(all-SP-$1 \cdot 2$) complex displays a reduction in the steric clashes produced by the spiropyran substituents compared to the homodimeric (CHCl$_3$)$\subset$(all-SP-**1**)$_2$ assembly (Figure 4.5b). Most likely, this effect causes an increase in the thermodynamic stability of the former assembly. In the

Chapter 4

heterodimer, the aromatic protons *ortho* to the urea groups of the two halves appear as sharp diastereotopic signals. This observation supports an increase in the energy barrier for the interconversion between the two senses of rotation of the unidirectional oriented urea groups owing to stronger hydrogen bonds. The formation of the heterocapsular assembly was also supported by the results of a DOSY experiment (Figure 4.5a). The calculated diffusion coefficient for $3\subset$(all-SP-**1**·**2**) is 4.36 ± 0.02 x 10^{-10} m²/s ($-\log D = 9.36$). This value corresponds to a spherical diffusing particle with a radius of 12.1 Å. The volume of the spherical diffusing particle fits nicely with the energy-minimized structure of the heterocapsule $3\subset$(all-SP-**1**·**2**) (Figure 4.5b).[49]

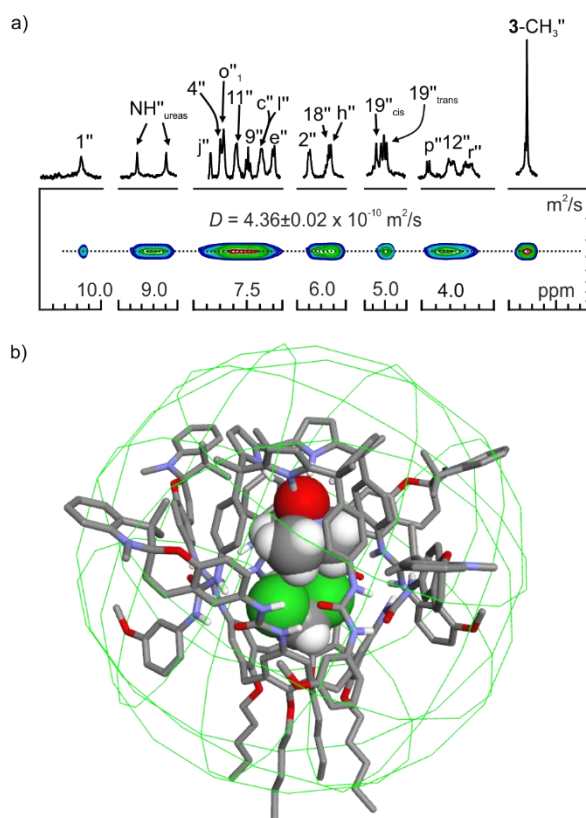**Figure 4.5** a) Selected regions of the *pseudo*-2D plot of the DOSY experiment performed with the solution containing $3\subset$(all-SP-**1**·**2**). Double primed letters and numbers correspond to proton signals of bound components. See Scheme 4.2 for proton assignment. b) Energy-minimized structure (MM3) of $(CH_2Cl_2 \cdot \mathbf{3})\subset$(all-SP-**1**·**2**) superimposed to a sphere with a radius of 12.1 Å centered at the geometrical centre of the capsule. The halves of the capsule are depicted in stick representation and the encapsulated guests as CPK models. The allylic chains in **2** were pruned to methoxy groups, and non-polar hydrogens of **1** and **2** were omitted for clarity.

Self-assembly of homo- and heterodimeric capsules based on a tetraspiropyran tetraurea calix[4]arene

4.2.5 Encapsulation studies of Me_4X^+ salts with all-SP-**1**

Similarly to the previous chapter, we carried out encapsulation studies using all-SP-**1** and tetramethyl-onium salts, Me_4X^+ salts (X = N, P). The addition of incremental amounts of $Me_4N^+BArF^-$ (**8**) to a millimolar dichloromethane solution of all-SP-**1** produced a sharpening of all proton signals belonging to the tetraurea (Figure 4.6). In the presence of 0.5 molar equiv. of **8**, a broad singlet appeared in the upfield region of the ^1H NMR spectrum, $\delta = 0.14$ ppm. The signal was assigned to the methyl protons of the encapsulated cation ($Me_4N^{+'}$) in the dimeric assembly. Upon the addition of more than 0.5 equiv. of **8** to the solution, we detected the singlet belonging to free Me_4N^+ resonating at $\delta = 3.19$ ppm ($\Delta\delta = 3.05$ ppm). We attribute the broadening of the methyl signal of the species $Me_4N^{+'}$ to the presence of multiple isomers of the hydrogen-bonded capsular dimer. The rotation barrier of the single bond connecting the spiropyran fragments to the ureas on the receptor's scaffold might increase in the capsular dimer and, as mentioned above, the energy barrier for the racemization of the spiropyran units may also be modified.
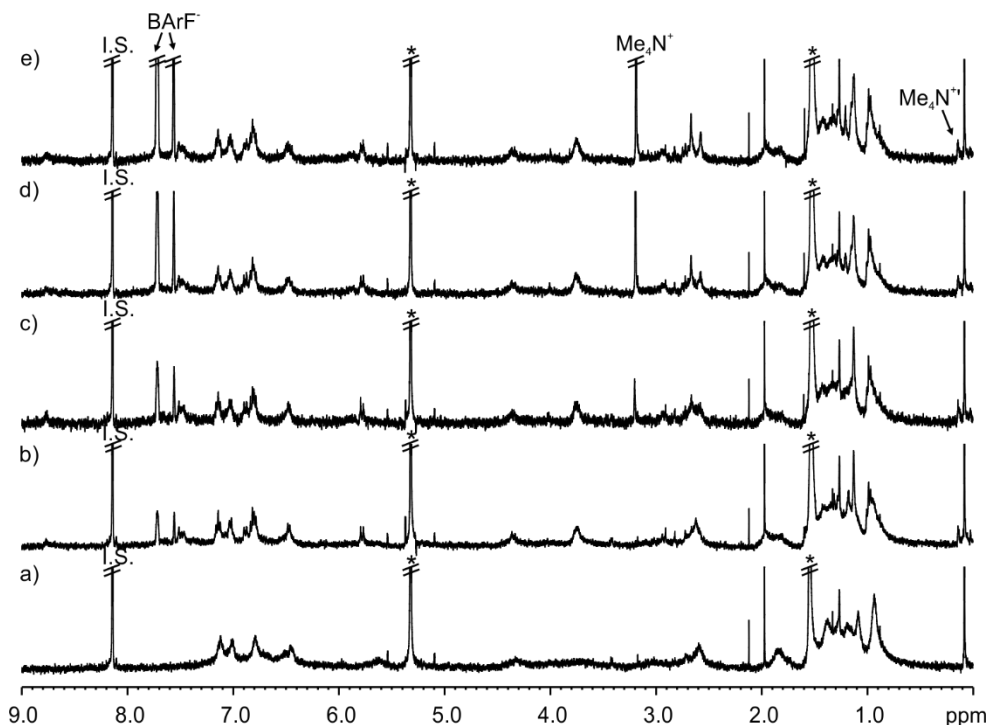

Figure 4.6 Selected regions of the ^1H NMR (CD_2Cl_2, 400 MHz) spectra at 298 K of a 1 mM solution of receptor all-SP-**1** + a) 0; b) 0.25; c) 0.5; d) 1 and e) 1.5 equiv. of **8**. Primed letters and numbers

Chapter 4

correspond to proton signals of bound components. 1,3,5-tris(trifluoromethyl)benzene was used as internal standard (I.S.). * Residual solvent peaks.

Next, we titrated a millimolar dichloromethane solution of all-SP-**1** with $Me_4P^+BArF^-$ (**7**). The addition of incremental amounts of **7** produced a sharpening of all proton signals belonging to the receptor. This result contrasts with our findings described in chapter 3 upon titrating the tetra-HTI tetraurea calix[4]arene with **7**, for which we did not observe any evidence of the formation of the dimeric assembly. In the presence of 0.5 molar equiv. of **7**, a broad doublet appeared in the highly upfield region of the ^1H NMR spectrum, δ = -0.90 ppm. The signal was assigned to the methyl protons of the encapsulated cation ($Me_4P^{+'}$). We also detected the doublet belonging to the methyl protons of free Me_4P^+ resonating at 1.90 ppm ($\Delta\delta$ = 2.80 ppm). When 1 equiv. of **7** was added to the solution, the peak for the free Me_4P^+ cation was observed at 25.8 ppm in its ^{31}P NMR spectrum. When a more concentrated CD_2Cl_2 solution of all-SP-**1** was prepared (2 mM) and 1 equiv. of **7** was added to the solution, the resulting ^1H NMR spectrum displayed a set of well-resolved proton peaks (Figure 4.7). Notably, the doublet belonging to the included cation appearing at -0.87 ppm was now sharp and indicative of the formation of the homocapsular assembly $7 \subset (all-SP-1)_2$. The phosphorus signal for the encapsulated cation was also evident in the corresponding ^{31}P NMR spectrum resonating at δ = 24.6 ppm (Figure 4.7, inset).
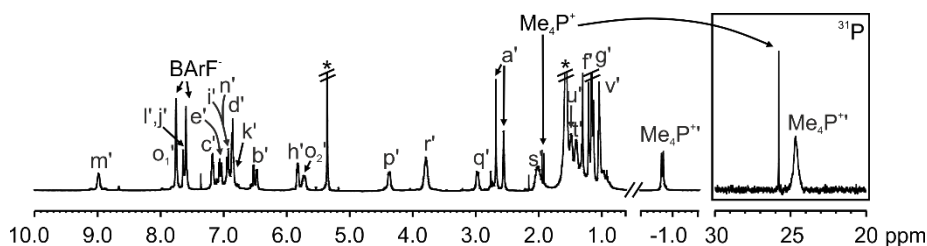
Figure 4.7 Selected regions of the ^1H and ^{31}P NMR (CD_2Cl_2, 400 and 162 MHz) spectra at 298 K of a 2 mM solution of receptor all-SP-**1** + 1 equiv. of **7**. Primed letters and numbers correspond to proton signals of bound components. * Residual solvent peaks.

In the experiments above, the detection of the Me_4P^+ free in solution in the presence of 0.5 equiv. of **7** indicated that the self-assembly of the dimeric capsule was not quantitative.

Self-assembly of homo- and heterodimeric capsules based on a tetraspiropyran tetraurea
calix[4]arene

4.2.6 Photochemical and acid-base modulation of the SP-to-MC isomerization processes of the tetraurea all-SP-**1** assembled in homo- and heterocapsules.

The light-irradiation experiments of the homocapsule (all-SP-**1**)$_2$ and heterocapsule **3**⊂(all-SP-**1·2**) in chloroform and dichloromethane solutions, respectively, were monitored using UV/Vis and ^{1}H NMR spectroscopy. For the UV/Vis experiments, aliquots (100 µl) of thermally equilibrated 1 mM solutions of the capsular assemblies, previously analyzed by ^{1}H NMR spectroscopy, were taken and diluted to 2 mL in a quartz cuvette affording 50 µM solutions. Based on literature precedents,[60] we assume that the dimerization constant is larger than 10^8 M^{-1}. For this reason, at 50 µM concentration of the tetraurea we estimate its quantitative assembly into the dimer. It is also known that some tetra-aryl tetraurea calix[4]arene derivatives dimerize exclusively at the dilution limit of the 600 MHz NMR spectrometer (i.e. 72 µM in CDCl$_3$). The UV/Vis absorption spectra of the initial solution and after irradiation at 365 nm up to 6 (Figure 4.8a) or 10 min (Figure 4.8b) (PSSs) were recorded. The solutions changed from colorless to red or pink after 2 min of irradiation. The absorption spectra of (all-SP-**1**)$_2$ in CHCl$_3$ showed the appearance of two intense bands at 393 and 490 nm upon irradiation with 365 nm light. Similarly to the results obtained for **1** in (CH$_3$)$_2$SO solution (*vide supra*), the observation of these two bands is consistent with the formation of open-ring merocyanine isomer units in **1**. The photoirradiation of **3**⊂(all-SP-**1·2**) also produced absorption spectra changes characteristic of the formation of open-ring merocyanines units in the calix[4]arene half.
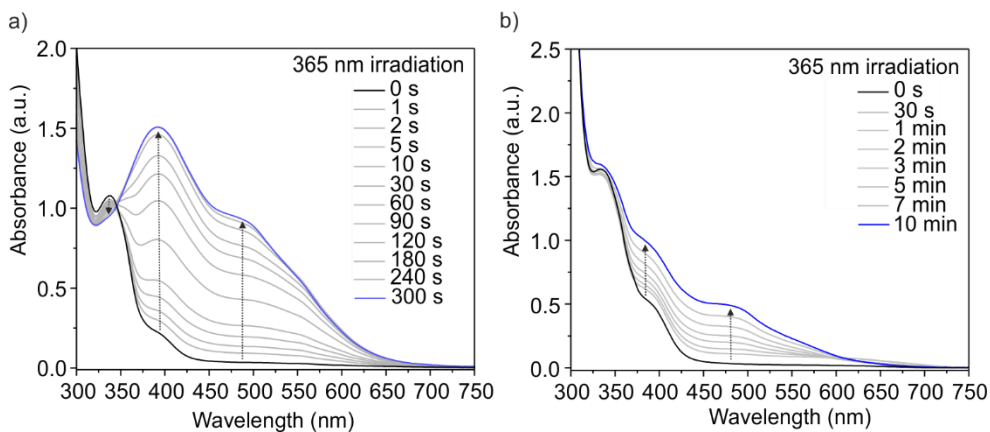

Figure 4.8 UV/Vis absorption spectra of a 50 µM solution of a) (all-SP-**1**)$_2$ in CDCl$_3$ and b) **3**⊂(all-SP-**1·2**) in CD$_2$Cl$_2$ light-irradiated at 365 nm at different times.

Chapter 4

Owing to the observation of the earmarks of the spiropyran ring-opening to the merocyanines by UV/Vis spectroscopy, we monitored the photoirradiation experiments of the homo- and heterocapsular assemblies using ^{1}H NMR spectroscopy.[61] The irradiation at 365 nm up to 7 min of a millimolar chloroform solution of homocapsule (all-SP-**1**)₂ produced a general broadening and decrease in intensity in the diagnostic signals of the assembly. The irradiation at 365 nm for 5 min of the **3**⊂(all-SP-**1**·**2**) capsular assembly did not lead to changes in its proton signals. This result indicates that the heterocapsule **3**⊂(all-SP-**1**·**2**) is stable and persists in solution after exposure to UV light. The photochromic SP units, probably acting as "inert filters", absorb the high-energy photons and form open-ring merocyanines to a reduced extent or dissipate the energy through a different pathway, either way protecting the other components of the assembly from photodegradation.

Next, we investigated the acid-base modulation of the SP-to-MC isomerization occurring in the spiropyran substituents of all-SP-**1** assembled as both the homo- and heterodimeric capsules. Rudkevich and co-workers[62] reported that the addition of up to 20 equiv. of trifluoroacetic acid to a solution of a polymeric capsule derived from a bis-tetraurea calix[4]arene did not break the self-assembling polymeric chain. Moreover, it is well-known that the acidochromism of 6'-nitroSP requires large amounts of trifluoroacetic acid. It manifests in small bathochromic shifts and results in the formation in minor amounts of the protonated MCH⁺ species.[63,64] On the contrary, in polar solvents, the use of strong acids like trifluoromethanesulfonic (TfOH; pK_a = 0.7) in near to stoichiometric amounts results in the extensive formation of the *Z*-isomer of the MCH⁺ form. The addition of 8 equiv. of TfOH to a 2 mM CDCl₃ solution of the homodimer (all-SP-**1**)₂ (1 equiv. of TfOH per spiropyran group) induced the colorless solution to adopt a deep red color. The analysis of the mixture using ^{1}H NMR spectroscopy displayed significant broadening of the proton signals all-SP-**1** (Figure 4.9b). Taken together, these results suggested the isomerization of, at least some, of the SP substituents of all-SP-**1** into the open MCH⁺-form. The exact quantification of the extent of the isomerization process is not trivial owing to signal broadening and reduced changes in chemical shifts. Likewise, it is difficult for us to ascertain if the SP-**1** derivatives enriched with MCH⁺ substituents are capable to assemble into capsular dimeric aggregates. Most likely, an equilibrium between dimeric and oligomeric aggregates deriving from the MCH⁺ enriched SP-**1** units is established in solution producing the observed broadening of the proton signals. We hypothesized that the MCH⁺ units of **1** have a strong tendency to aggregate and form large polymeric assemblies that are not detectable by ^{1}H NMR

Self-assembly of homo- and heterodimeric capsules based on a tetraspiropyran tetraurea calix[4]arene

spectroscopy. We support this hypothesis in the known tendency of merocyanine and cyanine dyes to aggregation.[65] The addition of base (8 equiv. of dry triethylamine to the above solution) restored the initial color and produced a ^{1}H NMR spectrum displaying the diagnostic proton signals of the (all-SP-**1**)$_2$ dimeric capsule (Figure 4.9c). This result evidenced the reversibility of the acid/base induced SP-to-MC isomerization and the chemical stability of the multiple isomers of the tetraurea calix[4]-arene **1** in the employed acid/base conditions.
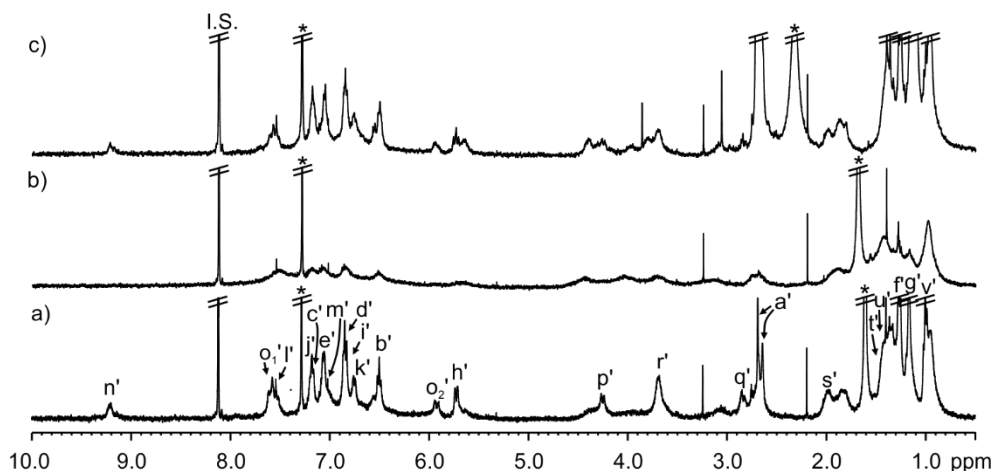

Figure 4.9 ^{1}H NMR (CDCl$_3$, 400 MHz) spectra at 298 K of a 2 mM solution of homocapsule (all-SP-**1**)$_2$ treated with a) 0, b) 8 equiv. of TfOH and c) 8 equiv. of Et$_3$N. 1,3,5-tris(trifluoromethyl)benzene was used as internal standard (I.S.). See Scheme 4.2 for proton assignment.* Residual solvent peaks.

The acid/base modulation of the SP-to-MC isomerization for (all-SP-**1**)$_2$ was also monitored by using UV/Vis spectroscopy (Figure 4.10). Briefly, the addition of TfOH to the solution of (all-SP-**1**)$_2$ produced the increase of the absorption band centered at 393 nm and the emergence of a new band with a maximum at 510 nm. The observed spectral changes are in agreement with the isomerization of the SP-substituents in all-SP-**1** into the open-ring protonated MCH$^+$-counterparts, thus, putatively producing all-MCH$^+$-**1** or a mixture of isomers of **1** enriched with MCH$^+$ units. The subsequent addition of triethylamine restored the absorption spectrum assigned to (all-SP-**1**)$_2$.
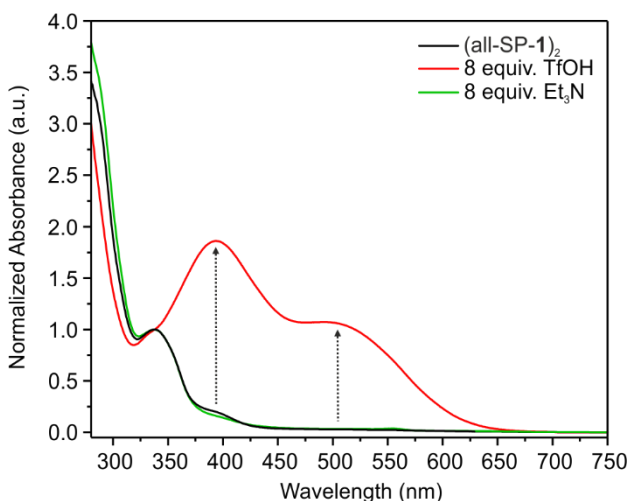
Chapter 4

Figure 4.10 Normalized UV/Vis absorption spectra of (all-SP-**1**)$_2$ in chloroform (50 µM): initial solution (black); treatment with 8 equiv. of TfOH (red) and neutralization with 8 equiv. of Et$_3$N (green). The spectra were normalized to the value of maximum absorbance of (all-SP-**1**)$_2$ (*ca.* 338 nm).

An analogous acid/base modulation of the SP-to-MCH$^+$ isomerization of the substituents of **1** was performed starting from the heterodimeric **3**⊂(all-SP-**1·2**) capsule in dichloromethane solution. In this case, the ^{1}H NMR spectrum of the solution acquired after the addition of TfOH (4 equiv.) still showed a set of sharp and well-defined proton signals of the heterodimeric capsule (Figure 4.11). Nevertheless, some broadened proton signals were also evident in the baseline of the ^{1}H NMR spectrum. Most likely, some of the added equiv. of TfOH acid protonated other basic centers of the assembly in addition to the SP-units. The observation of a broad singlet, resonating at δ = 2.95 ppm, was assigned to the partially protonated *N*-oxide **3** released to the bulk solution. The observation of two separate signals for the methyl protons of released and encapsulated *N*-oxide **3** indicated that they are involved in a chemical exchange process that is slow on the chemical shift timescale. On the other hand, the appearance of a broad and downfield shifted signal for the *N*-oxide **3** released to the bulk solution supports that the chemical exchange between the protonated and non-protonated forms is fast on the same timescale.

Self-assembly of homo- and heterodimeric capsules based on a tetraspiropyran tetraurea
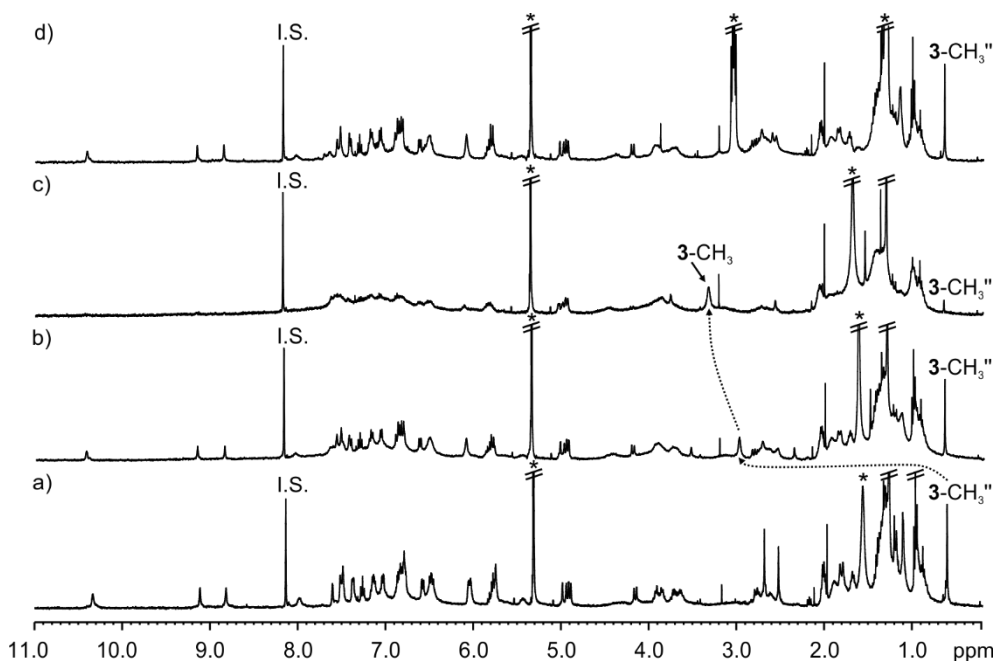*calix[4]arene*

Figure 4.11 ^{1}H NMR (CD$_2$Cl$_2$, 400 MHz) spectra at 298 K of a 2 mM solution of heterocapsule **3**⊂(all-SP-**1·2**) treated with a) 0, b) 4, c) 8 equiv. of TfOH and d) 4 equiv. of Et$_3$N. Double primed letters and numbers correspond to proton signals of bound **3**. 1,3,5-tris(trifluoromethyl)benzene was used as internal standard (I.S.). * Residual solvent peaks.

Based on the integral values, we estimated that the ratio of released and encapsulated *N*-oxide **3** was 55:45. Because the singlet of the methyl protons of the encapsulated *N*-oxide **3** shifted slightly downfield after the addition of TfOH acid, we must conclude that partially protonated capsular dimeric species in addition to **3**⊂(all-SP-**1·2**) might be present in solution. Most likely, the disassembly of the heterodimeric aggregates requires and extensive protonation of the SP units of **1**, i.e. dimeric assemblies having one or more MCH$^+$ units are thermodynamically stable (i.e. **3**⊂(1MCH$^+$-3SP-**1·2**)). The addition of 4 equiv. more of TfOH acid produced a significant increase and downfield shift of the broad singlet assigned to the *N*-oxide **3** in the bulk solution. This observation was concomitant with the broadening of the signals assigned to the two halves of the dimeric assemblies. This result further confirmed that the increase of MCH$^+$ units in **1** reduces the thermodynamic stability of the resulting dimers and induces the formation of non-capsular aggregates.[66] Finally, the addition of 8 equiv. of Et$_3$N to the latter solution produced a new set of sharpened proton signals that coincided with those of the **3**⊂(all-SP-**1·2**) capsule.[67] The obtained results demonstrated the

Chapter 4

reversibility of the acid-base modulation of the SP-to-MCH$^+$ isomerization process of the substituents of **1** and the stability of the capsular component to the used conditions.

4.3 Conclusions

In this chapter, we reported the synthesis of an unprecedented tetraurea calix[4]arene decorated with four upper rim spiropyran groups. The synthetized calix[4]arene self-assembles into a dimeric capsule in chloroform solution. The response of the homodimeric capsule to light-irradiation was only detected at micromolar concentrations by UV-Vis spectroscopy. However, the spiropyran groups of the calix[4]arene are isomerized to protonated merocyanines at both milli- and micromolar concentrations using TfOH. The tetraspiropyran tetraurea calix[4]arene all-SP-**1** and tetraurea calix[4]pyrrole **2** form a heterodimeric capsular assembly with one molecule of trimethylamine *N*-oxide (**3**) and one molecule of solvent in dichloromethane solution. The photo- and acid-behavior of the heterocapsule **3**⊂(all-SP-**1·2**) were also studied and suggest that the heterocapsule is disintegrated by the addition of a strong acid causing the release of the guest to the bulk solution. The initial state of the system is restored by addition of a suitable base. The work contained in this chapter constitutes an extension to our previous findings on hydrogen-bonded homo- and heterodimeric capsules, and explores the effect of upper rim substitution of the calix[4]arene scaffold with photo- and acidochromic spiropyran fragments on its self-assembly behavior in chlorinated solvents.

4.4 Experimental section

4.4.1 General information and instrumentation

All syntheses were carried out using chemicals as purchased from commercial sources unless otherwise noted. All commercial solvents and chemicals were of reagent grade quality and were used without further purification except as noted. Dry solvents were taken from a solvent system MB SPS 800 (*MBraun*) and freshly distilled unless otherwise stated. Thin-layer chromatography (TLC) was performed with DC-Alufolien Kieselgel 60 F$_{254}$ (*Merck*) or neutral Al$_2$O$_3$ F$_{254}$ (*Sigma-Aldrich*). Column chromatography was performed with silica gel 60 Å for chromatography (*Sigma-Aldrich*), or active neutral Al$_2$O$_3$ 90 for chromatography (*Merck*). Routine ^{1}H and ^{13}C NMR spectra were recorded on *Bruker* Avance 300 (300 MHz

for ^{1}H NMR), Avance 400 (400 MHz for ^{1}H NMR) or Avance 500 (500 MHz for ^{1}H NMR) ultrashield spectrometers, or on a *Bruker* Avance III 500 with a QNP cryoprobe. Deuterated solvents (*Euriso-Top*) used are indicated in the characterization and chemical shifts are given in ppm. Residual solvent peaks were used as reference. All NMR *J* values are given in Hz. Mass Spectrometry experiments were performed on a *MicroTOF*, *Bruker Daltonics ESI*. The diagnostic peaks are reported in m/z units. IR spectra were recorded on a *Bruker Optics* FT-IR Alpha spectrometer equipped with a DTGS detector, KBr beamsplitter at 4 cm^{-1} resolution using a one bounce ATR accessory with diamond windows. Melting points were measured on a *MP70 Melting Point System* instrument from *Mettler Toledo*. Irradiation experiments were conducted using a custom-made high power light source purchased from *Sahlmann Photochemical Solutions* and consisting of 3 LED-diodes from *Nichia* (365 nm, 241.5 mW·cm^{-2}). UV/Vis spectra were recorded on a *Shimadzu UV-2401PC* spectrophotometer (equipped with a photomultiplier detector, double beam optics and D_2 and W light sources). For the photo- and acidochromic studies, thermally stabilized millimolar solutions of the samples were analyzed by ^{1}H NMR technique. Afterwards, 10÷100 µl aliquots were taken and diluted to 2 mL in a quartz cuvette to afford *ca.* 50 µM solutions of the compounds in different solvents. UV/Vis absorption spectra of the plain samples, after acid/base additions and/or after irradiation at 365 nm were recorded in a quartz cuvette (10 mm path length). Solvents for spectroscopy are indicated in the characterization and were obtained from *Merck*. For the ^{1}H DOSY NMR experiments, working solutions of **1** and **2** were prepared by directly weighting the required amount of solid into the NMR tube. ^{1}H DOSY NMR experiments were performed on samples prepared as stated above and fixing the acquisition parameters to D20 = 0.10 s and P30 = 2 ms. The data were analyzed with the *Dynamics Centre* software (*Bruker*). The diffusion coefficient (*D*) value of each diagnostic signal was determined by applying a one-component exponential fit. The reported *D* values are an average of the *D* values of at least four different proton signals of two different experiments, giving the corresponding standard deviations. For the theoretical size, computational models were obtained by MM3 energy minimization (*SCIGRESS FJ 2.6*). Then, the structure centroid was calculated (*Biovia Discovery Studio Visualizer v16*) and used as the centre of an imaginary sphere with the diameter calculated from the corresponding DOSY data using the Stokes-Einstein equation:

$$R_H = \frac{k_B T}{6\pi n D}$$

Chapter 4

were R_H is the Stokes radius, k_B the Boltzmann constant ($1.38 \cdot 10^{-23}$ J·K^{-1}), T the temperature (298 K), n the viscosity of the solvent (CHCl$_3$ (298 K)= $5.36 \cdot 10^{-4}$ Pa·s; CH$_2$Cl$_2$ (298 K)= $4.13 \cdot 10^{-4}$ Pa·s) and D the diffusion coefficient.

4.4.2 Synthetic procedures

Tetra-amino calix[4]arene **6**, tetracarbamate calix[4]arene **5** and Me$_4$P$^+$BArF$^-$ **7** were synthesized following the methodology described in chapter 3.[35,39]

Tetraspiropyran tetraurea calix[4]arene SP-**1**: tetracarbamate calix[4]arene **5** (50 mg, 0.035 mmol, 1 equiv.) was added to an oven-dried 10 mL Schlenk tube purged 3x with Ar, and dissolved in 2 mL anhydrous DMF under Ar atmosphere. The SP-amine **4** (60 mg, 0.2 mmol, 5.8 equiv.) was dissolved in 2 mL anhydrous DMF and added dropwise to the tube under Ar flow. Finally, freshly distilled Et$_3$N (28 μl, 0.2 mmol, 5.8 equiv.) was added dropwise to the solution. The yellow solution was left stirring at RT protected from light, equipped with an Ar balloon. After 12 h the reaction was stopped, and 10 mL of HPLC DCM were added to the reaction vessel. The solution was transferred to a small extraction funnel. The organic phase was washed with 4% aq. NaHCO$_3$ solution (4x 10 mL) to remove *p*-nitrophenolate until the aqueous phase was clear, and citric acid 1 M solution (1x 10 mL) to remove residual Et$_3$N and excess amine. The organic blood red phase was again washed with 4% aq. NaHCO$_3$ (1x 10 mL) and finally with water (1x 10 mL). The light brown organic phase was dried over sodium sulfate and under reduced pressure to leave around 0.5 mL DCM. MeOH was added dropwise to the brown solution, and slowly a grey dispersion appeared. The suspended liquid was removed by filtration *in vacuo*, the solid collected and left drying overnight under high vacuum (48 mg, 67% yield). R$_f$ = 0.37 (CH$_2$Cl$_2$:CH$_3$OH 99:1). M.p. = >230 °C (decompose). ^{1}H NMR ((CD$_3$)$_2$SO, 500 MHz) δ (ppm): 8.11 (s, 4H); 8.09 (s, 4H); 7.22 (s, 4H); 7.08 (t, J = 7.8 Hz, 4H); 7.06 (d, *J* = 7.2 Hz, 4H); 6.95 (dd, *J* = 8.9, 2.3 Hz, 4H); 6.93 (d, *J* = 10.2 Hz, 4H); 6.78 (s, 8H); 6.75 (t, *J* = 7.3 Hz, 4H); 6.55 (d, *J* = 8.6 Hz, 4H); 6.52 (d, *J* = 7.7 Hz, 4H); 5.73 (d, *J* = 10.2 Hz, 4H); 4.32 (d, *J* = 12.0 Hz, 4H); 3.80 (s, 8H); 3.08 (d, *J* = 12.0 Hz, 4H); 2.61 (s, 12H); 1.90 (s, 8H); 1.38 (s, 16H); 1.18 (s, 8H); 1.06 (s, 8H); 0.93 (s, 12H). ^{13}C {^{1}H} NMR (CDCl$_3$, 126 MHz) δ (ppm): 152.6; 151.0; 148.9; 147.8; 136.3; 134.3; 133.5; 132.4; 129.4; 127.3; 121.3; 120.2; 119.7; 118.8; 118.4; 118.1; 117.0; 114.2; 106.7; 103.4; 74.8; 51.2; 30.7; 29.4; 28.5; 27.9; 25.6; 22.3; 19.8; 14.0. FT-IR ν (cm^{-1}) = 3368 (urea N-H stretching); 2955 (C-H stretching); 1666; 1606; 1539; 1483 (aromatic C=C stretching); 1376; 1301; 1206;

UNIVERSITAT ROVIRA I VIRGILI
STIMULI-RESPONSIVE HOST-GUEST SYSTEMS DECORATED WITH HEMITHIOINDIGO AND SPIROPYRAN UNITS
Giulia Moncelsi

*Self-assembly of homo- and heterodimeric capsules based on a tetraspiropyran tetraurea
calix[4]arene*

1119; 1016; 967; 873; 814; 739; 503. HRMS (MALDI/+) m/z: [M+H]⁺ Calcd. for $C_{128}H_{141}N_{12}O_{12}$: 2038.0786; found: 2038.0759.

Tetraurea calix[4]pyrrole **2** (**tuC[4]P**) was prepared according to a previously reported procedure.[58] ^{1}H NMR ((CD$_3$)$_2$CO, 400 MHz) δ ppm: 8.79 (s, 4H); 8.15 (s, 4H); 7.98 (s, 4H); 7.34 (d, J = 8.1 Hz, 8H); 7.16 (s, 4H); 7.09 (t, J = 8.4 Hz, 4H); 6.94 (d, J = 7.7 Hz, 4H); 6.97 (d, J = 8.4 Hz, 8H); 6.52 (dd, J = 8.1, 1.4 Hz, 4H); 5.98 (s, 8H); 5.81 (m, 4H); 4.99 (dd, J = 17.1, 1.7 Hz, 4H); 4.90 (d, J = 10.2 Hz, 4H); 3.91 (t, J = 6.3 Hz, 8H); 2.81 (m, 8H); 1.87 (s, 12H); 1.72 (quint., J = 7.3 Hz, 8H); 1.41 (m, 24H). The ^{1}H NMR spectrum is in total agreement with what is reported in the literature.

1',3',3'-trimethylspiro[2H-1-benzopyran-2,2′-(2H)-indol]-6-amine SP-**4** was synthesized adapting a reported procedure:[68] 1′,3′-dihydro-1′,3′,3′-trimethyl-6-nitrospiro[2H-1-benzopyran-2,2′-(2H)-indole] (**BIPS**) (210 mg, 0.65 mmol, 1 equiv.) and stannous dichloride dihydrate (728 mg, 3.22 mmol, 4.95 equiv.) were added to a 25 mL amber glass 2-neck round bottom flask purged 3x with argon. Then, the reagents were dissolved in 4 mL of anhydrous EtOH. The reaction mixture was refluxed and magnetically stirred under argon flow. After 2 h the reaction was stopped. The crude was rinsed with EtOH and filtered under vacuum to remove the unreacted stannous dichloride. The resulting turbid red solution was poured into a stirred mixture of 10 mL 1 N aq. NaOH and 5 mL CHCl$_3$. The solution became green and it was poured into a 100 mL separatory funnel. After shaking, the organic layer was separated and the aqueous layer extracted with CHCl$_3$ (1x 50 mL). The combined chloroform solutions were washed with water (2x 50 mL) and dried over sodium sulfate. The resulting brownish solution was dried *in vacuo* to afford a brown oil (152 mg, 80% yield). The amine is air- and light-sensitive and was used for the next step without further purification. R_f = 0. 66 (neutral Al$_2$O$_3$, EtOAc:Hex 1:1). ^{1}H NMR (CDCl$_3$, 400 MHz) δ (ppm): 7.18 (td, J = 7.7, 1.3 Hz, 1H); 7.08 (dd, J = 7.2, 1.1 Hz, 1H); 6.84 (td, J = 7.7, 1.3 Hz, 1H); 6.76 (d, J = 10.2 Hz, 1H); 6.56 (t, J = 8.4 Hz, 1H); 6.52 (d, J = 7.7 Hz, 1H); 6.49 (dd, J = 8.3, 2.7 Hz, 1H); 6.45 (d, J = 2.7 Hz, 1H); 5.67 (d, J = 10.2 Hz, 1H); 3.36 (br s, 2H); 2.73 ppm (s, 3H); 1.32 (s, 3H); 1.17 (s, 3H).

Tetramethylammonium tetrakis(3,5-bis(trifluoromethyl)phenyl)borate **8** (**Me₄N⁺BArF⁻**): a solution of sodium tetrakis(3,5-bis(trifluoromethyl)phenyl)borate (Na⁺BArF⁻, 362 mg, 0.41 mmol, 1.1 equiv.) in 4 ml of anhydrous methanol was added dropwise to a 3 ml solution of tetramethylammonium chloride (38 mg, 0.35 mmol, 1 equiv.) in the same solvent, under

argon flow. The colorless solution was stirred at room temperature and equipped with an Ar balloon. After 7 h the reaction was stopped. The solution was dried under reduced pressure and redissolved in 5 ml of Milli-Q water. The mixture was sonicated to generate a white suspension. The product was filtered out and washed several times with Milli-Q water, then dried under high vacuum to afford a white solid (271 mg, 83% yield). ^{1}H NMR (CD$_2$Cl$_2$, 400 MHz) δ (ppm): 7.76 (br s, 8H); 7.61 (s, 4H); 3.19 (s, 12H). ^{13}C {^{1}H} NMR (CD$_2$Cl$_2$, 101 MHz) δ (ppm): 162.16 (q, $^1J_{B-C}$ = 50 Hz); 135.21; 129.28 (q, $^2J_{C-F}$ = 33 Hz); 126.37; 123.66; 120.96; 117.92; 57.13. ^{19}F {^{1}H} NMR (CD$_2$Cl$_2$, 376 MHz) δ (ppm): -62.90. ^{11}B {^{1}H} NMR (CD$_2$Cl$_2$, 128 MHz) δ (ppm):-6.67.
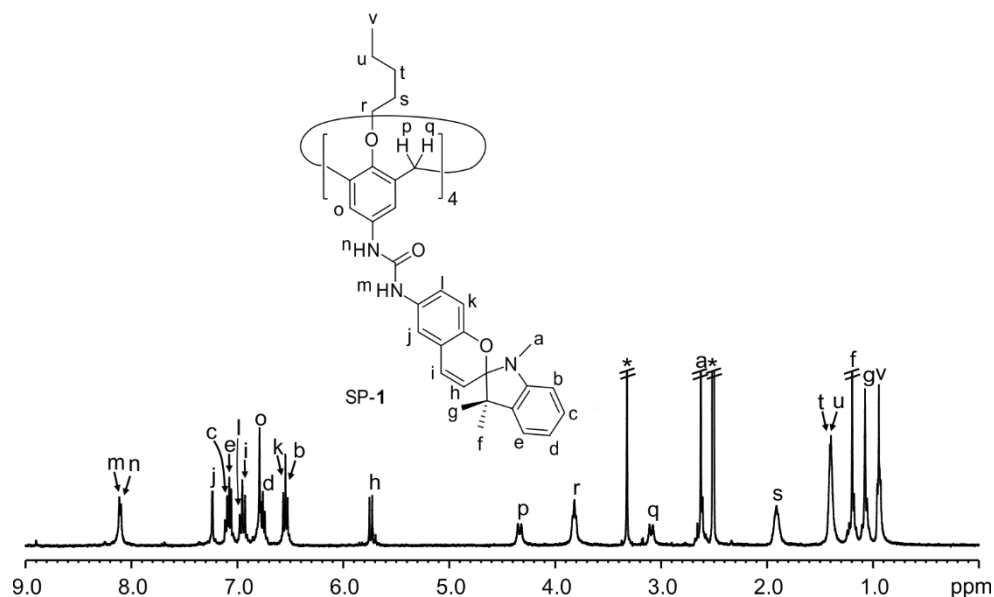
4.4.3 Figures and tables

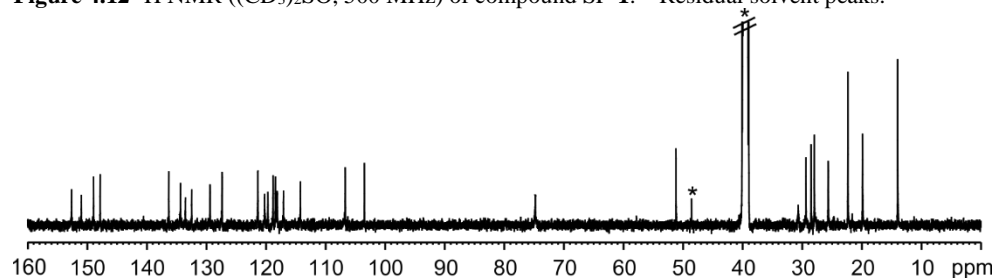**Figure 4.12** ^{1}H NMR ((CD$_3$)$_2$SO, 500 MHz) of compound SP-**1**. * Residual solvent peaks.

Figure 4.13 ^{13}C NMR ((CD$_3$)$_2$SO, 126 MHz) of compound SP-**1**. * Residual solvent peaks.

Self-assembly of homo- and heterodimeric capsules based on a tetraspiropyran tetraurea calix[4]arene
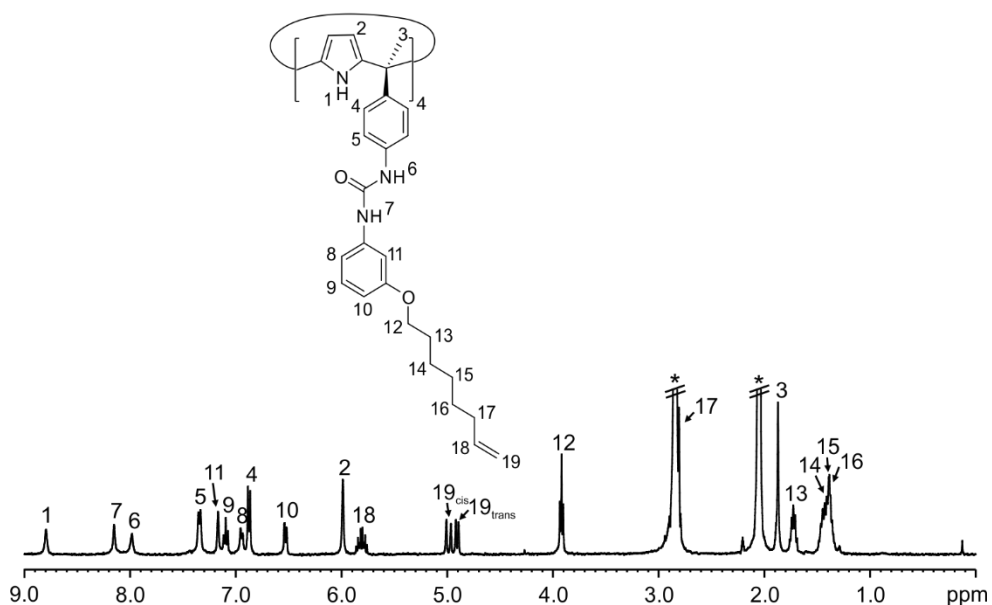

Figure 4.14 ^{1}H NMR ((CD$_3$)$_2$CO, 400 MHz) of a 1 mM solution of compound **2**. * Residual solvent peaks.
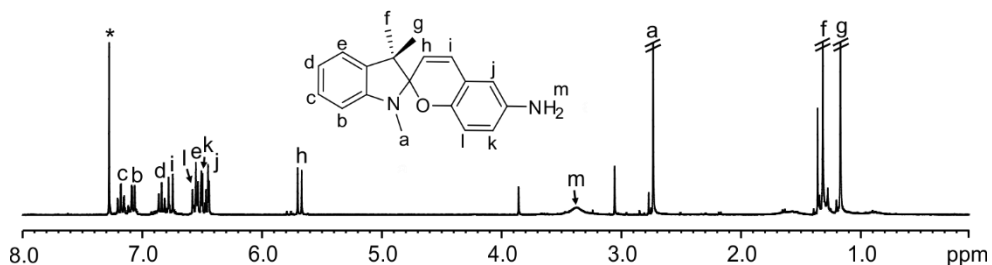

Figure 4.15 ^{1}H NMR (CDCl$_3$, 400 MHz) of 1',3',3'-trimethylspiro[2H-1-benzopyran-2,2'-(2H)-indol]-6-amine SP-**4**. * Residual solvent peaks.
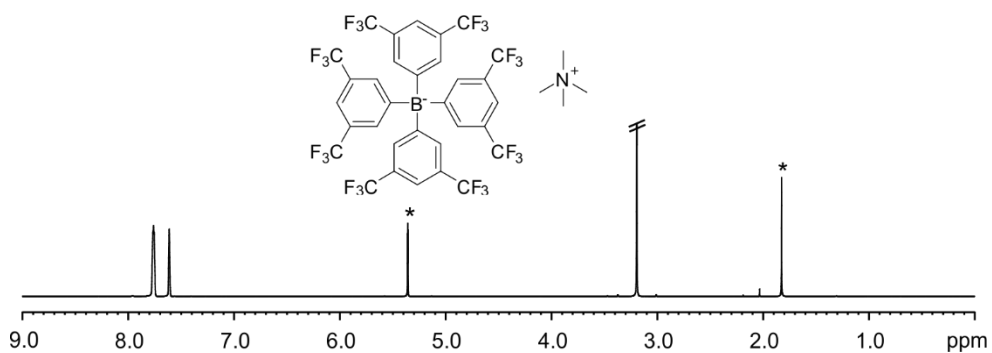

Figure 4.16 ^{1}H NMR (CD$_2$Cl$_2$, 400 MHz) of Me$_4$N$^+$BArF$^-$ **8**. * Residual solvent peaks.

Chapter 4

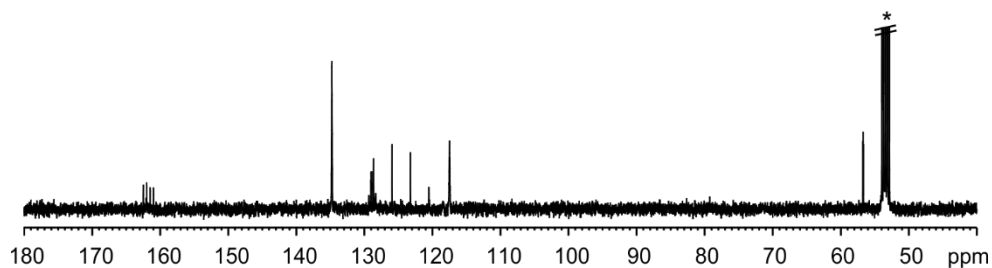**Figure 4.17** ^{13}C NMR (CD$_2$Cl$_2$, 101 MHz) of Me$_4$N$^+$BArF$^-$ **8**. * Residual solvent peaks.

Figure 4.18 Selected aromatic region of the ^1H COSY NMR spectrum ((CD$_3$)$_2$SO, 500 MHz) of SP-**1** showing the diagnostic cross-peaks for the indicated protons. * Residual solvent peaks.

Self-assembly of homo- and heterodimeric capsules based on a tetraspiropyran tetraurea
calix[4]arene

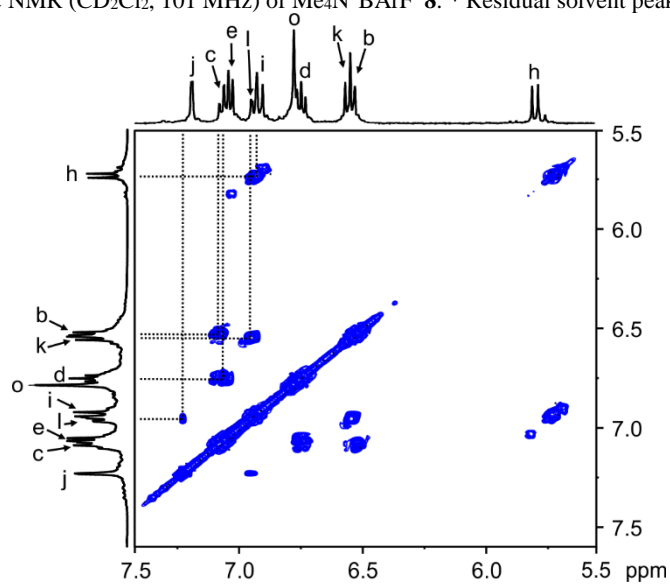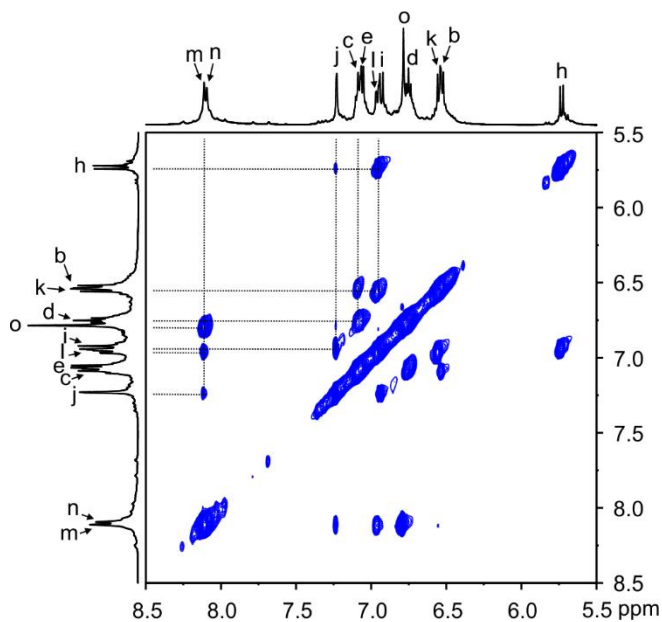**Figure 4.19** Selected aromatic region of the ^{1}H NOESY NMR spectrum ((CD$_3$)$_2$SO, 500 MHz) of SP-**1** showing the diagnostic cross-peaks for the indicated protons. * Residual solvent peaks.
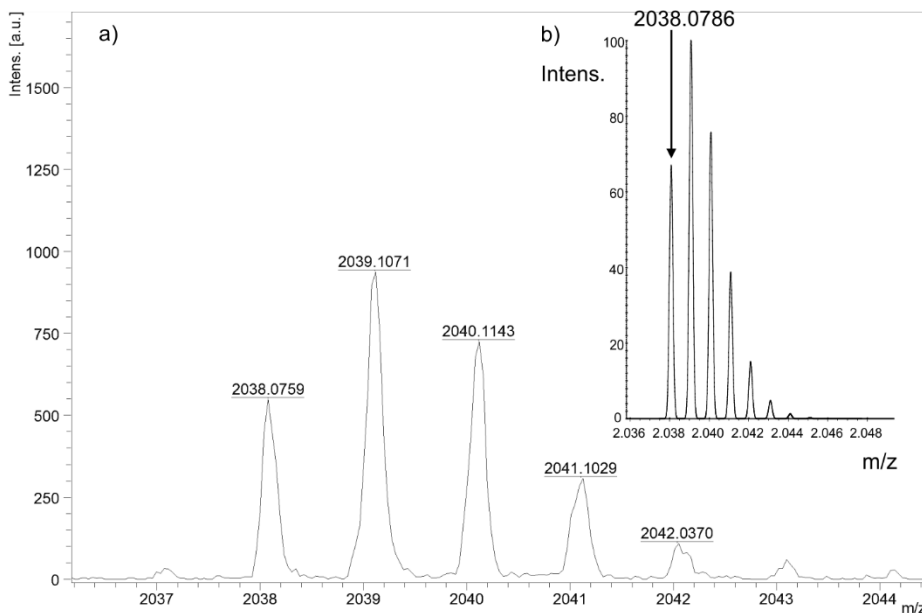

Figure 4.20 a) Experimental and b) theoretical isotopic distributions for [M+H]$^+$ of SP-**1**. The exact mass for the monoisotopic peak in a) and b) is indicated.

163

Chapter 4
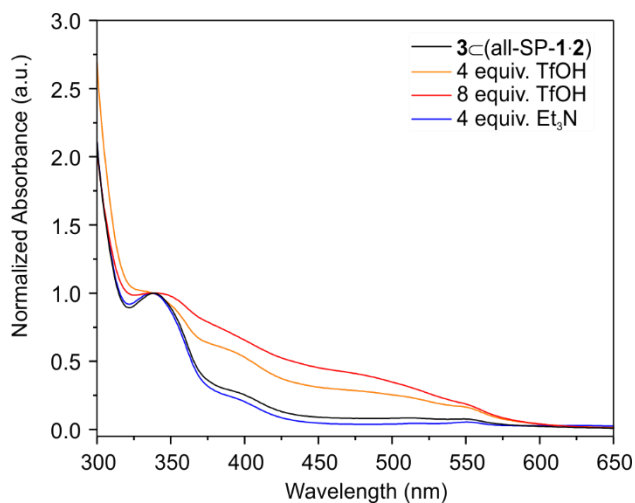
Figure 4.21 Normalized UV/Vis absorption spectra of a 50 µM CD_2Cl_2 solution of **3**⊂(all-SP-**1**·**2**) before (black) and after treatment with 4 equiv. of TfOH (orange), 8 equiv. of TfOH (red) and then with 4 equiv. of Et_3N (blue). The spectra were normalized to the value of maximum absorbance of the heterocapsule **3**⊂(all-SP-**1**·**2**) (*ca*. 338 nm).
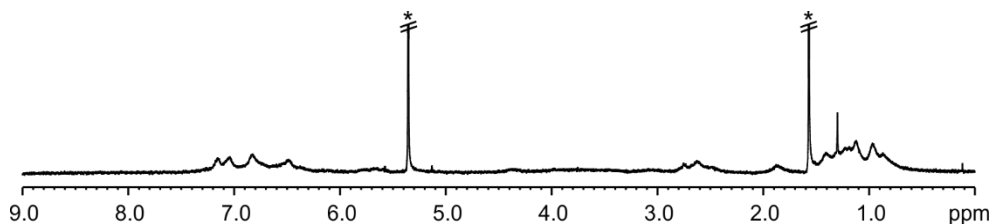
Figure 4.22 ^{1}H NMR (CD_2Cl_2, 400 MHz) spectrum at 298 K of a 1.1 mM solution of SP-**1**. * Residual solvent peaks.

Self-assembly of homo- and heterodimeric capsules based on a tetraspiropyran tetraurea calix[4]arene

Figure 4.23 ^{1}H NMR (CD$_2$Cl$_2$, 400 MHz) spectra at 298 K of a 1.3 mM solution of a) receptor **2**; b) **2** + 0.5 equiv. of **3**; c) 2 + 0.75 equiv. of **3**; d) 2 + 1 equiv. of **3** (**3**$_2$⊂**2**$_2$). Primed letters and numbers correspond to proton signals of bound components. 1,3,5-tris(trifluoromethyl)benzene was used as internal standard (I.S.). * Residual solvent peaks.

Chapter 4

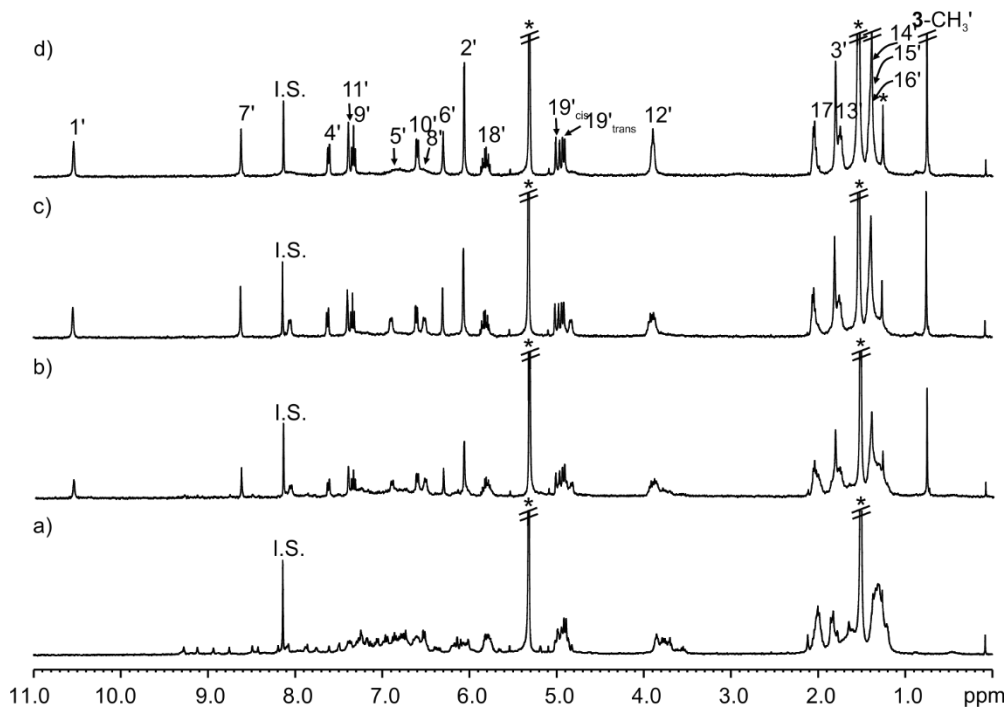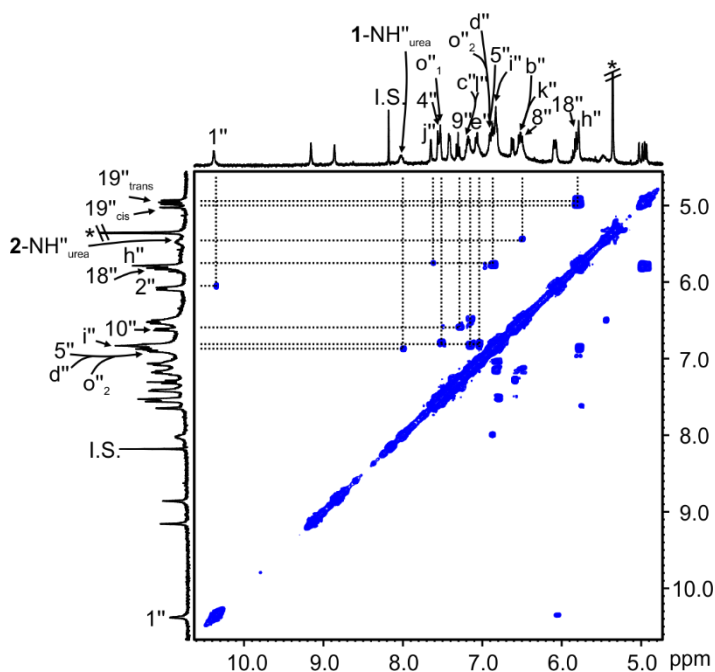**Figure 4.24** Selected region of the ¹H COSY NMR spectrum (CD₂Cl₂, 500 MHz) of **3**⊂(all-SP-**1**·**2**) showing the diagnostic cross-peaks for the indicated protons. Double primed letters and numbers correspond to proton signals of bound components involved in the heterocapsular assembly **3**⊂(all-SP-**1**·**2**). 1,3,5-tris(trifluoromethyl)benzene was used as internal standard (I.S.). * Residual solvent peaks.

Figure 4.25 Selected region of the ¹H NOESY NMR spectrum (CD₂Cl₂, 500 MHz) of **3**⊂(all-SP-**1**·**2**) showing the diagnostic cross-peaks for the indicated protons. Double primed letters and numbers correspond to proton signals of bound components involved in the heterocapsular assembly **3**⊂(all-SP-**1**·**2**). 1,3,5-tris(trifluoromethyl)benzene was used as internal standard (I.S.). * Residual solvent peaks.

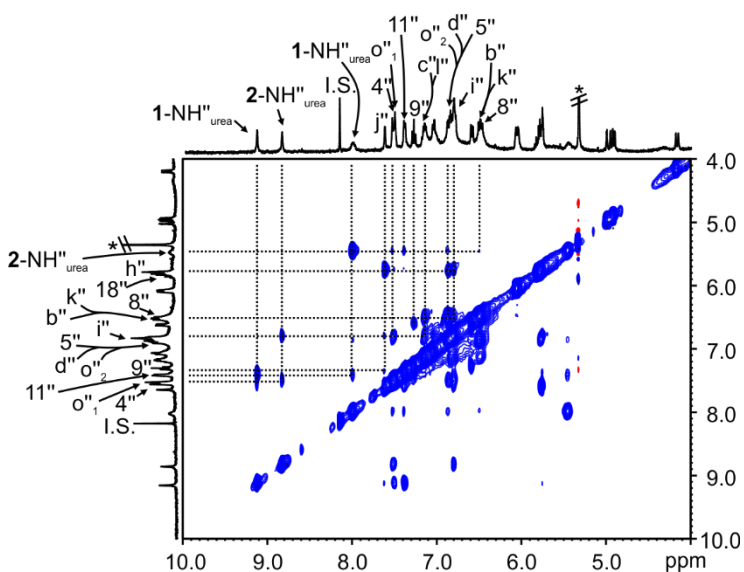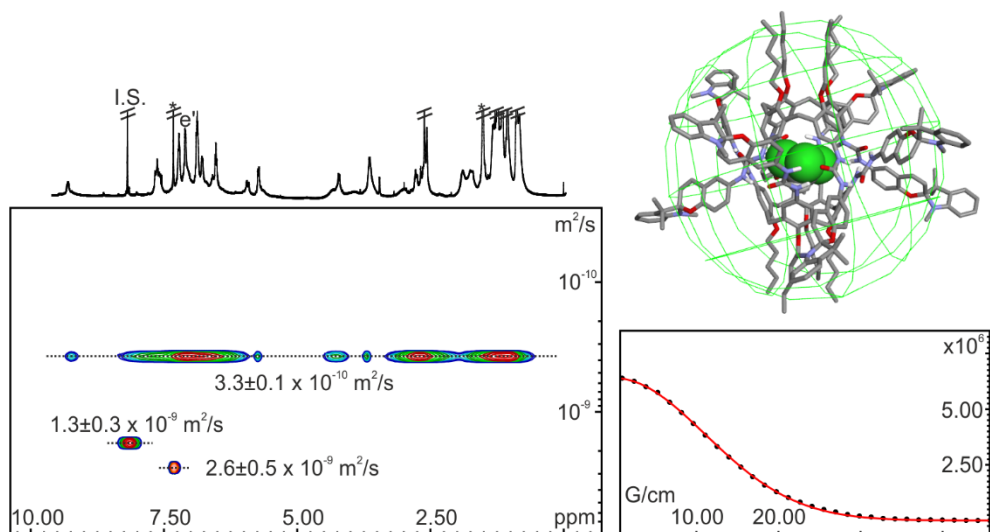*Self-assembly of homo- and heterodimeric capsules based on a tetraspiropyran tetraurea calix[4]arene*

Figure 4.26 (left) ^{1}H pseudo 2D-plot DOSY (500 MHz with cryoprobe, (CDCl$_3$, 298 K, D20 = 0.10 s; P30 = 2.0 ms) of (all-SP-**1**)$_2$ (2 mM). (right) Top: energy minimized molecular model (MM3) of (all-SP-**1**)$_2$. The host is depicted in stick representation and the encapsulated guest as CPK model. Non-polar hydrogen atoms of **1** were removed for clarity. The hydrodynamic radius r$_H$ defines a green sphere with diffusion coefficient *D* (Stokes-Einstein equation) from the respective ^{1}H DOSY NMR experiments in CDCl$_3$: 12.18 ± 0.44 Å. Bottom: fit of the decay of diagnostic proton signal e' of the capsular assembly to a mono-exponential function using *Dynamics Center* from *Bruker*. Errors are indicated as standard deviations. Primed letters correspond to proton signals of (all-SP-**1**)$_2$. * Solvent residual peaks.
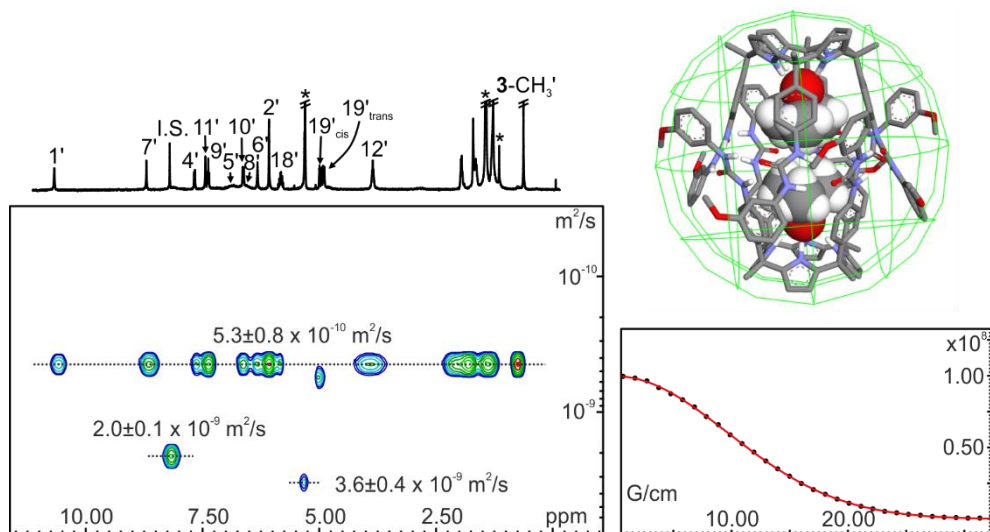
Figure 4.27 (left) ^{1}H pseudo 2D-plot DOSY (500 MHz, (CD$_2$Cl$_2$, 298 K, D20 = 0.10 s; P30 = 2.0 ms) of **3**$_2$⊂**2**$_2$ (1.9 mM). (right) Top: energy minimized molecular model (MM3) of **3**$_2$⊂**2**$_2$. The allylic chains in **2** were pruned to methoxy groups and non-polar hydrogen atoms were removed for clarity. Encapsulated guests are represented as CPK models. The hydrodynamic radius r$_H$ defines a green sphere with diffusion coefficient *D* (Stokes-Einstein equation) from the respective ^{1}H DOSY NMR experiments in CD$_2$Cl$_2$: 10.02 ± 1.50 Å. Bottom: fit of the decay of the diagnostic *β*-pyrrole proton

signal 2' of **2** in the capsular assembly to a mono-exponential function using *Dynamics Center* from *Bruker*. Errors are indicated as standard deviations. Primed letters correspond to proton signals of **3**$_2$⊂**2**$_2$. * Solvent residual peaks.
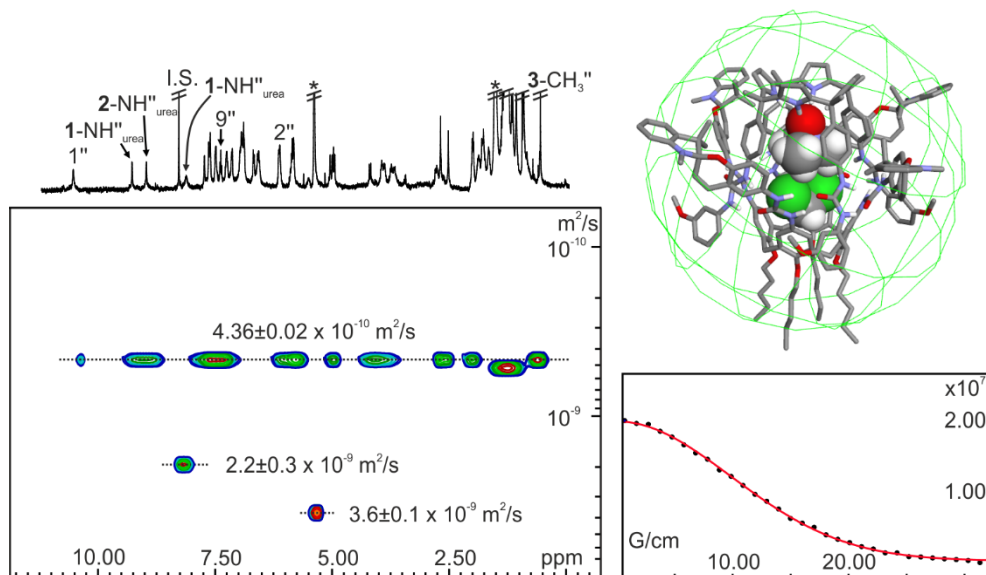
Figure 4.28 (left) ^{1}H pseudo 2D-plot DOSY (500 MHz, (CD$_2$Cl$_2$, 298 K, D20 = 0.10 s; P30 = 2.0 ms) of **3**⊂(all-SP-**1·2**) (2 mM). (right) Top: energy minimized molecular model (MM3) of **3**⊂(all-SP-**1·2**). The allylic chains in **2** were pruned to methoxy groups and non-polar hydrogen atoms of **1** and **2** were removed for clarity. Encapsulated guests are represented as CPK models. The hydrodynamic radius r$_H$ defines a green sphere with diffusion coefficient D (Stokes-Einstein equation) from the respective ^{1}H DOSY NMR experiments in CD$_2$Cl$_2$: 12.23 ± 0.05 Å. Bottom: fit of the decay of the diagnostic proton signal 9'' of **2** in the capsular assembly to a mono-exponential function using *Dynamics Center* from *Bruker*. Errors are indicated as standard deviations. Double primed letters correspond to proton signals of **3**⊂(all-SP-**1·2**). * Solvent residual peaks.

Capsule	D (10^{-10} m^2/s)	-log$D$	r$_H$ (Å)	PC (%)
(all-SP-**1**)$_2$	3.35 ± 0.12	9.47	12.18 ± 0.44	42
3$_2$⊂**2**$_2$	5.33 ± 0.8	9.27	10.02 ± 1.50	47
3⊂(all-SP-**1·2**)	4.36 ± 0.02	9.36	12.13 ± 0.05	63

Table 4.1 Diffusion coefficient (D) values obtained from the ^{1}H DOSY NMR experiments. Hydrodynamic radius (r$_H$) values corresponding to an imaginary sphere as calculated (Stokes-Einstein equation) from the respective experimental D values. Errors in D and r$_H$ are indicated as standard deviations. Packing coefficients (PC = (V$_{guest/s}$/V$_{host/s}$) x 100) of the capsular assemblies obtained from the energy-minimized structures (MM3). The internal volumes of the hosts and the external volumes of the guests were determined using the *Swiss PDB Viewer* software.

Self-assembly of homo- and heterodimeric capsules based on a tetraspiropyran tetraurea
calix[4]arene
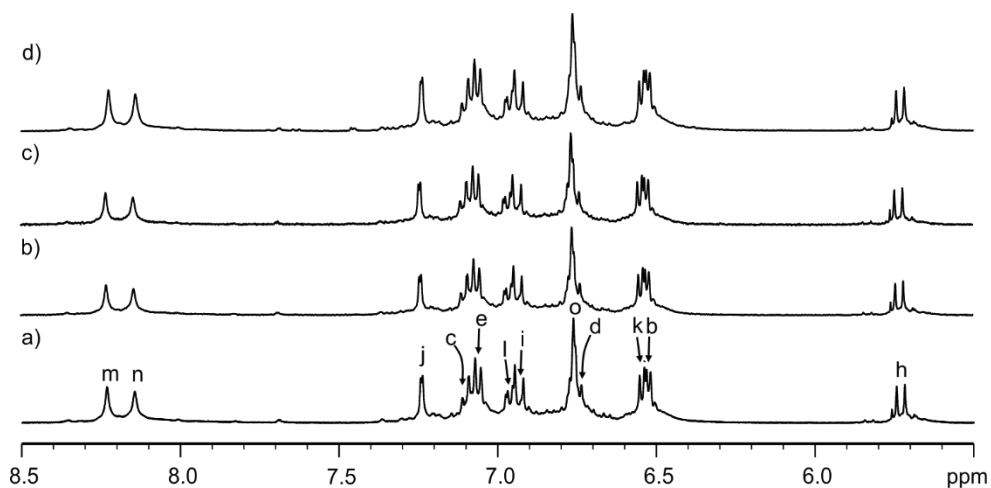
Figure 4.29 Selected aromatic region of the ^{1}H NMR ((CD$_3$)$_2$SO, 400 MHz) spectra at 298 K of a millimolar solution of SP-**1** irradiated at 365 nm for a) 0; b) 5, c) 10 min and d) after thermal equilibration at 60 ºC in the dark for 12 h.
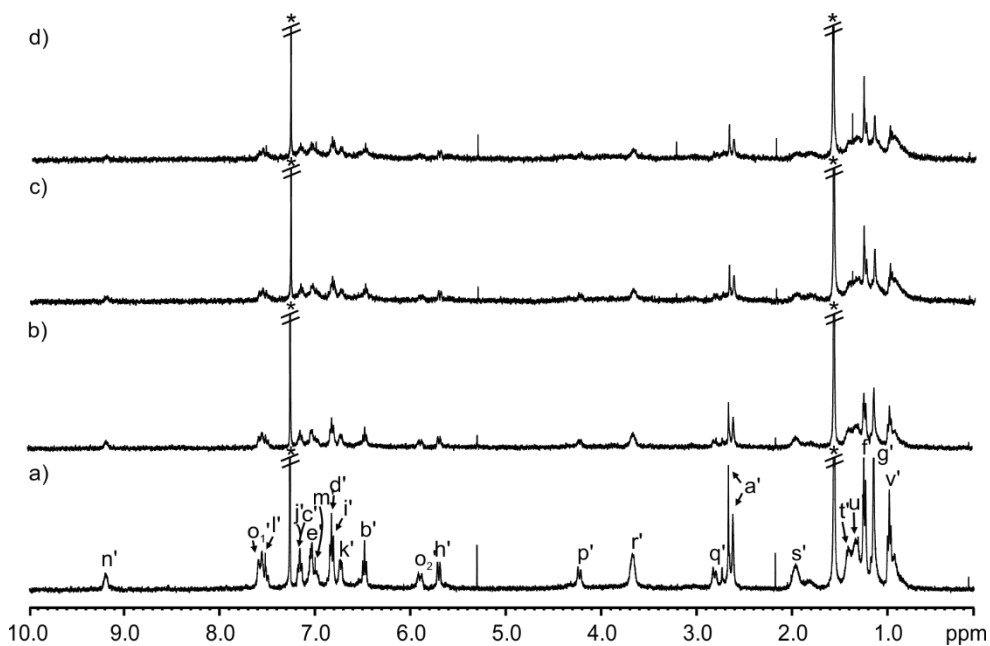
Figure 4.30 Selected aromatic region of the ^{1}H NMR (CDCl$_3$, 400 MHz) spectra at 298 K of a 1.1 millimolar solution of homocapsule (all-SP-**1**)$_2$ irradiated at 365 nm for a) 0; b) 1, c) 5 and d) 7 min. Primed letters and numbers correspond to proton signals of bound components. * Residual solvent peaks.

Chapter 4
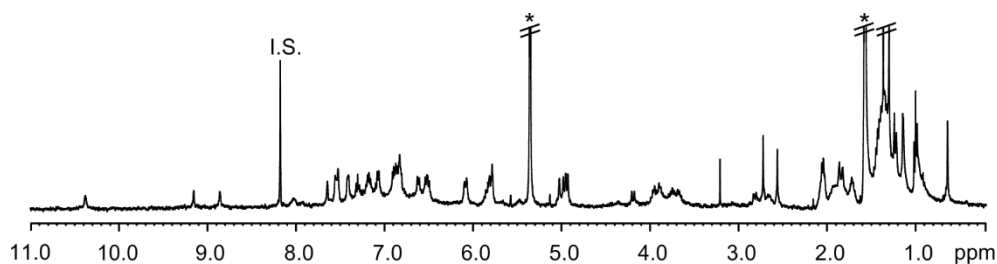
Figure 4.31 ^{1}H NMR (CDCl$_3$, 400 MHz) spectrum at 298 K of a 1 mM solution of heterocapsule **3**⊂(all-SP-**1**·**2**) photoirradiated at 365 nm for 5 min. 1,3,5-tris(trifluoromethyl)benzene was used as internal standard (I.S.). * Residual solvent peaks.
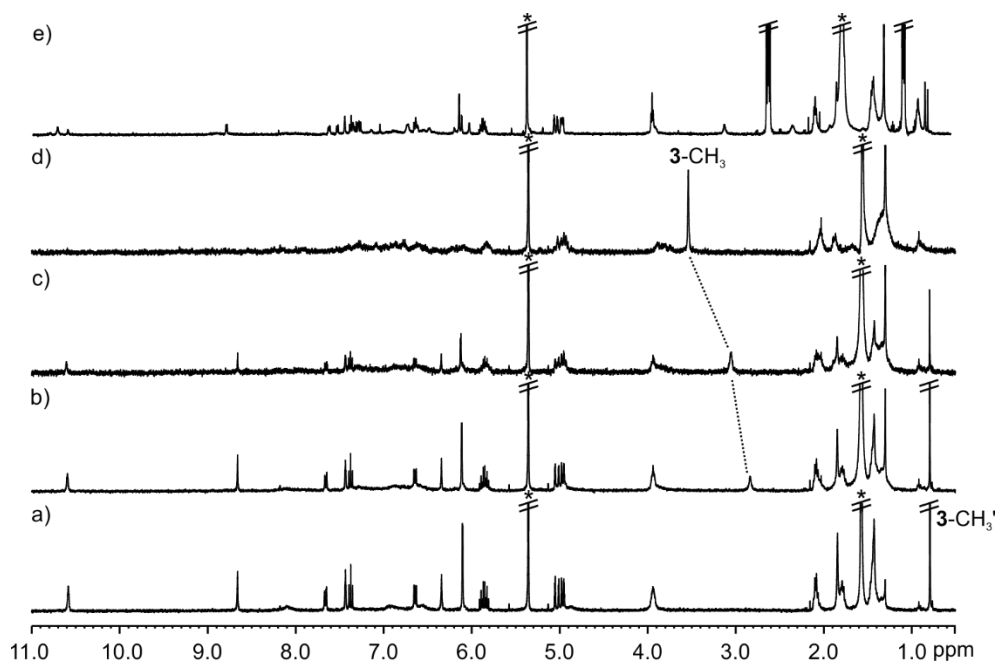
Figure 4.32 ^{1}H NMR (CDCl$_3$, 400 MHz) spectra at 298 K of a 1 mM solution of homocapsule **3**$_2$⊂**2**$_2$ treated with a) 0; b) 1; c) 4; d) 8 equiv. of TfOH and e) 8 equiv. of Et$_3$N. Primed letters and numbers correspond to proton signals of bound **3**. * Residual solvent peaks.

Self-assembly of homo- and heterodimeric capsules based on a tetraspiropyran tetraurea
calix[4]arene
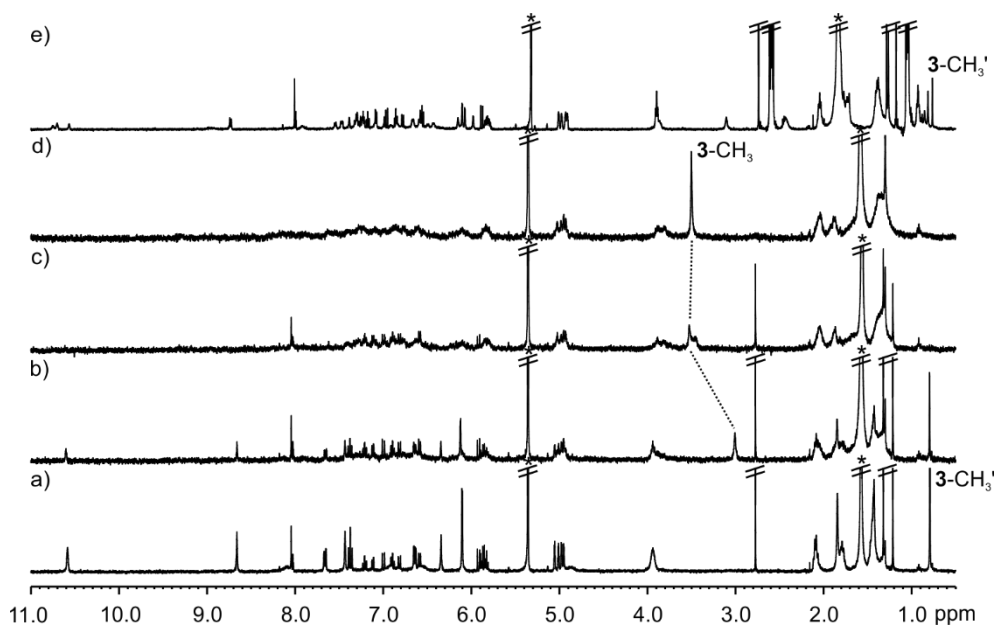
Figure 4.33 ^{1}H NMR (CDCl$_3$, 400 MHz) spectra at 298 K of a 1 mM equimolar solution of homocapsule $3_2 \subset 2_2$ and **BIPS** treated with a) 0; b) 1; c) 4; d) 8 equiv. of TfOH and e) 8 equiv. of Et$_3$N. Primed letters and numbers correspond to proton signals of bound **3**. * Residual solvent peaks.
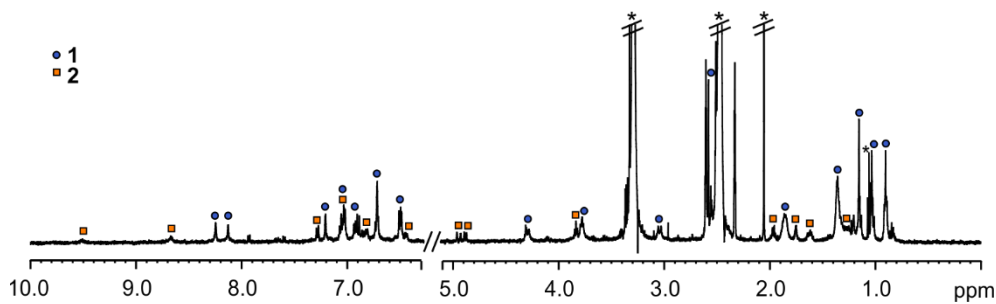
Figure 4.34 ^{1}H NMR ((CD$_3$)$_2$SO, 500 MHz) spectrum at 298 K of a photoirradiated mixture (365 nm) of **1** and **2** after centrifugation and separation from the supernatant, starting from an equimolar acetone solution of all-SP-**1**, **2** and **3**. The blue circles represent signals of **1** and the orange squares those of **2**. * Residual solvent peaks.

Chapter 4

4.5 References and notes

[1] J. D. Harris, M. J. Moran, I. Aprahamian, *Proc. Natl. Acad. Sci.* **2018**.

[2] H. M. D. Bandara, S. C. Burdette, *Chem. Soc. Rev.* **2012**, *41*, 1809-1825.

[3] S. Wiedbrauk, H. Dube, *Tetrahedron Lett.* **2015**, *56*, 4266-4274.

[4] D. J. van Dijken, P. Kovaříček, S. P. Ihrig, S. Hecht, *J. Am. Chem. Soc.* **2015**, *137*, 14982-14991.

[5] I. Aprahamian, *Chem. Commun.* **2017**, *53*, 6674-6684.

[6] V. I. Minkin, *Chem. Rev.* **2004**, *104*, 2751-2776.

[7] L. Kortekaas, W. R. Browne, *Chem. Soc. Rev.* **2019**. doi.org/10.1039/C9CS00203K

[8] M. Irie, *Chem. Rev.* **2000**, *100*, 1685-1716.

[9] M. Irie, T. Fukaminato, K. Matsuda, S. Kobatake, *Chem. Rev.* **2014**, *114*, 12174-12277.

[10] S. Helmy, F. A. Leibfarth, S. Oh, J. E. Poelma, C. J. Hawker, J. Read de Alaniz, *J. Am. Chem. Soc.* **2014**, *136*, 8169-8172.

[11] S. Helmy, S. Oh, F. A. Leibfarth, C. J. Hawker, J. Read de Alaniz, *J. Org. Chem.* **2014**, *79*, 11316-11329.

[12] M. M. Lerch, S. J. Wezenberg, W. Szymanski, B. L. Feringa, *J. Am. Chem. Soc.* **2016**, *138*, 6344-6347.

[13] O. B. Berryman, H. Dube, J. J. Rebek, *Isr. J. Chem.* **2011**, *51*, 700-709.

[14] D.-H. Qu, Q.-C. Wang, Q.-W. Zhang, X. Ma, H. Tian, *Chem. Rev.* **2015**, *115*, 7543-7588.

[15] P. Weis, S. Wu, *Macromol. Rapid Commun.* **2018**, 39, 1700220.

[16] W.-C. Geng, H. Sun, D.-S. Guo, *J. Inclusion Phenom. Macrocyclic Chem.* **2018**, 92, 1-79.

[17] E. Wagner-Wysiecka, N. Łukasik, J. F. Biernat, E. Luboch, *J. Inclusion Phenom. Macrocyclic Chem.* **2018**, 90, 189-257.

[18] A. A. Beharry, G. A. Woolley, *Chem. Soc. Rev.* **2011**, 40, 4422-4437.

[19] T. Masuda, Y. Kondo, *Supramol. Chem.* **1995**, 5, 129-131.

[20] E. J. Cho, I. Y. Jeong, S.-J. Lee, J.-B. Seo, H. J. Kim, E. Kim, S. S. Lee, J. K. Kang, J. S. Kim, J. Jong Hwa, *Bull. Korean Chem. Soc.* **2007**, 28, 2519-2522.

[21] P. Thuéry, M. Nierlich, É. Lamare, J.-F. Dozol, Z. Asfari, J. Vicens, *J. Inclusion Phenom. Macrocyclic Chem.* **2000**, *36*, 375-408.

[22] P. Neri, J. L. Sessler, M.-X. Wang, *Calixarenes and Beyond*, Springer, Cham, **2016**.

[23] K. D. Shimizu, J. Rebek, *Proc. Natl. Acad. Sci. U. S. A.* **1995**, *92*, 12403-12407.

[24] O. Mogck, V. Böhmer, W. Vogt, *Tetrahedron* **1996**, *52*, 8489-8496.

[25] J. J. Rebek, *Chem. Commun.* **2000**, 637-643.

[26] O. Mogck, M. Pons, V. Böhmer, W. Vogt, *J. Am. Chem. Soc.* **1997**, *119*, 5706-5712.

[27] R. K. Castellano, B. H. Kim, J. J. Rebek, *J. Am. Chem. Soc.* **1997**, *119*, 12671-12672.

[28] R. K. Castellano, C. Nuckolls, J. J. Rebek, *J. Am. Chem. Soc.* **1999**, *121*, 11156-11163.

[29] C. A. Schalley, R. K. Castellano, M. S. Brody, D. M. Rudkevich, G. Siuzdak, J. J. Rebek, *J. Am. Chem. Soc.* **1999**, *121*, 4568-4579.

[30] S. Zarra, D. M. Wood, D. A. Roberts, J. R. Nitschke, *Chem. Soc. Rev.* **2015**, *44*, 419-432.

[31] D. M. Rudkevich, *Bull. Chem. Soc. Jpn.* **2002**, *75*, 393-413.

[32] J. J. Rebek, *Chem. Soc. Rev.* **1996**, *25*, 255-264.

[33] F. Hof, S. L. Craig, C. Nuckolls, J. J. Rebek, *Angew. Chem., Int. Ed.* **2002**, *41*, 1488-1508.

[34] J. J. Rebek, *Angew. Chem., Int. Ed.* **2005**, *44*, 2068-2078.

[35] F. A. Arroyave, P. Ballester, *J. Org. Chem.* **2015**, *80*, 10866-10873.

[36] A. Diaz-Moscoso, F. A. Arroyave, P. Ballester, *Chem. Commun.* **2016**, *52*, 3046-3049.

[37] T. Sakano, T. Ohashi, M. Yamanaka, K. Kobayashi, *Org. Biomol. Chem.* **2015**, *13*, 8359-8364.

[38] T. Zimmermann, O. Brede, *J. Heterocycl. Chem.* **2003**, *40*, 611-616.

[39] R. A. Jakobi, V. Boehmer, C. Gruettner, D. Kraft, W. Vogt, *New J. Chem.* **1996**, *20*, 493−501.

[40] N. L. Zaichenko, A. V. Lyubimov, V. S. Marevtsev, M. I. Cherkashin, *Bull. Acad. Sci. USSR, DiV. Chem. Sci.* **1987**, *36*, 1543-1544.

[41] S. Swansburg, E. Buncel, R. P. Lemieux, *J. Am. Chem. Soc.* **2000**, *122*, 6594-6600.

[42] Y. Sheng, J. Leszczynski, *Struct. Chem.* **2014**, *25*, 667-677.

*Self-assembly of homo- and heterodimeric capsules based on a tetraspiropyran tetraurea calix[4]arene*

[43] J. T. C. Wojtyk, A. Wasey, N.-N. Xiao, P. M. Kazmaier, S. Hoz, C. Yu, R. P. Lemieux, E. Buncel, *J. Phys. Chem. A* **2007**, *111*, 2511-2516.

[44] W. Tian, J. Tian, *Dyes Pigm.* **2014**, *105*, 66-74.

[45] The proton signals of all-SP-**1** in $(CD_3)_2SO$ appeared slightly broad. Thus, we cannot exclude that all-SP-**1** experiences aggregation to a very reduced extent in this solvent.

[46] R. Sekiya, A. Díaz-Moscoso, P. Ballester, *Chem. Eur. J.* **2018**, *24*, 2182-2191.

[47] We were not able to determine the extent of the switching from the closed all-SP-**1** to the all-MC-**1** species by means of UV/Vis spectroscopy.

[48] We also followed the irradiation at 365 nm of a 1 mM acetone solution of all-SP-**1** by ^{1}H NMR. The formation of hydrogen-bonded capsules is highly disfavored by the competitive nature of this solvent. The sample was irradiated at 365 nm for 20 s: immediately, the colorless solution turned blue, and a blue precipitate appeared. The observation of the blue precipitate was attributed to the formation of supramolecular aggregates induced by the stacking of the photogenerated open-ring merocyanines of **1** in this solvent. Thermal equilibration at 40 ºC for 5 min recovered the initial state of the system, and the precipitate dissolved again.

[49] M. Chas, G. Gil-Ramírez, P. Ballester, *Org. Lett.* **2011**, *13*, 3402-3405.

[50] A. Galán, M. Espelt, P. Ballester, *Supramol. Chem.* **2016**, *28*, 455-463.

[51] S. Mecozzi, J. J. Rebek, *Chem. Eur. J.* **1998**, *4*, 1016-1022.

[52] L. Avram, Y. Cohen, *Chem. Soc. Rev.* **2015**, *44*, 586-602.

[53] A. V. Laptev, D. E. Pugachev, A. Y. Lukin, A. V. Nechaev, N. E. Belikov, O. V. Demina, P. P. Levin, A. A. Khodonov, A. F. Mironov, S. D. Varfolomeev, V. I. Shvets, *Mendeleev Commun.* **2013**, *23*, 199-201.

[54] A. Grün, P. Kerekes, I. Bitter, *Supramol. Chem.* **2008**, *20*, 255-263.

[55] A. Grün, É. Kőszegi, B. Balázs, G. Tóth, I. Bitter, *Supramol. Chem.* **2004**, *16*, 239-246.

[56] Z. Liu, L. Jiang, Z. Liang, Y. Gao, *J. Mol. Struct.* **2005**, *737*, 267-270.

[57] M. Lee, D. Cho, I. Kim, J. Lee, J. Y. Lee, C. Satheeshkumar, C. Song, *ChemistrySelect* **2017**, *2*, 3527-3533.

[58] M. Chas, P. Ballester, *Chem. Sci.* **2012**, *3*, 186-191.

[59] We performed a 1D GOESY NMR experiment of **3**⊂(all-SP-**1**·**2**) in a 9:1 CH_2Cl_2:CD_2Cl_2 solvent mixture. Unfortunately, we were not able to detect the signal corresponding to the bound CH_2Cl_2.

[60] R. K. Castellano, S. L. Craig, C. Nuckolls, J. Rebek, *J. Am. Chem. Soc.* **2000**, *122*, 7876-7882.

[61] We monitored by ^{1}H NMR spectroscopy the irradiation at 365 nm for 20 s of a 1 mM $(CD_3)_2CO$ solution of a 1:1:1 equimolar mixture of all-SP-**1**, **2** and **3**: again, the solution turned from colorless to blue, and a precipitate appeared. The tube was cooled inside the fridge for 5 min. Afterwards, the suspension was transferred to an Eppendorf vial and centrifuged for 2 min. The supernatant was removed using a pipette. The remaining blue solid was dried under nitrogen flow and redissolved in $(CD_3)_2SO$: interestingly, its ^{1}H NMR spectrum showed the diagnostic signals of both tetraureas, hinting to the existence of interaction between **1** and **2** in this polar solvent. The same studies performed in other moderately polar solvents ($CHCl_3$, CH_2Cl_2, THF) did not show a similar behavior.

[62] H. Xu, S. P. Stampp, D. M. Rudkevich, *Org. Lett.* **2003**, *5*, 4583-4586.

[63] L. Kortekaas, J. Chen, D. Jacquemin, W. R. Browne, *J. Phys. Chem. B* **2018**, *122*, 6423-6430.

[64] The treatment of separate millimolar dichloromethane solutions of all-SP-**1** and **3**⊂(all-SP-**1**·**2**) with 1 molar equiv. of deuterated trifluoroacetic acid and subsequent irradiation at 365 nm did not produce detectable changes in the composition of their NMR spectra.

[65] S. Gadde, E. K. Batchelor, J. P. Weiss, Y. Ling, A. E. Kaifer, *J. Am. Chem. Soc.* **2008**, *130*, 17114-17119.

[66] The homo-capsule **3**$_2$⊂**2**$_2$ was not detected in solution. Probably, both **1** and **2** were involved in non-capsular aggregates.

[67] The same acid-base treatments were performed on separate millimolar chloroform solutions containing the homocapsule **3**$_2$⊂**2**$_2$ in the absence and presence of 1 equiv. of **BIPS** in the bulk. In both control experiments, the addition of TfOH provoked the release of the fully protonated guest **3** in solution and the disintegration of the capsular dimer. Moreover, upon addition of Et_3N the original state of the system was not restored. Instead, we observed the appearance of several unknown capsular and non-capsular species of **2** in solution.

[68] Z. Thomas, B. Ortwin, *J. Heterocycl. Chem.* **2003**, *40*, 611-616.

UNIVERSITAT ROVIRA I VIRGILI
STIMULI-RESPONSIVE HOST-GUEST SYSTEMS DECORATED WITH HEMITHIOINDIGO AND SPIROPYRAN UNITS
Giulia Moncelsi

General conclusions

This thesis deals with the design, synthesis and comprehensive studies of a series of inclusion complexes and capsular assemblies covalently incorporating stimuli-responsive hemithioindigo or spiropyran units in either the receptor's or the guest's scaffold. The general objective of the research work was the efficient coupling of the isomerization of the molecular switches with the binding affinity and the encapsulation properties of host-guest systems derived from calix[4]arene and calix[4]pyrrole macrocyclic scaffolds.

In the first system, described in chapter 2, both the *Z*- and *E*-isomers of light-responsive HTI *N*-oxide guests formed highly thermodynamically and kinetically stable 1:1 complexes with a super aryl-extended calix[4]pyrrole in organic solvent. Surprisingly, the photoirradiation at 450 nm of the *Z*-HTI⊂**1** complexes produced mixtures enriched with the *E*-HTI⊂**1** counterparts and required extensive irradiation times to achieve the same levels of isomerization at the PSSs compared to the analogous experiments performed with the free *Z*-HTIs. In this project, we were able to modulate the kinetics of the reversible *Z/E* photoisomerization of the two HTI guests by inclusion into the polar aromatic cavity of the receptor, whereas the *Z/E* HTI isomeric ratio remained unaffected by the inclusion. We were also expecting a substantial decrease in the binding affinity of the receptor towards the *E*-HTIs with respect to the *Z*-isomers. However, the K_a values of all bound isomers were of the same order of magnitude (10^6 M^{-1}), meaning that the number and nature of the different interactions between the host-guest counterparts were not significantly modified by the photoisomerization process. At millimolar concentration, the *Z*-to-*E* photoisomerization of the guests did not induce their detectable release to the bulk solution.

The study of the photoisomerizable 1:1 inclusion complexes yielded valuable knowledge and know-how for devising related host-guest systems capable of efficient transport and release of cargo by application of a remote stimulus. We postulated that the modulation in the structure of the receptor, and not the guest, would provide the desired coupling. Accordingly, we designed hydrogen-bonded capsular dimers based on tetraurea calix[4]arene scaffolds equipped with four upper rim stimuli-responsive units.

In chapter 3, we isolated two tetra-HTI tetraurea calix[4]arenes. Our findings on the photoisomerization and self-assembly behavior in a variety of non-polar organic solvents and

in the presence of templating guests showed that these containers experience reduced switching of the photoresponsive HTI units, as well as a lack of quantitative dimerization into well-defined discrete capsules. Overall, the tetra-HTI tetraureas prepared herein are not the ideal candidates for the construction of photoresponsive capsular architectures capable of light-controlled release of molecular cargo.

Following a similar molecular design, in the last chapter we successfully synthesized an unprecedented light- and pH-responsive tetraspiropyran tetraurea calix[4]arene. The prepared tetraurea self-assembles into a homocapsule in chloroform solution or in dichloromethane using tetramethylphosphonium cation as the templating guest. Remarkably, in the presence of a calix[4]pyrrole counterpart and a suitable *N*-oxide template, the tetraureas experience a self-sorting process yielding exclusively the heterodimeric capsule including the *N*-oxide and one molecule of dichloromethane solvent. The SP/MC isomerization of the decorating units and the dimerization equilibrium are highly and inversely solvent-dependent: non-polar organic solvents favor the self-assembly of the tetra-SP tetraurea capsules over the light-induced formation of merocyanines, which is achieved to a reduced extent. Although the SP/MC response to light-irradiation was not efficient, the acid-base modulation between the SP/MCH[+] substituents using triflic acid and triethylamine was indeed effective towards the reversible capsular assembly/disintegration process at both micro- and millimolar concentrations, provoking the uptake and release of the *N*-oxide guest to the bulk solution. In conclusion, we were able to efficiently couple the acid-base modulated SP-to-MC isomerization of the appended switches to the assembly/disassembly processes of capsular dimers based on tetraurea scaffolds. Our results augur well for future studies of these assemblies as stimuli-responsive systems for the efficient transport of specific cargo.

List of abbreviations

ACN	—	Acetonitrile
ATR	—	Attenuated total reflectance
BArF$^-$	—	Tetrakis(3,5-bis(trifluoromethyl)phenyl)borate
BIPS	—	6'-Nitrospiropyran
C[4]A	—	Calix[4]arene
C[4]P	—	Calix[4]pyrrole
CB[n]	—	Cucurbit[n]uril
CD[n]	—	n-Membered cyclodextrin
COSY	—	Correlation spectroscopy
CPK	—	Corey-Pauling-Koltun space-filling model
Cys	—	Cysteine
DASA	—	Donor-acceptor Stenhouse Adduct
DCM	—	Dichloromethane
DMF	—	Dimethylformamide
DTGS	—	Deuterated triglycine sulfate
DOSY	—	Diffusion-ordered spectroscopy
ESI	—	Electrospray ionization
EXSY	—	Exchange spectroscopy
FT-IR	—	Fourier-transform infrared spectroscopy
GOESY	—	Gradient enhanced nuclear Overhauser effect
GSH	—	Glutathione

HCy	—	Homocysteine
HPLC	—	High performance liquid chromatography
HRMS	—	High resolution mass spectrometry
HTI	—	Hemithioindigo
IR	—	Infrared spectroscopy
ITC	—	Isothermal titration calorimetry
K_a	—	Association constant
LED	—	Light emitting diode
MALDI	—	Matrix-assisted laser desorption/ionization
MC	—	Merocyanine
MCH^+	—	Protonated merocyanine
MM3	—	Molecular Mechanics force field
MS	—	Mass spectrometry
MV	—	Methyl viologen
NMC	—	6'-Nitromerocyanine
NMR	—	Nuclear magnetic resonance
NOE	—	Nuclear Overhauser effect
NOESY	—	Nuclear Overhauser effect spectroscopy
NSP	—	6'-Nitrospiropyran
ORTEP	—	Oak Ridge thermal ellipsoid plot
PBS	—	Sodium perborate
PC	—	Packing coefficient
PIP	—	Piperidine

PSS	—	Photostationary State
QNP	—	Quattro nucleus probe
RT	—	Room temperature
SCXn	—	Sulfonatocalix[n]arene
SP	—	Spiropyran
TFA	—	Trifluoroacetic acid
THF	—	Tetrahydrofuran
TLC	—	Thin-layer chromatography
Tu	—	Tetraurea
UV	—	Ultraviolet
Vis	—	Visible

UNIVERSITAT ROVIRA I VIRGILI
STIMULI-RESPONSIVE HOST-GUEST SYSTEMS DECORATED WITH HEMITHIOINDIGO AND SPIROPYRAN UNITS
Giulia Moncelsi

UNIVERSITAT ROVIRA I VIRGILI
STIMULI-RESPONSIVE HOST-GUEST SYSTEMS DECORATED WITH HEMITHIOINDIGO AND SPIROPYRAN UNITS
Giulia Moncelsi

UNIVERSITAT ROVIRA I VIRGILI
STIMULI-RESPONSIVE HOST-GUEST SYSTEMS DECORATED WITH HEMITHIOINDIGO AND SPIROPYRAN UNITS
Giulia Moncelsi

UNIVERSITAT
ROVIRA i VIRGILI